EPFL

Thèse n° 9606

Dissecting the role of biliary epithelial cells during non-alcoholic fatty liver disease progression

Présentée le 14 décembre 2022

Faculté des sciences de la vie
Unité de la Prof. Schoonjans
Programme doctoral en biotechnologie et génie biologique

pour l'obtention du grade de Docteur ès Sciences

par

Ece YILDIZ

Acceptée sur proposition du jury

Prof. M. Dal Peraro, président du jury
Prof. K. Schoonjans, directrice de thèse
Prof. A. Ocampo, rapporteur
Prof. I. Leclercq, rapporteuse
Prof. G. D'Angelo, rapporteur

École polytechnique fédérale de Lausanne

2022

To all the women around the world fighting for human rights

Acknowledgments

In 2018, I started my Ph.D. program in EPFL without knowing that it would be the most challenging and longest journey to get to know myself more than ever. Even though I was pursuing a topic that was very interesting to me and my background was fitting well with it, it was never a bed of roses as I had to get into the details of this field on a cellular and molecular level together with techniques that I have not employed before. After 4.5 years, I am closing this chapter of my life, which was full of doubts, worries, and stress but also of self-awareness, personal growth, success, patience, and diligence. I finally say that I am ready for the next chapter with an open heart and a great enthusiasm for science, which I would not be able to accomplish without the help and support of the following people.

Foremost, I am immensely thankful to *Prof. Kristina Schoonjans*, my thesis director and advisor, who provided me the opportunity to join her laboratory on the liver organoid project. Throughout the years, her guidance and support encouraged me to push my limits, sharpen my thinking and develop a small follow-up project on the first project I joined. Without her feedback and trust, this study would never have come to an end.

I am also profoundly grateful to *Giovanni Sorrentino*, a fantastic scientist with a great approach to science, who initiated me on the liver organoid project when I first joined the lab. Our constant discussions and his scientific talent and passion made me the scientist I am proud to be today. Besides Giovanni, I am deeply grateful to be guided by *Alessia Perino*, who has been essential in the last two years when I was working on my follow-up project. Thanks to Alessia and her incredible insight and understanding of topics that are not even her field, I learned the best aspects of project management and experiment design. I deeply thank both of my Italian mentors; they are the best!

I would also like to thank my amazing collaborators: *Prof. Matthias Lutolf* for the insights and guidance on hydrogels and synthetic cultures (also for the times when I was a master's student in his lab), *Saba Rezakhani* for her manner, being open for collaboration, and helping with the understanding of PEG hydrogels, *Prof. Johan Auwerx* for his constructive suggestions, *Katharina Huber*, *Pierre-Damien Denechaud* and *Prof.Lluis Fajas* for the helpful feedback in addition to providing critical samples, and *Sandro Nuciforo* and *Prof. Markus Heim* for sharing their human liver samples and knowledge on biopsies.

My sincere thanks go to all the scientists and members of the EPFL facilities, without whom I could have not accomplished my Ph.D. research: *Olivier Burri, Romain Guiet,* and *Thierry Laroche* (Bioimaging and Optics platform), *Jessica Sordet-Dessimoz, Gian-Filippo Mancini, Agnès Hautier* and *Christine Göpfert* (Histology Core Facility), *Valérie Glutz, André Mozes,* and *Francesco Palumbo* (Flow Cytometry Core Facility) and Center of PhenoGenomics.

I enjoyed every single moment of the past four and a half years due to the presence of amazing UPSCHOONJANS and LISP lab members, and I would like to offer my special thanks to them. Firstly, a big thank you to great secretaries *Valerie Stengel*, *Rita Heiniger,* and *Adriana Marceta* for being very helpful with all the administrative tasks. Next, I can't thank enough our great lab technicians who facilitated the lab routine, assisted with animal experiments, ensured our safety, and sometimes made impossible things happen. Thank you sincerely, *Sabrina Bichet*, *Jéromine Imbach*, *Fabiana Fraga*, *Thibaud Clerc*, *Andréane Fouassier*, *Laure Vogeleisen-Delpech*, *Marie Janod*, *Carla Mendes*, *Borany Kim*, and *Penelope Stefanelli*! *Laure*, also, I am very happy that we started at the same time and shared so many great (professional cook-level) dinners!

Old and current members of LISP (no order): I thank warmly *Arwen Gao* and *Yasmine Liu* for their smiling faces and good energy, *Sandra Lopez* for her great humor and fun times, *Maxime Nachit* for being my NAFLD buddy and his great food suggestions, *Tanes Imamura de Lima* for his ability to listen and comfort even in bad times and being inspirational for multiskills in tennis, music, and science, *Maria Boulougouri* and *Gaby El Alam* for being the bioinformatic geniuses in addition to their great emotional company, and *Alessia De Masi*, *Amelia Lalou* and *Xiaoxu Li* for the good energy in the lab that always put a smile on my face.

Old and current members of UPSCHOONJANS (no order): I deeply thank *Marika Zietak* and *Laura Velasquez*, for all their support and scientific/non-scientific discussions, *Vera Lemos* for introducing me to Seahorse world, *Hadrien Demagny* for his effective feedback and fun aperos, *Sulagna Mukherjee* for the great spirit in social events, *Vasiliki Delitsikou* for being a great friend from a similar culture and openness to try all different cuisines, *Antoine Jalil* and *Alejandro Calleja* for helpful scientific/non-scientific coffee breaks, continuous support and fun in the lab, *Francesca Pontanari* for sushi making and nice dinner organizations, *Nadia Bresciani* and *Yu Sun* for being my best buddies in the lab who go through the same journey and for covering each other's backs.

Some of my appreciation goes to my mentors before my Ph.D., who continue to support me during my Ph.D. I want to thank *Nathalie Brandenberg* and *Sylke Hoechnel*, brilliant CEOs and co-founders of SUN Bioscience. Their initiative spirit, courage, and problem-solving skills impress me, and I am thankful to meet them. I also would like to thank *Maria Cabrer* for being my one and only master thesis student, for her contributions to the liver organoid culture in SUN Bioscience plates, and her hard work and great mood.

My life in Lausanne has also consisted of a Turkish gang, with whom we had countless parties and weekend getaways. I thank all of them sincerely for making Lausanne home. *Dilara Yilmaz*, *Murat Kaynak*, *Ece Ozelci*, *Ozge Uysal*, *Omer Ozdemir*, *Mustafa Kangul*, *Selen Keles*, *Furkan Ayhan*, and *Fazil Uslu*, thank you all for easing the hard times and making the easy times more joyful. As we all say proudly, "Everything has an end, but cigkofte does not." In addition to my Turkish gang in Lausanne, I also want to thank my dear friends in Turkey. *Zeynep Tolunay*, *Onur Calik*, *Mert Yilmaz*, *Elif Taskiran*, since high school years, you have been an essential part of my life; I love you guys! *Zeynep Saz*, we met when we were three years old. Since then, we

never even fought and were always supportive of each other. And now, we are traveling together; I can't wait to see our journey in the future. Thank you very much, my sister, from another mother!

In addition to my Turkish gang, I am deeply grateful for my international friends since my master's studies, with whom we grew together, started, and finished our Ph.Ds. together. *Eleonora Borda*, *Claudia Bigoni*, *Aileen Naef*, *Clementine Aguet*, *Claire Lugrin, Maria Cervera de la Rosa*, *Guillaume Magnien*, *Nikolaus Huwiler*, *Isabel Arenas*, *Nicolas Fumeaux*, *Hugo Ribet*. I can't wait to see where the future will take us.

I also want to thank very warmly the people I met on the road *Roeltje Maas*, *Fabian Schilling*, *John Leblanc*, *Lucie Moinvaziri*, and *Joanna Kowal,* for the fun, skiing, camping, biking, hiking, game nights, and dinner event. *Joanna*, you are the best neighbor we could ever ask for.

I am deeply grateful to have my big family around. *Ayla Dehni*, *Nevin Ersak*, *Mine Unalan*, *Burc Unalan*, *Baris Dehni*, *Yagmur Unalan*, *Dilek Yildiz*, *Ozlem Goynu*, *Bilgen Anakok*, *Ismail Yildiz*, *Micheline St-Jacques*, *Oktay Yildiz*, *Meryem Yildiz*, and *Amelié Martel*: I feel your support and love at every step. *Hatice Yildiz*, *Huseyin Yildiz*, *Zeliha Ersak*, and *Necmettin Ersak*, you constantly inspired me throughout my childhood; I miss you tremendously. Last but not least, I profoundly thank my parents: *Aynur Yıldız* and *Mehmet Yıldız*, for their endless love, support, and encouragement in every step I take. When I am down, they get me back on my feet. Thanks to them, I can continue learning, changing, and fighting.

Finally, there is *Paul Letainturier*, my Ph.D. surprise, and long-term flatmate since the COVID started. He helped me throughout my Ph.D. life, encouraging me to surpass difficult times with your non-ending support and belief in me. He made my life more exciting, challenging, and authentic. Thank you very much for showing me whom I want to become and always broadening my perspectives. Let's continue traveling, playing, laughing, growing, and working hard together!

03.10.2022

Lausanne

"Success is not final; failure is not fatal: It is the courage to continue that counts."

Winston S. Churchill

Abstract

The liver is the largest solid organ and the only one capable of using regenerative mechanisms to recover its mass fully. Although liver regeneration from acute injuries has been effective and extensively studied, chronic liver damage has adverse effects on hepatic histology, such as fibrosis or cirrhosis, suggesting that regenerative mechanisms have been disrupted. The most common form of chronic liver disorder, non-alcoholic fatty liver disease (NAFLD), is a growing cause of end-stage liver disease worldwide and is estimated to increase 2-3-fold by 2030. Despite the enormous amount of ongoing research on this topic, no treatment is available, leaving liver transplantation as the only current option.

One approach to revert this situation focuses on facultative liver stem cells derived from the biliary epithelium. This recent alternative comes from the breakthrough that biliary epithelial cells (BEC) can be assembled into complex three-dimensional organoid structures *in vitro* from bile duct-derived stem cells. These BEC-organoids can be expanded as stem cells, with a similar phenotype to injury-induced BECs *in vivo*, and also can be differentiated into functional hepatocyte-like cells with engraftment ability upon transplantation. Considering the potential of BEC-organoids, I focused on dissecting the role and unveiling the potential of BECs in the context of NAFLD. BECs undergo rapid reprogramming and proliferation in chronic liver diseases, including the fibrotic stage of NAFLD, a process known as ductular reaction (DR). Thus, studying DR provides new insights into the BEC expansion mechanisms. For this purpose, I first investigated the effect of hepatic overload on BECs to study the initiation of DR during the early stages of NAFLD. I demonstrated that lipid overload induces the conversion of adult cholangiocytes into proliferating BECs and promotes their expansion via the activation of the E2F transcription factors, which drives cell cycle progression while promoting glycolytic metabolism. These observations, while correlative, reveal unexpected connections between lipid metabolism and stemness, and set the ground for future research in understanding the role and the therapeutic potential of lipid metabolism and E2Fs in controlling BEC activation.

On the other hand, DR correlates closely with the severity of fibrosis in NAFLD, even though the function is largely unknown. Thus, I studied the effect of the mechanical properties of the fibrotic environment in BEC-organoid cultures by using the synthetic matrix we developed together with colleagues. The investigation of BECs cultured in a defined mechanical environment mimicking fibrotic stiffness revealed decreased stem cell capacities and increased inflammation, hepatic injury, and matrix metalloproteases. Finally, by using recently published data comparing BEC-organoid cultures from healthy and NASH patients, I revealed that hydrogels with fibrotic stiffness mimic the phenotype of organoids derived from NASH patients. As a result, investigating aberrant stiffness will enable the development of powerful DR models and future therapeutics for

enhancing stem cell-mediated liver regeneration. Overall, the results from this thesis should spark future enthusiasm for the potential of BECs in studying DR regenerative mechanisms and developing therapies.

Keywords

BECs, liver stem cells, steatosis, E2F, glycolysis, ductular reaction, proliferation, hydrogel, stiffness, fibrosis

Résumé

Le foie est le plus grand organe solide et le seul capable d'utiliser des mécanismes de régénération pour de récupérer entièrement sa masse. Bien que la régénération du foie à la suite de lésions aiguës soit efficace et largement étudiée, les lésions hépatiques chroniques ont des effets néfastes sur l'histologie hépatique, tels que la fibrose ou la cirrhose, suggérant une perturbation de la régénération tissulaire. La forme la plus courante de trouble hépatique chronique, la stéatose hépatique non alcoolique (NAFLD), est une cause croissante de pathologie hépatique dans le monde et pourrait être multipliée par 2 voire 3 d'ici 2030. Malgré la mise en place de moyens de recherche conséquents attribués à cette pathologie, aucun traitement n'est actuellement disponible, laissant la transplantation hépatique comme seule option actuelle.

Une approche pour pallier cette situation se focalise sur les cellules souches hépatiques dérivées de l'épithélium biliaire. Cette alternative récente a pour origine la découverte que les cellules épithéliales biliaires (CEB) peuvent être assemblées en structures organoïdes tridimensionnelles complexes *in vitro* à partir de cellules souches dérivées du canal biliaire. Ces organoïdes de cellules épithéliales biliaires peuvent être développés en tant que cellules souches, arborant un phénotype similaire à celui des cellules épithéliales biliaires induites par des lésions *in vivo*, et peuvent également être différenciés en cellules fonctionnelles de type hépatocyte avec une capacité de greffe lors de la transplantation.

Compte tenu du potentiel des organoïdes CEB, je me suis attachée à caractériser le rôle des CEB et à dévoiler leur potentiel dans un contexte de NAFLD. Les CEB subissent une reprogrammation et une prolifération rapides dans les maladies hépatiques chroniques, y compris au stade de fibrose de la NAFLD, processus connu sous le nom de réaction ductulaire (RD). J'ai d'abord étudié l'effet de la surcharge hépatique sur les CEBs afin de caractériser l'initiation de la réaction ductulaire au cours des premiers stades de la NAFLD. J'ai montré que la surcharge lipidique induit la conversion des cholangiocytes adultes en CEB et favorise leur expansion via l'activation des facteurs de transcription E2F, entraînant à leur tour la progression du cycle cellulaire tout en favorisant le métabolisme glycolytique. Ces observations, bien que corrélatives, révèlent des connexions inattendues entre le métabolisme lipidique et la régénération tissulaire, ouvrant la voie à de futures recherches visant à comprendre le rôle et le potentiel thérapeutique du métabolisme lipidique et des E2F dans le contrôle de l'activation des CEB.

D'autre part, la RD est en étroite corrélation avec la sévérité de la fibrose dans la NAFLD, même si sa fonction est largement inconnue. J'ai étudié l'effet des propriétés mécaniques de l'environnement fibrotique sur les cultures de CEB-organoïdes en utilisant une matrice extracellulaire synthétique que nous avons développée. L'étude de CEB en culture dans un environnement mécanique déstructuré mimant la rigidité caractéristique de

la fibrose a révélé une altération des capacités des cellules souches, une augmentation de l'inflammation et des lésions hépatiques ainsi que des métalloprotéases matricielles. Enfin, en utilisant des données récemment publiées comparant des cultures de CEB-organoïdes provenant de patients sains et de patients atteints de NASH, j'ai pu révéler que les hydrogels à rigidité fibrotique miment le phénotype des organoïdes dérivés de patients atteints de NASH. L'étude de la rigidité permettra le développement de puissants modèles de RD et de futures thérapies pour améliorer la régénération hépatique médiée par les cellules souches. Dans l'ensemble, les résultats de cette thèse pourraient susciter un enthousiasme futur quant au potentiel des cellules souches biliaires et des cultures de CEB-organoïdes dans l'étude des mécanismes de régénération de la RD et le développement de nouvelles stratégies thérapeutiques.

Mots-clés

CEBs, cellules souches hépatiques, stéatose, E2F, glycolyse, réaction ductulaire, prolifération, hydrogel, rigidité, fibrose

Contents

List of Figures

List of Tables

List of Drugs and Compounds

Fluorodeoxyglucose	FdG
Pioglitazone	
Elafibranor	
Cenicriviroc	CVC
Simtuzumab	SIM
Obeticholic acid	OCA
Acetaminophen (paracetamol)	APAP
Carbon tetrachloride	CCl4
Thioacetamide	TAA
3.5-diethoxycarbonyl-1.4-dihydrocollidine	DDC
2-acetylaminofluorene	AAF
4,4'-Methylene dianiline	DAPM
Dipeptidyl peptidase-IV	DPPIV
Rho-associated protein kinase inhibitor	ROCKi
Glycogen synthase kinase 3 inhibitor	GSK3i
Transforming growth factor beta inhibitor	TGF-βi
5-Ethynyl-2′-deoxyuridine	EdU
3.3'-diaminobenzidine	DAB
4′,6-diamidino-2-phenylindole	DAPI
Vinyl sulfone functionalized 8-arm PEG	PEG-VS
PEG with minimal integrin recognition peptide RGDSPG	PEG-RGD
Transglutaminase factor XIII	FXIIIa

DiI-conjugated acetylated low-density lipoproteins	Dil-Ac-LDL
Fatty acid mix	FA mix
Dimethyl sulfoxide	DMSO
Bis-2-(5-phenylacetamido-1,3,4-thiadiazol-2-yl)ethyl sulfide	BPTES
2-Cyano-3-(1-phenyl-1H-indol-3-yl)-2-propenoic acid	UK5099
2[6(4-chlorophenoxy)hexyl]oxirane-2-carboxylate	Etomoxir
Carbonyl cyanide-p-trifluoromethoxyphenylhydrazone	FCCP
Rotenone/Antimycin A	ROT/AA
2-Deoxy-D-glucose	2-DG
HLM006474	
PF-573228	PF
Dasatinib	DAS
Blebbistatin	BLEB
Verteporfin	VP
Y-27632 dihydrochloride	Y-27632

"When it feels scary to jump, that is exactly when you jump, otherwise you end up staying in the same place your whole life, and that I can't do."

A Most Violent Year

Chapter 1 Introduction

1.1 The liver: physiology and cellular organization

1.1.1 Physiology of the liver

The liver is the largest multifunctional organ in the human body and plays a key role in the control of physiological functions, such as bile formation and secretion, xenobiotic detoxification, macronutrient metabolism, plasma protein synthesis, and immune system support[1]. Everything that is eaten or consumed, including food, alcohol, drugs, and toxins, is absorbed from the intestine and travels through the liver first, highlighting the importance of liver metabolic functions that become apparent in patients with liver diseases or failure.

In addition to toxic substances, the liver metabolizes macronutrients such as glucose, fatty acids (FA), and amino acids. Liver energy metabolism is highly plastic based on the current availability of energy sources and will be explained in the section below (Chapter 1.1.4). Briefly, in the postprandial state, following a meal, the liver prioritizes storage and stores glucose as glycogen and FAs as triacylglycerol (TAG) molecules in lipid droplets or secretes TAGs into the circulation as very low-density lipoprotein (VLDL) particles[2]. Likewise, amino acids are metabolized to provide energy and/or nitrogen sources, or used to synthesize proteins, glucose, and/or other bioactive molecules. On the other hand, in the fasted state, the main function of the liver is to maintain blood glucose levels and to support extrahepatic tissues with energy. As such, glucose generated *de novo* from lactate, glycerol, or pyruvate (gluconeogenesis) is released from the liver into the circulation and subsequently metabolized by muscle, adipose tissue, and other extrahepatic tissues[2]. The liver also oxidizes long-chain fatty acids (LCFA) derived from adipose lipolysis in hepatic mitochondria through FA β-oxidation, resulting in ketone bodies (ketogenesis), which provide essential metabolic fuels for extrahepatic tissues, including the brain, heart, and skeletal muscle during sustained fasting[2].

Bile is an alkaline electrolyte solution (mostly water) that contains bile salts and pigments. Bile salts are sodium and potassium salts of bile acids (cholic and chenodeoxycholic acid) conjugated to glycine and taurine that are crucial to the digestion and absorption of lipids[1]. Besides being fundamental for facilitating fat digestion and intestinal lipid absorption, bile acids are important signaling molecules regulating glucose, lipid, and energy homeostasis[3,4]. Moreover, bile also helps with excretion as the liver detoxification products can be removed from the liver through bile or urine[5].

Liver detoxification is the transformation of xenobiotics mainly by converting them from a lipophilic form to a hydrophilic one through 2 reactions: phase I and phase II. Phase I involves cytochrome p450 (CYP450)

enzymes, which neutralize the substances by converting them to less harmful versions through oxidation, reduction, and hydrolysis. In contrast, the second step solubilizes the by-products of the initial step and other remaining toxins in water through conjugation[6].

Considering the presence of possible endotoxins and bacteria in the blood carried from the gastrointestinal tract, the residual immune support of the liver plays an essential role in alerting an immune response[1,7]. In case of an inflammatory stimulus, the liver produces cytokines, tumor necrosis factor, interleukin-1, and interleukin-6. Interestingly, this response can also stimulate the acute phase response, a change in liver plasma protein synthesis and distribution between the intravascular and extravascular spaces, to aid host defense against pathological damage[1]. In homeostasis, plasma protein synthesis in the liver consists of the production of albumin, globulin, and fibrinogen, which are involved in maintaining fluid balance in peripheral tissues, binding several substances, and forming part of the lipoprotein complexes that transport lipid molecules and cholesterol between the liver and the tissues[1].

1.1.2 Liver epithelium and non-parenchymal cells

The liver is composed of parenchymal and non-parenchymal cells acting synergistically to sustain hepatic functions. Parenchymal liver cells comprise two endoderm-derived epithelial cell types: hepatocytes and biliary epithelial cells (BECs), also known as cholangiocytes. On the other hand, hepatic non-parenchymal cells of non-endodermal origin represent about 30 percent of the liver cells and are composed of liver sinusoidal endothelial cells (LSECs), stellate cells (HSCs), and Kupffer cells. In general, non-parenchymal cells contribute to the maintenance of liver architecture and physiology and regulate hepatocyte proliferation[8].

The majority of the liver physiological functions mentioned in the previous section (Chapter 1.1.1) are accomplished by hepatocytes, which are parenchymal cells that comprise around 65 percent of the liver cells. In more detail, hepatocytes are the cellular factories of the liver with a large number of mitochondria and endoplasmic reticulum to produce large amounts of bile, albumin, urea, glutamine, clotting factors, and other serum proteins[9]. In addition to these synthetic activities, hepatocytes play a major role in detoxification through the production of CYP450 enzymes that recognize and modify various chemicals, enabling their elimination in bile or urine[9]. Finally, hepatocytes are involved in the metabolic pathways of glycogen storage/degradation, gluconeogenesis/glycolysis, and lipid production/storage/secretion/degradation as part of their macronutrient metabolism to maintain glucose homeostasis and meet energy demands based on the nutritional status[10].

Even though less metabolically active than hepatocytes, BECs (3-5 percent of liver cells) are as critical for bile acid homeostasis as hepatocytes, mainly through structural support and regulation of the bile ionic composition. In particular, BECs form a biliary network in which bile is collected and transported from the hepatocytes to the gallbladder. Hepatocytes initiate bile formation by secreting primary bile, composed primarily of water, solutes, and ions, into canaliculi. As canalicular bile flows along the biliary tree, it is subjected to BEC secretory (secrete Cl^-, $HCO3^-$, and water) and absorptive (bile acids, glucose, amino acids, and water) processes,

thus resulting in modified ductal bile[11]. Hormones, peptides, nucleotides, neurotransmitters, and other molecules, including bile acids, modulate the transport through various intracellular signaling pathways and regulatory cascades[9].

LSECs are the unique endothelial cells in the liver and reside at the interface between blood cells on the one side and hepatocytes and HSCs on the other. In a normal liver, differentiated LSECs are gatekeepers of fibrogenesis by maintaining HSCs in their inactive state[12]. LSECs regulate sinusoidal blood flow through their action on HSCs and thus maintain a low portal pressure, and are responsible for the clearance of blood from toxins, regulate immune system responses[13], and induce angiogenesis for liver regeneration[14].

HSCs are located in the perisinusoidal space between LSECs and hepatic epithelial cells. In a healthy liver, HSCs are quiescent and store numerous vitamin A-containing lipid droplets, constituting the largest reservoir of vitamin A in the body[15]. When the liver is injured, HSCs receive signals secreted by damaged hepatocytes and immune cells, which cause them to transdifferentiate into activated myofibroblast-like cells and produce the protective extracellular matrix (ECM), collagen[15]. In addition, they secrete cytokines and growth factors that promote the regeneration of hepatic epithelial cells. However, they also promote liver fibrosis and cirrhosis following chronic injury[16].

Kupffer cells are liver-resident macrophages and are inherently involved in the regulation of liver homeostasis. They are particularly important for the acute and chronic toxicity response of hepatocytes[17]. Kupffer cells are the first line of defense against potentially harmful material originally found in the gut, such as gut bacteria, bacterial endotoxins, and microbial debris, which can reach the liver from the portal circulation. They are therefore an integral part of the innate immune system responses[18].

In addition to the traditional roles of hepatic cells described above, recent techniques and tools available for tissue analysis contributed significantly to decoding tissue heterogeneity. Recent single-cell RNA sequencing (scRNA-seq) approaches revealed previously unknown subtypes of LSECs, Kupffer cells, hepatocytes, BECs, and HSCs, suggesting an unanticipated complexity in healthy and diseased liver. The study of liver cells at high resolution will open avenues for a detailed examination of the interplay between parenchymal and non-parenchymal compartments and help to uncover unexpected and novel functions of these cell subtypes.

1.1.3 Liver architecture and zonation

The liver has complex vascular, biliary, and lymph networks supported by the special arrangements of liver cells. Structurally the liver can be divided into five compartments: (1) vascular system, (2) hepatocytes and hepatic lobule, (3) hepatic sinusoids, (4) biliary system, and (5) space of Disse[19–24]. Moreover, it has a unique vascular system with two blood supplies from the portal vein and the hepatic artery (Figure 1.1). Blood enters via the portal vein and the hepatic artery, flows through hepatic sinusoids, and finally exits the liver through the central vein. On the other hand, bile acids, synthesized in hepatocytes, are secreted into bile canaliculi and

transported via the biliary system to end up in the gallbladder, where bile is stored until food intake triggers its release into the small intestine. Later, bile acids are reabsorbed by the intestine and return to the liver by the portal vein as part of the enterohepatic recycling system[25].

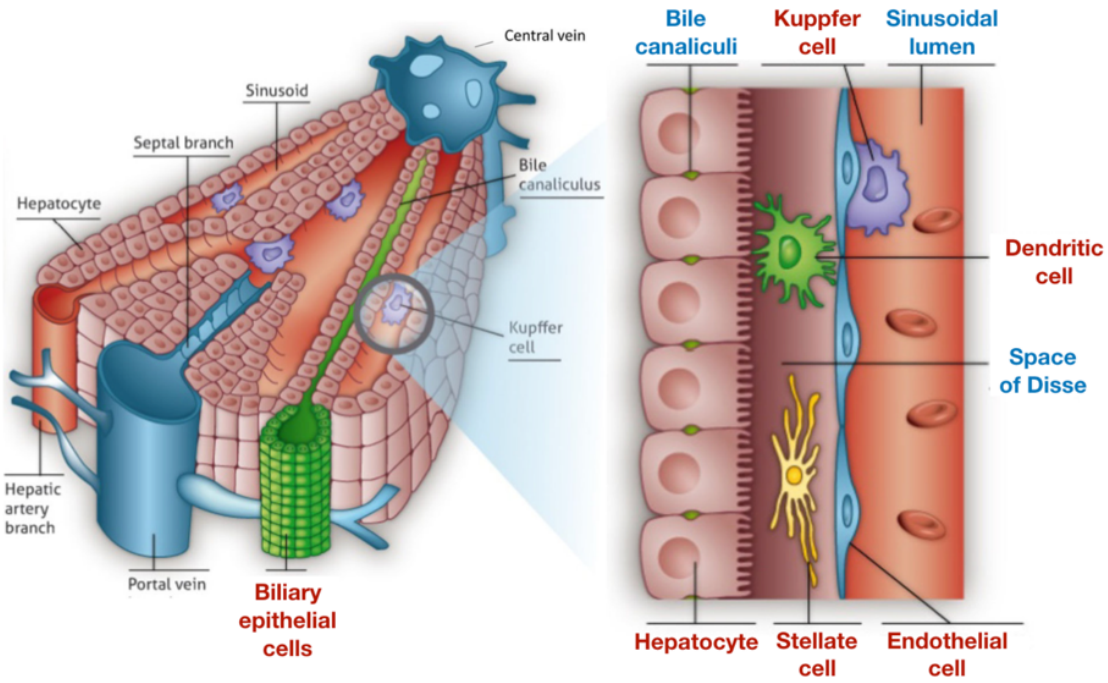

Figure 1.1 Cellular architecture of the liver.

Scheme depicting a liver lobule (smallest repeated functional tissue unit). Within a lobule, blood enters through the hepatic artery and portal vein and flows towards the central vein in sinusoidal vessels. On the other hand, bile flows in the opposite direction. In the sinusoidal vessels, hepatocytes interact closely with the non-parenchymal cells. Adapted from[26].

The complex structure of the liver is furthermore accentuated by distinct liver functions along the lobule radial axis, a phenomenon that has been termed "liver zonation"[27]. While blood flows from the portal vein to the central vein, hepatocytes take up and secrete nutrients and sense hormones. Together with local tissue morphogens, this phenomenon creates a graded microenvironment and results in liver zonation[27]. The existence of functional liver compartments helps hepatocytes to carry out their metabolic functions with maximum efficiency[28]. Each hepatic lobule is comprised of three different zones (Figure 1.2): hepatocytes close to the portal tract (zone 1), hepatocytes between the portal and the central vein (zone 2), and hepatocytes close to central veins (zone 3). Hepatocytes near the portal vein, also defined as periportal hepatocytes, are exposed to an oxygen-rich environment and perform more energetically demanding functions such as gluconeogenesis, urea production, and β-oxidation of FAs[27]. In contrast, pericentral hepatocytes are dedicated to glycolysis, xenobiotic metabolism, bile acid biosynthesis, and glutamine production, which are less energetically demanding processes[9]. In addition to these distinct functions, some tasks are oppositely zonated and maintain the balance throughout the lobule, such as periportal production and pericentral uptake of glucose, periportal synthesis of cholesterol and pericentral cholesterol consumption, and pericentral synthesis of bile acids and periportal

uptake of bile acids[27]. Thus, liver zonation is critical for energy homeostasis, the metabolism of nutrients and xenobiotics, and the production and recycling of various proteins[29].

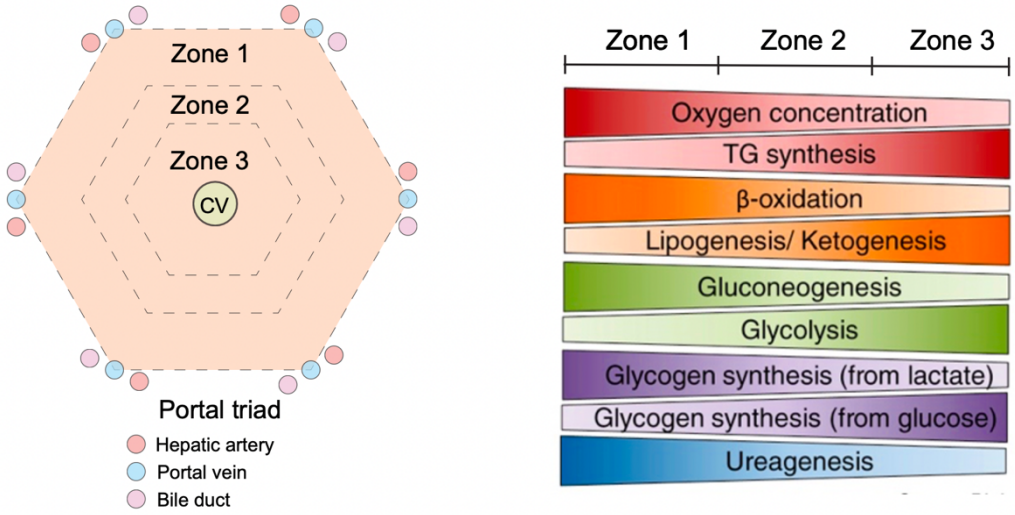

Figure 1.2 Liver zonation and functions.

CV, central vein, TG, triglyceride. Adapted from[10].

Interestingly, the distribution of biochemical functions within the liver also underlies the zonated damage in liver pathology. For example, in the case of overdoses of drugs such as acetaminophen, the zonated processes of xenobiotic metabolism lead to pericentral damage due to the accumulation of toxic intermediates exclusively in pericentral hepatocytes that have the detoxification machinery[30]. In addition, the higher lipogenic activity in pericentral hepatocytes most likely contributes to the development of non-alcoholic and alcohol-related liver diseases[31]. On the other hand, periportal damage is observed in autoimmune hepatitis, partly due to the zonated expression of antigens such as CD54 and CD58[30]. Finally, primary biliary cholangitis (PBC) and other biliary diseases occur in the periportal zone due to the damage to epithelial cells that form the periportal bile duct[31].

1.1.4 Energy metabolism in the liver

As mentioned in the previous section, hepatocytes are the main cell type of the liver that coordinate the key metabolic functions of the liver in energy homeostasis by regulating systemic glucose and lipid fluxes during feeding and fasting[32]. The metabolic switch between the fasted and fed states in the liver is tightly controlled by hormonal systems. Insulin suppresses glucose production and ketogenesis and stimulates glycolysis and lipogenesis, whereas glucagon counteracts insulin action. Within hepatocytes, mitochondria are important membrane-bound cell organelles that are the powerhouse of the cell and major actors in liver metabolism, involved in both hepatic anabolic pathways (*de novo* lipogenesis (DNL), gluconeogenesis) and catabolic pathways (tricarboxylic acid (TCA) cycle, β-oxidation, ketogenesis, and electron transport chain (ETC) linked to reactive oxygen species (ROS) production)[33].

In the liver, glucose metabolism (Figure 1.3) starts with its uptake in hepatocytes from the circulation via glucose transporter 2 (GLUT2), a plasma membrane glucose transporter. Intracellular glucose is then phosphorylated by glucokinase to generate glucose 6-phosphate (G6P), which can be metabolized via the pentose phosphate pathway to generate intermediates in nucleotide biosynthesis and NADPH that are required for scavenging ROS, lipogenesis, and biosynthesis of other bioactive molecules. Alternatively, G6P can act as a precursor for glycogen synthesis in the fed state, or it can be metabolized to generate pyruvate through glycolysis, controlled by hexokinase (HK), 6-phosphofructo-1 kinase (PFK), and liver pyruvate kinase (PKL). Later, pyruvate can be either channeled into the mitochondria and completely oxidized to generate ATP through the TCA cycle and oxidative phosphorylation or can be converted into lactate. The electron carriers produced in the TCA cycle (NADH and FADH2) donate electrons to the electron transport chain (ETC), and, through the reactions of the mitochondrial respiratory chain, ATP is generated. In more detail, the four protein complexes (complex I, II, III, IV) of ETC pump protons to the mitochondrial intermembrane space in sequential redox reactions. The proton gradient generated by complex I, III, and IV drives the rotation of a fifth complex (complex V), leading to phosphorylation of adenosine diphosphate (ADP), hence called ATP synthase[34]. In addition to ATP generation, citrate from the TCA cycle can be used to generate acetyl-CoA from which LCFAs are formed, elongated, and desaturated through enzymes like fatty acid synthase (FAS), acetyl-CoA carboxylase (ACC), acyl-CoA elongase (Elovl) and stearoyl-CoA desaturases (SCDs). Thus, the liver can make FAs from glucose through DNL.

On the other hand, in the short-term fasted state, glycogen is degraded into G6P molecules, which, upon dephosphorylation by glucose-6-phosphatase (G6Pase), is converted to glucose and released in circulation. During prolonged fasting, when glycogen is depleted, hepatocytes synthesize glucose through gluconeogenesis using lactate, pyruvate, glycerol, and amino acids, which are either generated in the liver or delivered to the liver through circulation from extrahepatic tissues.

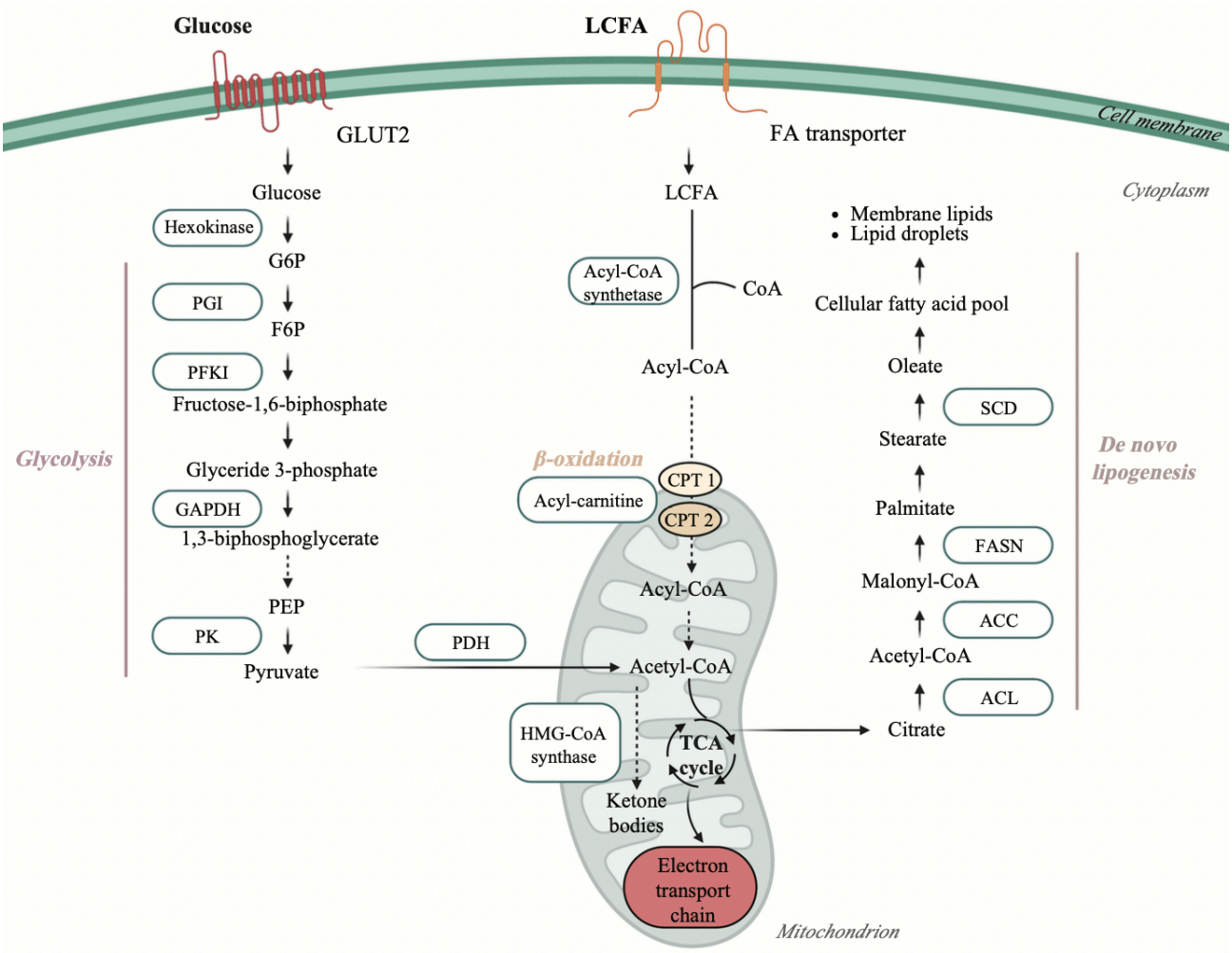

Figure 1.3 Overview of hepatic energy metabolism.

After entering the cell, glucose is phosphorylated to be used in glycolysis, and pyruvate generated by glycolysis is converted to acetyl-CoA, which enters the TCA cycle. Through acetyl-CoA, the cell can also synthesize and elongate fatty acids. PGI, phosphoglucose isomerase; PFK1, phosphofructokinase 1; PK, pyruvate kinase; GAPDH, glyceraldehyde-3-phosphate dehydrogenase; ACC, acetyl-CoA carboxylase; ACL, ATP citrate lyase; FASN, fatty acid synthase; PDH, pyruvate dehydrogenase; GLUT2, glucose transporter 2; G6P, glucose 6-phosphate; SCD, stearoyl-CoA desaturase; LCFA, long-chain fatty acid; FA, fatty acid; CPT, carnitine palmitoyltransferase. Adapted from[35] using BioRender.com.

Regarding lipid metabolism, chylomicrons (dietary fat processed by enterocytes) and LCFAs - the lipolysis products of adipose tissue, are the sources in the liver. LCFAs enter hepatocytes via transporters CD36 and fatty acid transport protein (FATP). Once inside, they are transported into peroxisomes by FATP2 and FATP4 for further conversion to long-chain-fatty-acid-coenzyme A (LCFA-CoA) by long-chain acyl-CoA synthetase (ACSL). They are then carried by fatty acid binding proteins (FABPs), which act as intracellular FA chaperones. LCFA-CoA translocation into mitochondria is mediated by carnitine palmitoyltransferase 1 (CPT1), a rate-limiting step for FA β-oxidation. β-oxidation mainly occurs in mitochondria but can also occur to a low extent in endoplasmic reticulum and peroxisomes. FA acid β-oxidation represents one of the main sources of FA disposal and energy production through the sequential breakdown of LCFA-CoA to acetyl-CoA. From acetyl-CoA, either ketone bodies are produced, or ATP is generated through the TCA cycle.

In summary, the liver is a metabolically highly plastic organ that adapts rapidly to the body's nutritional state by increasing DNL, and FA synthesis in the fed state, while upregulating β-oxidation, ketogenesis, and lipolysis during fasting.

1.2 Liver pathophysiology in non-alcoholic fatty liver disease (NAFLD)

1.2.1 Definition of NAFLD

NAFLD is defined as a spectrum of disorders caused by a build-up of fat in the liver of people who drink low or no alcohol. It is one of the most common liver disorders that initiates with fat accumulation, also referred to as steatosis, and can progress to steatohepatitis (NASH) with inflammation, cirrhosis with fibrosis, and hepatocellular carcinoma (HCC). The prevalence of NAFLD is almost one-third of the general population in Western nations and is linked to obesity, insulin resistance, metabolic syndrome, and type 2 diabetes mellitus (T2DM)[36,37]. With the decreased incidence of hepatitis and rising emergence of obesity[38,39], NAFLD is predicted to become the primary cause of end-stage liver disease in the next few decades[36,40,41], and is recognized as an etiology of HCC, even without underlying cirrhosis[42].

NAFLD usually initiates with steatosis, the appearance of intrahepatic fat droplets due to the storage of excess calories in hepatocytes as lipids, unlike a healthy person whose liver consists of less than 5% fat. Although this process is considered benign and does not damage the liver per se, it can progress to more severe conditions like NASH, fibrosis/cirrhosis, and HCC (Figure 1.4)[30]. Usually, steatosis is considered benign, and only 44% of patients with baseline NAFLD showed progression to NASH[31]. However, emerging data showed that patients with only steatosis developed fibrosis[31–33], suggesting that fat accumulation may not be entirely benign.

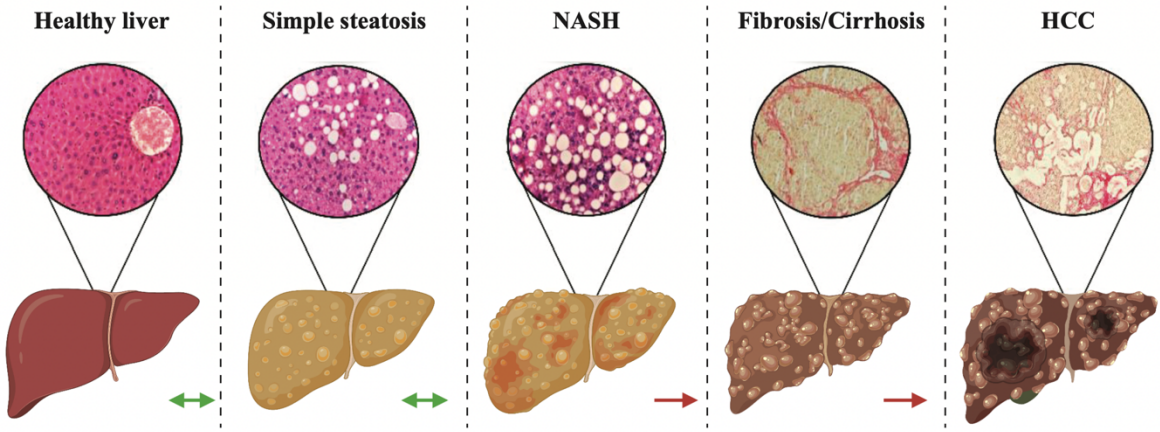

Figure 1.4 Scheme of NAFLD progression.

NAFLD initiates with steatosis, characterized by lipid accumulation, and can further progress into NASH, characterized by inflammation and liver injury. Even though these stages are considered reversible, further development of fibrosis/cirrhosis, characterized by excessive deposition of scar tissue, is not reversible, and patients with fibrosis/cirrhosis are at risk of HCC. Adapted from[43] using BioRender.com.

While the first manifestation of the disease is mainly represented by lipid accumulation, the next stages comprise a myriad of structural disruptions and compromised liver function. In case of the oxidative stress, proinflammatory cytokines, and mitochondrial dysfunction, the liver is susceptible to inflammation and hepatocyte ballooning, characterized by cell swelling and enlargement[44,45]. This stage, called NASH, leads to a considerable risk for fibrosis, characterized by the deposition of aberrant ECM caused by scar tissue, increased liver stiffness and a change in mechanical properties, and compromised liver functions. NASH, if combined with fibrosis, is an irreversible condition, and patients with fibrosis are at a higher risk of liver failure and developing cirrhosis. In cirrhosis, aberrant ECM and fibrous tissue distort the hepatic architecture and zonation and cause hepatic insufficiency and portal hypertension. Patients who progress to cirrhosis are at risk of liver-related complications such as portal hypertension, hepatic failure, and HCC[46–49], the end-stage of NAFLD is considered a life-threatening disorder.

1.2.2 Diagnosis of NAFLD

Although there have been developments in the diagnosis of NAFLD, currently, the gold-standard diagnostic approach is liver biopsy, which remains challenging due to its invasiveness and sampling variability[50]. To overcome these drawbacks, non-invasive methods have been developed and include magnetic resonance imaging (MRI) and transient elastography, which estimate the liver composition in terms of fat and fibrosis. However, these approaches must be interpreted together with the clinical data and biological and morphological information obtained through liver biopsy. Considering that there is a growing demand not only to detect NAFLD precisely but also to better identify and follow up the individuals with a high risk of developing NASH and liver-related clinical outcomes, further development of cheaper and more effective non-invasive approaches to be used as follow-up tools is highly relevant[51].

The non-invasive methods mentioned above are very useful for diagnosing steatosis[52,53]. To diagnose NASH, some clinical markers are used to detect the well-known risk factors associated with NASH, including T2DM, elevated aspartate aminotransferase (AST), and alanine aminotransferase (ALT) levels, increasing age, and body mass index (BMI)[54]. However, to detect the NASH stage precisely, liver fibrosis needs to be quantified. For this purpose, there are some scoring metrics for noninvasive fibrosis estimation, including fibrosis-4 index (FIB4) and the NAFLD fibrosis score (NFS), calculated by considering age, the AST:platelet ratio index (APRI), ALT for FIB4, and age, BMI, IGF/diabetes, ALT/AST ratio, platelet count and albumin for NFS[55,56]. These clinical features, together with the stiffness quantification with Fibroscan[55,56], serve as tools to determine which individuals should be referred for a liver biopsy to confirm the presence of NASH, which remains the reference standard. In the case of high fibrosis score along with the diagnosis of advanced fibrosis (liver stiffness >11-12 kPa with vibration-controlled transient elastography (VCTE) such as Fibroscan), cirrhosis is often diagnosed, triggering the follow-up and management decisions[50,55]. The classification of NAFLD diagnosis is presented in Figure 1.5.

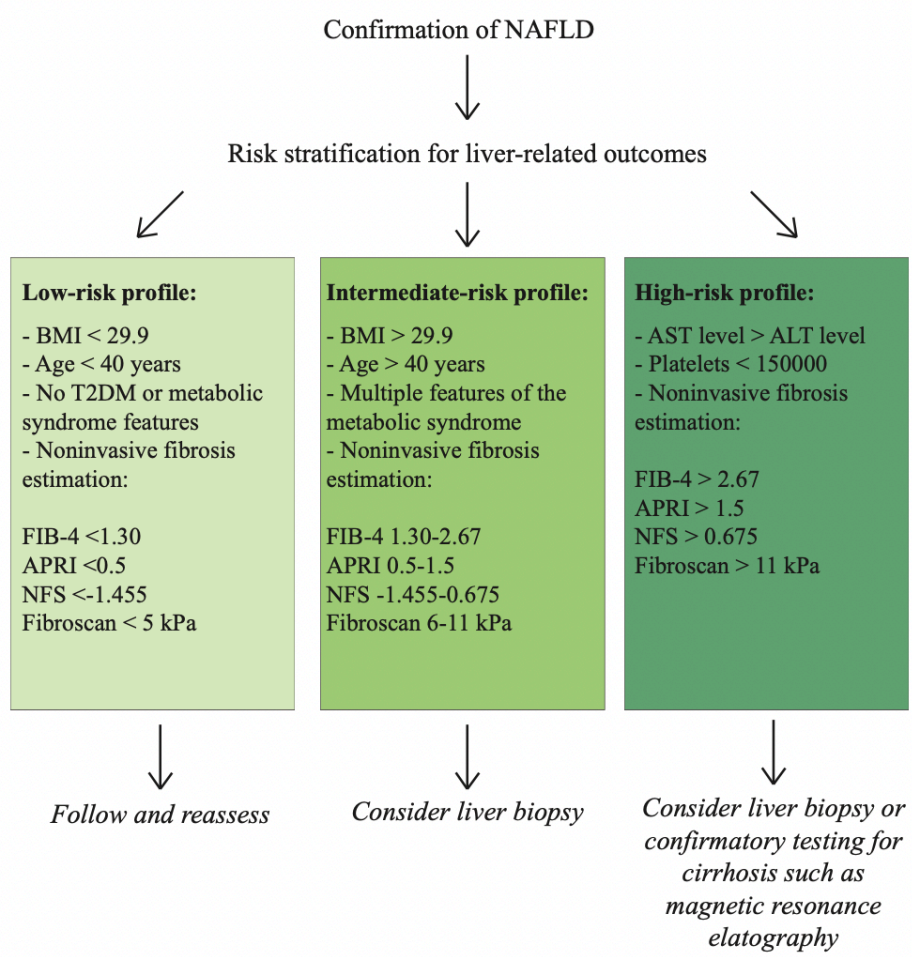

Figure 1.5 NAFLD risk stratification.

In the case of confirmed NAFLD, there are several risk stratifications based on the patient profile, which are decided upon clinical data and fibrosis estimation. After the profile classification, the appropriate strategy is undertaken. Adapted from[55].

1.2.3 Energy metabolism alterations in NAFLD

NAFLD is often accompanied by systemic metabolic disorders such as hyperglycemia, insulin resistance, and obesity, collectively called metabolic syndrome. Since the liver is the hub of the glucose and lipid metabolism and plays a major role in orchestrating metabolic homeostasis, targeting certain metabolic pathways in the liver can be a potential therapeutic for NAFLD.

One major hallmark of NAFLD is the accumulation of TG as lipid droplets in hepatocytes, suggesting alterations in lipid metabolism. The excessive accumulation of TG in the liver with NAFLD results from an imbalance between the uptake and disposal of FAs. Increased adipose tissue or diet-derived FA uptake and DNL are the main initiation phenotypes in steatosis[57–59]. A study using multiple stable isotopes followed by liver biopsies demonstrated that a higher percentage of dietary TG is taken up by the liver in the fed state in NAFLD compared to healthy patients[60]. Likewise, people with NAFLD have higher hepatic CD36 levels[61], indicating increased FA uptake from plasma[62]. Moreover, DNL is 5-fold greater in NAFLD than in normal livers, and the expression of lipogenic genes, including sterol regulatory element-binding protein-1C (SREBP1c), fatty

acid synthase (FAS), the liver x receptor (LXR), carbohydrate-responsive element binding protein (ChREBP) and acetyl-CoA carboxylase 1 (ACC1) increases in NAFLD[63–65].

On the other hand, the disposal of FAs from the liver through VLDL secretion and FA oxidation can be compromised in NAFLD, especially during NASH. Even though simple steatosis can be tolerated by a compensatory effort to dispose of excess acyl-CoA[66–68], the chronic exposure, in turn, leads to a failure in these mechanisms with a concomitant decrease in mitochondrial function and energetics[66]. Thus, as a result, dysfunctional VLDL synthesis and release[69], together with a decreased ability of FA oxidation and mitochondrial function, are observed in NASH mouse model[70] and patients[71]. In patients with obesity or fatty liver, hepatic mitochondrial respiration is increased compared to healthy subjects, whereas 31–40% of patients with NASH display lower levels of hepatic mitochondrial respiration than obese people[72,73]. As attenuated mitochondrial respiration is inadequate to the increased TCA cycle[74], the excess electrons cannot be captured by oxygen appropriately, and acyl-carnitines, ceramides, and diacylglycerols accumulate, which increased ROS production and DNA damage[72], and can trigger the inflammatory response, the key feature of NASH[70]. Moreover, in the case of FA overload, LCFAs are oxidized in the endoplasmic reticulum; however, this also forces ROS production and lipid peroxidation[75], thus facilitating the progression from liver steatosis to steatohepatitis[176]. Interestingly, ketogenesis, which is regulated by β-oxidation and TCA cycle flux, is also impaired in NASH, as shown by reduced serum b-hydroxybutyric acid concentrations, the major ketone body type[77]. While mitochondrial function, ATP synthesis, and ketogenesis are impaired, the TCA cycle is even upregulated as a futile attempt to sustain the high energy demand in NASH[70], probably supporting this toxic environment in a vicious cycle.

In addition to FA metabolism, glucose metabolism, including glycolysis, lactate production, and gluconeogenesis, is markedly affected in NAFLD, most likely because of its association with insulin. For example, in HFD diet-induced NAFLD hepatocytes, the mRNA levels of several key glycolysis-related enzymes, such as HK2, PFKM, and PKM, are increased compared to chow-diet controls[78]. Likewise, Seahorse analysis shows an increased extracellular acidification rate in HFD-fed mice, indicating enhanced glycolysis[78]. Moreover, the isotopically labeled glucose derivative tracer fluorodeoxyglucose (FdG) in positron emission tomography-computer tomography (PET-CT) imaging shows higher FdG phosphorylation in the livers of patients with steatohepatitis, indicative of an increase in the glycolytic rate[79]. As a result, both outcomes of glycolysis, TCA cycle, and lactate production are increased in NAFLD compared to normal livers[78,80].

1.2.4 Treatment of NAFLD

Even though there are no current therapies to treat NAFLD, several approaches can be useful in managing the disease by choosing an approach based on its stage. In general, for any stage of NAFLD except cirrhosis and HCC, strict lifestyle intervention with diet and exercise should be pursued and can show significant improvements in some patients.

In the case of early NAFLD, pharmacological interventions are not suggested considering the low risk of progression. Instead, weight loss with diet and exercise is suggested unless there is underlying obesity, for which bariatric surgery can be envisioned. In NASH, in the intermediate stage, in addition to the suggestion of bariatric surgery, pharmacological intervention starts. For example, Vitamin E and peroxisome proliferator-activated receptor γ (PPARγ) activator pioglitazone show improvement in hepatic steatosis and ballooning during NAFLD progression[50,81]. More recently, Farnesoid X receptor (FXR) agonist obeticholic acid (OCA)[82,83], and a PPARα and PPARδ dual-agonist, elafibranor[84], were also shown to be beneficial in reversing fibrosis and increasing lipid oxidation, and reducing inflammation, respectively[50]. In addition to metabolic approaches, specific anti-inflammatory and anti-fibrotic drugs have also been utilized for the intermediary stage. For example, the CC-chemokine receptor 2 (CCR2) - CCR5 antagonist, Cenicriviroc (CVC), reduced fibrosis without changing steatosis or ballooning injury[85]. On the other hand, using a monoclonal antibody directed against Lysyl oxidase-like 2 (LOXL2), Simtuzumab (SIM), did not inhibit fibrosis, suggesting that either more potent anti-fibrotic therapies are needed or that anti-fibrotic strategies should be combined with metabolically targeted therapeutics[50,86]. In the case of late-stage NAFLD with cirrhosis, there are no more pharmacological interventions, and patients started to be screened for HCC, highlighting the importance of early diagnosis and follow-up.

1.3 Cell renewal capacity of the liver in the healthy and diseased state

The liver is well-known for its capacity to regenerate following injuries such as partial hepatectomy and drug-induced injury[9]. For example, in rodent models, after removing two-thirds of the liver, the remaining liver tissue expands and fully recovers in a week[87]. During this acute damage process, the regeneration of hepatocytes and other cell types is orchestrated by the transient activation of complex signaling cascades of growth factors and cytokines[88]. As a result, the liver successfully restores its size to its pre-injury state. Thus, a better understanding of the mechanisms underlying the positive and negative consequences of the regenerative process, both in healthy and diseased states, could create therapeutic opportunities.

1.3.1 Turnover of hepatic epithelium in healthy liver

Under normal physiological conditions, maintenance of normal liver size and the required number of hepatocytes is controlled by a homeostatic process. In an adult healthy liver, hepatocytes hold a low turnover rate, with less than 0.2% of hepatocytes undergoing DNA synthesis at any given moment[87,89]. Early research on normal liver homeostasis suggested that periportal hepatocytes hold a high replicative capacity and stream along the portal-to-central path to renew the population, referred to as the “streaming liver hypothesis”[90]. Even though this model was later corroborated by lineage-tracing[91], it has also been challenged by other studies, in which no evidence for hepatocyte movement could be found[92,93]. Instead, replication of pre-existing hepatocytes was identified as the mechanism occurring under physiological conditions as supported by lineage-tracing of novel hepatocytes[94,95]. While some studies identified a subset of periportal hepatocytes as the source of

these replicative hepatocytes[96], others proposed pericentral hepatocytes expressing axis inhibition protein 2 (AXIN2$^+$)[97], or hepatocytes in all zones[92]. However, recently, two new studies demonstrated that hepatocytes in the midlobular zone seem to proliferate at higher rates than those in pericentral and periportal zones and that, during aging, the midlobular zone expands, whereas pericentral and periportal zones decrease in size[98,99]. These results open new insights into liver regeneration and raise questions about the mechanisms behind homeostatic liver regeneration.

1.3.2 Regeneration of hepatic epithelium in acute injury

Regenerative activities in acute liver injury are characterized by phenotypic fidelity: hepatic epithelial cells (hepatocytes and BECs) proliferate to make more of the same (Figure 1.6). The liver has adopted multiple regenerative strategies to enable recovery from injury, and the signaling mechanisms of this type of repair are reasonably well understood[88]. Partial hepatectomy is one of the textbook examples of liver regeneration triggered by a two-third surgical removal of the liver. In this process, in which all cell types recreate themselves, most of the liver mass is re-established within 7–8 days, with complete restoration achieved within 3 weeks in rodents[88].

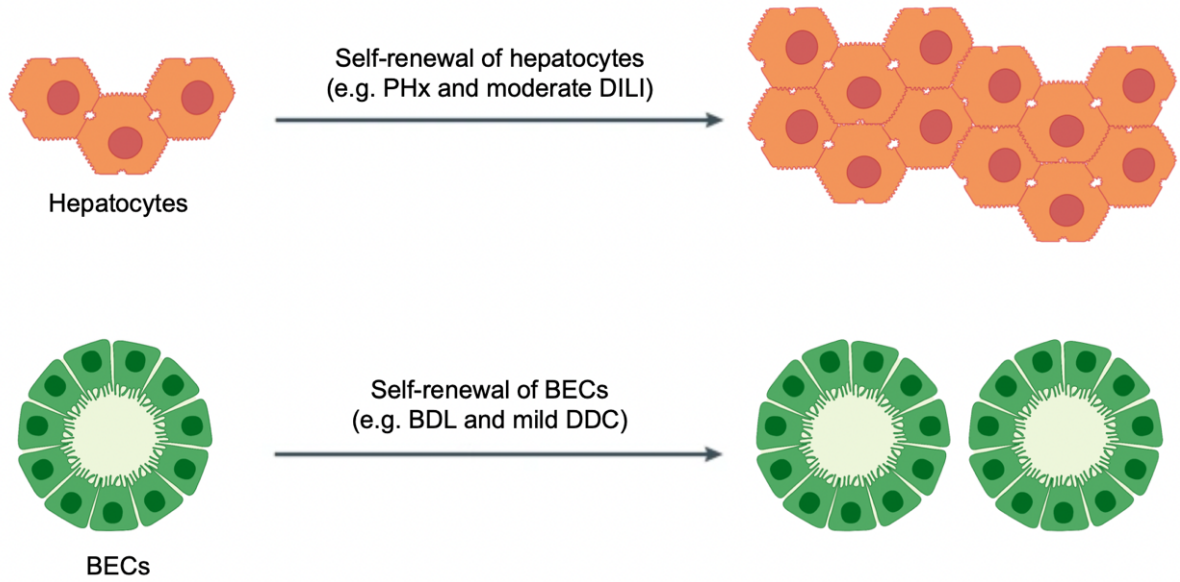

Figure 1.6 Scheme of regenerative activities in acute liver injury.

In the regeneration ongoing behind the acute liver injury, there is phenotypic fidelity, meaning that new hepatocytes and BECs derive from homotypic precursors. PHx, partial hepatectomy, DILI, drug-induced liver injury, BDL, bile duct ligation, DDC, 3.5-diethoxycarbonyl-1.4-dihydrocollidine. Adapted from[88] using BioRender.com.

Drug-induced liver injury (DILI) also induces liver regeneration and is critical for the recovery of patients with DILI. Acetaminophen (paracetamol) overdose is a major cause of acute liver failure in the Western world[100]. In mouse models, carbon tetrachloride (CCl_4) and thioacetamide (TAA) are widely studied hepatotoxins. At low doses, these hepatotoxins cause centrilobular liver necrosis and inflammation upon metabolization, followed by hepatocyte proliferation to replace the dead cells and regenerate the liver[100]. In this process,

macrophages are specifically involved in cleaning the cell debris and secreting proliferative signals. In terms of regenerative hepatocyte activities, epidermal growth factor receptor (EGFR) and MET receptor tyrosine kinase (MET) activation[101,102] and hepatocyte growth factor (HGF)[103], vascular endothelial growth factor (VEGF)[104], fibroblast growth factor 15 (FGF15)[105] and WNT/β-catenin[106] pathways were also shown to be activated after acetaminophen administration. Moreover, the impairment of these pathways blocks regeneration. As a result, hepatocytes are at the center of the coordinated histogenesis by restoring the histologically complete hepatic tissue.

However, in the case of a drug overdose, liver regeneration is significantly impaired, even in the presence of a critical liver mass (>50% viable hepatocytes)[100,102]. Even though EGFR, MET, and extracellular signal-regulated kinase (ERK) signaling remain highly activated after a severe acetaminophen overdose, they fail to initiate a regenerative response due to cell cycle arrest pathways, including p21 and p53[102,107,108]. Drug overdose also induces double-strand DNA breaks and failure of DNA repair mechanisms, possibly contributing to the observed cell cycle arrest. For example, transforming growth factor beta-1 (TGFβ1) was shown to promote cell cycle arrest through p21 and p53 and impair regeneration[108]. Thus, to advance regenerative therapeutics, understanding the mechanisms that impair or activate liver regeneration is primordial.

In addition to the hepatocyte-mediated regeneration described above, BECs also regenerate in acute liver injury, especially by forming larger bile ductules[87–89,109]. Bile duct obstruction, when the bile ducts become blocked, is a textbook example of BEC regeneration, performed by bile duct ligation (BDL) and 3.5-diethoxycarbonyl-1.4-dihydrocollidine (DDC) diet. During this process, massive BEC proliferation and the formation of multiple portal ductules occur. Even though the signals controlling this process are not fully understood, the peak of BEC proliferation occurs only a few hours after that of hepatocytes[110]. Like hepatocytes, BECs express MET and EGFR, whereas HGF and interleukin-6 (IL-6) are cholangiocyte mitogens *in vitro*[111]. In contrast to hepatocyte regenerative signals, cholangiocytes express high levels of YAP[112–114], and there is evidence showing that the interplay between YAP and bile acids also has a role in cholangiocyte proliferation. Single-cell RNA sequencing studies have shown that there is a 'fluctuating' activation of YAP-dependent gene expression in cholangiocytes, and this phenomenon is regulated by bile acids[112,114].

1.3.3 Epithelial plasticity in chronic injury and a brief history of liver stem cells

Even though the regenerative activities in the liver follow phenotypic fidelity, in chronic injuries where one of the two epithelial compartments fails to regenerate, alternative regenerative schemes through 'facultative liver stem cells' are activated[115]. Thus, discovering the source of regeneration remains a challenging yet important task.

In the 1950s, the emergence of small oval-shaped cells, which have a high nuclear/cytoplasmic ratio and display a hepatoblast phenotype between hepatocytes and BECs, was identified after hepatotoxic and carcinogenic treatments in rats. Moreover, oval cells were found to expand from the portal triads and gradually

transform into small and mature hepatocytes in hepatectomized livers exposed to 2-acetylaminofluorene (AAF), a chemical carcinogen that forms DNA adducts[109,116–121]. Considering their bipotential phenotype and similarity with bile ducts, these cells were proposed to have BEC origins and to arise from the canal of Hering, a strategic point lined by hepatocytes on one site and BECs on the other[122,123]. This phenomenon was defined as a "ductular reaction" (DR), and the regenerative capacity of the liver upon injury led to the hypothesis that adult liver facultative stem cells may exist, whose activity is conditioned by injury-driven signals[124]. Thus, in this situation, oval cells can function as "facultative stem cells" to replace liver epithelium.

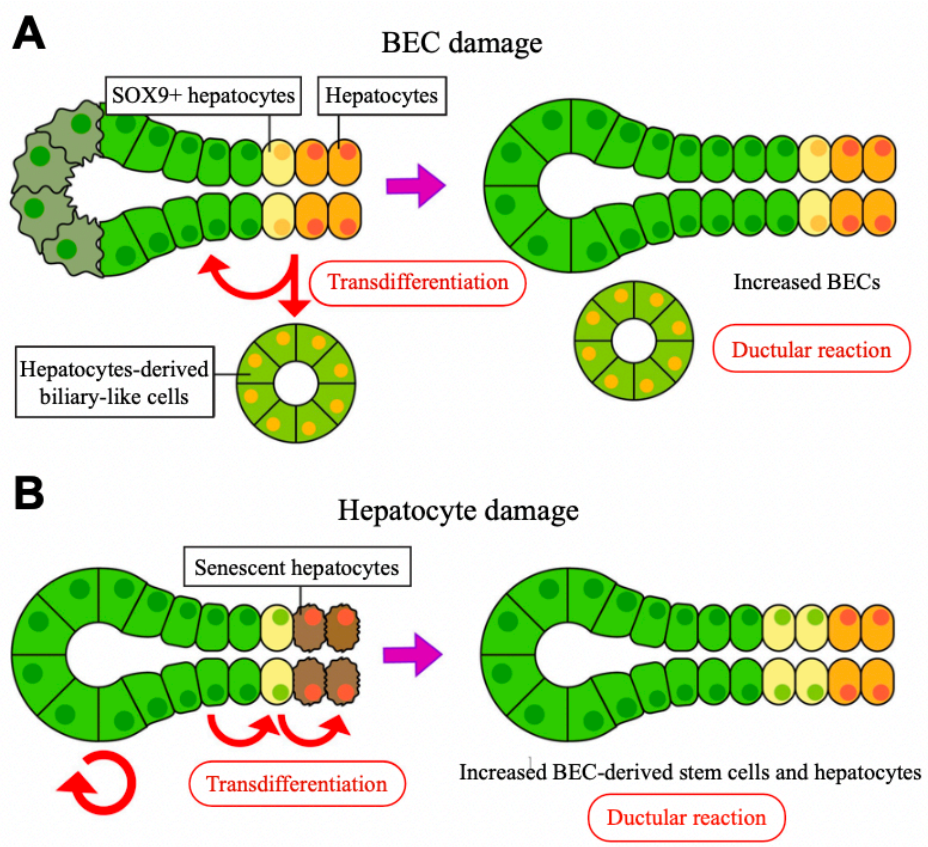

Figure 1.7 Scheme of ductular reaction in chronic injuries.

Alternative regenerative schemes in (A) BEC and (B) hepatocyte chronic injuries through ductular reaction. Adapted from[125] using BioRender.com.

Experiments such as clonogenic growth, cellular transplantation, and lineage tracing have been conducted to characterize the source and identity of the oval cells[9]. However, findings are contradictory and much depend on the model used to induce liver injury. Several reports support the notion that stem cells originate from hepatocytes, renew themselves and differentiate into hepatocytes and cholangiocytes in case of injury[95,96,126]. In this case, fully differentiated BECs do not seem to have a major role in generating new hepatocytes[95]. Other studies, on the other hand, demonstrate that stem cells originate from biliary cells after liver injury. In a mouse model of long-term chronic hepatic injury (i.e. MDM2$^{hep-/-}$ mice), biliary cells gave rise to new hepatocytes upon hepatocyte death, but not in the mouse model of liver injury induced by choline-deficient, methionine-

supplemented (CDE) diet[127]. Similar findings were also obtained in mice by BEC lineage tracing in a DR triggered by knockdown of β1-integrin[128] or β-catenin[129] in hepatocytes. Likewise, both short-term and long-term liver injury induced by DDC and TAA caused impairment in hepatocyte proliferation, and BECs were identified as the source of new hepatocytes[130]. Additional studies demonstrated that BECs could have subpopulations with an enhanced capacity to function as bipotential stem cells[131,132]. More recently, scRNA-seq analysis of hepatic cells in healthy liver revealed a new marker, Trophoblast Cell Surface Antigen 2 (TROP2), for bipotential stem cells[20]. Altogether, the current view is that when hepatocytes are damaged and no longer proliferate, facultative liver stem cells originate from BECs and have the potential to differentiate into hepatocyte- and cholangiocyte-like cells *in vitro* and *in vivo,* as depicted in Figure 1.7.

Comparable but reverse mechanisms arise when BECs fail to regenerate in the case of PBC[133], severe bile duct obstruction[134], and BDL[135], which are associated with acute inflammation and proliferation of portal bile ductules. In a study using dipeptidyl peptidase-IV (DPPIV)-negative rats and injection of DPPIV-positive hepatocytes upon partial hepatectomy, 1.4% of BECs were positive for the hepatocyte marker DPPIV following BDL[135]. Moreover, when these rats were exposed to the biliary-necrotizing toxin 4,4'-Methylene dianiline (DAPM) and then subjected to BDL, 53% of BECs in the newly formed ductules expressed the hepatocyte marker DPPIV[135].

To sum up, the transdifferentiation between hepatocytes and BECs is a highly plastic regenerative approach in chronic injuries to rescue one of the two compartments in the event of selective failure. Importantly, the suppression of hepatocyte proliferation and triggering of the expansion of biliary stem cells through DR (Figure 1.7A) is seen in many chronic liver diseases[125], including Hepatitis C virus (HCV) infection[136,137], alcoholic hepatitis[138], and NASH[139,140]. Thus, a better understanding of the regenerative mechanisms underlying stem cell activation derived from BECs can help to discover new therapeutics.

1.3.4 Established DR mechanisms in BECs

Apart from regeneration, the DR process is a pathological histological observation, reflecting bile duct proliferation and/or hyperplasia. It is commonly identified in biliary disorders such as PBC, primary sclerosing cholangitis (PSC), and biliary atresia (BA), as well as in chronic liver injuries such as alcoholic and non-alcoholic fatty liver disease[125,139,141].

Several previously identified liver stem cell signature proteins are increased in the DR process, and used as molecular markers to track and characterize the DR. These include Epithelial Cell Adhesion Molecule (EPCAM), Sex-Determining Region Y-Box 9 (SOX9), Cytokeratin-7 (KRT7), Cytokeratin-19 (KRT19), forkhead box L1 (FOXL1)[142], TROP2[20] and leucine-rich repeat-containing G-protein coupled receptor 5 (LGR5)[143]. Using these markers, several studies have shown that BECs —through DR— can contribute to hepatocyte regeneration in case of chronic hepatocyte injury. Despite the importance of the DR to promote liver regeneration in response to injury, the mechanisms regulating BEC activation and expansion to drive this process are

incompletely understood. Several reports have focused on the mechanisms underlying DDC-induced injury, a well-established *in vivo* DR model for biliary damage and portal fibrosis[112–114]. From these studies, multiple signaling pathways such as NOTCH[144], YAP[113,140,145], Wnt/β-catenin[146], tumor necrosis factor-like weak inducer of apoptosis (TWEAK)/FN14[127], mTORC1[113], neural cell adhesion molecule 1 (NCAM1)[147], and Tet Methylcytosine Dioxygenase 1 (TET1)-mediated hydroxymethylation[148] have been reported to be critical for initiating and sustaining the DR process.

Besides its need for activated BECs, the DR is also associated with inflammatory cells infiltrated in the portal zone[139], HSCs, and portal fibroblasts contributing to liver fibrogenesis[149]. Moreover, several studies have suggested that proliferating cholangiocytes have a role in the induction of fibrosis, either directly via epithelial-mesenchymal transition (EMT) or indirectly via activation of other liver cell types[150,151]. Supporting this claim, the inhibition of BEC proliferation has been shown to attenuate liver fibrosis via decreased TGF-β1 signaling[152]. Moreover, scRNA-seq analysis of $EPCAM^+$ BECs from DDC-injured livers revealed hepatocyte-like and inflammatory subsets of BECs[112], suggesting that BECs can exacerbate the inflammatory environment and thus support fibrogenesis during DR. These demonstrations reveal the close relationship between DR and HSC fibrogenesis and implicate the importance of DR and its grade as a sign of liver conditions, fibrosis and regeneration during liver injury. Considering that DR is associated with inflammation and fibrosis, but is also an important factor for hepatocyte regeneration[153–160], the study of DR mechanisms not only in the context of late NAFLD progression but also in the initial stages, could unveil new pathways that can be targeted in the future as therapies to increase hepatic regeneration in NAFLD.

1.4 *Ex vivo* cultures as a model for liver regenerative medicine

1.4.1 Two-dimensional (2D) liver cultures

As mentioned in the previous section (Chapter 1.3), even though the mammalian liver has a remarkable capacity for regeneration[9,87], its regenerative capacity is impaired in late-stage NAFLD due to chronic inflammation and scarring, which leaves liver transplantation as the only treatment[161,162]. Unfortunately, liver transplantation is limited by organ shortages, emphasizing the need for alternative technologies and cell-based therapies[163]. Primary hepatocytes hold a great synthetic and metabolic capacity; therefore, they could be used for therapeutical approaches such as drug screening or transplantation[164]. However, culturing primary hepatocytes as *ex vivo* monolayers has been challenging as they do not expand and rapidly dedifferentiate[164]. Therefore, alternative ways to culture expandable human hepatocytes have been developed, such as inducing hepatocyte-like cells from human induced pluripotent stem cells (iPSCs) by *in vitro* differentiation or from human somatic cells like fibroblasts by direct transdifferentiation[165]. However, transdifferentiated human hepatocytes showed limited engraftment capability[165].

Immortalized hepatocytes with human telomerase reverse transcriptase (hTERT) and viral genes such as *SV40, E6, and E7* have also been studied[166]. However, overexpression of hTERT and viral oncogenes holds a

potential risk of tumorigenesis, discarding their clinical potential. More recently, a chemical cocktail consisting of rho-associated protein kinase (ROCK), TGF-β, and glycogen synthase kinase 3 (GSK3) inhibitors was identified[167]. This cocktail converts rodent hepatocytes into proliferative bipotent liver cells as 2D *in vitro* cultures, which could then be differentiated into cholangiocytes and hepatocytes and were able to repopulate chronically injured liver tissue[167]. However, the researchers mentioned that they observed chromosomal abnormalities; therefore, possible risks regarding oncogenic transformation should be carefully investigated[167].

On the other hand, investigating stem cell markers that appear upon injury, as mentioned in the previous section (Chapter 1.3.4), led to the discovery of 2D stem cell cultures using collagen I coated plates. One of them, FOXL1, is strongly induced in the periportal region upon DDC treatment, and $FOXL1^+$ cells can be cultured *in vitro* and potentially differentiate into cholangiocyte and hepatocyte-like cells[168]. Similar clonogenic and differentiation properties have also been observed for $EPCAM^+$ cells[169] that can grow and survive for more than 6 months while maintaining a homogenous morphology[127,169]. By default, these cultures have a high proliferative capacity and a phenotype similar to cholangiocytes, but they can also differentiate into hepatocyte- and cholangiocyte-like lineages[127,169], thus opening new perspectives in hepatic cultures.

1.4.2 Three-dimensional (3D) liver organoid cultures

Organoids are 3D tissue-like structures, which can be derived from adult stem cells, embryonic stem cells, or iPSCs. Through their dynamic interactions with the ECM microenvironment, stem cells can form organoids with self-renewal and self-organization abilities. Moreover, organoids can recapitulate distinct physiological aspects of their tissue-of-origin[170]. In addition to basic biological applications, their derivation from healthy and diseased individuals provides advances in precision medicine and disease modeling, considering approaches including cell therapy, drug development, genetic engineering, metabolomic analyses, and screening for disease-related genetic variants (Figure 1.8)[171]. Thus, a breakthrough in hepatic cultures came with the identification that liver organoids can be derived *in vitro* as 3D cultures from mouse and human bile duct-derived stem cells[143,172], iPSCs[173–175] as well as primary hepatocytes[176,177].

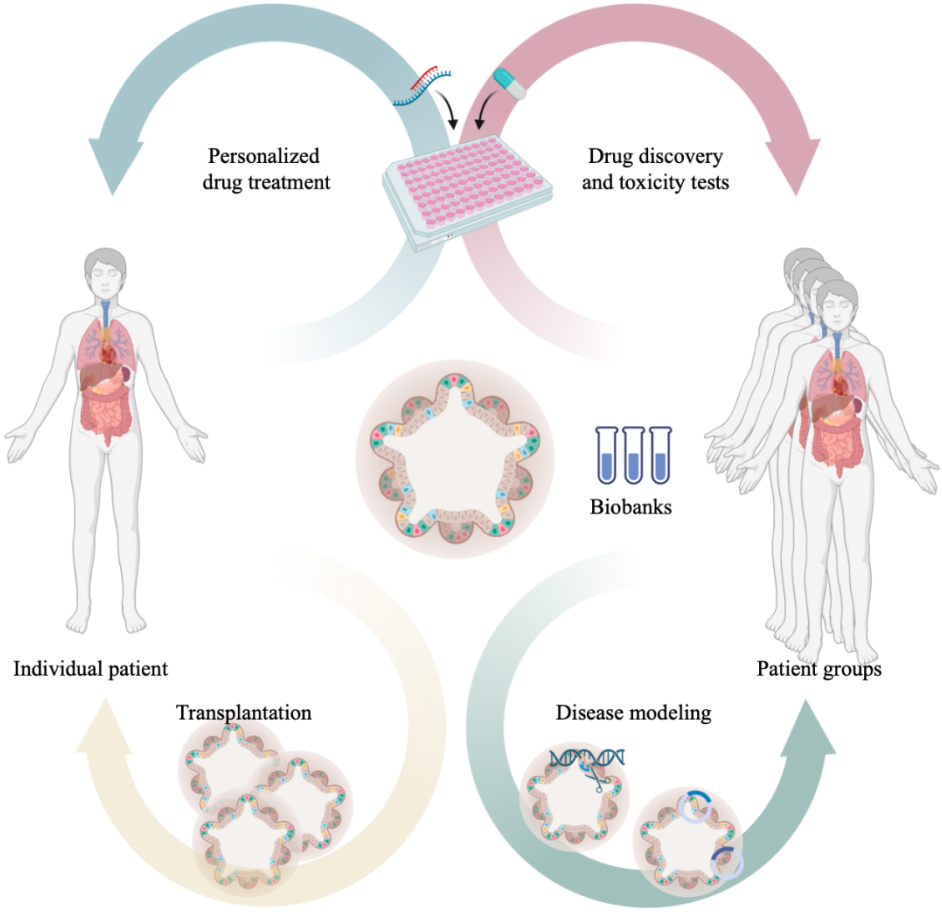

Figure 1.8 The advantages of organoid cultures.

Organoid technology offers various benefits for individual patients, such as personalized drug treatment, and in the future, it may serve as autologous transplantation. In addition, organoids grown from patient groups can be used for disease modeling and identifying genetic mutations. Finally, biobanked organoids from patient groups are a very promising tool for drug discovery. Adapted from[178] using BioRender.com.

One of the first liver organoid systems was generated from human iPSCs differentiated into hepatic endoderm cells and cultured with human umbilical vein endothelial cells and mesenchymal stem cells to mimic early organogenesis[127,169]. This 3D vascularized liver model not only formed functional vascular networks but also mimicked *in vitro* liver-specific functions such as human-specific drug metabolism and rescued drug-induced liver failure after transplantation *in vivo* [173]. However, iPSC-derived liver organoids have a long protocol that generally takes almost a month, and specific growth factor cocktails are to be added at each differentiation step[173–175,179]. Moreover, once the organoids are fully differentiated, they usually lose their ability to further expand[179]. In addition, these organoids include complex cellular compartments, including mesenchymal, epithelial, and even endothelial cells, however, the composition and differentiation of these cells can vary heavily from batch to batch and are not well-controlled[173–175,179]. Moreover, they are more suitable for studying early organogenesis as these processes only occur during embryonic development[179], thus limiting their use for experimental research.

Other studies have employed biliary-derived bi-potent adult stem cells. Huch and colleagues established the long-term organoid expansion cultures of single $LGR5^+$ stem cells and $EPCAM^+$ ductal cells, which express stem cell and ductal markers such as SOX9 and KRT19[143,172]. The authors established culture conditions for differentiation of BEC-organoids into functional hepatocyte-like cells *in vitro* and showed successful engraftment following their transplantation into mice with drug-induced liver failure[143]. The same laboratory also established human liver organoid cultures derived from bile duct-derived bi-potent stem cells, which were shown to be genetically stable, and readily converted into functional hepatocytes *in vitro* and *in vivo* upon transplantation[172]. In both cases, the transplanted organoids increased the survival of the mice, providing proof that a cellular therapy for liver disease is possible[143,172]. Thus, liver biliary stem cells can be expanded *in vitro* as 3D organoid cultures and differentiated into hepatocytes to study hepatocyte function.

More recently, liver organoids have also been established from human and mouse primary hepatocytes, which can be maintained for multiple months while keeping their morphological, functional, and gene expression features[176]. Another recent study illustrated that adding inflammatory cytokine tumor necrosis alpha (TNF-α) further promotes the proliferation of liver organoids derived from mouse primary hepatocytes[177]. Upon transplantation, these liver organoids showed a better engraftment efficiency compared to differentiated BEC-organoids[176,177]. However, they had a lower proliferative rate and longer passaging interval than liver organoids derived from BECs, thus limiting their use for experimental research.

Considering the limitations in iPSC-derived and hepatocyte organoid culture and that BECs were demonstrated to be the facultative liver stem cells, BEC-organoid culture is a promising tool in liver regenerative medicine. These self-renewing bipotent organoids are capable of expressing stem cell markers and of differentiating into functional cholangiocyte- and hepatocyte-like lineages, which can engraft and repair bile ducts[180,181] and improve liver function when transplanted into a mouse with liver disease[131,143,172]. Moreover, the efficiency of BECs to generate organoids *in vitro* has been shown to mirror their regenerative capacity, and organoid formation has also been shown to have similarities with the regenerative process in DDC-induced DR[148]. Thus, these results imply that BEC-organoids provide a good tool for regenerative cell therapy and for studying the mechanisms behind the DR process.

As mentioned in the previous section (Chapter 1.3.4), YAP activation is necessary to support DR in the late fibrotic NAFLD stages and thus is a known regulator of DR. However, it is not observed in steatosis[182], thus leaving the early molecular mechanisms of BEC activation during DR initiation unexplored. Studying the early stages in NAFLD could help to understand BEC activation without the interference of further complex traits like inflammation/fibrosis, and BEC-organoid cultures provide a great model system to study this phenomenon.

Chapter 2 Research Aims

Despite the increasing prevalence of NAFLD, effective drugs are still lacking, and novel therapeutic approaches are urgently needed. To this end, a better understanding of the molecular mechanisms of liver regeneration is essential. To do so, one approach is to get more insights into the biology of BECs and to study facultative liver stem cells using BEC-organoid cultures, which mimic the cellular diversity, spatial organization, and functionality of their *in vivo* counterparts. This makes them a powerful tool for studying DR and regenerative mechanisms.

The main focus of my doctoral work was to dissect the behavior of liver BECs in the context of NAFLD progression. BECs undergo the DR process, one of the possible mechanisms in place to regenerate the liver in chronic liver injuries such as NAFLD. However, the mechanisms underlying DR initiation and BEC activation or whether they can be used to boost regeneration are not known and can lay the foundations for the development of new therapeutics. Moreover, DR correlates closely with the severity of fibrosis in human liver diseases, and whether fibrosis is unintentionally exacerbated by DR is unknown due to the underestimation of tissue stiffness and the absence of synthetic matrices with modular physical properties. Altogether, these issues have major implications for developing antifibrotic or pro-regenerative therapies.

To address these major bottlenecks, I investigated the role of BEC phenotype in the context of NAFLD as described below:

Aim 1 (Chapter 4): Hepatic lipid overload potentiates BEC activation. I investigated the regenerative mechanisms using biliary-derived liver stem cells in the context of NAFLD. Considering that DR is observed in late-stage NAFLD patients with fibrosis and portal inflammation, how it initiates or if steatosis, the early stage of NAFLD, affects BEC activation is still unexplored. In this aim, I demonstrated that lipid overload induces the conversion of adult cholangiocytes into proliferating BECs and promotes their expansion via the activation of the E2F transcription factors.

Aim 2 (Chapter 5): Mechano-modular PEG hydrogels unveil the role of liver stiffness on BEC activation. Together with collaborators, we developed a simple synthetic BEC-organoid culture in PEG hydrogels. Using this mechano-modular synthetic hydrogel, I studied the effect of stiffness on BEC-organoids as an *in vitro* model of DR and liver regeneration in the physiological and fibrotic stiffness of mouse liver. Finally, I demonstrated that the response to fibrotic stiffness was preserved in BEC-organoids derived from NASH patients compared to healthy controls.

Chapter 3 Experimental Procedures

Mouse studies and ethical approval. All the animal experiments were authorized by the Veterinary Office of the Canton of Vaud, Switzerland, under license authorizations VD3263, VD3721 and VD2627.b. C57BL/6JRj mice were obtained from Janvier Labs, and *E2f1*$^{+/+}$ and *E2f1*$^{-/-}$ (B6;129S4-E2f1tm1 Meg/J) mice were purchased from The Jackson Laboratory. 8-week-old C57BL/6JRj male mice were fed with Chow Diet (CD - SAFE Diets, SAFE 150) or High Fat Diet (HFD - Research Diets Inc, D12492i) for 15 weeks. 7-week-old *E2f1*$^{+/+}$ and *E2f1*$^{-/-}$ male mice were fed with Chow Diet (CD – Kliba Nafag 3336) or High Fat Diet (HFD - Envigo, TD93075) for 29 weeks. The mice were housed in groups of five per cage with access to food and water. The temperature of the animal facility was set at 22 ± 2 °C, the hygrometry at 40–60%, and the light cycle (12:12) from 7:00 to 19:00. The well-being of the animals was monitored daily, and body weight was monitored once per week until the end of the experiment. All mice had unrestricted access to water and food, and liver tissues were harvested at the end of the experiment.

Data reporting. Mice were randomized into different groups according to their genotype. A previous HFD experiment was used to calculate the sample size for C57BL/6JRj mouse experiments. Mice showing any sign of severity, predefined by the Veterinary Office of the Canton of Vaud, Switzerland were sacrificed and excluded from the data analyses. *In vitro* experiments were repeated with at least 3 biological replicates (BEC-organoids from different mice) or were repeated at least twice by pooling 4 mice per condition (for Seahorse analysis).

Proliferation Assay with EdU. Cell proliferation was assessed by EdU assay (Click-iT EdU Alexa Fluor 647, ThermoFisher, C10340) following the manufacturer's instructions. For *in vivo* studies, EdU was resuspended in phosphate-buffered saline (PBS- ThermoFisher, 10010002), and 200 µL of the solution was injected intraperitoneally (50 µg per g of mouse weight) 16 hours before the sacrifice. For *in vitro* quantification of EdU+ cells, one section per organoid showing the largest dimension of the organoid was analyzed (15 organoids per condition), and from each section EdU+ cells were manually counted and expressed as a percentage of cells calculated from nuclear labeling with DAPI.

EPCAM^{+} BEC isolation and FACS analysis. 23-week-old CD/HFD-fed C57BL/6JRj male mice were used for this experiment and sacrificed in the fed state. To isolate the BECs, mouse livers were harvested and digested enzymatically as previously reported[183]. Briefly, livers were minced and incubated in a digestion solution (1% fetal bovine serum (FBS) (Merck/Sigma, F7524) in DMEM/Glutamax (ThermoFisher, 31966-021) supplemented with HEPES (ThermoFisher, 15630-056) and Penicillin/Streptomycin (ThermoFisher, 15140-122) containing 0.0125% (mg/ml) collagenase (Merck/Sigma, C9407), 0.0125% (mg/ml) dispase II

(ThermoFisher, 17105-041) and 0.1 mg/ml of DNAase (Merck/Sigma, DN25). This incubation lasted 2-3h on a shaker at 37°C at 150 rpm. Livers were then dissociated into single cells with TrypLE (GIBCO, 12605028) and washed with washing buffer (1% FBS (Merck/Sigma, F7524) in Advanced DMEM/F-12 (GIBCO, 12634010) supplemented with Glutamax (ThermoFisher, 35050061), HEPES (ThermoFisher, 15630-056) and Penicillin/Streptomycin (ThermoFisher, 15140-122)). Single cells were filtered with a 40 μm cell strainer (Falcon, 352340) and incubated with fluorophore-conjugated antibodies CD45–PE/Cy7 (BD Biosciences, 552848), CD11b–PE/Cy7 (BD Biosciences, 552850), CD31–PE/Cy7 (Abcam, ab46733) and EPCAM–APC (eBioscience, 17-5791-82) for 30 min on ice. BECs were sorted using FACSAria Fusion (BD Biosciences) as previously described[184]. Briefly, individual cells were sequentially gated based on cell size (forward scatter (FSC) versus side scatter (SSC)) and singlets. BECs were then selected based on EPCAM positivity after excluding leukocytes ($CD45^+$), myeloid cells ($CD11b^+$), and endothelial cells ($CD31^+$), yielding a population of single $CD45^-$/$CD11b^-$/ $CD31^-$/$EPCAM^+$ cells. All flow cytometry data were analyzed with FlowJo v10.8 software (BD Life Sciences).

RNA preparation from $EPCAM^+$ BECs and bulk RNA-seq data analysis. RNA was isolated from sorted BECs using the RNeasy micro kit (QIAGEN, 74104), and the amount and quality of RNA were measured with the Agilent Tapestation 4200 (Agilent Technologies, 5067-1511). As a result, RNA-seq of 5 CD and 7 HFD samples was performed by BGI with the BGISEQ-500 platform. FastQC was used to verify the quality of the reads[185]. No low-quality reads were present, and no trimming was needed. Alignment was performed against the mouse genome (GRCm38) following the STAR (version 2.6.0a) manual guidelines[186]. The obtained STAR gene counts for each alignment were analyzed for differentially expressed genes using the R package DESeq2 (version 1.34.0)[187]. A threshold of 1 log2 fold change and adjusted p-value smaller than 0.05 were considered when identifying the differentially expressed genes. A principal component analysis (PCA)[188] was used to explore the variability between the different samples.

Bulk RNA-seq data analysis from publicly available human NASH BEC-organoids dataset. The raw counts were obtained from the deposited gene expression data (GSE180882). A threshold of 1 log2 fold change and adjusted p-value smaller than 0.05 were considered when identifying the differentially expressed genes.

Gene set enrichment analysis (GSEA). We used the clusterProfiler R package[189] to conduct GSEA analysis on various gene sets. Gene sets were retrieved from http://ge-lab.org/gskb/ for *M.musculus* and *H.sapiens*. We ordered the differentially expressed gene list by log2 (Fold-changes) for the analysis with default parameters.

Over-representation enrichment analysis. All significantly changing genes (adjusted p-value < 0.05 and an absolute fold change > 1) were split into 2 groups based on the direction of the fold change (genes significantly up- & down-regulated). An over-representation analysis using the clusterProfiler R package was performed on these groups to identify biologically overrepresented terms.

Figure generation with R. The R packages ggplot2[190] retrieved from https://ggplot2.tidyverse.org and ggpubr were used to generate figures.

Liver immunohistochemistry (IHC) and immunofluorescence (IF). For liver paraffin histology, livers were washed in PBS (Gibco, 10010023), diced with a razor blade, and fixed overnight in 10% formalin (ThermoFisher, 9990244) while shaking at 4°C. The next day fixed livers were washed twice with PBS, dehydrated in ascending ethanol steps, followed by xylene, and embedded in paraffin blocks. 4 µm thick sections were cut from paraffin blocks, dewaxed, rehydrated, and quenched with 3% H_2O_2 for 10 minutes to block the endogenous peroxidase activity (for IHC). Antigen retrieval was performed by incubating the sections in 10 mM citrate buffer (pH 6.0) for 20 min at 95 °C. After the sections cooled to room temperature, they were washed and blocked with blocking buffer (1% BSA (Sigma, A7906) and 0.5% Triton X-100 (Sigma, X100) in PBS), for 1 h at room temperature. The primary antibodies anti-Ki67 (ThermoFisher, MA5-14520), anti-PANCK (Novusbio, NBP600-579), anti-OPN (R&D Systems, AF808), anti-Cleaved caspase-3 (Cell Signaling, 9661) were diluted in a 1:100 dilution of the blocking buffer and incubated overnight at 4 °C. For IHC, ImmpRESS HRP conjugated secondary (VectorLabs MP-74-01-15 and MP-74-02) were incubated for 30 min, and detection was performed using a 3.3'-diaminobenzidine (DAB) reaction. Sections were counterstained with Harris and mounted. For IF, sections were washed and incubated for 1 h with Alexa Fluor conjugated secondary antibodies (1:1000 in blocking solution; Invitrogen). Following extensive washing, sections were counterstained with DAPI (ThermoFisher, 62248), and mounted in ProLong Gold Antifade Mountant (Thermo Fischer, P36930).

For IF of liver cryosections, the livers were frozen in O.C.T. compound (VWR chemicals) on dry ice-filled with isopentane. 10 µm liver sections were cut from O.C.T embedded samples, hydrated, and washed twice in PBS. The sections were blocked in blocking buffer for 1h at room temperature and incubated with BODIPY 558/568 (Invitrogen, D38D35) for 20 minutes. After fixation with 4% paraformaldehyde (PFA) solution (Sigma, 1004960700) for 15 minutes, sections were washed with PBS. Then, sections were permeabilized using 5% BSA in TBS-T and stained with primary antibody anti-PANCK diluted in blocking buffer for 16 h at 4 °C. The next day, the sections were washed three times with PBS and the appropriate Alexa Fluor secondary antibodies were diluted in blocking buffer (1:1000) and incubated with the sections for 1 h at room temperature. The sections were washed in PBS and incubated with DAPI diluted 1:1000 in PBS for 1 h at room temperature. Finally, the sections were mounted in ProLong Gold Antifade Mountant.

Stained sections were imaged by a virtual slide microscope (VS120, Olympus) and analysis was performed using QuPath software[191].

Enzymatically crosslinked hydrogel precursor synthesis: Hydrogel precursors were synthesized as previously reported by using vinyl sulfone functionalized 8-arm PEG (PEG-VS), and substrate peptides mentioned below[192]. Briefly, PEG-VS was purchased from NOF. The transglutaminase (TG) factor XIII (FXIIIa) substrate

peptides Ac-FKGGG*PQGIWGQ*-ERCG-NH2 with matrix metalloproteinases (MMPs)-sensitive sequence (in italics), Ac-FKGG-GDQGIAGF-ERCG-NH2, and H-NQEQVSPLERCGNH2) were purchased from GL Biochem. FXIIIa substrate peptides and 8-arm PEG-VS were dissolved in triethanolamine (0.3 M, pH 8.0) and mixed at 1.2 stoichiometric excess (peptide-to-VS group) and allowed to react for 2 h under an inert atmosphere. The reaction solution was dialyzed (Snake Skin, MWCO 10 K, PIERCE) against ultrapure water for 3 days at 4 °C, after which the products were lyophilized and dissolved in ultrapure water to make 13.33% w/v stock solutions.

Formation and dissociation of PEG hydrogels: PEG precursor solutions described above were mixed in stoichiometrically balanced ratios to form hydrogel networks of a desired final PEG content. The addition of thrombin-activated FXIIIa (10 U ml−1; Galexis) triggered the hydrogel formation in Tris-buffered saline (TBS; 50 mM, pH 7.6) and 50 mM CaCl2. The spare reaction volume was used to incorporate dissociated liver stem cells, fragments of liver bile ducts, and RGD-presenting adhesion peptide (H-NQEQVSPLRGDSPG-NH2, purchased from GL Biochem). Gels cast on a PDMS-coated 24-well plate were allowed to crosslink by incubation at 37 °C for 10 min. To release the grown colonies for further processing, gels were detached from the bottom of the plates using a tip of a metal spatula and transferred to a 15-ml Falcon tube containing 1 ml of Dispase (1 mg/ml, Thermo Fisher Scientific). After 10 minutes of enzymatic digestion, the reaction was quenched using 10% FBS containing 1 mM EDTA, organoids were washed with a cold basal medium (Advanced DMEM/F-12 (Gibco,12634010) supplemented with Glutamax (ThermoFisher, 35050061), HEPES (ThermoFisher, 15630-056), and Penicillin/Streptomycin (ThermoFisher, 15140-122)), and centrifuged for 3 min at 1000 rpm.

Mechanical characterization of PEG hydrogels: Elastic modulus (G') of hydrogels was measured by performing small-strain oscillatory shear measurements on a Bohlin CVO 120 rheometer with plate-plate geometry. Briefly, 1–1.4 mm thick hydrogel discs were prepared and allowed to swell in water for 24 h. The mechanical response of the hydrogels sandwiched between the parallel plates of the rheometer was recorded by performing frequency sweep (0.1–10 Hz) measurements in a constant strain (0.05) mode at 25 °C.

Culture of mouse liver BEC-organoids from biliary duct fragments or single bile duct cells. BEC-organoids were established from bile ducts as previously described[183,193]. Thus, the liver was digested as detailed above ($EPCAM^+$ BEC isolation), and bile ducts were isolated. Ducts were pelleted by centrifugation at 200 rpm for 5 min at 4°C, washed with PBS twice and resuspended in Matrigel (Corning, 356231) or PEG hydrogels and cast in 10 µl droplets in 48-well plates. To obtain single bile duct cells, the isolated ducts were dissociated into single cells using TrypLE Express (Gibco, 12604013). Then, single cells were counted, and 15000 single cells were resuspended in Matrigel or PEG hydrogels. When gels were formed, 250 µl of isolation medium (IM- Advanced DMEM/F-12- Gibco,12634010) supplemented with Glutamax (ThermoFisher, 35050061), HEPES (ThermoFisher, 15630-056), and Penicillin/Streptomycin (ThermoFisher, 15140-122), 1X B27 (Gibco, 17504044), 1mM *N*-acetylcysteine (Sigma-Aldrich, A9165), 10 nM gastrin (Sigma-Aldrich,

G9145), 50 ng/ml EGF (Peprotech, AF-100-15), 1 µg/ml Rspo1 (produced in-house), 100 ng/ml FGF10 (Peprotech, 100-26), 10 mM nicotinamide (Sigma-Aldrich, N0636), 50 ng/ml HGF (Peprotech, 100-39), Noggin (100 ng/ml produced in-house), 1µg/ml Wnt3a (Peprotech, 315-20) and 10 µM Y-27632 (Sigma, Y0503) was added to each well. Plasmids for Rspo1 and Noggin production were a kind gift from Joerg Huelsken. After the first 4 days, IM was replaced with the expansion medium (EM), which was the IM without Noggin, Wnt3a, and Y-27632.

BEC-organoids were collected using Cell Recovery Solution (Corning, 354253, passaging in Matrigel) and 1 ml of Dispase (1 mg/ml, Thermo Fisher Scientific, passaging in PEG hydrogels) a maximum of one week after seeding and dissociated into single cells using TrypLE Express (Gibco, 12604013). Single cells were then transferred to fresh Matrigel and PEG. Passaging was performed in a 1:3 split ratio.

For the FA-treatment of BEC-organoids, palmitic acid (Sigma, P0500) and oleic acid (Sigma, O1008) were dissolved in 100% ethanol into 500 and 800 µM stock solutions, respectively, and kept at -20 °C. For each experiment, palmitic acid and oleic acid were conjugated to 1% FA-free bovine serum albumin (BSA) (Sigma, A7030), in EM through 1:2000 dilution each (Malhi et al., 2006). The concentration of vehicle, ethanol, was 0.1% ethanol in final incubations and 1% FA-free BSA in EM was used as the control for FA treatment.

Quantification of BEC-organoid formation efficiency in PEG hydrogels: Phase contrast z-stacks images were collected through the entire thickness of the PEG gels (every 15 µm) at four different locations within the gels (Nikon Eclipse Ti). The Cell Counter plugin in ImageJ (NIH) was used to quantify the percentage of single cells that formed colonies after 3 days of culture in the expansion medium.

BEC-organoid growth assay in Matrigel. BEC-organoid formation efficiency was quantified by counting the total number of cystic/single layer (lumen-containing) CD/HFD-derived BEC-organoids 6 days after seeding and normalizing it to the total number of cells seeded initially (15000 cells). Organoids were imaged by DM IL LED inverted microscope (Leica), selected as regions of interest (ROI) using widefield 4x magnification, and counted manually.

BEC-organoid whole-mount immunofluorescence. BEC-organoids were incubated with BODIPY 558/568 for 20min, washed with PBS, and extracted from Matrigel using Cell Recovery Solution (Corning, 354253). After fixing with 4% PFA in PBS (30 min, on ice), they were pelleted by gravity to remove the PFA and were washed with PBS and ultra-pure water. BEC-organoids were then spread on glass slides and allowed to attach by drying. The attached BEC-organoids were rehydrated with PBS and permeabilized with 0.5% Triton X-100 in PBS (1 h, room temperature) and blocked for 1 h in the blocking buffer. After washing with PBS, samples were incubated overnight with Alexa Fluor Phalloidin 488 (Invitrogen, A12379) and primary antibodies against EPCAM (1:50, eBioscience, G8.8), KRT19 (1:100, Abcam, ab15463), E-CADHERIN (1:100, Cell Signaling, 24E10), SOX9 (1:50, Millipore, AB5535), ALBUMIN (1:50, R&D systems, MAB1455), HNF4α (1:50, Santa Cruz, C19), ZO-1 (1:50, Invitrogen, 61-7300); YAP (1:50, Cell Signaling, 4912 S). Samples were

washed with PBS and incubated for 3 h with secondary antibodies Alexa 488 donkey-α-rabbit, Alexa 568 donkey-α-mouse, Alexa 647 donkey-α-goat (1:1000 in blocking solution; Invitrogen). Following extensive washing, stained organoids were imaged by confocal (Zeiss LSM 710) mode. DAPI was used to stain nuclei. Signal intensity was adjusted on each channel using Fiji software[194].

Quantitative real-time qPCR for mRNA quantification. BEC-organoids were extracted from Matrigel PEG hydrogels as mentioned previously. RNA was extracted from organoid pellets using the RNAqueous total RNA isolation kit (Invitrogen, AM1931) and the RNeasy Micro Kit (Qiagen, 74004) following the manufacturer's instructions. RNA was transcribed to complementary DNA using QuantiTect Reverse Transcription Kit (Qiagen, 205314) following the manufacturer's instructions. PCR reactions were run on the LightCycler 480 System (Roche) using SYBR Green (Roche, 4887352001) chemistry. Real-time quantitative polymerase chain reaction (RT-qPCR) results were presented relative to the mean of *36b4* and *Gapdh* (comparative ΔCt method). Expression values shown as heatmap are reported as delta cycle threshold (ΔCt) values normalized using *Gapdh* (ΔCt values were calculated as ΔCt = Ct[target gene] − Ct[*Gapdh*] and represented by scale color of ΔCt values [Green-low expression; Red-high expression]). Primers for qRT-PCR are listed in Table 1.

E2F inhibition. For the E2F inhibition experiment, single BECs were grown for 7 days and allowed to form organoids. For the Seahorse experiment, BEC-organoids were treated with E2F inhibitor, HLM006474 (10 μM, Merck, 324461), overnight before the metabolic assay. For RT-qPCR analysis, BEC-organoids were treated with HLM006474 chronically for 4 days.

Bioenergetics with Seahorse extracellular flux analyzer. The oxygen consumption rate (OCR), extracellular acidification rate (ECAR), and proton-efflux rate (PER) of the BEC-organoids were analyzed by an XFe96 extracellular flux analyzer (Agilent) following the manufacturer's instructions according to assay type.

For the Mito Stress Test on CD/HFD-derived BEC-organoids, the organoids were grown with FA mix for 7 days. On day 7, 10 μM HLM006474 or DMSO as vehicle were added overnight. The next morning, BEC-organoids were dissociated, and 20000 cells were seeded with Seahorse Assay Medium in XFe96 Cell Culture Microplates (Agilent, 101085-004), which were previously coated with 10% Matrigel in Advanced DMEM/F-12. Seahorse Assay Medium was unbuffered, serum-free pH 7.4 DMEM supplemented with 10 mM glucose (Agilent, 103577-100), 10 mM pyruvate (Gibco, 11360070), and 2 mM glutamine (Agilent, 103579-100), and 10 μM HLM006474 or DMSO (vehicle) were added when indicated. After 2 h incubation for cell attachment, plates were transferred to a non-CO^2 incubator at 37 °C for 45 minutes. Mitochondrial OCR was measured in a time course before and after the injection of 1.5 μM Oligomycin (Millipore, 495455), 2.5 μM FCCP (Sigma, C2920), and 1 μM Rotenone (Sigma, R8875)/Antimycin A (Sigma, A8674).

For Glycolytic Rate Assay, CD BEC-organoids were grown without FA mix and CD/HFD-derived BEC-organoids were grown with FA mix for 7 days. The Seahorse assay preparations including the E2F inhibitor were

the same as mentioned above. GlycoPER was measured in a time course before and after the injection of 1 μM Rotenone/Antimycin A, and 500 μM 2-DG (Sigma, D8375).

For the Substrate Oxidation Assay, CD BEC-organoids were grown without FA mix for 7 days. On day 8, they were dissociated and prepared for Seahorse assay without E2F inhibitor. Mitochondrial OCR was measured in a time course before and after the injection of Oligomycin (1.5 μM), FCCP (2.5 μM), and Rotenone/Antimycin A (1 μM) with or without UK5099 (Sigma, PZ0160), Etomoxir (E1905) and BPTES (SML0601), inhibitors of glucose oxidation, FA oxidation and glutamine oxidation, respectively, in separate experiments.

All Seahorse experiments were normalized by cell number through injection of 10 μM of Hoechst (ThermoFisher,62249) in the last Seahorse injection. Hoechst signal (361/486 nm) was quantified by SpectraMax iD3 microplate reader (Molecular Devices).

BEC-organoid functional analysis. Grown BEC-organoids were treated with the FA-mix for 4 days and triglyceride levels were measured with a Triglyceride kit (Abcam, ab65336) following the manufacturer's instructions. Cell-titer Glo (Promega, G7570) was used to investigate cell viability. For functional assays involving single BECs, grown organoids were dissociated into single cells. 10000 BECs were seeded, and organoid formation was allowed for 7 days. Cell viability, apoptosis, and cell death were investigated using Cell-titer Glo, Caspase 3/7 activity (Promega, G8091), and Nucgreen Dead 488 staining (Invitrogen, R37109), respectively, according to the protocol of manufacturers. For cell death staining, organoids were imaged using ECLIPSE Ts2 inverted microscope (Nikon).

LDL uptake was detected with DiI-Ac-LDL (Biomedical Technologies). Mouse albumin secretion was detected with an ELISA kit (Abcam, ab108792). Urea secretion was assessed with QuantiChrom™ Urea Assay Kit (BioAssay Systems). All experiments were performed according to the manufacturers' instructions.

Western blotting: Samples were lysed in lysis buffer (50 mM Tris (pH 7.4), 150 mM KCl, 1 mM EDTA, 1% NP-40, 5 mM NAM, 1 mM sodium butyrate, protease, and phosphatase inhibitors). Proteins were separated by SDS–PAGE and transferred onto nitrocellulose or polyvinylidene difluoride membranes. Blocking (30 min) and antibody incubations (overnight) were performed in 5% BSA in TBST. YAP1 (Santa Cruz sc101199, 1:1000), phospho-YAP1Y357 (Abcam ab62751, 1:1000), ACTIN (Santa Cruz sc47778, 1:1000), CXCL10 (RD system AF-466-NA, 1:1000), CCL2 (Novus Biologicals NBP2-22115, 1:1000), COL1A2 (Santa Cruz, 1:1000).

Quantification and statistical analysis. Data were presented as mean ± standard deviation (mean ± SD.) unless it is stated otherwise in the figure legend. n refers to biological replicates and is represented by the number of dots in the plot or stated in the figure legends. For the Seahorse experiments, n refers to technical replicates pooled from 4 biological replicates and is represented by the number of dots in the plot or stated in the figure legends. The statistical analysis of the data from bench experiments was performed using Prism

(Prism 9, GraphPad). The differences with $p<0.05$ were considered statistically significant. No samples (except outliers) or animals were excluded from the analysis. Data are expected to have a normal distribution.

For two groups comparison, data significance was analyzed using a two-tailed, unpaired Student's t-test. In case of comparisons between more than two groups, one- or two-way ANOVA was used. Dunnet's, Tukey's, or Sidak's tests were used to correct for multiple comparisons. Statistical details of each experiment can be found in the respective figure legends.

Table 3.1 List of primer sequences used.

Gene	Species	Forward	Reverse
Cyr61	Mouse	CTGCGCTAAACAACTCAACGA	GCAGATCCCTTTCAGAGCGG
Ctgf	Mouse	GCTTGGCGATTTTAGGTGTC	CAGACTGGAGAAGCAGAGCC
Cyp3a11	Mouse	TGGTCAAACGCCTCTCCTTGCTG	ACTGGGCCAAAATCCCGCCG
Alb	Mouse	GCGCAGATGACAGGGCGGAA	GTGCCGTAGCATGCGGGAGG
Ttr	Mouse	ATGGTCAAAGTCCTGGATGC	AATTCATGGAACGGGGAAAT
Fxr	Mouse	ACAGCTAATGAGGACGACAG	GATTTCCTGAGGCATTCTCTG
Glut-2	Mouse	GACCGTGGTGAACCTGCTAT	TGCGGGAATCATAGTCCTTC
Glul	Mouse	CAAGTGTGTGGAAGAGTTACCTGAGT	TGGCAACAGGATGGAGGTACA
Lxr	Mouse	TGCCATCAGCATCTTCTCTG	GGCTCACCAGCTTCATTAGC
Lgr5	Mouse	ATTCGGTGCATTTAGCTTGG	CGAACACCTGCGTGAATATG
Gapdh	Mouse	GGAGAGTGTTTCCTCGTCCC	ACTGTGCCGTTGAATTTGCC
Tnfa	Mouse	GTAGCCCACGTCGTAGCAAAC	AGTTGGTTGTCTTTGAGATCCATG
Mmp3	Mouse	GGAAATCAGTTCTGGGCTATACGA	TAGAAATGGCAGCATCGATCTTC
Ccl2	Mouse	AGGTCCCTGTCATGCTTCTG	GCTGCTGGTGATCCTCTTGT
Col1a2	Mouse	AAGGAGTTTCATCTGGCCCT	AGCAGGTCCTTGGAAACCTT
Mmp2	Mouse	AACTACGATGATGACCGGAAGTG	TGGCATGGCCGAACTCA
Tgfb1	Mouse	GAATGACGGTGCGCAACTCT	CAGCCCCAATAACCGTATGAA
Cxcl1	Mouse	TCTCCGTTACTTGGGGACAC	CCACACTCAAGAATGGTCGC
Mmp13	Mouse	ACAAAGATTATCCCCGCCTCATA	CACAATGCGATTACTCCAGATACTG
Cxcl10	Mouse	CCACGTGTTGAGATCATTGCC	GAGGCTCTCTGCTGTCCATC
Cygb	Mouse	GCTGTATGCCAACTGCGAG	CCTCCATGTGTCTAAACTGGC
Gfap	Mouse	TCGAGATCGCCACCTACAG	GTCTGTACAGGAATGGTGATGC
Acta2	Mouse	GTCCCAGACATCAGGGAGTAA	TCGGATACTTCAGCGTCAGGA
Lrat	Mouse	TACACAGGCCTGGCATCATA	TCCACAAGCAGAATGGGATA
Clec4f	Mouse	ACTGAAGTACCAAATGGACAATGTTAGT	GTCAGCATTCACATCCTCCAGA
Vsig4	Mouse	TCACCTATGGCCACCCCACC	AGGCGGCCTCTGTACTTTGCCT
Stab2	Mouse	TGTCCAGACGGCTACATCAA	CCAGGGATATCCAGGACGTA
Lyve1	Mouse	CCTCCAGCCAAAAGTTCAAA	TCCAACACGGGGTAAAATGT
Scd1	Mouse	TTCTTGCGATACACTCTGGTGC	CGGGATTGAATGTTCTTGTCGT
Hmgcs2	Mouse	GTGGTCTGTGGTGACATTGC	CGCAGGTAGCACTGGATAGA
Pdk4	Mouse	CCGCTGTCCATGAAGCA	GCAGAAAAGCAAAGGACGTT
Aldh1a1	Mouse	TGACCAGGTGCTTTCCATTG	TCACAACACCTGGGGAACAG
Ccnd1	Mouse	CAAGTGTGACCCGGACTGC	TTGACTCCAGAAGGGCTTCAA
Ccna2	Mouse	CAAGACTCGACGGGTTGCTC	GCTGGCCTCTTCTGAGTCTC
Rad51c	Mouse	CGGGAGTTGGTGGGTTATCC	CCGGCACATCTTGGTTTATTTGT
Foxm1	Mouse	ATCGCTACTTGACATTGGACCA	GATTGGGTCGTTTCTGCTGTG
Tpx2	Mouse	ATAGGCGAGCCTTTTCAGGG	CAACTGCCTTCAACGGTGTG

Hk1	Mouse	GAGGTCTACGACACCCCAGA	GAAGTCTCCGAGGCATTCAG
Pfkfb3	Mouse	TCATGGAATAGAGCGCC	GTGTGCTCACCGATTCTACA
Glut2	Mouse	GTCACTATGCTCTGGTCTCTG	CAAGAGGGCTCCAGTCAATG

Chapter 4 Hepatic lipid overload potentiates BEC activation

4.1 BECs and BEC-organoids efficiently accumulate lipids *in vivo* and *in vitro*

To gain insight into how chronic lipid exposure, an inducer of liver steatosis, affects biliary stem cell function *in vitro*, we incubated single BECs with a fatty acid mixture (FA mix) of oleic acid (OA) and palmitic acid (PA) – the two most abundant FAs found in livers of NAFLD patients[195], for 7 days and allowed BEC-organoid formation using two doses of FA treatment (Figure 4.1A). Surprisingly, we observed that BEC-organoids efficiently accumulated lipid droplets in a dose-dependent manner (Figure 4.1B), and this process did not affect organoid viability measured by Cell-titer Glo (ATP-based cell viability), Caspase 3/7 (caspase activity) and a dead cell staining (Figures 4.1C, D).

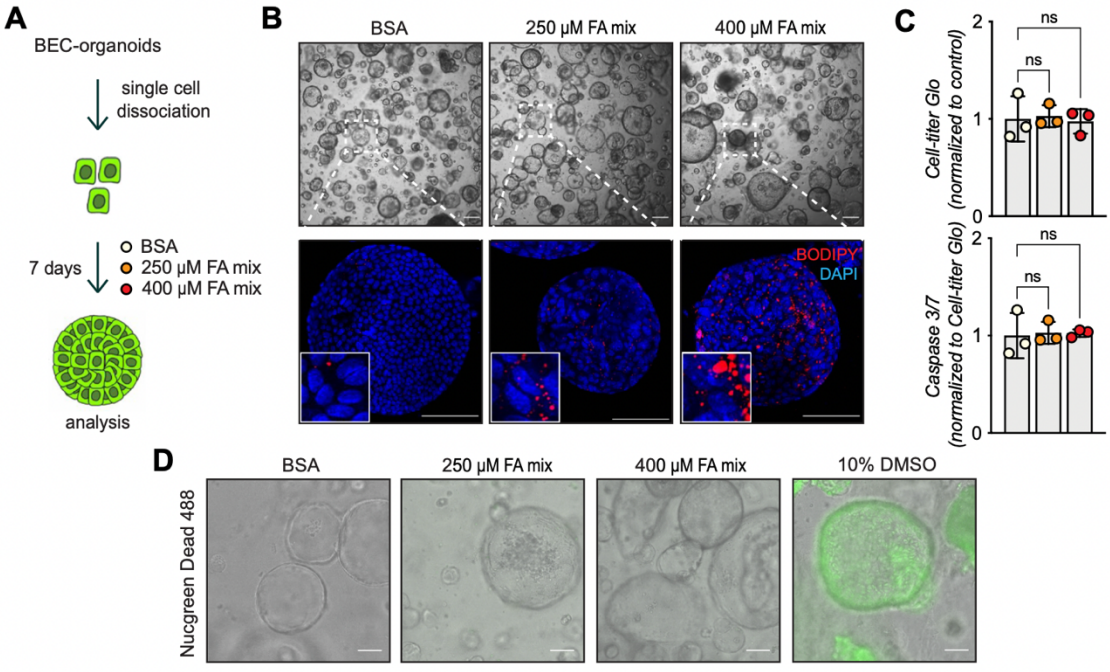

Figure 4.1 BEC-organoids accumulate lipids *in vitro*.

A) Schematic depicting fatty acid (FA) treatment of BEC-organoids *in vitro*. **(B)** Representative brightfield and immunofluorescence (IF) images of lipids (BODIPY) in control (BSA) and FA-treated organoids. Close-up IF images were digitally zoomed in four times. n=3. **(C)** Cell-titer Glo and Caspase 3/7 activity measurement for viability and apoptosis detection relative to panel A. n=3. **(D)** Representative Nucgreen Dead 488 staining as composite images from brightfield and fluorescent microscopy. n=3. Data are shown as mean ± SD. Absence of stars or ns, not significant ($p > 0.05$); one-way ANOVA with Dunnett's test (C) was used. Scale bars, 200 µm (B-brightfield), 100 µm (B- IF, D).

We then investigated how cells adapt their metabolism to lipid overload by monitoring the expression of key genes involved in lipid metabolism, including *Scd1* (*de novo* lipogenesis) (Figure 4.2A), *Hmgcs2*

(ketogenesis), *Pdk4* (inhibition of pyruvate oxidation), and *Aldh1a1* (prevention against lipid peroxidation products) (Figure 4.2B). While we found an increase in lipid usage through the increased expression of *Pdk4*, *Hmgcs2*, and *Aldh1a1*, we also found that *Scd1* was decreased, suggesting that BEC-organoids actively reprogram their metabolism to cope with aberrant lipid overload.

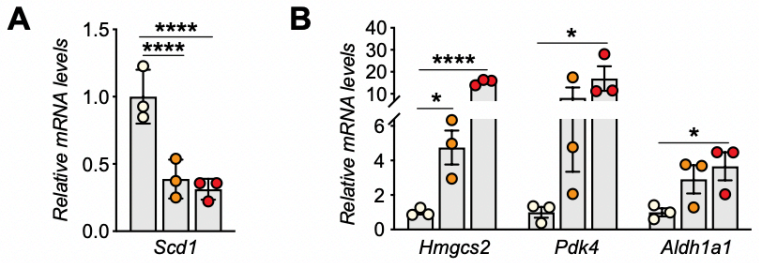

Figure 4.2 Metabolic response of BEC-organoids to fatty acids.

(A-B) Quantification of *Scd1* (**A**) and *Hmgcs2*, *Pdk4,* and *Aldh1a1* (**B**) mRNA in control (BSA) and FA-treated organoids. n=3. Data are shown as mean ± SD. *p < 0.05; ****p < 0.0001; Fisher's LSD test (A, B) was used.

To determine whether the observed phenotype was preserved in fully formed organoids, we treated already established BEC-organoids with the FA mix for 4 days (Figure 4.3A). In line with our previous observations, BODIPY staining (Figure 4.3B), and triglyceride (TG) quantification (Figure 4.3C) showed a pronounced increase in lipid accumulation after 4 days, without affecting cell viability (Figure 4.3D).

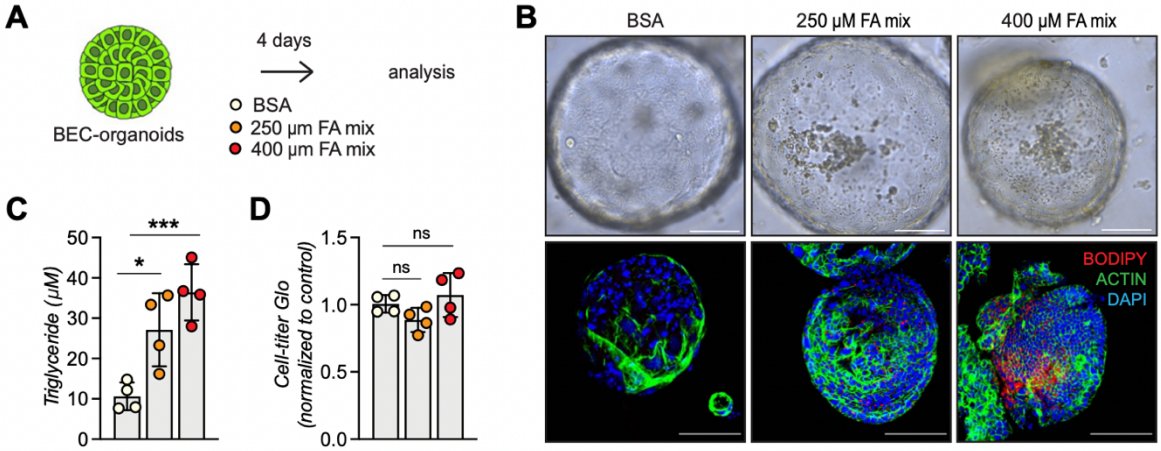

Figure 4.3 Further characterization of lipid accumulation in fully formed BEC-organoids.

(A) Scheme depicting FA mix treatment for already grown BEC-organoids for 4 days. **(B)** Representative brightfield and immunofluorescence (IF) images of lipids (BODIPY) and ACTIN co-staining, relative to panel A. n=4. **(C)** Measurement of triglyceride concentration upon FA mix treatment relative to panel A. n=4. **(D)** Cell-titer Glo measurement for viability detection relative to panel A. n=4. Data are shown as mean ± SD. Absence of stars or ns, not significant (p > 0.05); *p < 0.05; ***p < 0.001; one-way ANOVA with Dunnet's test (C, D) was used. Scale bars, 100 µm (B).

In the next step, we wished to assess whether chronic lipid exposure also affects BECs *in vivo*. To do this, we fed C57BL/6JRj mice for 15 weeks with CD or HFD and analyzed their bile ducts. As expected, HFD-fed mice gained weight and developed liver steatosis (Figure 4.4A), but no apparent epithelial damage (Figures 4.4B, C).

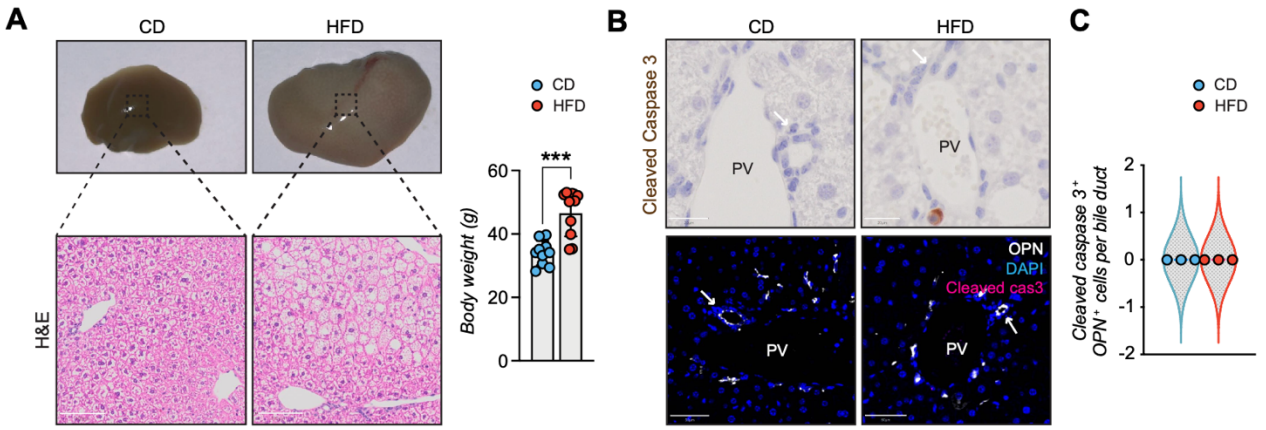

Figure 4.4 Further characterization of steatosis upon HFD.

(A) Representative images of CD/HFD-fed mouse livers, hematoxylin, and eosin (H&E) staining, and the final body-weight measurement at the end of the experiment. n=10. **(B)** Representative cleaved caspase 3 stainings and **(C)** quantification of apoptotic cells in bile ducts**.** n=3. Data are shown as mean ± SD. Absence of stars or ns, not significant ($p > 0.05$); *$p < 0.05$; ***$p < 0.001$; two-tailed Student's t-test (A, C) was used. PV, portal vein. Arrowheads mark bile ducts. Scale bars, 100 µm (A), 50 µm (B-IF), and 20 µm (B-brightfield).

Of note, HFD-feeding led to an accumulation of lipid droplets in the periportal zone and within bile ducts, as reflected by colocalization of BODIPY with PANCK, a BEC marker (Figure 4.5A). To investigate whether individual BECs can accumulate lipids, we isolated BECs from livers of CD/HFD-fed mice using EPCAM, a pan-BEC marker[112,113,148], by fluorescence-activated cell sorting (FACS) (Figures 4.5B, C). Prelabelling of the cells with the lipid marker BODIPY allowed us to quantify the accumulation of this dye in the cells and revealed an increased BODIPY signal in HFD-derived $EPCAM^+$ BECs (Figures 4.5D, E). Together, these *in vitro* and *in vivo* results demonstrate that BECs accumulate lipids upon chronic FA exposure, raising the question of the functional consequences of this previously unrecognized event on BEC behavior.

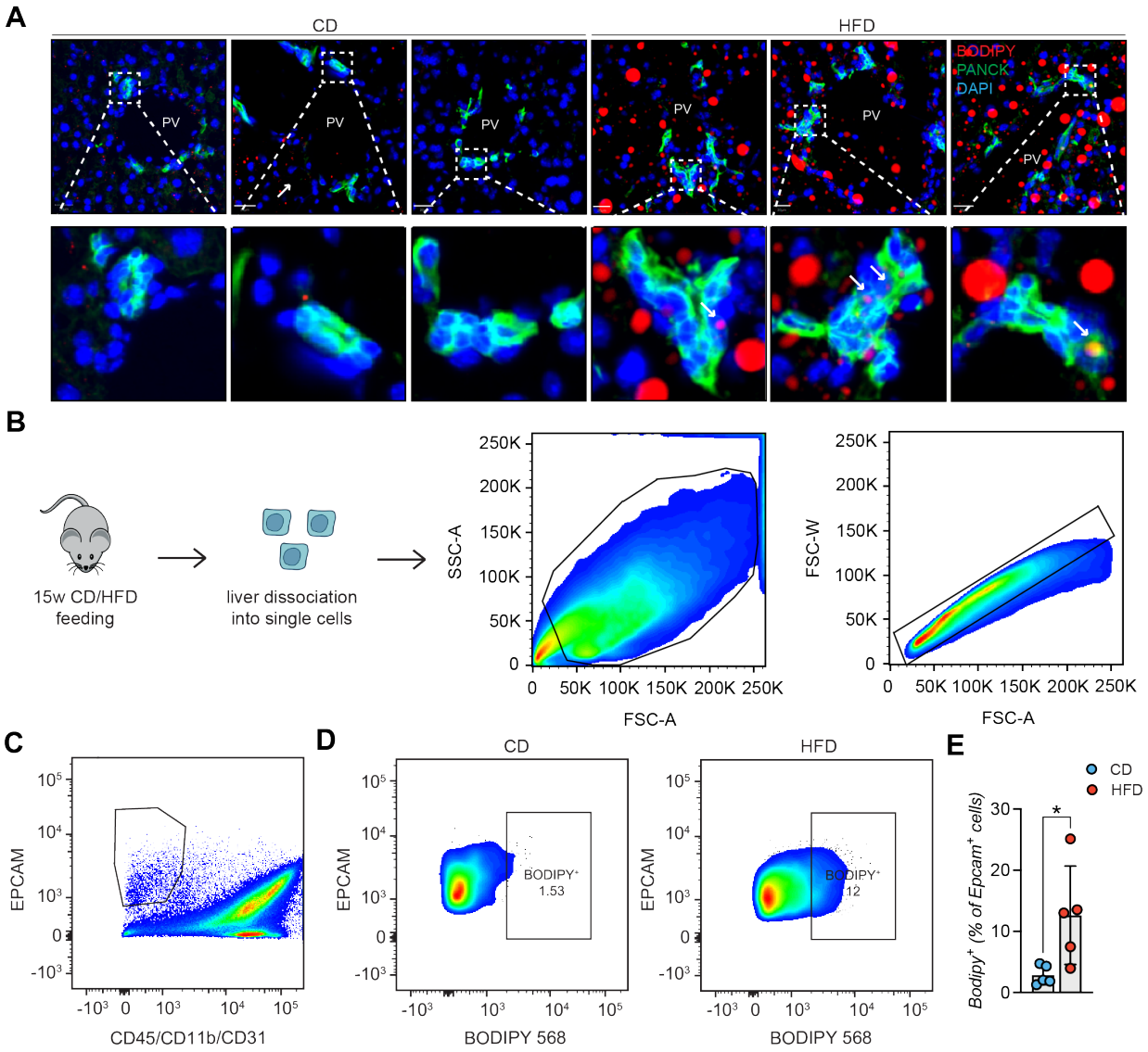

Figure 4.5 BECs accumulate lipids *in vivo*.

(A) Representative images for co-staining of BODIPY and PANCK. Close-up IF images were digitally zoomed in four times. n=5. PV, portal vein. Arrowheads mark bile ducts. **(B)** Scheme depicting the isolation of EPCAM$^+$ BECs from livers of CD- and HFD-fed mice by FACS. **(C)** FACS gating strategy for isolation of CD45$^-$/CD11b$^-$/CD31$^-$/EPCAM$^+$ BECs: individual cells were sequentially gated based on cell size (FSC versus SSC) and singlets. BECs were then selected based on EPCAM positivity after excluding leukocytes (CD45$^+$), myeloid cells (CD11b$^+$), and endothelial cells (CD31$^+$), yielding a population of single CD45$^-$/CD11b$^-$/CD31$^-$/EPCAM$^+$ BECs. **(D-E)** Representative analysis **(D)** and quantification **(E)** of BODIPY$^+$ EPCAM$^+$ BECs in CD and HFD samples. Data are shown as mean ± SD. *p < 0.05; two-tailed Student's t-test (E) was used. Scale bars, 20 µm (A).

4.2 HFD feeding promotes BEC activation and increases organoid formation capacity

We next characterized at the molecular level the impact of chronic lipid overload on BECs *in vivo* by isolating EPCAM$^+$ BECs from livers of CD/HFD-fed mice using FACS (Figure 4.6A) and performing bulk RNA sequencing (RNA-seq). Principal Component Analysis of the RNA-seq data revealed a diet-dependent clustering (Figure 4.6B), indicating that HFD feeding induces considerable transcriptional changes in BECs *in vivo*. Differential expression analysis further revealed 495 significantly changed genes, 121 upregulated and 374 downregulated (Figure 4.6C). At the same time, HFD promoted the upregulation of *Ncam1* (Figure 4.6D), a well-established mediator of BEC activation.

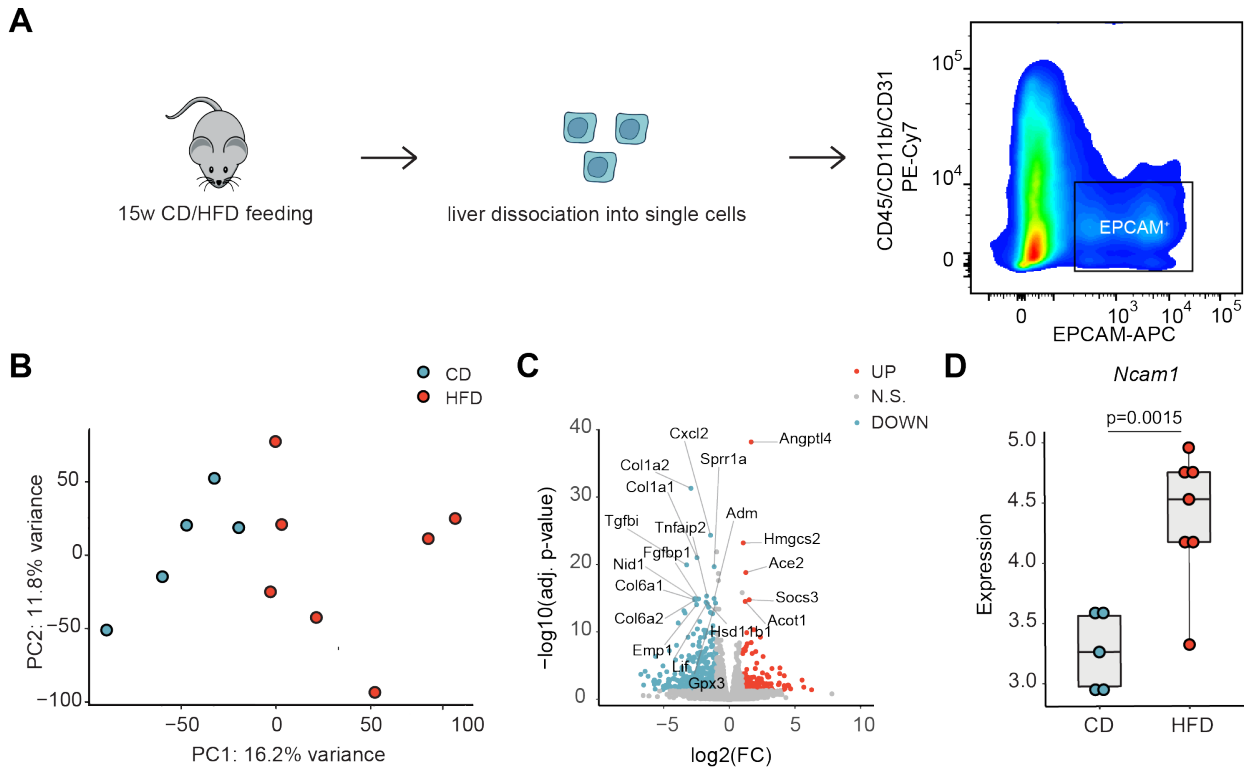

Figure 4.6 RNA-seq analysis of EPCAM$^+$ BECs upon HFD feeding.

(A) Scheme depicting the isolation of EPCAM$^+$ BECs from CD- and HFD-fed mice by FACS. **(B)** Principal component analysis (PCA) of mRNAs measured in mice fed CD or HFD by RNA-seq. **(C)** Volcano plot of HFD vs CD differential expression analysis. The top 20 differentially expressed genes were labeled. Blue dots represent downregulated genes (log2(FC) < -1 & adj. p-value < 0.05). Red dots represent upregulated genes (log2(FC) > 1 & adj. p-value < 0.05). Grey dots represent genes not changing significantly. **(D)** Box plot representing the differential gene expression of *Ncam1*. n= 5 for CD, n=7 for HFD. The Y-axis depicts log2(cpm+1) values.

To further explore transcriptional changes, we performed gene set enrichment analysis (GSEA) on Gene Ontology (GO) terms (Figure 4.7A) and KEGG (Figure 4.7B) pathways and identified cell proliferation, the most prevalent feature of BEC activation[125], as the major upregulated process in these cells upon HFD feeding. Expansion of the reactive BECs requires detachment from their niche and invasion of the parenchyma toward the damaged hepatic area. This process is made possible by reorganizing the ECM and reducing focal adhesion, effectively downregulated in EPCAM$^+$ BECs upon HFD (4.7A, B).

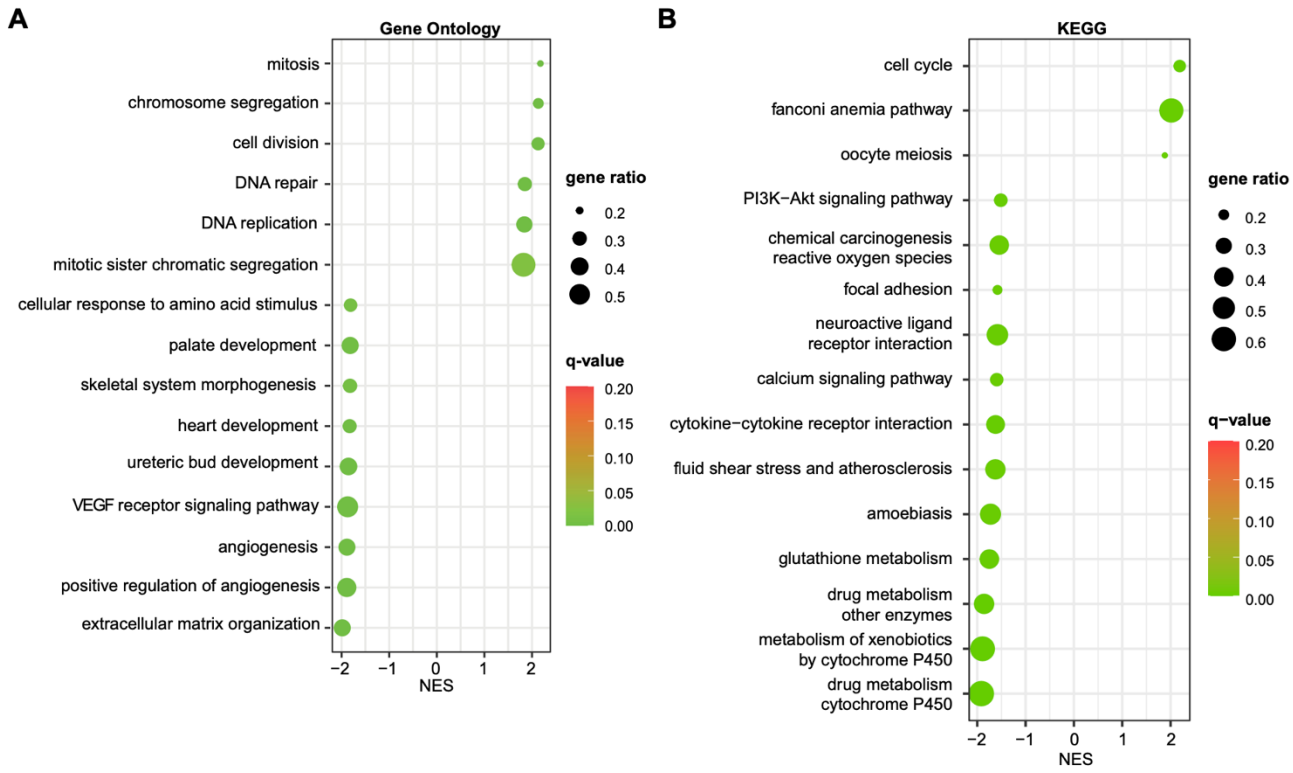

Figure 4.7 HFD feeding induces a proliferative signature on EPCAM$^+$ BECs.

(A) Gene set enrichment analysis (GSEA) of Gene Ontology (GO) terms. Top 15 upregulated biological processes (BP), ordered by normalized enrichment score (NES). **(B)** Gene set enrichment analysis (GSEA) of KEGG terms. Top 15 enriched pathways (sorted by q-value). q-value: false discovery rate adjusted p-values. NES: normalized enrichment score.

In the next step, we monitored the activation of BECs in vivo by measuring the number of proliferating BECs in the portal region of the livers of mice fed either CD or HFD to validate the RNA-seq data. Of note, we found that HFD feeding was sufficient to induce a marked increase in the number of active BECs (i.e., cell proliferation antigen (Ki67)$^+$/osteopontin (OPN)$^+$ cells- Figures 4.8A, B). Similar results were observed in an independent cohort of mice challenged with HFD and injected with EdU to track proliferating cells (Figures 4.8C, D), confirming that chronic lipid exposure stimulates the appearance of reactive BECs within the bile ducts.

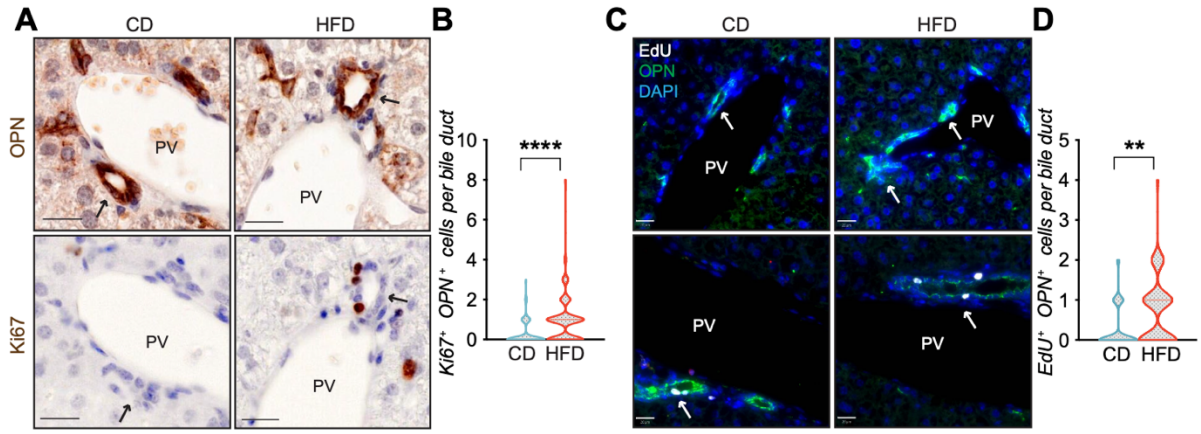

Figure 4.8 HFD feeding induces BEC proliferation.

(A-D) Representative co-staining images **(A, C)** and quantification **(B, D)** of BECs stained for OPN and Ki67 **(A-B)** and OPN and EdU **(C-D)** in livers of CD/HFD-fed mice. n=10 for Ki67 and n=5 for EdU. Violin graphs depict the distribution of data points i.e the width of the shaded area represents the proportion of data located there. **p < 0.01; ****p < 0.0001; unpaired, two-tailed Student's t-test was used. PV, portal vein. Arrowheads mark bile ducts. Scale bars, 20 µm (A, C).

The efficiency of BECs to generate organoids *in vitro* has been shown to mirror their regenerative capacity[148]. To functionally assess the impact of lipid overload on this process, we measured the organoid forming capacity of isolated BECs, as a read-out of their regenerative functions. To this aim, we quantified the organoid formation efficiency of BECs isolated from CD- and HFD-fed mouse livers (Figure 4.9A). Strikingly, we observed that HFD-derived BECs were significantly more efficient in generating organoids than their CD counterparts (Figure 4.9B). Altogether, these results demonstrate that HFD feeding is sufficient to induce, *in vivo*, the exit of BECs from a quiescent state and the acquisition of both proliferative and pro-regenerative features.

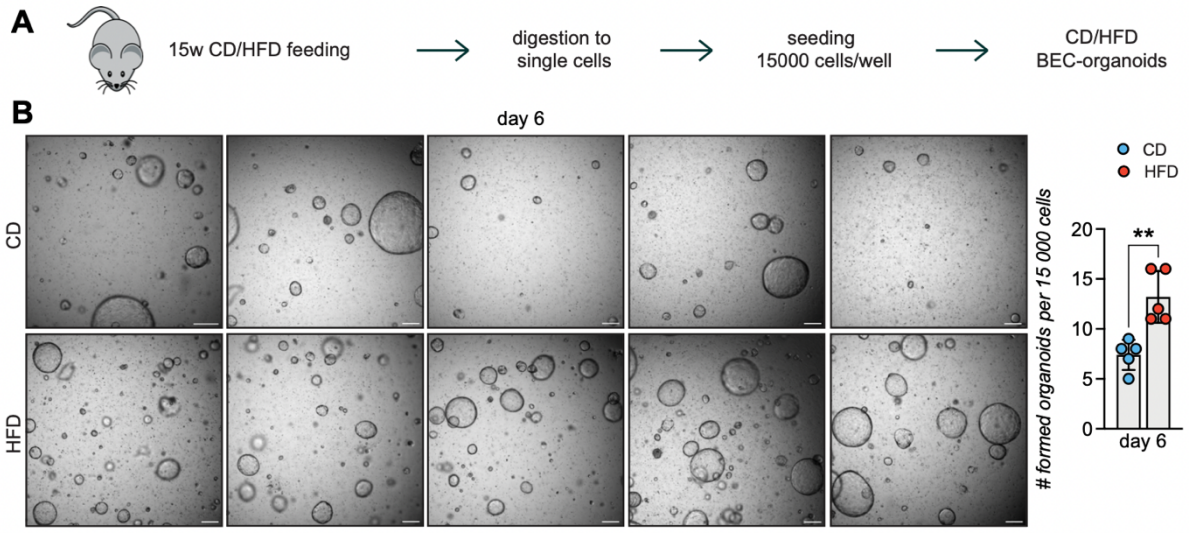

Figure 4.9 HFD feeding increases the organoid formation capacity of BECs.

(A) Schematic depicting BEC-organoid formation *in vitro* from CD/HFD-fed mouse livers. **(B)** Images of organoid colonies formed 6 days after seeding, and quantification of organoids per well. n=5. Data are shown as mean ± SD. **p < 0.01; unpaired, two-tailed Student's t-test was used. Scale bars, 200 µm (B).

4.3 HFD feeding initiates BEC activation via E2Fs

To understand whether the mechanisms underlying BEC activation upon HFD *in vivo* involve canonical processes found in chronically damaged livers, we compared the transcriptional profile of BECs upon HFD with those of DDC-activated BECs[112]. We identified the most pronounced changes in HFD and DDC samples by separate over-representation enrichment analyses and overlapped the results to determine the shared pathways. Cell division, mitosis, and chromosome segregation were the shared enriched pathways for upregulated genes in HFD and DDC samples (Figure 4.10A). At the same time, ECM organization was the shared enriched pathway for the downregulated genes in HFD and DDC conditions (Figure 4.10B). As a result, we concluded that

the mechanisms of BEC activation induced by lipid overload overlap with those induced by biliary epithelial damage.

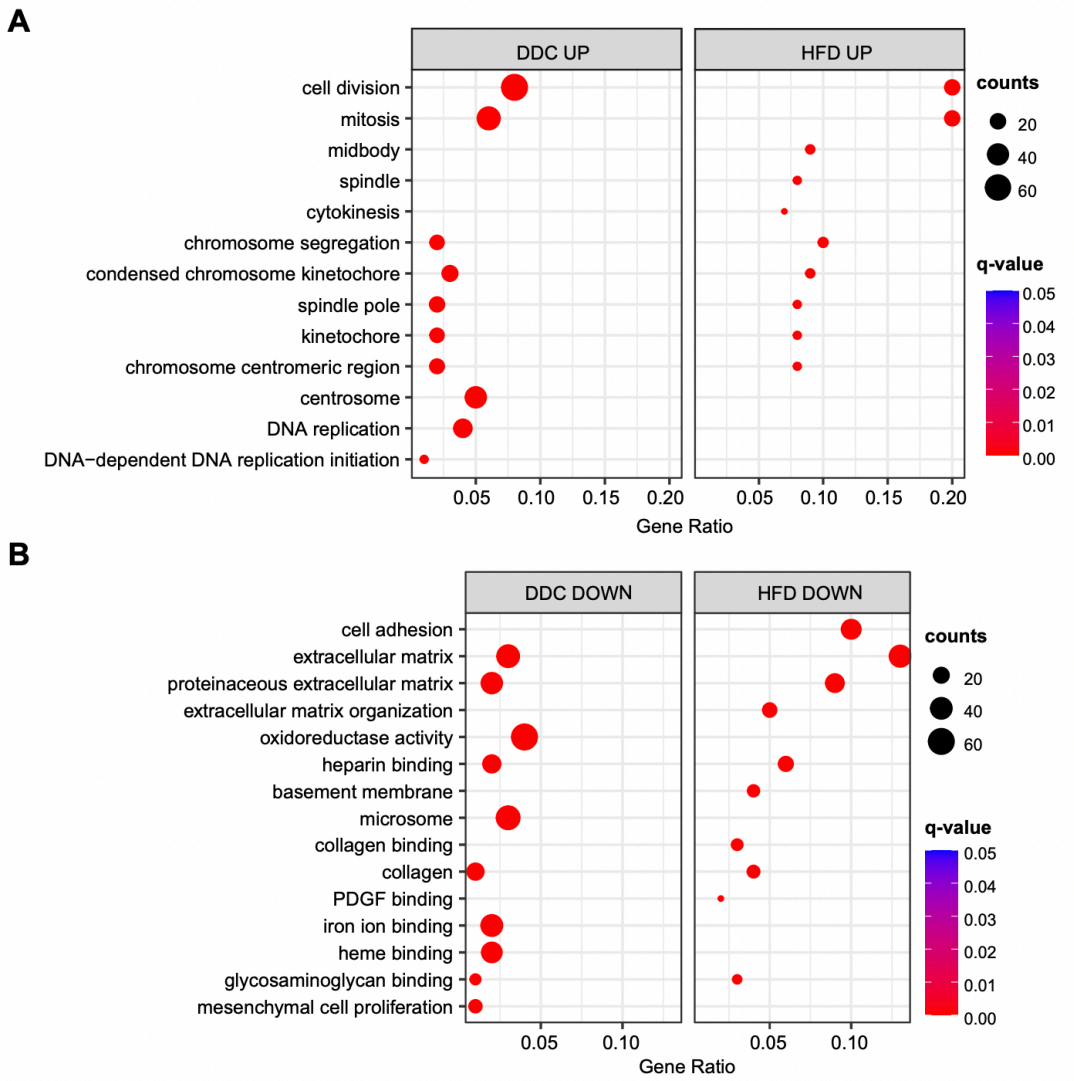

Figure 4.10 Shared enriched pathways in DDC and HFD datasets.

(A-B) Over-representation analysis depicting the shared enriched pathways for **(A)** upregulated and **(B)** downregulated genes. Top 13 **(A)** and top 15 **(B)** enriched biological processes (BP) upon HFD (own data) and DDC (GSE125688) treatment. q-value: false discovery rate adjusted p-values, counts: number of found genes within a given gene set.

Of note, a more detailed analysis of DDC- and HFD-derived BECs, revealed the concomitant enrichment of 4 overlapping transcription factor (TF) gene sets, E2F1-4 (Figure 4.11A), which have not been linked to DR previously. Further analysis of the E2F target genes in the HFD dataset unveiled that E2F1 targets were the most deregulated upon HFD (Figures 4.11A, B). Moreover, we used another publicly available dataset of adult BECs and BEC-organoids to investigate the organoid formation process *in vitro* as a proxy of DR. During organoid formation, we identified enrichment of the E2F and cell division pathways (Figures 4.11C, D) for the upregulated genes, further corroborating the role of E2Fs in the two DR models[148].

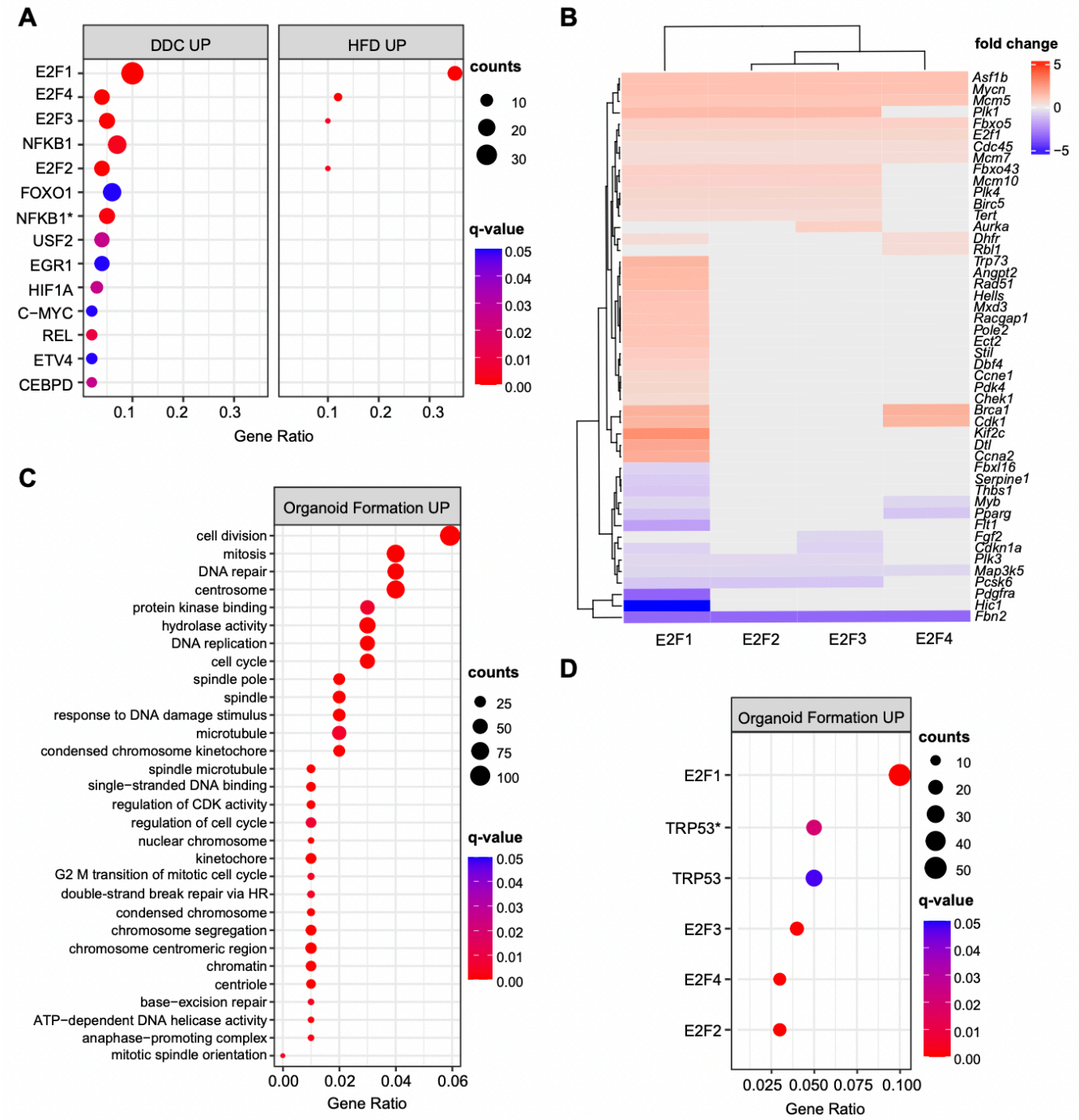

Figure 4.11 E2Fs are enriched in DDC, HFD, and organoid-formation datasets.

(A) Enriched transcription factors (TFs) of upregulated genes identified by over-representation analysis in HFD (own data) and DDC (GSE125688) treatment. Asterisk (*) marks TFs of the "TF_ZHAO" gene set. **(B)** Heatmap of E2F1-4 target genes from TF gene sets. Genes with absolute fold change lower than 0.5 were not shown. **(C-D)** Over-representation analysis of upregulated genes using gene ontology **(C)** and enriched TF **(D)** genesets during organoid formation from single BECs (Organoids vs T0) (GSE123133).

E2Fs are a large family of TFs with complex functions in cell cycle progression, DNA replication, repair, and G2/M checkpoints[196–199]. Therefore, we hypothesized that activation of E2Fs might represent a key event in the process of BEC activation, which is necessary for exiting the quiescent state and driving DR initiation. To test this hypothesis, we focused on E2F1, as it was the most enriched TF in our analysis, and assessed its role

in BECs by feeding E2f1$^{+/+}$ and E2f1$^{-/-}$ mice with HFD (Figure 4.12A). Remarkably, E2f1$^{-/-}$ mice were refractory to BEC activation induced by lipid overload upon HFD, as opposed to E2f1$^{+/+}$ mice (Figures 4.12B, C). These results *in vivo* demonstrate a previously unrecognized role of E2F1 in controlling BEC activation during HFD-induced hepatic steatosis.

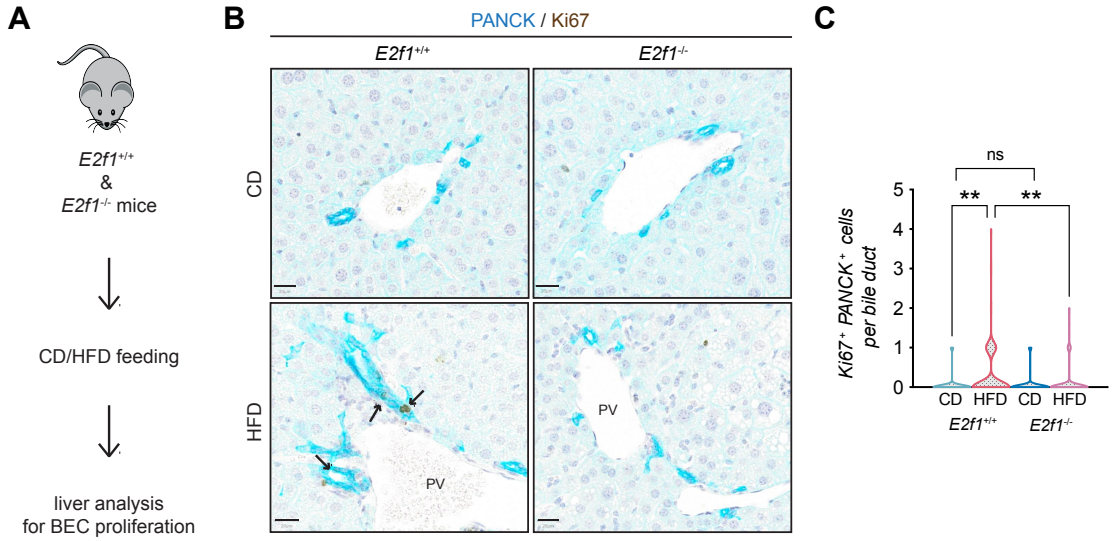

Figure 4.12 E2F1 mediates BEC expansion upon HFD *in vivo*.

(A) Schematic depicting *in vivo* E2F1 analysis. **(B-C)** Representative images of PANCK/Ki67 co-staining in livers of *E2f1*$^{+/+}$ and *E2f1*$^{-/-}$ mice fed with CD or HFD **(B)** and the quantification of proliferative BECs in the indicated mice **(C)**. For CD, n=5 for *E2f1*$^{+/+}$ and *E2f1*$^{-/-}$. For HFD, n=7 for *E2f1*$^{+/+}$, and n=8 for *E2f1*$^{-/-}$. Violin graphs depict the distribution of data points i.e the width of the shaded area represents the proportion of data located there. ns, not significant; **p < 0.01; two-way ANOVA with Tukey's test was used. PV, portal vein. Arrowheads mark bile ducts. Scale bars, 20 µm (B).

4.4 E2F promotes BEC activation by upregulating glycolysis

The exit of terminally differentiated cells from their quiescent state requires both energy and building block availability to support cell proliferation. Proliferative cells, therefore, reprogram their glucose metabolism to meet their increased need for biomass and energy[200]. Supporting this notion, our interrogation of *in vitro* BEC-organoid formation dataset[148] revealed the enrichment of purine and pyrimidine metabolism, as well as the pentose-phosphate pathway (Figure 4.13A), which are tightly connected to glycolysis (see Introduction). In line with these findings, a substrate oxidation test in BEC-organoids revealed a preference for glucose, as reflected by the decrease in maximal respiration, when UK5099, a mitochondrial pyruvate carrier inhibitor, was used (Figures 4.13D, E), while no changes were observed with inhibitors of glutamine (BPTES) and FA (Etomoxir) metabolism (Figure 4.13B, C).

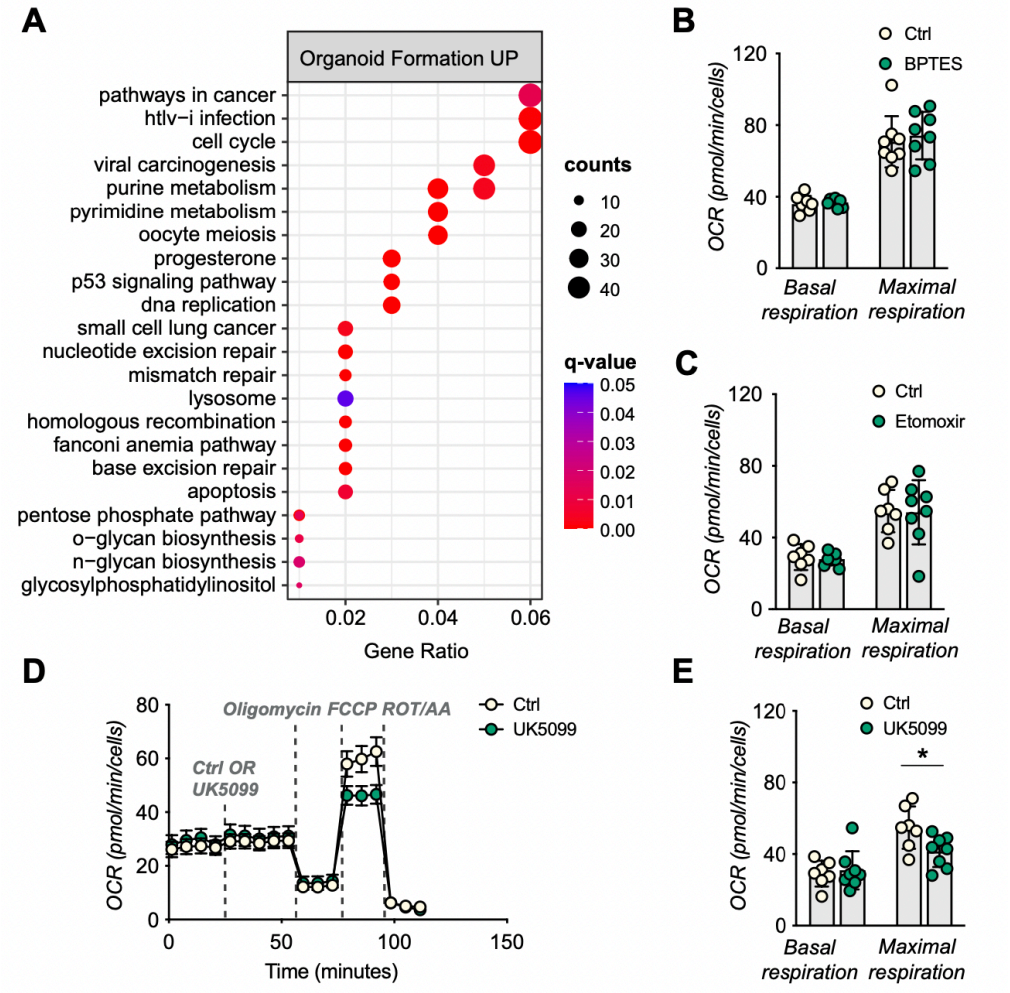

Figure 4.13 BEC-organoids have a glycolytic metabolism.

(A) Over-representation analysis results. Top 22 enriched KEGG and EHMN pathways during the process of organoid formation from single BECs (Organoids vs T0) (GSE123133). q-value: false discovery rate adjusted p-values, counts: number of found genes within a given gene set. **(B-C)** Seahorse substrate oxidation assay using BPTES, n=8 **(B)**, or Etomoxir, n=7 for control (Ctrl) and n=8 for inhibitor conditions **(C)** in CD-derived BEC-organoids. **(D-E)** Seahorse substrate oxidation assay using UK5099, a mitochondrial pyruvate carrier inhibitor **(D)**, and assessment of the glucose dependency **(E)** in CD-derived BEC organoids. n=7 for control (Ctrl), n=8 for UK5099. Data are shown as mean ± SD (SEM for D). Absence of stars or ns, not significant ($p > 0.05$); *$p < 0.05$; two-way ANOVA with Sidak's test (B, C, E) were used.

To investigate the metabolic changes in BEC-organoids upon HFD, we treated CD/HFD BEC-organoids with an FA mix to mimic steatotic conditions in vitro (Figure 4.14A). We hypothesized that the presence of glucose and FA in culture media would reveal a metabolic shift of BEC-organoids. Consistent with our hypothesis, HFD-FA BEC-organoids demonstrated increased compensatory glycolytic rates (Figures 4.14B-D). Of note, there was a reduction in oxidative phosphorylation in HFD-FA BEC-organoids, as evidenced by the decrease in maximal respiration (Figures 4.14E-G), which might reflect their preference for the glycolytic pathway to generate biomass.

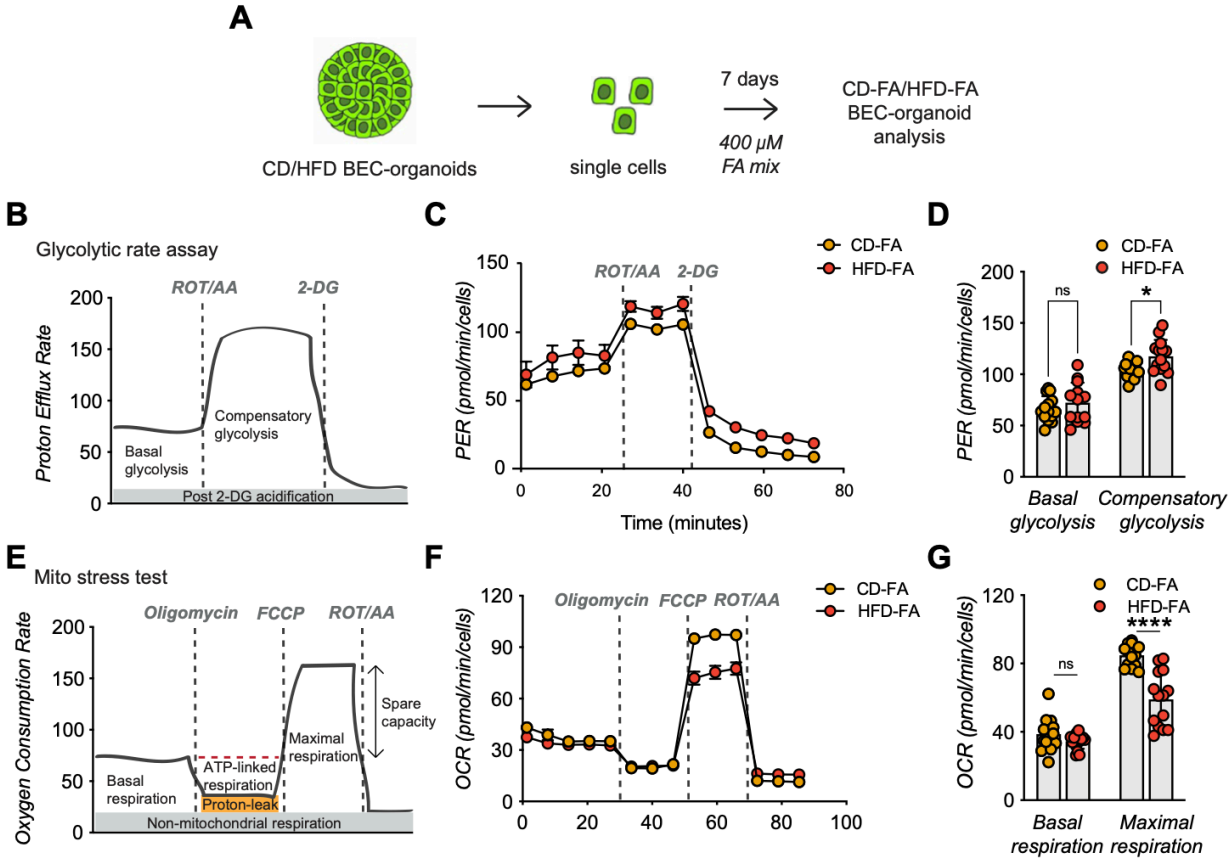

Figure 4.14 HFD-FA BEC-organoids demonstrate a shift towards glycolysis.

(A) Scheme depicting the treatment of CD/HFD-derived BEC-organoids with FA mix. **(B)** Scheme depicting Seahorse glycolytic rate assay. **(C-D)** Proton efflux rate (PER) **(C)** and basal and compensatory glycolysis **(D)** were measured using Seahorse XF glycolytic rate assay. Relative to panel A. n=13. **(E)** Scheme depicting Seahorse mito stress test. **(F-G)** Oxygen consumption rate (OCR) **(F)** and basal and maximal respiration **(G)** were measured using the Seahorse XF mito stress test. Relative to panel A. n=14. Data are shown as mean ± SD (SEM for C, F). Absence of stars or ns, not significant ($p > 0.05$); *$p < 0.05$; ****$p < 0.0001$; two-way ANOVA with Sidak's test (D, G) were used.

Besides their prominent role in cell cycle progression, E2Fs coordinate several aspects of cellular metabolism[201,202], and promote glycolysis in different contexts[203–205]. These findings prompted us to postulate that E2F might control glycolysis and thus the glucose preference observed in BEC-organoids. To investigate this hypothesis, we treated BEC-organoids with an E2F inhibitor, HLM006474 (Figure 4.15A). As expected, HLM006474 treatment reduced the transcriptional levels of several genes involved in cell cycle progression and glycolytic metabolism (Figure 4.15B) and decreased the glycolytic flux, as evidenced by the blunted proton efflux rate (PER) (Figures 4.15C, D). Moreover, E2F inhibition was able to reverse the metabolic phenotype only in HFD-FA BEC-organoids (Figures 4.15A-B).

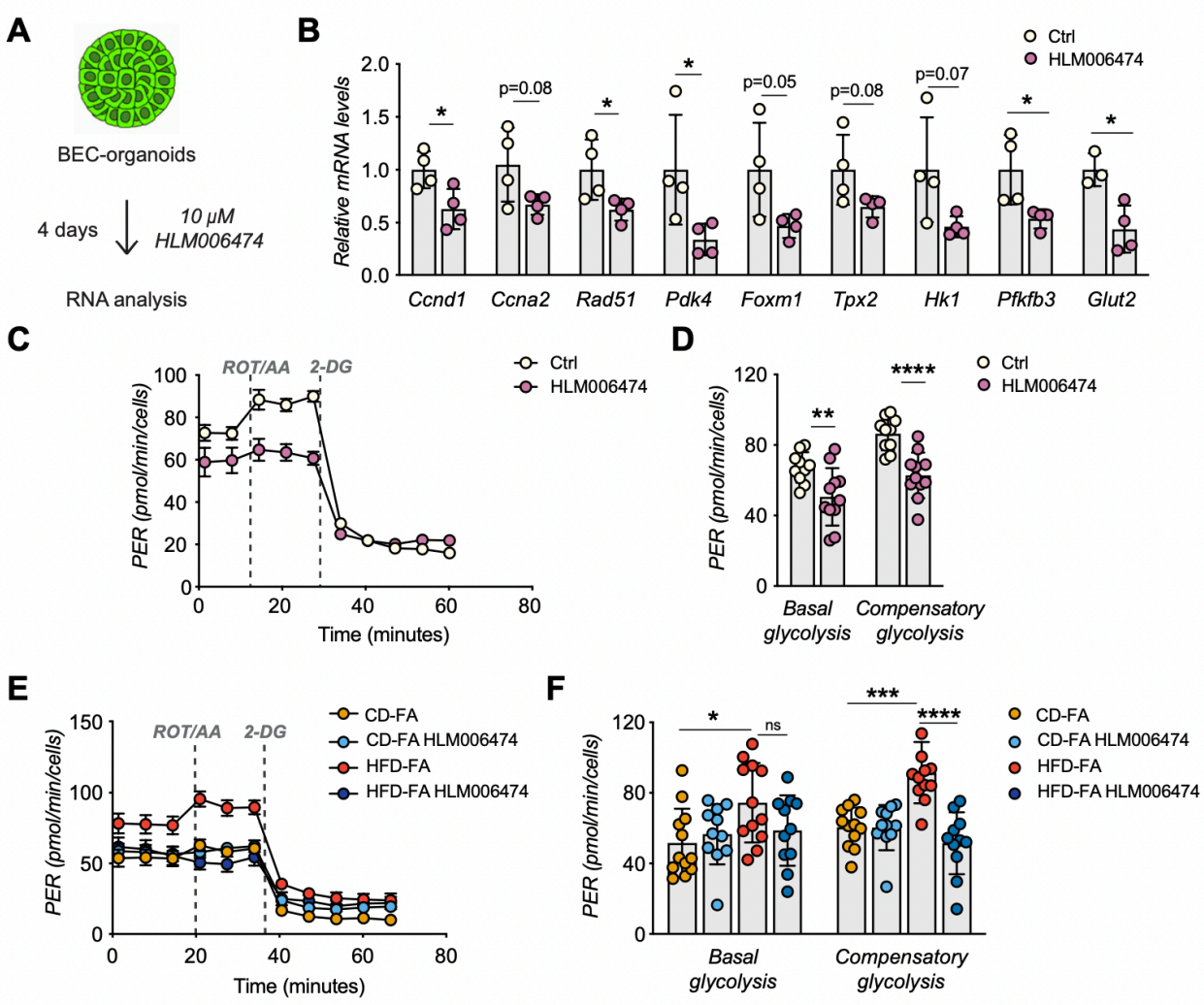

Figure 4.15 E2F inhibition decreases canonical E2F targets and reverses the glycolytic phenotype in HFD-FA BEC-organoids.

(A) Scheme depicting the treatment of CD-derived BEC-organoids with E2F inhibitor, HLM006474. **(B)** RT-qPCR of selected cell cycle and glycolytic genes, relative to panel A. n=4. **(C-D)** PER during the Seahorse XF glycolytic rate assay **(C)**, and basal and compensatory glycolysis **(D)**, relative to panel A. n=10 for control (Ctrl), n=11 for HLM006474. **(E-F)** PER during the Seahorse XF glycolytic rate assay **(E)**, and basal and compensatory glycolysis **(F)**. n=12 for control (Ctrl), n=11 for HLM006474. Data are shown as mean ± SD (SEM for C, E). Absence of stars or ns, not significant ($p > 0.05$); *$p < 0.05$; **$p < 0.01$; ***$p < 0.001$; ****$p < 0.0001$; unpaired, two-tailed Student's t-test (B), two-way ANOVA with Sidak's test (D, F) were used.

In conclusion, these results demonstrate that HFD-induced E2F activation controls the conversion of BECs from quiescent to active stem cells by promoting the expression of cell cycle genes while simultaneously driving a shift towards glycolysis

Chapter 5 Mechano-modular PEG hydrogels unveil the role of liver stiffness on BEC activation

Partially adapted from

Mechano-modulatory synthetic niches for liver organoid derivation. Giovanni Sorrentino[1,†], Saba Rezakhani[2,†], Ece Yildiz[1], Sandro Nuciforo[3], Markus H. Heim[3,4], Matthias P. Lutolf[2,*], Kristina Schoonjans[1,*]. Nature Communications 2020.

†These authors contributed equally to this work.

*Correspondence should be addressed to: M.P.L. (matthias.lutolf@epfl.ch) and K.S. (kristina.schoonjans@epfl.ch).

Author contributions: G.S., S.R., M.L., and K.S. conceived the project and wrote the manuscript. G.S., S.R., and E.Y. planned and performed experiments and analyzed data. S.N. and M.H. provided human biopsy samples and critically revised the manuscript.

5.1 PEG-based synthetic hydrogels for organoid cultures

Despite the enormous potential of organoids as an ex vivo model, there are still some bottlenecks linked to this system when it comes to clinical application. For example, Matrigel, the animal-derived matrix that supports organoid growth, renders organoids unsuitable for cell therapy, as it is an ECM derived from a mouse tumor line and may hold tumorigenic properties. Moreover, due to its origin, it contains various defined and undefined components, including many growth factors, and its composition can show batch-to-batch variability[178]. Thus, new matrices are needed, and synthetic hydrogels are at the forefront of these applications. Among these novel chemical entities, PEG hydrogels[206] are particularly interesting due to their hydrophilicity, user-defined crosslinking chemistry, and integration of ligands for cell adhesion and matrix modelling[206]. Moreover, they have modifiable mechanical properties. As a result, they have been heavily employed for 3D cell culture for cell therapy and regenerative medicine purposes[207–211], thanks to their controllable chemical and mechanical properties[206].

PEG hydrogels for intestinal stem cell culture and organoid derivation have already been used[192,209], and opened the path for the culture of stem cells from different tissues. Especially in the last two years, there have been a handful of advances in the synthetic BEC-organoid cultures incorporating polyisocyanopeptides (PIC)[212], or PEG-gelatin mix[213] with laminin or fibronectin. Moreover, liver fibrosis, an emerging pathological condition, is characterized by the accumulation of abnormal and stiff ECM. Thus, studying how cells within a stiff matrix behave is important to further expand our understanding in terms of disease outcomes and the design of future treatments [214]. In addition to their application for cell therapy and regeneration, synthetic hydrogels can also be used to model the mechanical properties of fibrosis and investigate its outcome on the regenerative potential of BECs.

5.2 Generation of a PEG-based synthetic niche for BEC-organoid cultures

To circumvent the disadvantages of Matrigel, our main goal was to develop a synthetic matrix allowing efficient proliferation and differentiation of biliary stem cells. To achieve this aim, an important criterium was to recapitulate the key physical and biochemical characteristics of the hepatic microenvironment. The liver contains collagen type I, III, IV, V, and VI, laminin, fibronectin, glycosaminoglycans, and proteoglycans, as ECM[215], and the appropriate synthetic hydrogels for BEC-organoid cultures should contain some of these ECM components. Thus, we generated inert PEG hydrogels enzymatically crosslinked by the activated transglutaminase factor XIIIa (FXIIIa) and incorporated them with minimal integrin recognition peptide RGDSPG (Arg-Gly-Asp-Ser-Pro-Gly)[216]. In addition, to mimic the mechanical properties of the mouse liver[217,218], we tuned the stiffness of PEG gels to physiological values (≈1.3 kPa)[216]. Using these conditions, we demonstrated that the PEG-RGD matrix is as efficient as Matrigel for both biliary stem cell expansion and their differentiation into hepatocyte-like cells[216].

5.3 Matrix stiffness controls BEC-organoid growth in an actomyosin-independent manner

Mechanical signals play a critical role in controlling stem cell behavior and tissue homeostasis[219], but also contribute to the manifestation of diseases[219–221], especially of NAFLD[222]. Despite the recent progress in establishing novel 3D liver model systems, relatively little is known about the role of mechanics in regulating biliary stem cell physiology and pathophysiology. To test whether matrix mechanics affect BEC-organoid growth, we grew BEC-organoids in PEG-RGD of variable stiffness, ranging from values below normal mouse liver stiffness (0.3 kPa) to those reaching physiological stiffness (1.3 kPa)[217,218]. Organoid formation efficiency was profoundly affected by the mechanical properties of the matrix, with values mimicking physiological liver stiffness (between 1.3 and 1.7 kPa) being optimal (Figures 5.1A, B).

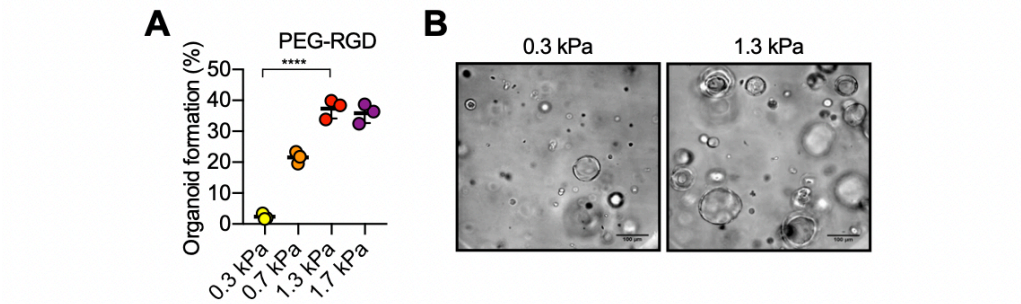

Figure 5.1 PEG-RGD stiffness impacts BEC-organoid formation and proliferation

(A) Effect of matrix stiffness on organoid formation efficiency. **(B)** Representative images of **BEC**-organoids 3 days after embedding in PEG-RGD hydrogels of indicated stiffness. Graphs show individual data points derived from n=3 independent experiments and means ± s.d. ****P<0.0001 one-way Anova. Scale bars, 100 µm (B).

Given the pivotal role of YAP signaling in the transduction of mechanical and cytoskeletal signals[226] and the regulation of BEC expansion during the DR process[112–114,140], we next tested whether YAP activation could control BEC growth and potentially explain the observed matrix stiffness dependence. We monitored the expression of canonical YAP target genes and YAP subcellular localization in BEC-organoids cultured in soft (0.3 kPa) and physiologically stiff (1.3 kPa) matrices. Interestingly, in stiffer PEG-RGD hydrogels, YAP target gene expression and nuclear accumulation were increased compared to soft matrices (Figures 5.2A, B). To examine whether an activated integrin/YAP signaling axis is functionally required for organoid derivation in physiologically-stiff matrices, we treated BEC-organoids with PF-573228 (PF), an inhibitor of the integrin effector focal adhesion kinase (FAK), or with Verteporfin (VP), a YAP inhibitor (Figure 5.2C)[227]. Both treatments prevented the increase in organoid formation induced in stiffer matrices (Figures 5.2D, E), indicating that the integrin/YAP module is required in coordinating the growth of BECs in response to mechanical stimuli.

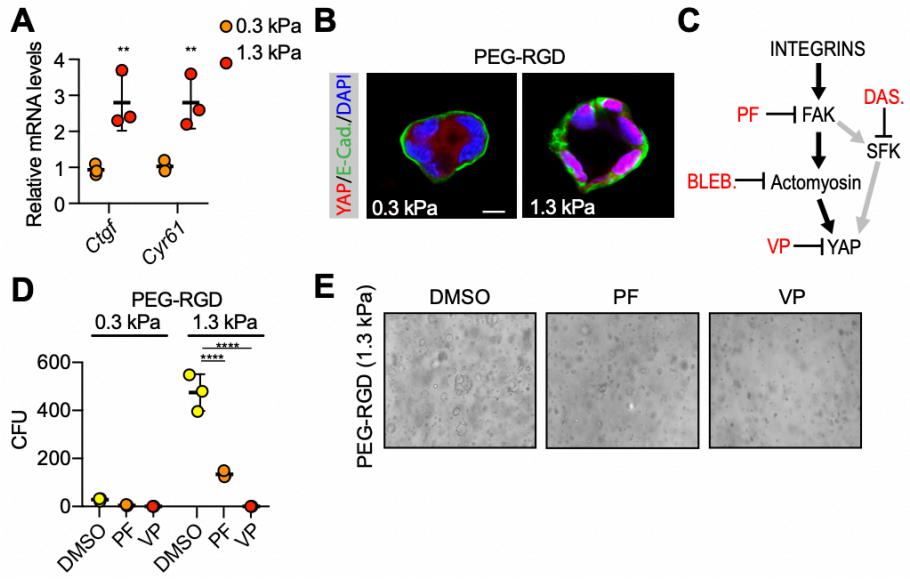

Figure 5.2 Integrin/YAP module controls the BEC-organoid growth in PEG-RGD.

(A) Gene expression was analyzed by qRT-PCR in liver organoids 6 days after embedding in PEG-RGD hydrogels with indicated stiffness. n=3. **(B)** Representative images of YAP subcellular localization in liver organoids 1 day after embedding in soft (0.3 kPa) or physiologically stiff (1.3 kPa) PEG-RGD hydrogels. **(C)** Schematic representation of cellular mechano-signaling pathways. Inhibitors of key elements are depicted in red. **(D)** Effect of indicated inhibitors on organoid formation efficiency in soft (0.3 kPa) and physiologically stiff (1.3 kPa) PEG-RGD hydrogels. CFU (colony forming unit). n=3. **(E)** Representative images of BEC-organoids treated with DMSO, PF, and VP. Data are shown as means ± SD. ns or absence of star, not significant; ** P<0.01; ***P<0.001; unpaired Student's two-tailed t-test (A), two-way ANOVA (D). PF, PF-573228, BLEB, blebbistatin, VP, verteporfin, DAS, dasatinib, SFK, Src family kinase, FAK, focal adhesion kinase, YAP, yes-associated protein.

We then sought to identify the other components of the FAK-YAP cascade that may play a role in modulating the stiffness response in our system. Since remodeling of the actin cytoskeleton has been identified as a key event upstream of YAP activation[228–230], we assessed its putative involvement in physiological stiffness-induced BEC-organoid growth by inhibiting actomyosin contractility with blebbistatin[231]. Of interest, treatment with Dasatinib[232], an FDA-approved SFK inhibitor, fully abolished YAP phosphorylation and organoid growth in physiologically stiff (1.3 kPa) matrices (Figures 5.3A, B). Moreover, tyrosine phosphorylation of YAP by the SFK, an alternative route for integrin-dependent and actomyosin-independent YAP activation[171,233–239], was increased by matrix stiffness (Figure 5.3B). Surprisingly, blebbistatin treatment significantly enhanced organoid formation (Figure 5.3A) with an efficiency comparable to ROCK inhibitors (Figure 5.3C), indicating that matrix stiffness promotes organoid growth independently of cytoskeletal dynamics and actomyosin contractility. These results corroborate the importance of the integrin/SFK/YAP signaling pathway in BEC proliferation in response to differential mechanical inputs.

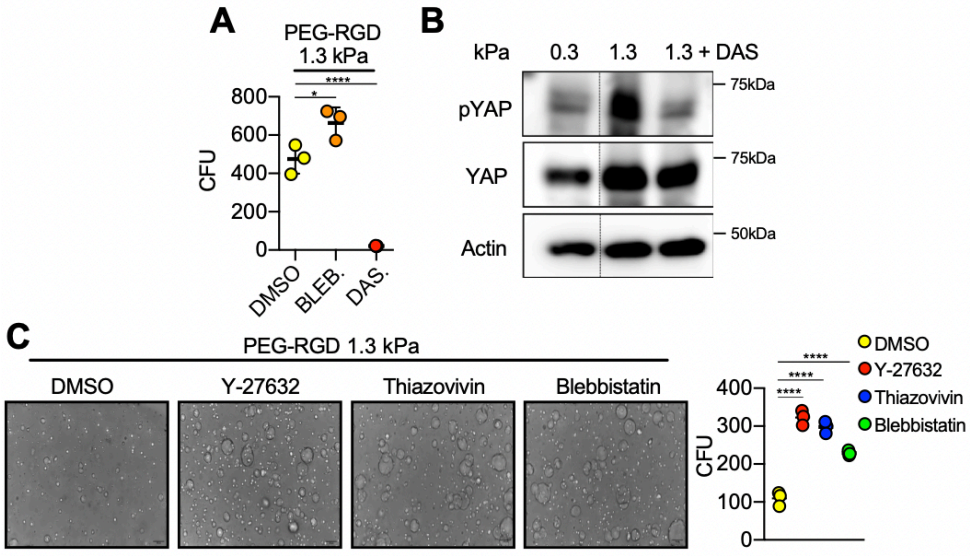

Figure 5.3 Integrin/SFK/YAP signaling controls BEC-organoid growth in PEG-RGD.

(A) Effect of indicated inhibitors on organoid formation efficiency in physiologically stiff (1.3 kPa) PEG-RGD hydrogels. CFU (colony forming unit). n=3. **(B)** Western blot showing YAP phosphorylation in mouse BECs 6 hours after embedding in soft (0.3 kPa) and physiologically stiff (1.3 kPa) PEG-RGD hydrogels with or without DAS treatment. **(C)** Matrigel-derived BECs were embedded in physiologically stiff PEG-RGD hydrogels and cultured in the expansion medium containing ROCK inhibitors (Y-27632 and Thiazovivin) or Blebbistatin. Colony forming units (CFU) were quantified after 3 days. n=3. Data are shown as means ± SD (SEM for C). *P<0.05, ****P<0.0001; one-way ANOVA (A, C). Scale bars, 100 µm. DAS, dasatinib.

5.4 PEG hydrogels can be tuned to model fibrotic liver mechanics

Liver disease progression is strongly associated with abnormal tissue architecture and mechanotransduction[217,240,241]. In NAFLD patients with fibrosis, as a direct effect of aberrant ECM deposition, liver stiffness increases in time and severely compromises its function[242–245]. As a result, the changes in liver stiffness associated with NAFLD are used for diagnostics based on longitudinal non-invasive monitoring[52,53,55,246]. We reasoned that BEC-organoids grown in defined PEG-RGD hydrogels recapitulating the stiffness of fibrotic liver could serve as a relevant 3D model to investigate how stem cells translate aberrant mechanical inputs into disease-relevant phenotypes. To this aim, we generated fibrosis-mimicking hydrogels with a stiffness of 4 kPa[217,218]. Strikingly, these hydrogels led to a significant impairment of organoid formation (Figures 5.4A, B), demonstrating that an abnormal ECM stiffness is sufficient to decrease the liver stem cell proliferative capacity and the expression of hepatic stem cell markers (Figure 5.4C, D).

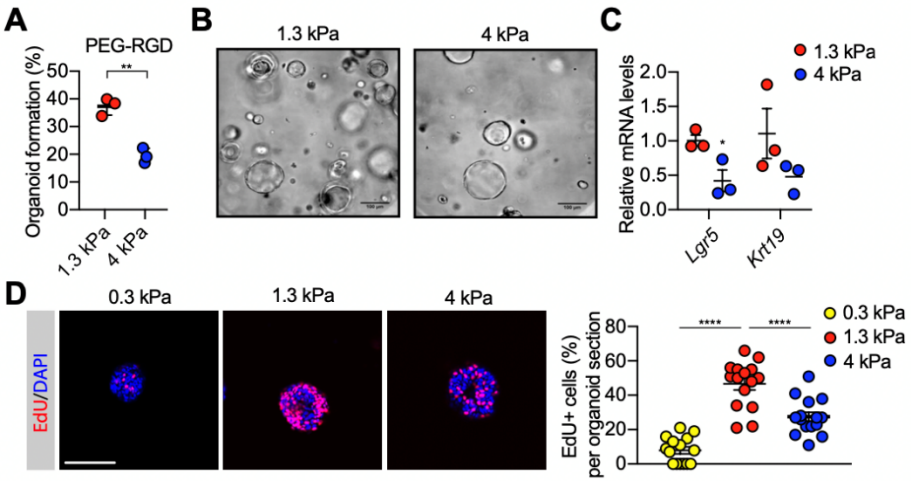

Figure 5.4 BEC-organoid formation is altered in fibrosis-mimicking PEG-RGD.

(**A)** Effect of matrix stiffness on organoid formation efficiency. n=3. **(B)** Representative image of organoids 3 days after embedding in PEG-RGD hydrogels of indicated stiffness. (**C)** Gene expression was analyzed by qRT-PCR in liver organoids 6 days after embedding in PEG-RGD hydrogels with indicated stiffness. n=3. **(D)** Representative images of EdU staining of BEC-organoids, 3 days after embedding in PEG-RGD hydrogels with indicated stiffness. Data are shown as means ± SEM (A, C, D). *P<0.05, ** P<0.01, ****P<0.0001; unpaired Student's two-tailed t-test (A), two-way ANOVA (C) or one-way ANOVA. Scale bars: 100 µm (B, D).

Furthermore, BEC-organoids cultured in a hyper-stiff matrix showed an upregulation of genes involved in the cellular response to hepatic injury (Figures 5.5A, B), indicating that the reduced stemness potential (Figure 5.4) is associated with concomitant induction of a stress response. Finally, fibrosis-mimicking hydrogels led to an increase in the expression of matrix metalloproteases (Figure 5.5C), a compensatory phenomenon known to be induced in response to increased ECM stiffness[247–249]. Surprisingly, in these conditions, YAP activation was not affected (Figure 5.5D), suggesting the existence of other pathways controlling liver stem cell growth in response to increased stiffness. These results suggest that synthetic hydrogels may be a useful tool to assess the contribution of mechanical inputs to NAFLD and other liver diseases.

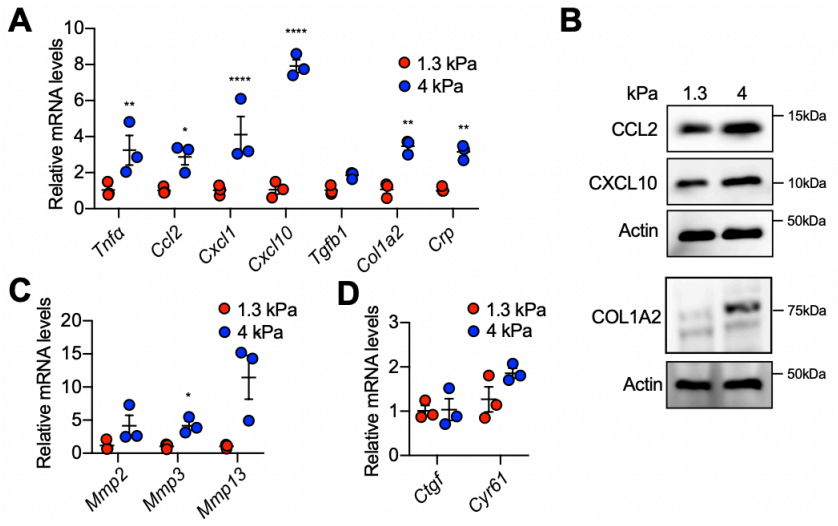

Figure 5.5 Fibrosis-mimicking PEG-RGD alters the phenotype of BEC-organoids.

(**A)** Gene expression was analyzed by qRT-PCR in BEC-organoids 6 days after embedding in PEG-RGD hydrogels with indicated stiffness. n=3. **(B)** Western blot of BECs 6 days after embedding in PEG-RGD hydrogels with indicated stiffness. **(C-D)** Gene expression was analyzed by qRT-PCR in

BWC-organoids 6 days after embedding in PEG-RGD hydrogels with indicated stiffness. n=3. Data are shown as means ± SEM (A, C, D). ns or absence of stars, not significant; *P<0.05; ** P<0.01; ****P<0.0001; two-way ANOVA (A, C, D).

5.5 Human BEC-organoids derived from fibrotic livers mimic the BEC phenotype in stiff PEG hydrogels

To further increase the relevance of our findings, we used publicly available mRNA expression profiling data of BEC-organoids derived from advanced NASH patients with fibrosis and healthy controls (GSE180882)[250], and performed a differential expression analysis that revealed 708 and 567 significantly upregulated and downregulated genes, respectively (Figure 5.6A). Of note, the top differentially expressed genes were downregulated (*mKi67*, *Top2a, Cenpf*, *Cdk1,* and *Rrm2*) and were master regulators of cell cycle and DNA synthesis, suggesting a decreased BEC proliferation and expansion in NASH. To further explore these transcriptional changes, we performed a gene set enrichment analysis (GSEA) using Gene Ontology (GO) terms and found that in the top 15 pathways, there were only downregulated biological processes associated with cell cycle and DNA replication (Figure 5.6B). These unexpected results are in line with the reduced proliferation of BECs in stiff PEG-RGD hydrogels (Figure 5.4) and highlight that the effect of the fibrosis-mimicking stiff environment on BEC-organoid formation is preserved in NASH BECs *in vivo*.

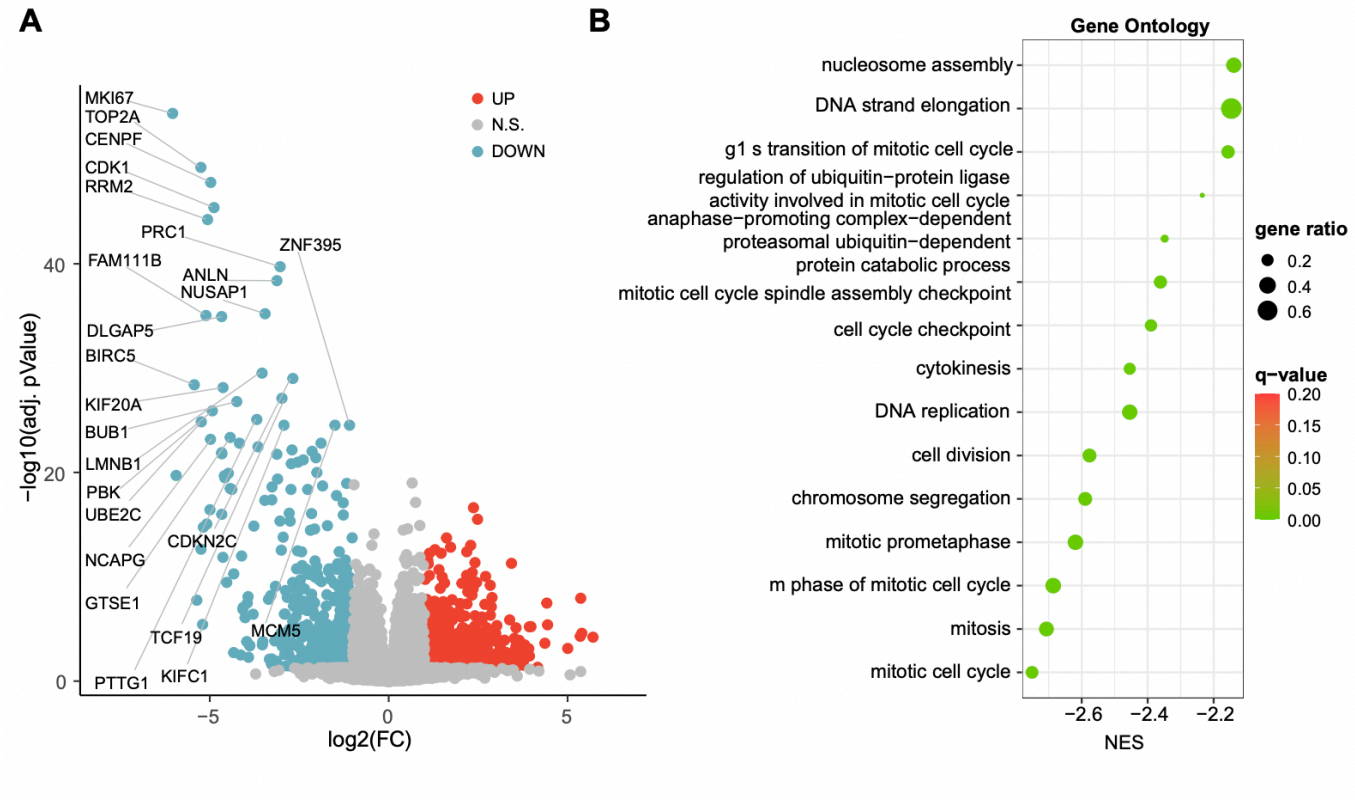

Figure 5.6 Cell cycle is significantly perturbed in NASH BEC-organoids.

(A) Volcano plot of NASH vs control BEC-organoids differential expression analysis. The 24 top differentially expressed genes were labeled. Blue dots represent downregulated genes (log2(FC) < -1 & adj. p-value < 0.05). Red dots represent upregulated genes (log2(FC) > 1 & adj. p-value < 0.05). Grey dots represent genes not changing significantly. **(B)** Gene set enrichment analysis (GSEA) of Gene Ontology (GO) terms. Top 15 pathways, ordered by NES. q-value: false discovery rate adjusted p-values. NES: normalized enrichment score.

Additional analysis of the same dataset with KEGG and Hallmark (Figures 5.7A, B) revealed a decrease in mTORC1 signaling, an established regulator of DR[113], further supporting the initial observation that BEC expansion was prevented in NASH BEC-organoids (Figure 5.7B). Moreover, we identified the downregulation of E2F targets and glycolysis (Figure 5.7B), supporting our previous results (Chapter 4) and increasing the relevance of these TFs as previously uncharacterized modulators of the BEC phenotype during NAFLD progression.

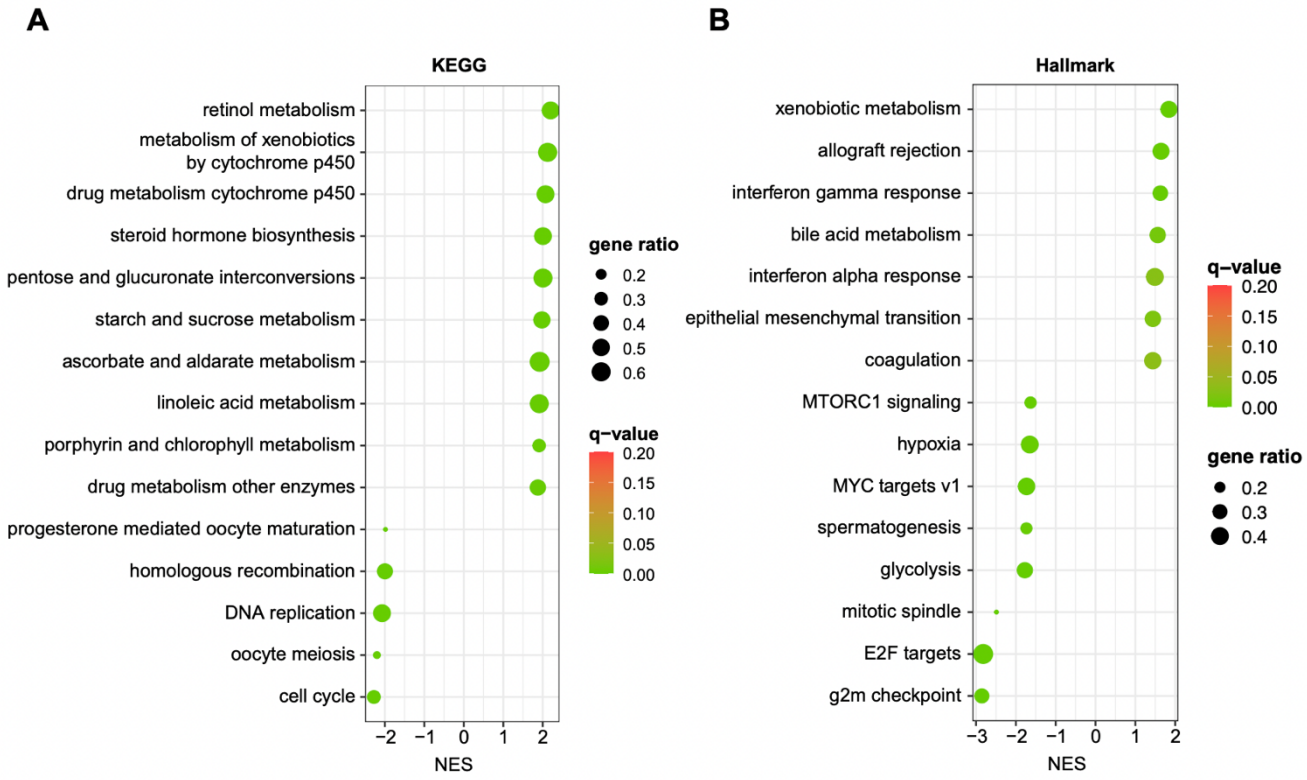

Figure 5.7 NASH BEC-organoids have alterations in metabolism and cell cycle.

(A-B) Gene set enrichment analysis (GSEA) of KEGG **(A)** and Hallmark **(B)** terms. Top 15 pathways, ordered by NES. q-value: false discovery rate adjusted p-values. NES: normalized enrichment score.

On the other hand, our GSEA analysis revealed a significant upregulation in cytokine-receptor interactions (Figure 5.7A) and interferon-gamma response (Figure 5.7B), suggesting an increased immune response. These results once more mirrored our observations in pathologically stiff PEG-RGD hydrogels (Figures 5.4, 5.5). Moreover, the analysis of the upregulated pathways revealed the xenobiotic metabolic process, bile acid metabolism, and retinol metabolism (Figures 5.7A, B), which reflect specific functions of differentiated hepatocytes. In conclusion, this preliminary analysis demonstrates that NASH halts BEC expansion while simultaneously promoting hepatocyte-like features, indicating the loss of stem cell properties *in vivo*, which is kept in BEC-organoid culture.

Chapter 6 Conclusion and perspectives

6.1 Achieved results

NAFLD is an emerging cause of end-stage liver disease worldwide and is estimated to increase 2-3-fold by 2030. Despite this rather pessimistic forecast, no effective treatments are available, and liver transplantations, limited by organ shortages, remain the only option. Moreover, HCC caused by NAFLD significantly increased over the years[251], emphasizing the need for a better understanding of NAFLD and the development of novel treatments. One approach to gain further insight into the pathology of NAFLD is to study the behavior of BECs during the different stages of NAFLD development. BECs are a good candidate as they lie at the intersection of liver regeneration and pathophysiology, and represent an essential reservoir of stem cells crucial for coordinating hepatic epithelial regeneration in the context of chronic liver diseases by triggering the so-called DR reaction[153–160]. However, until now, knowledge of the mechanisms underlying BEC activation and DR in NAFLD progression is limited. Therefore, the work of my thesis focused on identifying and characterizing these mechanisms to gather new knowledge that could form the basis of future therapies centered on enhancing stem cell-mediated liver regeneration.

To achieve these goals, I started by investigating the BEC phenotype upon steatosis, the initial stage of NAFLD. Aberrant lipid accumulation is a hallmark of early NAFLD, and imbalances in lipid metabolism are known to affect hepatocyte homeostasis, including the induction of lipotoxicity and cell death[252–256]. However, the role of lipid dysregulation in BECs and its impact on DR initiation remains unexplored in the context of NAFLD. Here, using an HFD-fed mouse model, I first characterized BECs *in vivo* and demonstrated that these cells can accumulate lipids but are resistant to lipid-induced toxicity. To fully understand the molecular changes induced by lipid overload in these primary $EPCAM^+$ BECs, I characterized their transcriptome and observed significant changes occurring during HFD compared to the CD control condition. Of note, the HFD model used in this study was not associated with inflammation, fibrosis, or overt hepatocyte damage, suggesting that lipids alone are sufficient to alter the phenotype of BECs. The most significant upregulated signature in HFD-derived BECs was cell cycle and DNA replication, which was associated with an increase in EdU^+ and $Ki67^+$ BECs in liver sections from HFD-fed mice. BECs have previously been shown to serve as a cell source for regenerative cellular expansion via the DR process when hepatocyte replication is impaired in chronic liver injury[153–160]. My results demonstrated that BEC activation however may already occur before this event and emerge after chronic lipid exposure, adding another layer of complexity to the chronology of DR initiation in chronic liver disease and extending the therapeutic potential of BECs to an earlier NAFLD stage.

BEC proliferation and activation is a pathophysiological marker of DR[125,134]. It is known that BEC activation is tightly controlled by the transcriptional co-activator YAP[257–259], and previous studies have demonstrated that YAP activation is required for DR in fibrotic livers but does not occur in steatosis in the context of NAFLD[140], leaving the early molecular mechanisms of BEC activation and DR unexplored. To understand whether the mechanisms underlying BEC activation by HFD in vivo involve already established canonical DR processes, I compared the transcriptional profile of BECs upon HFD with publicly available well-studied DDC-induced DR datasets[112,148] (GSE125688 and GSE123133). The common transcriptional changes between the two conditions not only suggested that the mechanisms of BEC activation induced by lipid overload overlap with those induced by biliary epithelial damage but also revealed the concomitant enrichment of 4 TFs, E2F1-4, that have not been linked to DR previously. E2Fs comprise a family of TFs, which are well known for their function in cell cycle progression, DNA synthesis, and cellular proliferation[260]. Of note, among the 4 E2Fs, E2F1 had the most enriched target genes in our analysis. To further validate its implication in the regulation of HFD-induced DR, we used an $E2f1^{-/-}$ mouse model and analyzed BEC proliferation in the liver. While BEC proliferation was not different in CD, HFD-feeding triggered a significant BEC expansion in $E2f1^{+/+}$ mice, and this phenotype was blunted in mice lacking E2F1. These data consolidate the important role of E2F1 in driving lipid-mediated activation of BECs upon HFD feeding and feature E2F1 as an essential mediator of DR in the first stages of NAFLD progression, a condition in which the well-known modulator of DR, YAP[112–114], is dispensable.

Since BEC organoids mirror the DR process *in vitro*[184], this system can be used as a model to study BEC activation. By using BEC-organoids, I demonstrated that FAs directly target BECs, without any involvement of hepatocytes and that BECs functionally respond to lipid overload. Moreover, to functionally assess the impact of lipid overload on BEC regenerative capacity, I measured the organoid forming capacity of isolated BECs from CD- and HFD-fed mouse livers and observed that HFD-derived BECs were significantly more efficient in organoid proliferation than their CD counterparts. Considering that specific metabolic states play instructive roles in controlling cell fate and tissue regeneration[261–264], and the prominent role of E2Fs in metabolic regulation[196–199,201–205], I investigated the metabolism of BEC-organoids and demonstrated a shift towards glycolysis. These findings demonstrated for the first time that BECs are affected by steatosis, and their physiological response to the environment with lipid overload can be an initiating factor for the early DR process. Moreover, activation of E2Fs allows BECs to exit from a quiescent state and the simultaneous acquisition of stem cell functions, such as proliferation and organoid-initiating capacity, through metabolic adaptation.

Besides characterizing the impact of lipid overload on BEC functionality, I also investigated how BECs respond to changes in the stiffness of the microenvironment, which is an important hallmark in fibrosis[46,53,78,221,240–243] in the context of NAFLD. To study the microenvironment stiffness, I used a synthetic PEG-RGD hydrogel with tunable stiffness and demonstrated that BEC-organoids change their growth capacity depending on the rigidity of the matrix. Firstly, by growing BEC-organoids in the hydrogel of variable stiffness

ranging from values below the normal mouse liver stiffness (0.3 kPa) to those reaching physiological stiffness (1.7 kPa)[265,266], I showed that organoid formation efficiency and proliferation were optimal in values mimicking physiological liver stiffness (between 1.3 and 1.7 kPa) and were comparable to Matrigel cultures. YAP is crucial in the transduction of mechanical cues[267]. In line with the pivotal role of YAP in BEC activation, I found that in physiologically stiff hydrogels, YAP nuclear accumulation and transcriptional activity were increased compared to soft matrices. Further analysis with a series of inhibitors indicated that the activation of the integrin-SFK-YAP pathway is required to elicit BEC expansion in response to mechanical stimuli[216]. These findings align with the previous DR studies in BECs[112–114], and highlight the importance of YAP for DR and BEC expansion in response to changes in ECM mechanical cues, even though its activation is not required in steatosis.

Similar to soft gels, the pathologically stiff PEG-RGD profoundly impaired organoid formation and proliferation. Considering that DR has been especially observed in the late-stage NAFLD patients with fibrosis and portal inflammation[125,139,141], I leveraged the modularity of synthetic matrices to recapitulate the liver fibrotic microenvironment in NAFLD and used this configuration to study DR in BEC-organoids. As a result, I provided evidence that aberrant stiffness negatively impacts the organoid formation capacity and proliferation of biliary stem cell. The significance of the role of fibrotic-mimicking matrix stiffness on the BEC phenotype was supported by a decreased proliferative capacity and by an increase of markers of inflammation, hepatic injury, and matrix metalloproteases. Surprisingly, in these conditions, YAP activation was not affected, suggesting the existence of other pathways controlling BEC growth in response to increased stiffness. To understand the relevance of the BEC phenotype in the pathologically stiff hydrogels to NASH *in vivo*, I compared the publicly available datasets of BEC-organoids derived from healthy and advanced NASH patients with severe fibrosis (GSE180882). This analysis highlighted that NASH BEC-organoids had reduced cell cycle and DNA replication compared to healthy controls, revealing that hydrogels with fibrotic stiffness mimic the phenotype of organoids derived from fibrotic livers. Moreover, in NASH BEC-organoids, E2F targets were downregulated, suggesting that E2F inhibition may also contribute to the regulation of late DR and constitute a previously unrecognized TF family that controls BEC proliferation throughout the progression of NAFLD.

In conclusion, the experiments conducted in this thesis unveiled a critical role of BECs in the initiation and maintenance of DR in the context of NAFLD. These findings set the ground for future research aimed at understanding the role and the therapeutic potential of E2Fs in controlling BEC activation, thus initiating DR in humans. Moreover, the results obtained with the use of PEG-RGD hydrogels that mimic the aberrant mechanical properties of the fibrotic liver provide evidence that abnormal liver stiffness negatively impacts BEC proliferation and instead induces an inflammatory phenotype, thus hindering the regenerative potential of fibrotic livers. These findings highlight that the BEC phenotype in DR may depend on the NAFLD stage and suggest that even though the proliferation of BECs characterizes DR, BEC exhaustion can occur especially in the fibrotic stage, which would correlate with liver failure. Moreover, our results not only further increase the

translational relevance of BECs through the use of a clinically compatible synthetic matrix instead of Matrigel, but also provide useful tools to assess the contribution of mechanical and metabolic inputs to liver diseases, which may enable the development of powerful DR models and future therapeutics to enhance stem cell-mediated liver regeneration.

6.2 Future outlook

In this doctoral work, I discovered that lipid exposure of BECs unleashes their activation and initiates the DR in the livers of HFD-fed animals. Integrative molecular, cellular and metabolic profiling demonstrated that lipid overload is sufficient to induce BEC activation in steatotic livers, placing BECs as sensors and possibly effectors in the initial NAFLD progression. Contrary to the previous understanding that DR occurs when hepatocyte replication is impaired in chronic liver injury, BEC activation preceded parenchymal damage, thus resolving a long-lasting debate on the chronology of DR initiation in chronic liver diseases. In addition to the increased cell cycle and DNA replication, our RNA sequencing analysis revealed alterations in cell-ECM interactions of $EPCAM^+$ BECs after HFD feeding, as suggested by the downregulation of ECM organization (Figure 4.7). Indeed, ECM remodeling is an important factor in NAFLD pathology[243,268,269], and could significantly impact BEC biology. In addition to downregulated cell-ECM binding through collagen (Figure 4.10), we identified another ECM receptor, hyaluronan-mediated motility receptor (*Hmmr*), which is an important driver of liver fibrosis[270], to be upregulated upon HFD. Interestingly, cell-to-cell connections through E-cadherin may also regulate BEC activation as loss of E-cadherin causes liver fibrosis in sclerosing cholangitis[271]. It is hence conceivable that these additional ECM proteins could also contribute to BEC activation and emerge as novel markers for early DR. Further investigations will be required to corroborate this possibility.

Cellular lipid components mediate the activation of transcription factors, highlighting the link between lipid composition and transcriptional programs. The changes in lipid composition occur in numerous diseases, such as cancer[272] or type 2 diabetes[273]. Since the first demonstration that cholesterol depletion results in SREBP activation and increase of its target genes[274], other pathways, including fatty acid regulation of PPARs[261,275], oxysterol regulation of LXR[276], and bile acid regulation of FXR[277]. Moreover, lipids are important components of the cell membrane[278], and recent studies demonstrated that specific sphingolipid composition in the cell membrane also plays instructive roles in controlling cell fate and tissue regeneration through FGF2[262]. Thus, further studies are warranted to investigate the impact of HFD feeding on the lipidome of $EPCAM^+$ BECs, as our data only show an increase in lipid droplets and TGs, without characterizing changes at the levels of specific lipid species.

Several molecular signaling pathways involving YAP[112–114], mTORC1[259], TET1-mediated hydroxymethylation[184], and NCAM1[279] have been reported to drive BEC activation in late DR. Interestingly, our RNA sequencing analysis highlighted a previously unrecognized E2F-mediated mechanism for BEC activation in steatosis, and genomic removal of the *E2f1* locus was sufficient to prevent BEC activation upon HFD. Given that

E2F is a group of genes that encodes a family of transcription factors (three activators, six repressors), how other E2Fs contribute to BEC activation remains uninvestigated. Furthermore, how E2Fs are regulated upon HFD and whether they are interconnected with the already known YAP, mTORC1, and TET1 pathways will require further investigation. Given that E2Fs were listed as binding targets of the DNA-demethylation factor TET1 in a bioinformatics analysis in DR upon DDC[148], further assessment of the extent of epigenetic remodeling may uncover additional molecular phenotypes in BECs induced by HFD. Moreover, in NAFLD, while mitochondrial function, ATP synthesis, and ketogenesis are impaired, glycolysis and the TCA cycle were shown to increase to generate sufficient energy and building blocks for cellular anabolism[70,74,78,80]. Some intermediates of the TCA cycle, such as α-ketoglutarate (α-KG), are substrates of chromatin-modifying enzymes, including the TET1-3[280]. Considering that TET1 was shown to regulate DR[148], investigating the TCA cycle intermediates by targeted metabolomics might reveal the relationship between FA overload and cellular reprogramming during BEC activation.

Liver disease progression is strongly associated with fibrosis, a direct effect of aberrant ECM deposition and mechanotransduction[217,240,241]. YAP activation is considered a driver of liver fibrosis[140,281–284] and an important pathway controlling BEC activation during late DR[112–114]. BEC-organoid proliferation closely mimics DR *in vitro*[148], and using this model, I demonstrated that BEC-organoid growth strongly depends on YAP signaling for mechanotransduction in synthetic hydrogels with physiological stiffness but no longer in PEG-RGD hydrogels with fibrotic stiffness[216]. As a result, it would be interesting to perform drug and small molecule screening on BEC-organoids in PEG-hydrogels with fibrotic stiffness to identify new signaling pathways and targets for reversing their regenerative capacities and potentially liver fibrosis. Even though the biological importance of the recovered regenerative capacity should ultimately be demonstrated *in vivo*, this experimental setup could significantly advance the field and shortlist molecules that could counteract the progression of fibrosis and/or promote the regeneration and healing of damaged tissue.

Evidence suggests that, in addition to regeneration, DR can contribute to inflammation, fibrosis, and EMT[150] during chronic diseases. Although the studies described in this thesis have helped in gaining insight into the BEC phenotype (proliferation) during NAFLD progression, tamoxifen-induced lineage tracing experiments[285] using KRT19 (e.g. $Krt19^{Cre}TdTomato^{LSL}$ reporter mouse[128]) and OPN (e.g. OPN-$iCreER^{T2}$;$ROSA26R^{YFP}$ reporter mouse[286]) markers would allow further investigation of the functional contribution of lipid-activated BECs in liver regeneration during the late stages of NAFLD and address the functional significance of DR. Furthermore, how the regulation of BEC proliferation affects liver function, and regeneration would provide a clinical setting to investigate BEC activation during disease progression.

Synthetic hydrogels are important for clinical applications as they lack animal-derived material for culture derivation. Considering that BEC-organoid culture in PEG-hydrogels is suitable for clinical application, one could question whether they can be transplanted. In this context, it is noteworthy that two studies recently demonstrated that BEC-organoids cultured in laminin 1 (suitable for clinical applications) could engraft and

repair bile ducts in a mouse model of biliary disease[180], and perfused human livers[287]. Since this explant was performed in diseased human donor livers undergoing *ex vivo* perfusion, further investigation will be needed to confirm if the same approach works in patients with dysfunctional or damaged bile canaliculi. Finally, as previously demonstrated with BEC-organoids from murine origin[143,172], the potential to transplant human BEC-organoids in patients with fibrosis and rescue hepatic function should be tested in the future. If successful, these studies would constitute a breakthrough in the field of liver regeneration.

References

1. Campbell, I. Liver: metabolic functions. *Anaesthesia & Intensive Care Medicine* **7**, 51–54 (2006).

2. Rui, L. Energy Metabolism in the Liver. in *Comprehensive Physiology* (ed. Terjung, R.) 177–197 (Wiley, 2014). doi:10.1002/cphy.c130024.

3. Chiang, J. Y. L. Bile Acid Metabolism and Signaling. in *Comprehensive Physiology* (ed. Terjung, R.) 1191–1212 (Wiley, 2013). doi:10.1002/cphy.c120023.

4. Perino, A., Demagny, H., Velazquez-Villegas, L. & Schoonjans, K. Molecular Physiology of Bile Acid Signaling in Health, Disease, and Aging. *Physiol Rev* **101**, 683–731 (2021).

5. Hodges, R. E. & Minich, D. M. Modulation of Metabolic Detoxification Pathways Using Foods and Food-Derived Components: A Scientific Review with Clinical Application. *Journal of Nutrition and Metabolism* **2015**, 1–23 (2015).

6. Grant, D. M. Detoxification pathways in the liver. *J Inherit Metab Dis* **14**, 421–430 (1991).

7. Gao, B., Jeong, W.-I. & Tian, Z. Liver: An organ with predominant innate immunity. *Hepatology* **47**, 729–736 (2007).

8. Malik, R., Selden, C. & Hodgson, H. The role of non-parenchymal cells in liver growth. *Seminars in Cell & Developmental Biology* **13**, 425–431 (2002).

9. Stanger, B. Z. Cellular Homeostasis and Repair in the Mammalian Liver. *Annu. Rev. Physiol.* **77**, 179–200 (2015).

10. Trefts, E., Gannon, M. & Wasserman, D. H. The liver. *Current Biology* **27**, R1147–R1151 (2017).

11. Tabibian, J. H., Masyuk, A. I., Masyuk, T. V., O'Hara, S. P. & LaRusso, N. F. Physiology of cholangiocytes. *Compr Physiol* **3**, 541–565 (2013).

12. Poisson, J. *et al.* Liver sinusoidal endothelial cells: Physiology and role in liver diseases. *Journal of Hepatology* **66**, 212–227 (2017).

13. Connolly, M. K. *et al.* In Hepatic Fibrosis, Liver Sinusoidal Endothelial Cells Acquire Enhanced Immunogenicity. *J.I.* **185**, 2200–2208 (2010).

14. Ding, B.-S. *et al.* Inductive angiocrine signals from sinusoidal endothelium are required for liver regeneration. *Nature* **468**, 310–315 (2010).

15. Yin, C., Evason, K. J., Asahina, K. & Stainier, D. Y. R. Hepatic stellate cells in liver development, regeneration, and cancer. *J. Clin. Invest.* **123**, 1902–1910 (2013).

16. Mederacke, I. *et al.* Fate tracing reveals hepatic stellate cells as dominant contributors to liver fibrosis independent of its aetiology. *Nat Commun* **4**, 2823 (2013).

17. Roberts, R. A. *et al.* Role of the Kupffer Cell in Mediating Hepatic Toxicity and Carcinogenesis. *Toxicological Sciences* **96**, 2–15 (2006).

18. Dixon, L. J., Barnes, M., Tang, H., Pritchard, M. T. & Nagy, L. E. Kupffer Cells in the Liver. in *Comprehensive Physiology* (ed. Terjung, R.) 785–797 (Wiley, 2013). doi:10.1002/cphy.c120026.

19. Ishibashi, H., Nakamura, M., Komori, A., Migita, K. & Shimoda, S. Liver architecture, cell function, and disease. *Semin Immunopathol* **31**, 399–409 (2009).

20. Aizarani, N. *et al.* A human liver cell atlas reveals heterogeneity and epithelial progenitors. *Nature* **572**, 199–204 (2019).

21. MacParland, S. A. *et al.* Single cell RNA sequencing of human liver reveals distinct intrahepatic macrophage populations. *Nat Commun* **9**, 4383 (2018).

22. Payen, V. L. *et al.* Single-cell RNA sequencing of human liver reveals hepatic stellate cell heterogeneity. *JHEP Reports* **3**, 100278 (2021).

23. Su, Q. *et al.* Single-cell RNA transcriptome landscape of hepatocytes and non-parenchymal cells in healthy and NAFLD mouse liver. *iScience* **24**, 103233 (2021).

24. Andrews, T. S. *et al.* Single-Cell, Single-Nucleus, and Spatial RNA Sequencing of the Human Liver Identifies Cholangiocyte and Mesenchymal Heterogeneity. *Hepatology Communications* **6**, 821–840 (2022).

25. Fuchs, C. D. & Trauner, M. Role of bile acids and their receptors in gastrointestinal and hepatic pathophysiology. *Nat Rev Gastroenterol Hepatol* **19**, 432–450 (2022).

26. Bhatia, S. N., Underhill, G. H., Zaret, K. S. & Fox, I. J. Cell and tissue engineering for liver disease. *Sci Transl Med* **6**, 245sr2 (2014).

27. Manco, R. & Itzkovitz, S. Liver zonation. *Journal of Hepatology* **74**, 466–468 (2021).

28. Gebhardt, R. Liver zonation: Novel aspects of its regulation and its impact on homeostasis. *WJG* **20**, 8491 (2014).

29. Annunziato, S. & Tchorz, J. S. Liver zonation—a journey through space and time. *Nat Metab* **3**, 7–8 (2021).

30. Anundi, I., Lähteenmäki, T., Rundgren, M., Moldeus, P. & Lindros, K. O. Zonation of acetaminophen metabolism and cytochrome P450 2E1-mediated toxicity studied in isolated periportal and perivenous hepatocytes. *Biochemical Pharmacology* **45**, 1251–1259 (1993).

31. Halpern, K. B. *et al.* Single-cell spatial reconstruction reveals global division of labour in the mammalian liver. *Nature* **542**, 352–356 (2017).

32. Oosterveer, M. H. & Schoonjans, K. Hepatic glucose sensing and integrative pathways in the liver. *Cell. Mol. Life Sci.* **71**, 1453–1467 (2014).

33. Morio, B., Panthu, B., Bassot, A. & Rieusset, J. Role of mitochondria in liver metabolic health and diseases. *Cell Calcium* **94**, 102336 (2021).

34. Mansouri, A., Gattolliat, C.-H. & Asselah, T. Mitochondrial Dysfunction and Signaling in Chronic Liver Diseases. *Gastroenterology* **155**, 629–647 (2018).

35. Buchakjian, M. R. & Kornbluth, S. The engine driving the ship: metabolic steering of cell proliferation and death. *Nat Rev Mol Cell Biol* **11**, 715–727 (2010).

36. Younossi, Z. M. *et al.* The economic and clinical burden of nonalcoholic fatty liver disease in the United States and Europe. *Hepatology* **64**, 1577–1586 (2016).

37. Byrne, C. D. & Targher, G. NAFLD: A multisystem disease. *Journal of Hepatology* **62**, S47–S64 (2015).

38. Fan, J.-G., Kim, S.-U. & Wong, V. W.-S. New trends on obesity and NAFLD in Asia. *Journal of Hepatology* **67**, 862–873 (2017).

39. Wu, L.-M. *et al.* Associations between obesity and metabolic health with nonalcoholic fatty liver disease in elderly Chinese. *Hepatobiliary & Pancreatic Diseases International* **19**, 252–257 (2020).

40. Burra, P., Becchetti, C. & Germani, G. NAFLD and liver transplantation: Disease burden, current management and future challenges. *JHEP Reports* **2**, 100192 (2020).

41. Younossi, Z. *et al.* Global burden of NAFLD and NASH: trends, predictions, risk factors and prevention. *Nat Rev Gastroenterol Hepatol* **15**, 11–20 (2018).

42. Estes, C., Razavi, H., Loomba, R., Younossi, Z. & Sanyal, A. J. Modeling the epidemic of nonalcoholic fatty liver disease demonstrates an exponential increase in burden of disease: Estes et al. *Hepatology* **67**, 123–133 (2018).

43. Chhimwal, J., Patial, V. & Padwad, Y. Beverages and Non-alcoholic fatty liver disease (NAFLD): Think before you drink. *Clinical Nutrition* **40**, 2508–2519 (2021).

44. Paschos, P. & Paletas, K. Non alcoholic fatty liver disease and metabolic syndrome. *Hippokratia* **13**, 9–19 (2009).

45. Caldwell, S. *et al.* Hepatocellular ballooning in NASH. *Journal of Hepatology* **53**, 719–723 (2010).

46. Bataller, R. & Brenner, D. A. Liver fibrosis. *J Clin Invest* **115**, 209–218 (2005).

47. Ascha, M. S. *et al.* The incidence and risk factors of hepatocellular carcinoma in patients with nonalcoholic steatohepatitis. *Hepatology* **51**, 1972–1978 (2010).

48. Bhala, N. *et al.* The natural history of nonalcoholic fatty liver disease with advanced fibrosis or cirrhosis: An international collaborative study. *Hepatology* **54**, 1208–1216 (2011).

49. McPherson, S. *et al.* Evidence of NAFLD progression from steatosis to fibrosing-steatohepatitis using paired biopsies: Implications for prognosis and clinical management. *Journal of Hepatology* **62**, 1148–1155 (2015).

50. Sanyal, A. J. Past, present and future perspectives in nonalcoholic fatty liver disease. *Nat Rev Gastroenterol Hepatol* **16**, 377–386 (2019).

51. Kleiner, D. E. *et al.* Design and validation of a histological scoring system for nonalcoholic fatty liver disease. *Hepatology* **41**, 1313–1321 (2005).

52. Idilman, I. S. *et al.* Hepatic Steatosis: Quantification by Proton Density Fat Fraction with MR Imaging versus Liver Biopsy. *Radiology* **267**, 767–775 (2013).

53. Siddiqui, M. S. *et al.* Vibration-Controlled Transient Elastography to Assess Fibrosis and Steatosis in Patients With Nonalcoholic Fatty Liver Disease. *Clinical Gastroenterology and Hepatology* **17**, 156-163.e2 (2019).

54. Hossain, N. *et al.* Independent Predictors of Fibrosis in Patients With Nonalcoholic Fatty Liver Disease. *Clinical Gastroenterology and Hepatology* **7**, 1224-1229.e2 (2009).

55. Rinella, M. E. & Sanyal, A. J. Management of NAFLD: a stage-based approach. *Nat Rev Gastroenterol Hepatol* **13**, 196–205 (2016).

56. Castera, L., Vilgrain, V. & Angulo, P. Noninvasive evaluation of NAFLD. *Nat Rev Gastroenterol Hepatol* **10**, 666–675 (2013).

57. Donnelly, K. L. *et al.* Sources of fatty acids stored in liver and secreted via lipoproteins in patients with nonalcoholic fatty liver disease. *J. Clin. Invest.* **115**, 1343–1351 (2005).

58. Fabbrini, E. *et al.* Alterations in Adipose Tissue and Hepatic Lipid Kinetics in Obese Men and Women With Nonalcoholic Fatty Liver Disease. *Gastroenterology* **134**, 424–431 (2008).

59. Diraison, F., Moulin, P. & Beylot, M. Contribution of hepatic de novo lipogenesis and reesterification of plasma non esterified fatty acids to plasma triglyceride synthesis during non-alcoholic fatty liver disease. *Diabetes & Metabolism* **29**, 478–485 (2003).

60. Lambert, J. E. & Parks, E. J. Postprandial metabolism of meal triglyceride in humans. *Biochimica et Biophysica Acta (BBA) - Molecular and Cell Biology of Lipids* **1821**, 721–726 (2012).

61. Bechmann, L. P. *et al.* Apoptosis is associated with CD36/fatty acid translocase upregulation in non-alcoholic steatohepatitis: FATPs and apoptosis in NASH. *Liver International* **30**, 850–859 (2009).

62. Greco, D. *et al.* Gene expression in human NAFLD. *American Journal of Physiology-Gastrointestinal and Liver Physiology* **294**, G1281–G1287 (2008).

63. Kohjima, M. *et al.* Re-evaluation of fatty acid metabolism-related gene expression in nonalcoholic fatty liver disease. *Int J Mol Med* **20**, 351–358 (2007).

64. Higuchi, N. *et al.* Liver X receptor in cooperation with SREBP-1c is a major lipid synthesis regulator in nonalcoholic fatty liver disease. *Hepatology Research* **38**, 1122–1129 (2008).

65. Repa, J. J. *et al.* Regulation of mouse sterol regulatory element-binding protein-1c gene (SREBP-1c) by oxysterol receptors, LXRα and LXRβ. *Genes Dev.* **14**, 2819–2830 (2000).

66. Sunny, N. E., Bril, F. & Cusi, K. Mitochondrial Adaptation in Nonalcoholic Fatty Liver Disease: Novel Mechanisms and Treatment Strategies. *Trends in Endocrinology & Metabolism* **28**, 250–260 (2017).

67. Miele, L. *et al.* Hepatic Mitochondrial Beta-Oxidation in Patients With Nonalcoholic Steatohepatitis Assessed by 13C-Octanoate Breath Test. *American Journal of Gastroenterology* **98**, 2335–2336 (2003).

68. Iozzo, P. *et al.* Fatty Acid Metabolism in the Liver, Measured by Positron Emission Tomography, Is Increased in Obese Individuals. *Gastroenterology* **139**, 846-856.e6 (2010).

69. Fujita, K. *et al.* Dysfunctional very-low-density lipoprotein synthesis and release is a key factor in nonalcoholic steatohepatitis pathogenesis. *Hepatology* **50**, 772–780 (2009).

70. Patterson, R. E. *et al.* Lipotoxicity in steatohepatitis occurs despite an increase in tricarboxylic acid cycle activity. *American Journal of Physiology-Endocrinology and Metabolism* **310**, E484–E494 (2016).

71. Moore, M. P. *et al.* Compromised hepatic mitochondrial fatty acid oxidation and reduced markers of mitochondrial turnover in human NAFLD. *Hepatology* hep.32324 (2022) doi:10.1002/hep.32324.

72. Koliaki, C. *et al.* Adaptation of Hepatic Mitochondrial Function in Humans with Non-Alcoholic Fatty Liver Is Lost in Steatohepatitis. *Cell Metabolism* **21**, 739–746 (2015).

73. Pérez-Carreras, M. *et al.* Defective hepatic mitochondrial respiratory chain in patients with nonalcoholic steatohepatitis. *Hepatology* **38**, 999–1007 (2003).

74. Sunny, N. E., Parks, E. J., Browning, J. D. & Burgess, S. C. Excessive Hepatic Mitochondrial TCA Cycle and Gluconeogenesis in Humans with Nonalcoholic Fatty Liver Disease. *Cell Metabolism* **14**, 804–810 (2011).

75. Reddy, J. K. III. Peroxisomal β-oxidation, PPARα, and steatohepatitis. *American Journal of Physiology-Gastrointestinal and Liver Physiology* **281**, G1333–G1339 (2001).

76. Satapati, S. *et al.* Elevated TCA cycle function in the pathology of diet-induced hepatic insulin resistance and fatty liver. *Journal of Lipid Research* **53**, 1080–1092 (2012).

77. Fletcher, J. A. *et al.* Impaired ketogenesis and increased acetyl-CoA oxidation promote hyperglycemia in human fatty liver. *JCI Insight* **4**, e127737 (2019).

78. Liu, J. *et al.* Geranylgeranyl diphosphate synthase (GGPPS) regulates non-alcoholic fatty liver disease (NAFLD)-fibrosis progression by determining hepatic glucose/fatty acid preference under high-fat diet conditions: GGPPS regulates NAFLD-fibrosis by glycolysis. *J. Pathol.* **246**, 277–288 (2018).

79. Keramida, G., Hunter, J. & Peters, A. M. Hepatic glucose utilization in hepatic steatosis and obesity. *Bioscience Reports* **36**, e00402 (2016).

80. Wang, T. *et al.* Acetylation of lactate dehydrogenase B drives NAFLD progression by impairing lactate clearance. *Journal of Hepatology* **74**, 1038–1052 (2021).

81. Sanyal, A. J. *et al.* A pilot study of vitamin E versus vitamin E and pioglitazone for the treatment of nonalcoholic steatohepatitis. *Clinical Gastroenterology and Hepatology* **2**, 1107–1115 (2004).

82. Neuschwander-Tetri, B. A. *et al.* Farnesoid X nuclear receptor ligand obeticholic acid for non-cirrhotic, non-alcoholic steatohepatitis (FLINT): a multicentre, randomised, placebo-controlled trial. *The Lancet* **385**, 956–965 (2015).

83. Mudaliar, S. *et al.* Efficacy and Safety of the Farnesoid X Receptor Agonist Obeticholic Acid in Patients With Type 2 Diabetes and Nonalcoholic Fatty Liver Disease. *Gastroenterology* **145**, 574-582.e1 (2013).

84. Ratziu, V. *et al.* Elafibranor, an Agonist of the Peroxisome Proliferator−Activated Receptor−α and −δ, Induces Resolution of Nonalcoholic Steatohepatitis Without Fibrosis Worsening. *Gastroenterology* **150**, 1147-1159.e5 (2016).

85. Friedman, S. *et al.* Efficacy and safety study of cenicriviroc for the treatment of non-alcoholic steatohepatitis in adult subjects with liver fibrosis: CENTAUR Phase 2b study design. *Contemporary Clinical Trials* **47**, 356–365 (2016).

86. Harrison, S. A. *et al.* Simtuzumab Is Ineffective for Patients With Bridging Fibrosis or Compensated Cirrhosis Caused by Nonalcoholic Steatohepatitis. *Gastroenterology* **155**, 1140–1153 (2018).

87. Michalopoulos, G. K. Liver regeneration. *J. Cell. Physiol.* **213**, 286–300 (2007).

88. Michalopoulos, G. K. & Bhushan, B. Liver regeneration: biological and pathological mechanisms and implications. *Nat Rev Gastroenterol Hepatol* **18**, 40–55 (2021).

89. Michalopoulos, G. K. & DeFrances, M. C. Liver Regeneration. *Science* **276**, 60–66 (1997).

90. Zajicek, G., Oren, R. & Weinreb, M. The streaming liver. *Liver* **5**, 293–300 (2008).

91. Furuyama, K. *et al.* Continuous cell supply from a Sox9-expressing progenitor zone in adult liver, exocrine pancreas and intestine. *Nat Genet* **43**, 34–41 (2011).

92. Kennedy, S., Rettinger, S., Flye, M. W. & Ponder, K. P. Experiments in transgenic mice show that hepatocytes are the source for postnatal liver growth and do not stream. *Hepatology* **22**, 160–168 (1995).

93. Magami, Y. *et al.* Cell proliferation and renewal of normal hepatocytes and bile duct cells in adult mouse liver: Proliferation of hepatocytes. *Liver* **22**, 419–425 (2002).

94. Malato, Y. *et al.* Fate tracing of mature hepatocytes in mouse liver homeostasis and regeneration. *J. Clin. Invest.* **121**, 4850–4860 (2011).

95. Yanger, K. *et al.* Robust cellular reprogramming occurs spontaneously during liver regeneration. *Genes Dev.* **27**, 719–724 (2013).

96. Font-Burgada, J. *et al.* Hybrid Periportal Hepatocytes Regenerate the Injured Liver without Giving Rise to Cancer. *Cell* **162**, 766–779 (2015).

97. Wang, B., Zhao, L., Fish, M., Logan, C. Y. & Nusse, R. Self-renewing diploid Axin2+ cells fuel homeostatic renewal of the liver. *Nature* **524**, 180–185 (2015).

98. Wei, Y. *et al.* Liver homeostasis is maintained by midlobular zone 2 hepatocytes. *Science* **371**, eabb1625 (2021).

99. He, L. *et al.* Proliferation tracing reveals regional hepatocyte generation in liver homeostasis and repair. *Science* **371**, eabc4346 (2021).

100. Bhushan, B. & Apte, U. Liver Regeneration after Acetaminophen Hepatotoxicity. *The American Journal of Pathology* **189**, 719–729 (2019).

101. Bhushan, B. *et al.* Dual Role of Epidermal Growth Factor Receptor in Liver Injury and Regeneration after Acetaminophen Overdose in Mice. *Toxicol. Sci.* **155**, 363–378 (2017).

102. Bhushan, B. *et al.* Pro-Regenerative Signaling after Acetaminophen-Induced Acute Liver Injury in Mice Identified Using a Novel Incremental Dose Model. *The American Journal of Pathology* **184**, 3013–3025 (2014).

103. Hughes, R. D., Zhang, L., Tsubouchi, H., Daikuhara, Y. & Williams, R. Plasma hepatocyte growth factor and biliprotein levels and outcome in fulminant hepatic failure. *Journal of Hepatology* **20**, 106–111 (1994).

104. Donahower, B. *et al.* Vascular endothelial growth factor and hepatocyte regeneration in acetaminophen toxicity. *American Journal of Physiology-Gastrointestinal and Liver Physiology* **291**, G102–G109 (2006).

105. Alvarez-Sola, G. *et al.* Engineered fibroblast growth factor 19 protects from acetaminophen-induced liver injury and stimulates aged liver regeneration in mice. *Cell Death Dis* **8**, e3083–e3083 (2017).

106. Bhushan, B., Poudel, S., Manley, M. W., Roy, N. & Apte, U. Inhibition of Glycogen Synthase Kinase 3 Accelerated Liver Regeneration after Acetaminophen-Induced Hepatotoxicity in Mice. *The American Journal of Pathology* **187**, 543–552 (2017).

107. Borude, P., Bhushan, B. & Apte, U. DNA Damage Response Regulates Initiation of Liver Regeneration Following Acetaminophen Overdose. *gene expr* **18**, 115–123 (2018).

108. Bird, T. G. *et al.* TGFβ inhibition restores a regenerative response in acute liver injury by suppressing paracrine senescence. *Sci. Transl. Med.* **10**, eaan1230 (2018).

109. Fausto, N. Liver regeneration and repair: Hepatocytes, progenitor cells, and stem cells. *Hepatology* **39**, 1477–1487 (2004).

110. Grisham, J. W. A morphologic study of deoxyribonucleic acid synthesis and cell proliferation in regenerating rat liver; autoradiography with thymidine-H3. *Cancer Res* **22**, 842–849 (1962).

111. Matsumoto, K., Fujii, H., Michalopoulos, G., Fung, J. J. & Demetris, A. J. Human biliary epithelial cells secrete and respond to cytokines and hepatocyte growth factors in vitro: interleukin-6, hepatocyte growth factor and epidermal growth factor promote DNA synthesis in vitro. *Hepatology* **20**, 376–382 (1994).

112. Pepe-Mooney, B. J. *et al.* Single-Cell Analysis of the Liver Epithelium Reveals Dynamic Heterogeneity and an Essential Role for YAP in Homeostasis and Regeneration. *Cell Stem Cell* **25**, 23-38.e8 (2019).

113. Planas-Paz, L. *et al.* YAP, but Not RSPO-LGR4/5, Signaling in Biliary Epithelial Cells Promotes a Ductular Reaction in Response to Liver Injury. *Cell Stem Cell* **25**, 39-53.e10 (2019).

114. Meyer, K. *et al.* Bile canaliculi remodeling activates YAP via the actin cytoskeleton during liver regeneration. *Mol Syst Biol* **16**, (2020).

115. Michalopoulos, G. K. & Khan, Z. Liver Stem Cells: Experimental Findings and Implications for Human Liver Disease. *Gastroenterology* **149**, 876–882 (2015).

116. Trautwein, C. *et al.* 2-Acetaminofluorene blocks cell cycle progression after hepatectomy by p21 induction and lack of Cyclin E expression. *Oncogene* **18**, 6443–6453 (1999).

117. Evarts, R. P. *et al.* Precursor-product relationship between oval cells and hepatocytes: comparison between tritiated thymidine and bromodeoxyuridine as tracers. *Carcinogenesis* **17**, 2143–2151 (1996).

118. Shiojiri, N., Lemire, J. M. & Fausto, N. Cell lineages and oval cell progenitors in rat liver development. *Cancer Res* **51**, 2611–2620 (1991).

119. Dezső, K. *et al.* Structural analysis of oval-cell-mediated liver regeneration in rats. *Hepatology* **56**, 1457–1467 (2012).

120. Farber, E. Similarities in the sequence of early histological changes induced in the liver of the rat by ethionine, 2-acetylaminofluorene, and 3'-methyl-4-dimethylaminoazobenzene. *Cancer Res* **16**, 142–148 (1956).

121. Popper, H., Kent, G. & Stein, R. Ductular cell reaction in the liver in hepatic injury. *J Mt Sinai Hosp N Y* **24**, 551–556 (1957).

122. Canals of Hering: Recent Insights and Current Knowledge. *Semin Liver Dis* **24**, 43–48 (2004).

123. Miyajima, A., Tanaka, M. & Itoh, T. Stem/Progenitor Cells in Liver Development, Homeostasis, Regeneration, and Reprogramming. *Cell Stem Cell* **14**, 561–574 (2014).

124. Zipori, D. The nature of stem cells: state rather than entity. *Nat Rev Genet* **5**, 873–878 (2004).

125. Sato, K. *et al.* Ductular Reaction in Liver Diseases: Pathological Mechanisms and Translational Significances: Liver Injury and Regeneration. *Hepatology* **69**, 420–430 (2019).

126. Tarlow, B. D., Finegold, M. J. & Grompe, M. Clonal tracing of Sox9 $^{+}$ liver progenitors in mouse oval cell injury. *Hepatology* **60**, 278–289 (2014).

127. Lu, W.-Y. *et al.* Hepatic progenitor cells of biliary origin with liver repopulation capacity. *Nat Cell Biol* **17**, 971–983 (2015).

128. Raven, A. *et al.* Cholangiocytes act as facultative liver stem cells during impaired hepatocyte regeneration. *Nature* **547**, 350–354 (2017).

129. Russell, J. O. *et al.* Hepatocyte-Specific β-Catenin Deletion During Severe Liver Injury Provokes Cholangiocytes to Differentiate Into Hepatocytes. *Hepatology* **69**, 742–759 (2019).

130. Deng, X. *et al.* Chronic Liver Injury Induces Conversion of Biliary Epithelial Cells into Hepatocytes. *Cell Stem Cell* **23**, 114-122.e3 (2018).

131. Li, B. *et al.* Adult Mouse Liver Contains Two Distinct Populations of Cholangiocytes. *Stem Cell Reports* **9**, 478–489 (2017).

132. Isse, K. *et al.* Preexisting epithelial diversity in normal human livers: A tissue-tethered cytometric analysis in portal/periportal epithelial cells. *Hepatology* **57**, 1632–1643 (2013).

133. Crosby, H. A. *et al.* Immunolocalization of putative human liver progenitor cells in livers from patients with end-stage primary biliary cirrhosis and sclerosing cholangitis using the monoclonal antibody OV-6. *Am J Pathol* **152**, 771–779 (1998).

134. Gouw, A. S. H., Clouston, A. D. & Theise, N. D. Ductular reactions in human liver: Diversity at the interface. *Hepatology* **54**, 1853–1863 (2011).

135. Michalopoulos, G. K., Barua, L. & Bowen, W. C. Transdifferentiation of rat hepatocytes into biliary cells after bile duct ligation and toxic biliary injury. *Hepatology* **41**, 535–544 (2005).

136. Sclair, S. N. *et al.* Increased hepatic progenitor cell response and ductular reaction in patients with severe recurrent HCV post-liver transplantation. *Clin Transplant* **30**, 722–730 (2016).

137. Kasprzak, A. *et al.* p21/Wafl/Cipl cellular expression in chronic long-lasting hepatitis C: correlation with HCV proteins (C, NS3, NS5A), other cell-cycle related proteins and selected clinical data. *Folia Histochem Cytobiol.* **47**, 385–394 (2010).

138. Sancho-Bru, P. *et al.* Liver progenitor cell markers correlate with liver damage and predict short-term mortality in patients with alcoholic hepatitis. *Hepatology* **55**, 1931–1941 (2012).

139. Gadd, V. L. *et al.* The portal inflammatory infiltrate and ductular reaction in human nonalcoholic fatty liver disease. *Hepatology* **59**, 1393–1405 (2014).

140. Machado, M. V. *et al.* Accumulation of duct cells with activated YAP parallels fibrosis progression in non-alcoholic fatty liver disease. *Journal of Hepatology* **63**, 962–970 (2015).

141. Sorrentino, P. *et al.* A Clinical–Morphological Study on Cholestatic Presentation of Nonalcoholic Fatty Liver Disease. *Dig Dis Sci* **50**, 1130–1135 (2005).

142. Sackett, S. D. *et al.* Foxl1 is a marker of bipotential hepatic progenitor cells in mice. *Hepatology* **49**, 920–929 (2009).

143. Huch, M. *et al.* In vitro expansion of single Lgr5+ liver stem cells induced by Wnt-driven regeneration. *Nature* **494**, 247–250 (2013).

144. Zhang, X. *et al.* Inhibition of notch signaling pathway prevents cholestatic liver fibrosis by decreasing the differentiation of hepatic progenitor cells into cholangiocytes. *Lab Invest* **96**, 350–360 (2016).

145. Yimlamai, D. *et al.* Hippo Pathway Activity Influences Liver Cell Fate. *Cell* **157**, 1324–1338 (2014).

146. Okabe, H. *et al.* Wnt signaling regulates hepatobiliary repair following cholestatic liver injury in mice: Okabe et al. *Hepatology* **64**, 1652–1666 (2016).

147. Tsuchiya, A. *et al.* Polysialic acid/neural cell adhesion molecule modulates the formation of ductular reactions in liver injury: HEPATOLOGY, Vol. XX, No. X, 2014 TSUCHIYA ET AL. *Hepatology* **60**, 1727–1740 (2014).

148. Aloia, L. *et al.* Epigenetic remodelling licences adult cholangiocytes for organoid formation and liver regeneration. *Nat Cell Biol* **21**, 1321–1333 (2019).

149. Perepelyuk, M. *et al.* Hepatic stellate cells and portal fibroblasts are the major cellular sources of collagens and lysyl oxidases in normal liver and early after injury. *American Journal of Physiology-Gastrointestinal and Liver Physiology* **304**, G605–G614 (2013).

150. Glaser, S. S., Gaudio, E., Miller, T., Alvaro, D. & Alpini, G. Cholangiocyte proliferation and liver fibrosis. *Expert Rev. Mol. Med.* **11**, e7 (2009).

151. Díaz, R. *et al.* Evidence for the epithelial to mesenchymal transition in biliary atresia fibrosis. *Human Pathology* **39**, 102–115 (2008).

152. Wu, N. *et al.* The secretin/secretin receptor axis modulates liver fibrosis through changes in transforming growth factor-β1 biliary secretion in mice. *Hepatology* **64**, 865–879 (2016).

153. Choi, T., Ninov, N., Stainier, D. Y. R. & Shin, D. Extensive Conversion of Hepatic Biliary Epithelial Cells to Hepatocytes After Near Total Loss of Hepatocytes in Zebrafish. *Gastroenterology* **146**, 776–788 (2014).

154. Deng, X. *et al.* Chronic Liver Injury Induces Conversion of Biliary Epithelial Cells into Hepatocytes. *Cell Stem Cell* **23**, 114-122.e3 (2018).

155. Español–Suñer, R. *et al.* Liver Progenitor Cells Yield Functional Hepatocytes in Response to Chronic Liver Injury in Mice. *Gastroenterology* **143**, 1564-1575.e7 (2012).

156. Huch, M. *et al.* In vitro expansion of single Lgr5+ liver stem cells induced by Wnt-driven regeneration. *Nature* **494**, 247–250 (2013).

157. Lu, W.-Y. *et al.* Hepatic progenitor cells of biliary origin with liver repopulation capacity. *Nat Cell Biol* **17**, 971–983 (2015).

158. Raven, A. *et al.* Cholangiocytes act as facultative liver stem cells during impaired hepatocyte regeneration. *Nature* **547**, 350–354 (2017).

159. Rodrigo-Torres, D. *et al.* The biliary epithelium gives rise to liver progenitor cells: RODRIGO-TORRES ET AL. *Hepatology* **60**, 1367–1377 (2014).

160. Russell, J. O. *et al.* Hepatocyte-Specific β-Catenin Deletion During Severe Liver Injury Provokes Cholangiocytes to Differentiate Into Hepatocytes. *Hepatology* **69**, 742–759 (2019).

161. Klein, A. S. *et al.* Organ Donation and Utilization in the United States, 1999-2008. *American Journal of Transplantation* **10**, 973–986 (2010).

162. Williams, R., Schalm, S. W. & O'Grady, J. G. Acute liver failure: redefining the syndromes. *The Lancet* **342**, 273–275 (1993).

163. Dhawan, A., Puppi, J., Hughes, R. D. & Mitry, R. R. Human hepatocyte transplantation: current experience and future challenges. *Nat Rev Gastroenterol Hepatol* **7**, 288–298 (2010).

164. Forbes, S. J. Organoid cultures boost human liver cell expansion: HEPATOLOGY *ELSEWHERE*. *Hepatology* **62**, 1635–1637 (2015).

165. Ji, S., Zhang, L. & Hui, L. Cell fate conversion: Direct induction of hepatocyte-like cells from fibroblasts. *J. Cell. Biochem.* **114**, 256–265 (2013).

166. Levy, G. *et al.* Long-term culture and expansion of primary human hepatocytes. *Nat Biotechnol* **33**, 1264–1271 (2015).

167. Katsuda, T. *et al.* Conversion of Terminally Committed Hepatocytes to Culturable Bipotent Progenitor Cells with Regenerative Capacity. *Cell Stem Cell* **20**, 41–55 (2017).

168. Shin, S. *et al.* Foxl1-Cre-marked adult hepatic progenitors have clonogenic and bilineage differentiation potential. *Genes Dev.* **25**, 1185–1192 (2011).

169. Okabe, M. *et al.* Potential hepatic stem cells reside in EpCAM+ cells of normal and injured mouse liver. *Development* **136**, 1951–1960 (2009).

170. Fatehullah, A., Tan, S. H. & Barker, N. Organoids as an in vitro model of human development and disease. *Nat Cell Biol* **18**, 246–254 (2016).

171. Kim, J., Koo, B.-K. & Knoblich, J. A. Human organoids: model systems for human biology and medicine. *Nat Rev Mol Cell Biol* **21**, 571–584 (2020).

172. Huch, M. *et al.* Long-Term Culture of Genome-Stable Bipotent Stem Cells from Adult Human Liver. *Cell* **160**, 299–312 (2015).

173. Takebe, T. *et al.* Vascularized and functional human liver from an iPSC-derived organ bud transplant. *Nature* **499**, 481–484 (2013).

174. Takebe, T. *et al.* Generation of a vascularized and functional human liver from an iPSC-derived organ bud transplant. *Nat Protoc* **9**, 396–409 (2014).

175. Takebe, T. *et al.* Massive and Reproducible Production of Liver Buds Entirely from Human Pluripotent Stem Cells. *Cell Reports* **21**, 2661–2670 (2017).

176. Hu, H. *et al.* Long-Term Expansion of Functional Mouse and Human Hepatocytes as 3D Organoids. *Cell* **175**, 1591-1606.e19 (2018).

177. Peng, W. C. *et al.* Inflammatory Cytokine TNFα Promotes the Long-Term Expansion of Primary Hepatocytes in 3D Culture. *Cell* **175**, 1607-1619.e15 (2018).

178. Bartfeld, S. & Clevers, H. Stem cell-derived organoids and their application for medical research and patient treatment. *J Mol Med* **95**, 729–738 (2017).

179. Tang, X.-Y. *et al.* Human organoids in basic research and clinical applications. *Sig Transduct Target Ther* **7**, 168 (2022).

180. Hallett, J. M. *et al.* Human biliary epithelial cells from discarded donor livers rescue bile duct structure and function in a mouse model of biliary disease. *Cell Stem Cell* **29**, 355-371.e10 (2022).

181. Sampaziotis, F. *et al.* Cholangiocyte organoids can repair bile ducts after transplantation in the human liver. *Science* **371**, 839–846 (2021).

182. Machado, M. V. *et al.* Accumulation of duct cells with activated YAP parallels fibrosis progression in non-alcoholic fatty liver disease. *Journal of Hepatology* **63**, 962–970 (2015).

183. Broutier, L. *et al.* Culture and establishment of self-renewing human and mouse adult liver and pancreas 3D organoids and their genetic manipulation. *Nature Protocols* **11**, 1724–1743 (2016).

184. Aloia, L. *et al.* Epigenetic remodelling licences adult cholangiocytes for organoid formation and liver regeneration. *Nature Cell Biology* **21**, 1321–1333 (2019).

185. Andrews, S. FastQC: a quality control tool for high throughput sequence data. (2010).

186. Dobin, A. *et al.* STAR: ultrafast universal RNA-seq aligner. *Bioinformatics* **29**, 15–21 (2013).

187. Love, M. I., Huber, W. & Anders, S. Moderated estimation of fold change and dispersion for RNA-seq data with DESeq2. *Genome Biol* **15**, 550 (2014).

188. Lê, S., Josse, J. & Husson, F. **FactoMineR** : An *R* Package for Multivariate Analysis. *J. Stat. Soft.* **25**, (2008).

189. Yu, G., Wang, L.-G., Han, Y. & He, Q.-Y. clusterProfiler: an R Package for Comparing Biological Themes Among Gene Clusters. *OMICS: A Journal of Integrative Biology* **16**, 284–287 (2012).

190. Wickham, H. *ggplot2: Elegant Graphics for Data Analysis*. (Springer International Publishing : Imprint: Springer, 2016). doi:10.1007/978-3-319-24277-4.

191. Bankhead, P. *et al.* QuPath: Open source software for digital pathology image analysis. *Sci Rep* **7**, 16878 (2017).

192. Gjorevski, N. *et al.* Designer matrices for intestinal stem cell and organoid culture. *Nature* **539**, 560–564 (2016).

193. Sorrentino, G. *et al.* Mechano-modulatory synthetic niches for liver organoid derivation. *Nature Communications* **11**, 1–10 (2020).

194. Schindelin, J. *et al.* Fiji: an open-source platform for biological-image analysis. *Nat Methods* **9**, 676–682 (2012).

195. Araya, J. *et al.* Increase in long-chain polyunsaturated fatty acid n−6/n−3 ratio in relation to hepatic steatosis in patients with non-alcoholic fatty liver disease. *Clinical Science* **106**, 635–643 (2004).

196. Dimova, D. K. & Dyson, N. J. The E2F transcriptional network: old acquaintances with new faces. *Oncogene* **24**, 2810–2826 (2005).

197. Dyson, N. The regulation of E2F by pRB-family proteins. *Genes Dev.* **12**, 2245–2262 (1998).

198. Dyson, N. J. *RB1* : a prototype tumor suppressor and an enigma. *Genes Dev.* **30**, 1492–1502 (2016).

199. Ren, B. *et al.* E2F integrates cell cycle progression with DNA repair, replication, and G $_2$ /M checkpoints. *Genes Dev.* **16**, 245–256 (2002).

200. Vander Heiden, M. G., Cantley, L. C. & Thompson, C. B. Understanding the Warburg Effect: The Metabolic Requirements of Cell Proliferation. *Science* **324**, 1029–1033 (2009).

201. Denechaud, P.-D., Fajas, L. & Giralt, A. E2F1, a Novel Regulator of Metabolism. *Front. Endocrinol.* **8**, 311 (2017).

202. Nicolay, B. N. & Dyson, N. J. The multiple connections between pRB and cell metabolism. *Current Opinion in Cell Biology* **25**, 735–740 (2013).

203. Blanchet, E. *et al.* E2F transcription factor-1 regulates oxidative metabolism. *Nat Cell Biol* **13**, 1146–1152 (2011).

204. Denechaud, P.-D. *et al.* E2F1 mediates sustained lipogenesis and contributes to hepatic steatosis. *Journal of Clinical Investigation* **126**, 137–150 (2015).

205. Huber, K., Mestres-Arenas, A., Fajas, L. & Leal-Esteban, L. C. The multifaceted role of cell cycle regulators in the coordination of growth and metabolism. *FEBS J* **288**, 3813–3833 (2021).

206. Caliari, S. R. & Burdick, J. A. A practical guide to hydrogels for cell culture. *Nat Methods* **13**, 405–414 (2016).

207. Chrisnandy, A., Blondel, D., Rezakhani, S., Broguiere, N. & Lutolf, M. P. Synthetic dynamic hydrogels promote degradation-independent in vitro organogenesis. *Nat. Mater.* **21**, 479–487 (2022).

208. Cruz-Acuña, R. *et al.* PEG-4MAL hydrogels for human organoid generation, culture, and in vivo delivery. *Nat Protoc* **13**, 2102–2119 (2018).

209. Cruz-Acuña, R. *et al.* Synthetic hydrogels for human intestinal organoid generation and colonic wound repair. *Nat Cell Biol* **19**, 1326–1335 (2017).

210. Ehrbar, M. *et al.* Biomolecular Hydrogels Formed and Degraded via Site-Specific Enzymatic Reactions. *Biomacromolecules* **8**, 3000–3007 (2007).

211. Below, C. R. *et al.* A microenvironment-inspired synthetic three-dimensional model for pancreatic ductal adenocarcinoma organoids. *Nat. Mater.* **21**, 110–119 (2022).

212. Ye, S. *et al.* A Chemically Defined Hydrogel for Human Liver Organoid Culture. *Adv. Funct. Mater.* **30**, 2000893 (2020).

213. Klotz, B. J. *et al.* A Versatile Biosynthetic Hydrogel Platform for Engineering of Tissue Analogues. *Adv. Healthcare Mater.* **8**, 1900979 (2019).

214. Davidson, M. D., Burdick, J. A. & Wells, R. G. Engineered Biomaterial Platforms to Study Fibrosis. *Adv. Healthcare Mater.* **9**, 1901682 (2020).

215. Rojkind, M. & Ponce-Noyola, P. The Extracellular Matrix of the Liver. *Collagen and Related Research* **2**, 151–175 (1982).

216. Sorrentino, G. *et al.* Mechano-modulatory synthetic niches for liver organoid derivation. *Nat Commun* **11**, 3416 (2020).

217. Yin, M. *et al.* Quantitative assessment of hepatic fibrosis in an animal model with magnetic resonance elastography. *Magn. Reson. Med.* **58**, 346–353 (2007).

218. Kumar, P. *et al.* Periostin promotes liver fibrogenesis by activating lysyl oxidase in hepatic stellate cells. *Journal of Biological Chemistry* **293**, 12781–12792 (2018).

219. Ingber, D. Mechanobiology and diseases of mechanotransduction. *Annals of Medicine* **35**, 564–577 (2003).

220. Humphrey, J. D., Dufresne, E. R. & Schwartz, M. A. Mechanotransduction and extracellular matrix homeostasis. *Nat Rev Mol Cell Biol* **15**, 802–812 (2014).

221. Duscher, D. *et al.* Mechanotransduction and fibrosis. *Journal of Biomechanics* **47**, 1997–2005 (2014).

222. Heyens, L. J. M., Busschots, D., Koek, G. H., Robaeys, G. & Francque, S. Liver Fibrosis in Non-alcoholic Fatty Liver Disease: From Liver Biopsy to Non-invasive Biomarkers in Diagnosis and Treatment. *Front. Med.* **8**, 615978 (2021).

223. Huch, M. *et al.* In vitro expansion of single Lgr5 + liver stem cells induced by Wnt-driven regeneration. *Nature* (2013) doi:10.1038/nature11826.

224. Hu, H. *et al.* Long-Term Expansion of Functional Mouse and Human Hepatocytes as 3D Organoids. *Cell* **175**, 1591-1606.e19 (2018).

225. Takebe, T. *et al.* Generation of a vascularized and functional human liver from an iPSC-derived organ bud transplant. *Nature Protocols* (2014) doi:10.1038/nprot.2014.020.

226. Halder, G., Dupont, S. & Piccolo, S. Transduction of mechanical and cytoskeletal cues by YAP and TAZ. *Nat Rev Mol Cell Biol* **13**, 591–600 (2012).

227. Liu-Chittenden, Y. *et al.* Genetic and pharmacological disruption of the TEAD–YAP complex suppresses the oncogenic activity of YAP. *Genes Dev.* **26**, 1300–1305 (2012).

228. Dupont, S. *et al.* Role of YAP/TAZ in mechanotransduction. *Nature* **474**, 179–183 (2011).

229. Sorrentino, G. *et al.* Metabolic control of YAP and TAZ by the mevalonate pathway. *Nat Cell Biol* **16**, 357–366 (2014).

230. Sorrentino, G. *et al.* Glucocorticoid receptor signalling activates YAP in breast cancer. *Nat Commun* **8**, 14073 (2017).

231. Kovács, M., Tóth, J., Hetényi, C., Málnási-Csizmadia, A. & Sellers, J. R. Mechanism of Blebbistatin Inhibition of Myosin II. *Journal of Biological Chemistry* **279**, 35557–35563 (2004).

232. Araujo, J. & Logothetis, C. Dasatinib: A potent SRC inhibitor in clinical development for the treatment of solid tumors. *Cancer Treatment Reviews* **36**, 492–500 (2010).

233. Taniguchi, K. *et al.* A gp130–Src–YAP module links inflammation to epithelial regeneration. *Nature* **519**, 57–62 (2015).

234. Li, P. *et al.* αE-catenin inhibits a Src–YAP1 oncogenic module that couples tyrosine kinases and the effector of Hippo signaling pathway. *Genes Dev.* **30**, 798–811 (2016).

235. Lamar, J. M. *et al.* The Hippo pathway target, YAP, promotes metastasis through its TEAD-interaction domain. *Proc. Natl. Acad. Sci. U.S.A.* **109**, (2012).

236. Abu-Absi, S. F., Hu, W.-S. & Hansen, L. K. Dexamethasone Effects on Rat Hepatocyte Spheroid Formation and Function. *Tissue Engineering* **11**, 415–426 (2005).

237. Smoot, R. L. *et al.* Platelet-derived growth factor regulates YAP transcriptional activity via Src family kinase dependent tyrosine phosphorylation. *J. Cell. Biochem.* **119**, 824–836 (2018).

238. Sugihara, T. *et al.* YAP Tyrosine Phosphorylation and Nuclear Localization in Cholangiocarcinoma Cells Are Regulated by LCK and Independent of LATS Activity. *Molecular Cancer Research* **16**, 1556–1567 (2018).

239. Tamm, C., Böwer, N. & Annerén, C. Regulation of mouse embryonic stem cell self-renewal by a Yes–YAP–TEAD2 signaling pathway downstream of LIF. *Journal of Cell Science* **124**, 1136–1144 (2011).

240. Tschumperlin, D. J., Ligresti, G., Hilscher, M. B. & Shah, V. H. Mechanosensing and fibrosis. *Journal of Clinical Investigation* **128**, 74–84 (2018).

241. Mueller, S. & Sandrin, L. Liver stiffness: a novel parameter for the diagnosis of liver disease. *Hepat Med* **2**, 49–67 (2010).

242. Schwabe, R. F., Tabas, I. & Pajvani, U. B. Mechanisms of Fibrosis Development in Nonalcoholic Steatohepatitis. *Gastroenterology* **158**, 1913–1928 (2020).

243. Herrera, J., Henke, C. A. & Bitterman, P. B. Extracellular matrix as a driver of progressive fibrosis. *Journal of Clinical Investigation* **128**, 45–53 (2018).

244. Liu, F. *et al.* Mechanosignaling through YAP and TAZ drives fibroblast activation and fibrosis. *American Journal of Physiology-Lung Cellular and Molecular Physiology* **308**, L344–L357 (2015).

245. Liu, L. *et al.* Mechanotransduction-modulated fibrotic microniches reveal the contribution of angiogenesis in liver fibrosis. *Nature Mater* **16**, 1252–1261 (2017).

246. Degos, F. *et al.* Diagnostic accuracy of FibroScan and comparison to liver fibrosis biomarkers in chronic viral hepatitis: A multicenter prospective study (the FIBROSTIC study). *Journal of Hepatology* **53**, 1013–1021 (2010).

247. Haage, A. & Schneider, I. C. Cellular contractility and extracellular matrix stiffness regulate matrix metalloproteinase activity in pancreatic cancer cells. *FASEB j.* **28**, 3589–3599 (2014).

248. Xie, J. *et al.* Substrate stiffness-regulated matrix metalloproteinase output in myocardial cells and cardiac fibroblasts: Implications for myocardial fibrosis. *Acta Biomaterialia* **10**, 2463–2472 (2014).

249. Peeters, S. A. *et al.* Circulating matrix metalloproteinases are associated with arterial stiffness in patients with type 1 diabetes: pooled analysis of three cohort studies. *Cardiovasc Diabetol* **16**, 139 (2017).

250. McCarron, S. *et al.* Functional Characterization of Organoids Derived From Irreversibly Damaged Liver of Patients With NASH. *Hepatology* **74**, 1825–1844 (2021).

251. Myers, S. *et al.* NAFLD and MAFLD as emerging causes of HCC: A populational study. *JHEP Rep* **3**, 100231 (2021).

252. Wang, X. *et al.* Hepatocyte TAZ/WWTR1 Promotes Inflammation and Fibrosis in Nonalcoholic Steatohepatitis. *Cell Metabolism* **24**, 848–862 (2016).

253. Sano, A. *et al.* Steatotic Hepatocytes Release Mature VLDL Through Methionine and Tyrosine Metabolism in a Keap1-Nrf2–Dependent Manner. *Hepatology* **74**, 1271–1286 (2021).

254. De Gottardi, A. *et al.* Microarray analyses and molecular profiling of steatosis induction in immortalized human hepatocytes. *Lab Invest* **87**, 792–806 (2007).

255. Wobser, H. *et al.* Lipid accumulation in hepatocytes induces fibrogenic activation of hepatic stellate cells. *Cell Res* **19**, 996–1005 (2009).

256. Ipsen, D. H., Lykkesfeldt, J. & Tveden-Nyborg, P. Molecular mechanisms of hepatic lipid accumulation in non-alcoholic fatty liver disease. *Cell. Mol. Life Sci.* **75**, 3313–3327 (2018).

257. Meyer, K. *et al.* Bile canaliculi remodeling activates YAP via the actin cytoskeleton during liver regeneration. *Mol Syst Biol* **16**, (2020).

258. Pepe-Mooney, B. J. *et al.* Single-Cell Analysis of the Liver Epithelium Reveals Dynamic Heterogeneity and an Essential Role for YAP in Homeostasis and Regeneration. *Cell Stem Cell* **25**, 23-38.e8 (2019).

259. Planas-Paz, L. *et al.* YAP, but Not RSPO-LGR4/5, Signaling in Biliary Epithelial Cells Promotes a Ductular Reaction in Response to Liver Injury. *Cell Stem Cell* **25**, 39-53.e10 (2019).

260. Chen, H.-Z., Tsai, S.-Y. & Leone, G. Emerging roles of E2Fs in cancer: an exit from cell cycle control. *Nat Rev Cancer* **9**, 785–797 (2009).

261. Beyaz, S. *et al.* High-fat diet enhances stemness and tumorigenicity of intestinal progenitors. *Nature* **531**, 53–58 (2016).

262. Capolupo, L. *et al.* Sphingolipids control dermal fibroblast heterogeneity. *Science* **376**, eabh1623 (2022).

263. Miao, Z.-F. *et al.* A Metformin-Responsive Metabolic Pathway Controls Distinct Steps in Gastric Progenitor Fate Decisions and Maturation. *Cell Stem Cell* **26**, 910-925.e6 (2020).

264. Zhang, H. *et al.* NAD $^+$ repletion improves mitochondrial and stem cell function and enhances life span in mice. *Science* **352**, 1436–1443 (2016).

265. Yin, M. *et al.* Quantitative assessment of hepatic fibrosis in an animal model with magnetic resonance elastography. *Magnetic Resonance in Medicine* (2007) doi:10.1002/mrm.21286.

266. Kumar, P. *et al.* Periostin promotes liver fibrogenesis by activating lysyl oxidase in hepatic stellate cells. *Journal of Biological Chemistry* (2018) doi:10.1074/jbc.RA117.001601.

267. Halder, G., Dupont, S. & Piccolo, S. Transduction of mechanical and cytoskeletal cues by YAP and TAZ. *Nature reviews. Molecular cell biology* **13**, 591–600 (2012).

268. Munsterman, I. D. *et al.* Extracellular matrix components indicate remodelling activity in different fibrosis stages of human non-alcoholic fatty liver disease. *Histopathology* **73**, 612–621 (2018).

269. Arriazu, E. *et al.* Extracellular Matrix and Liver Disease. *Antioxidants & Redox Signaling* **21**, 1078–1097 (2014).

270. Kyrönlahti, A. *et al.* Evolving Up-regulation of Biliary Fibrosis–Related Extracellular Matrix Molecules After Successful Portoenterostomy. *Hepatol Commun* **5**, 1036–1050 (2021).

271. Nakagawa, H. *et al.* Loss of liver E-cadherin induces sclerosing cholangitis and promotes carcinogenesis. *Proc. Natl. Acad. Sci. U.S.A.* **111**, 1090–1095 (2014).

272. Perrotti, F. *et al.* Advances in Lipidomics for Cancer Biomarkers Discovery. *IJMS* **17**, 1992 (2016).

273. Wigger, L. *et al.* Plasma Dihydroceramides Are Diabetes Susceptibility Biomarker Candidates in Mice and Humans. *Cell Reports* **18**, 2269–2279 (2017).

274. Horton, J. D., Goldstein, J. L. & Brown, M. S. SREBPs: activators of the complete program of cholesterol and fatty acid synthesis in the liver. *J. Clin. Invest.* **109**, 1125–1131 (2002).

275. Kliewer, S. A. *et al.* Fatty acids and eicosanoids regulate gene expression through direct interactions with peroxisome proliferator-activated receptors α and γ. *Proc. Natl. Acad. Sci. U.S.A.* **94**, 4318–4323 (1997).

276. Lehmann, J. M. *et al.* Activation of the Nuclear Receptor LXR by Oxysterols Defines a New Hormone Response Pathway. *Journal of Biological Chemistry* **272**, 3137–3140 (1997).

277. Wang, H., Chen, J., Hollister, K., Sowers, L. C. & Forman, B. M. Endogenous Bile Acids Are Ligands for the Nuclear Receptor FXR/BAR. *Molecular Cell* **3**, 543–553 (1999).

278. Harayama, T. & Riezman, H. Understanding the diversity of membrane lipid composition. *Nat Rev Mol Cell Biol* **19**, 281–296 (2018).

279. Tsuchiya, A. *et al.* Polysialic acid/neural cell adhesion molecule modulates the formation of ductular reactions in liver injury: HEPATOLOGY, Vol. XX, No. X, 2014 TSUCHIYA ET AL. *Hepatology* **60**, 1727–1740 (2014).

280. Martínez-Reyes, I. & Chandel, N. S. Mitochondrial TCA cycle metabolites control physiology and disease. *Nat Commun* **11**, 102 (2020).

281. Xu, L., Wettschureck, N., Bai, Y., Yuan, Z. & Wang, S. Myofibroblast YAP/TAZ is dispensable for liver fibrosis in mice. *Journal of Hepatology* **75**, 238–241 (2021).

282. Mannaerts, I. *et al.* The Hippo pathway effector YAP controls mouse hepatic stellate cell activation. *Journal of Hepatology* **63**, 679–688 (2015).

283. Martin, K. *et al.* PAK proteins and YAP-1 signalling downstream of integrin beta-1 in myofibroblasts promote liver fibrosis. *Nat Commun* **7**, 12502 (2016).

284. Mooring, M. *et al.* Hepatocyte Stress Increases Expression of Yes-Associated Protein and Transcriptional Coactivator With PDZ-Binding Motif in Hepatocytes to Promote Parenchymal Inflammation and Fibrosis. *Hepatology* **71**, 1813–1830 (2020).

285. Lemaigre, F. P. Determining the fate of hepatic cells by lineage tracing: Facts and pitfalls: VIRAL HEPATITIS. *Hepatology* **61**, 2100–2103 (2015).

286. Español–Suñer, R. *et al.* Liver Progenitor Cells Yield Functional Hepatocytes in Response to Chronic Liver Injury in Mice. *Gastroenterology* **143**, 1564-1575.e7 (2012).

287. Sampaziotis, F. *et al.* Cholangiocyte organoids can repair bile ducts after transplantation in the human liver. *Science* **371**, 839–846 (2021).

Curriculum Vitae

Ece Yildiz

ece.yildiz@hotmail.com.tr, +41787356448

Chemin des Cottages 8, 1007 Lausanne

EDUCATION

Ph.D. in Biotechnology and Bioengineering, Expected Graduation 2022
École Polytechnique Fédérale de Lausanne (EPFL), Switzerland

M.Sc in Bioengineering, September 2015 - September 2017
Honor Degree, École Polytechnique Fédérale de Lausanne (EPFL), Switzerland

B.Sc in Molecular Biology and Genetics, September 2011 - June 2015
Honor Degree, Bilkent University, Turkey

RESEARCH EXPERIENCE

(March 2018 - Present)
Laboratory of Metabolic Signaling, École Polytechnique Fédérale de Lausanne (EPFL), Switzerland
Ph.D. thesis under the supervision of Prof. Kristina Schoonjans "*Dissecting the role of biliary epithelial cells during the progression of non-alcoholic fatty liver disease.*"

(October 2017 - February 2018)
Micro Biorobotic Systems Laboratory, École Polytechnique Fédérale de Lausanne (EPFL), Switzerland
Internship under the supervision of Prof. Selman Sakar

(February 2017 - August 2017)
Griffith Lab, Department of Biological Engineering, Massachusetts Institute of Technology (MIT), USA
Master thesis under the supervision of Prof. Linda Griffth "*Engineering a modifiable in vitro vascularized liver model.*"

(October 2016 - January 2017)
Laboratory of Stem Cell Biology, École Polytechnique Fédérale de Lausanne (EPFL), Switzerland
Semester project under the supervision of Prof. Matthias Lutolf "*Investigating the effects of a characteristic microbiome lysate on intestinal organoid self-renewal and differentiation.*"

(September 2014 - May 2015)
Therapeutic Oligonucleotide Research Laboratory, Bilkent University, Turkey
Undergraduate assistant under the supervision of Prof. Ihsan Gursel "Studying the factors that control microparticle uptake of macrophages and host that the microparticles are released from."

(June 2014 – September 2014)
Ploegh Lab, Whitehead Institute, USA
Summer Intern under the supervision of Hidde Ploegh "Receptor-mediated B Cell response generation by targeting dendritic cells with payloads linked to single-domain antibodies."

PROFESSIONAL QUALIFICATION

- Leadership & Teaching Experience

(March 2018 - Present)
- Teaching assistant for "Integrated Laboratory in Life Sciences" and "Physiology Laboratory" undergraduate courses
- Supervised a master's thesis student

(January 2018 – November 2019)
- A member of Innovation Forum Lausanne and worked in a team of 10 and organized 7 events and workshops
- Interviewed start-ups and wrote online articles about the start-up of the month
- Managed event announcements on the club website and social media

- Techniques & Skills

Experimental Skills: Cell culture & organoid culture / Assay development / qPCR / Bulk RNA-sequencing / Metabolic flux analysis / Tissue immunohistochemistry / Drug screening / Flow cytometry / Microscopy / ELISA / Western immunoblotting / Hydrogel preparation

Computational Skills: Image processing (Image J) / Graphpad prism / Adobe illustrator / R / Microsoft office (excel, word, powerpoint) / QuPATH

AWARDS

(2017)
Mention d'excellence, Master's degree, École Polytechnique Fédérale de Lausanne (EPFL), Switzerland

(2015)
High honor degree: graduated second out of forty students in Faculty of Science (GPA: 3.93/4.00), Bilkent University, Turkey

(2011)
Awarded full scholarship for undergraduate studies in Bilkent University, Turkey

(2011)
High school honor degree: class valedictorian, Turkey

PATENTS

Three-dimensional models of tissue fibrosis. S.Rezakhani, **E.Yildiz**, K.Schoonjans, M.Lutolf, G.Sorrentino. EP Patent Application Nr 19177445.4.

PUBLICATIONS

Yildiz, E., El Alam, G*., Perino A*., Jalil A., Denechaud P.D., Huber K., Fajas L., Auwerx J., Sorrentino G., Schoonjans, K. (2022). Hepatic lipid overload potentiates biliary epithelial cell activation via E2Fs. *eLife*. Under revision.

Wang, A. J., Allen, A., Sofman, M., Sphabmixay, P., **Yildiz, E**., & Griffith, L. G. (2022). Engineering Modular 3D Liver Culture Microenvironments In Vitro to Parse the Interplay between Biophysical and Biochemical Microenvironment Cues on Hepatic Phenotypes. *Advanced NanoBiomed Research*, *2*(1), 2100049.

Sorrentino, G*., Rezakhani, S*., **Yildiz, E**., Nuciforo, S., Heim, M. H., Lutolf, M. P., & Schoonjans, K. (2020). Mechano-modulatory synthetic niches for liver organoid derivation. *Nature communications*, *11*(1), 1-10.

Sorrentino, G., Perino, A., **Yildiz, E**., El Alam, G., Sleiman, M. B., Gioiello, A., ... & Schoonjans, K. (2020). Bile acids signal via TGR5 to activate intestinal stem cells and epithelial regeneration. *Gastroenterology*, *159*(3), 956-968.

CONFERENCE PARTICIPATION

E.Yildiz, G.El Alam, A.Perino, A.Jalil, P.D.Denechaud, K.Huber, L.Fajas, J.Auwerx, G.Sorrentino, K.Schoonjans. Hepatic lipid overload potentiates biliary epithelial cell activation via E2Fs. The Molecular and Cellular Basis of Regeneration and Tissue Repair, EMBO Workshop. Barcelona, September 2022.

S.Rezakhani, G.Sorrentino, **E.Yildiz**, S.Nuciforo, M.H.Heim, M.P.Lutolf, K.Schoonjans. Synthetic hydrogels for hepatic organoid culture. Organoids: Modelling Organ Development and Disease in 3D Culture, EMBO | EMBL. Virtual Symposium, October 2020.

D.Bayik, **E.Yildiz,** T.Kahraman, and I.Gursel. Scavenger-Receptor Mediated and Clathrin-Dependent Endocytosis Regulate Internalization of Extracellular Vesicles by Immune Cells. 2nd International Molecular Immunology & Immunogenetics Congress (MIMIC-II). Antalya, Turkey. 27-30 Apr. 2014. (Turkish Society of Immunology Bursary)

INTERESTS

Photography / Tennis / Painting / Playing the piano / Bike travel / Puzzles

nature COMMUNICATIONS

ARTICLE

https://doi.org/10.1038/s41467-020-17161-0 OPEN

Mechano-modulatory synthetic niches for liver organoid derivation

Giovanni Sorrentino[1,5], Saba Rezakhani[2,5], Ece Yildiz[1], Sandro Nuciforo[3], Markus H. Heim[3,4], Matthias P. Lutolf[2✉] & Kristina Schoonjans[1✉]

The recent demonstration that primary cells from the liver can be expanded in vitro as organoids holds enormous promise for regenerative medicine and disease modelling. The use of three-dimensional (3D) cultures based on ill-defined and potentially immunogenic matrices, however, hampers the translation of liver organoid technology into real-life applications. We here use chemically defined hydrogels for the efficient derivation of both mouse and human hepatic organoids. Organoid growth is found to be highly stiffness-sensitive, a mechanism independent of acto-myosin contractility and requiring instead activation of the Src family of kinases (SFKs) and yes-associated protein 1 (YAP). Aberrant matrix stiffness, on the other hand, results in compromised proliferative capacity. Finally, we demonstrate the establishment of biopsy-derived human liver organoids without the use of animal components at any step of the process. Our approach thus opens up exciting perspectives for the establishment of protocols for liver organoid-based regenerative medicine.

[1] Laboratory of Metabolic Signaling, Institute of Bioengineering, School of Life Sciences and School of Engineering, Ecole Polytechnique Fédérale de Lausanne, 1015 Lausanne, Switzerland. [2] Laboratory of Stem Cell Bioengineering, Institute of Bioengineering, School of Life Sciences and School of Engineering, École Polytechnique Fédérale de Lausanne (EPFL), 1015 Lausanne, Switzerland. [3] Department of Biomedicine, University Hospital Basel, University of Basel, 4031 Basel, Switzerland. [4] Clinic of Gastroenterology and Hepatology, University Hospital Basel, University of Basel, 4031 Basel, Switzerland. [5] These authors contributed equally: Giovanni Sorrentino, Saba Rezakhani. ✉email: matthias.lutolf@epfl.ch; kristina.schoonjans@epfl.ch

Although the liver has a remarkable regenerative potential, chronic inflammation and scarring severely impair liver regeneration[1], making organ transplantation the only treatment option for patients with severe liver failure[2]. This therapeutic approach, however, is limited by the lack of liver donors, emphasizing the urgent need for cell-based therapies[3]. A promising alternative to liver transplantation comes from the recent breakthrough that liver organoids can be generated in vitro within animal-derived matrices (e.g. Matrigel) from mouse and human bile duct-derived bipotential facultative progenitor cells[4–6] or primary hepatocytes[4,5,7–9]. The first type of organoids are largely composed of progenitor cells that are genetically stable and can be differentiated into functional hepatocyte-like cells, which are able to engraft and increase survival when transplanted in a mouse model of liver disease[4,5]. However, the batch-to-batch variability of the three-dimensional (3D) matrices currently used for organoid derivation, as well as their mouse-tumour-derived origin, makes them unsuited for therapeutic ends. Recent work has suggested that composite matrices of fibrin and laminin-111, optimized for intestinal organoid culture, could also be used for liver organoid growth[10,11]. Owing to the mouse-tumour-derived laminin, these matrices are, however, incompatible with clinical use, and to the best of our knowledge there is no protocol available to expand and differentiate clinical-grade hepatic organoids[12,13].

In this study, we report the establishment of a chemically defined and mechano-modulatory 3D culture system for mouse and human hepatic progenitors and organoids for basic research and regenerative medicine applications. We optimized the efficiency of liver organoid derivation by tuning the mechanical properties of the synthetic microenvironment to match the physiological stiffness of the mouse liver. Finally, we accurately modelled the stiffness of the fibrotic liver, and demonstrate that aberrant liver mechanics negatively impact liver progenitor proliferation.

Results

Generation of a PEG-based synthetic niche for liver organoid culture. We previously reported chemically defined 3D matrices for intestinal stem cell culture and organoid derivation[12], identifying design principles that could be adopted to mimic stem cell niches from different tissues. Here, we sought to develop a synthetic matrix for the efficient proliferation of liver progenitor cells by recapitulating key physical and biochemical characteristics of the hepatic microenvironment as an alternative to the established natural matrices Matrigel and collagen[4,14] (Supplementary Fig. 1a). To this aim, we first generated inert poly(ethylene glycol) (PEG) hydrogels enzymatically crosslinked by the activated transglutaminase factor XIIIa (FXIIIa)[15]. To mimic the mechanical properties of the mouse liver, we tuned the stiffness of PEG gels to physiological values (≈1.3 kPa)[16,17]. Key ECM proteins found in the native liver[18], such as laminin-111, collagen IV and fibronectin, were then incorporated in the PEG network, and soluble factors found in the hepatic niche, such as hepatocyte growth factor (HGF)[19], the Wnt agonist R-Spondin[4,20] and fibroblast growth factor 10 (FGF10)[21], were added to the culture medium, referred to as expansion medium (EM)[4].

Single dissociated mouse liver progenitor cells derived from Matrigel-expanded liver organoids were embedded into either Matrigel or PEG hydrogels and cultured in EM (Supplementary Fig. 1b). The functionalization of PEG hydrogels with fibronectin and laminin-111 led to efficient organoid generation, comparable to Matrigel (Fig. 1a, b). Replacement of the full-length fibronectin with its minimal integrin recognition peptide RGDSPG (Arg-Gly-Asp-Ser-Pro-Gly) led to similar results, suggesting that the addition of a minimal adhesive moiety to the otherwise inert matrix is sufficient to promote extensive proliferation of liver progenitors (Fig. 1a, b). Cells expanding in PEG hydrogels modified with RGDSPG ('PEG-RGD') generated cystic structures characterized by a central lumen and a surrounding epithelium (Fig. 1c, e). Histology and gene expression analyses showed that these PEG-RGD-derived organoids possess a progenitor phenotype expressing stem/ductal markers such as *Lgr5*, *Epcam*, *Krt19* and *Sox9* (Fig. 1d, e and Supplementary Fig. 1c) and, in terms of morphology and gene expression, are indistinguishable from organoids grown in Matrigel (Fig. 1d, e). As expected, markers of fully differentiated hepatocytes such as *Cyp3a11* were not expressed (Fig. 1d).

A major limitation of all current protocols for culturing epithelial organoids is an obligatory requirement of Matrigel (or similar natural ECM-derived matrices) in the first step of organoid generation. To test whether mouse liver organoids can be established in synthetic matrices without any initial Matrigel culture step, biliary duct fragments were isolated from mouse liver and directly embedded in PEG-RGD hydrogels (Supplementary Fig. 1b). Strikingly, after 6 days of culture, organoids emerged that could be serially passaged in culture (Fig. 1f and Supplementary Fig. 1d). PEG-RGD gels allowed organoid growth for more than 14 days (Supplementary Fig. 1e) without any significant structural deterioration. In contrast, Matrigel softened and no longer provided sufficient mechanical support already after 6 days of culture (Supplementary Fig. 1f), highlighting the importance of having a stably crosslinked matrix for long-term organoid culture.

Liver organoids cultured in PEG hydrogel efficiently differentiate into hepatocyte-like cells. Liver organoids can be differentiated in vitro into functional hepatocyte-like cells when cultured in the presence of specific differentiation medium (DM) containing inhibitors of Notch and TGF-β pathways[4,9] (Supplementary Fig. 2a). To test whether organoids derived in the synthetic matrix preserved the capacity for differentiation and hepatocyte maturation, we grew organoids in PEG-RGD gels and replaced the expansion medium with differentiation medium after 6 days, and analysed the expression of differentiated hepatocyte markers after 12 days (Supplementary Fig. 2d)[4]. Similar to Matrigel cultures, synthetic gels promoted a robust increase in the transcript levels of mature hepatocyte markers such as *Cyp3a11*, *Alb*, *Ttr*, *Nr1h4* (*Fxr*), *Slc2a2* (*Glut2*), *Glul* and *Nr1h3* (*Lxr*) (Fig. 2a) and expression of ALB and HNF4α proteins (Fig. 2b), while markers of stem cells, such as *Lgr5*, disappeared (Supplementary Fig. 2b). As expected, during the differentiation process, cells acquired a characteristic hepatocyte-like morphology, as evidenced by a polygonal shape and expression of junction proteins such as ZO-1 and E-cadherin (Fig. 2c, d). Occasionally, hepatocyte-like cells showed poly-nucleation, a typical feature of hepatocytes (Fig. 2c, d and Supplementary Fig. 2e).

Next, to test whether hepatocyte-like cells generated in PEG-RGD hydrogels display hepatocyte-specific functions, we monitored albumin secretion. Liver organoids grown in DM showed a marked increase in albumin secretion, as compared to organoids cultured in EM (Fig. 2e). Moreover, hepatocyte-like cells were able to produce and secrete urea, as well as to accumulate glycogen, two enzymatically regulated processes that occur in mature hepatocytes (Fig. 2f, g). Moreover, the majority of differentiated cells were capable of internalizing low-density lipoproteins (LDL) from the culture medium, indicating that LDL receptor-mediated cholesterol uptake is functional (Fig. 2h). Finally, differentiation of organoids directly derived in PEG-RGD hydrogels was as efficient as in Matrigel (Supplementary Fig. 2c).

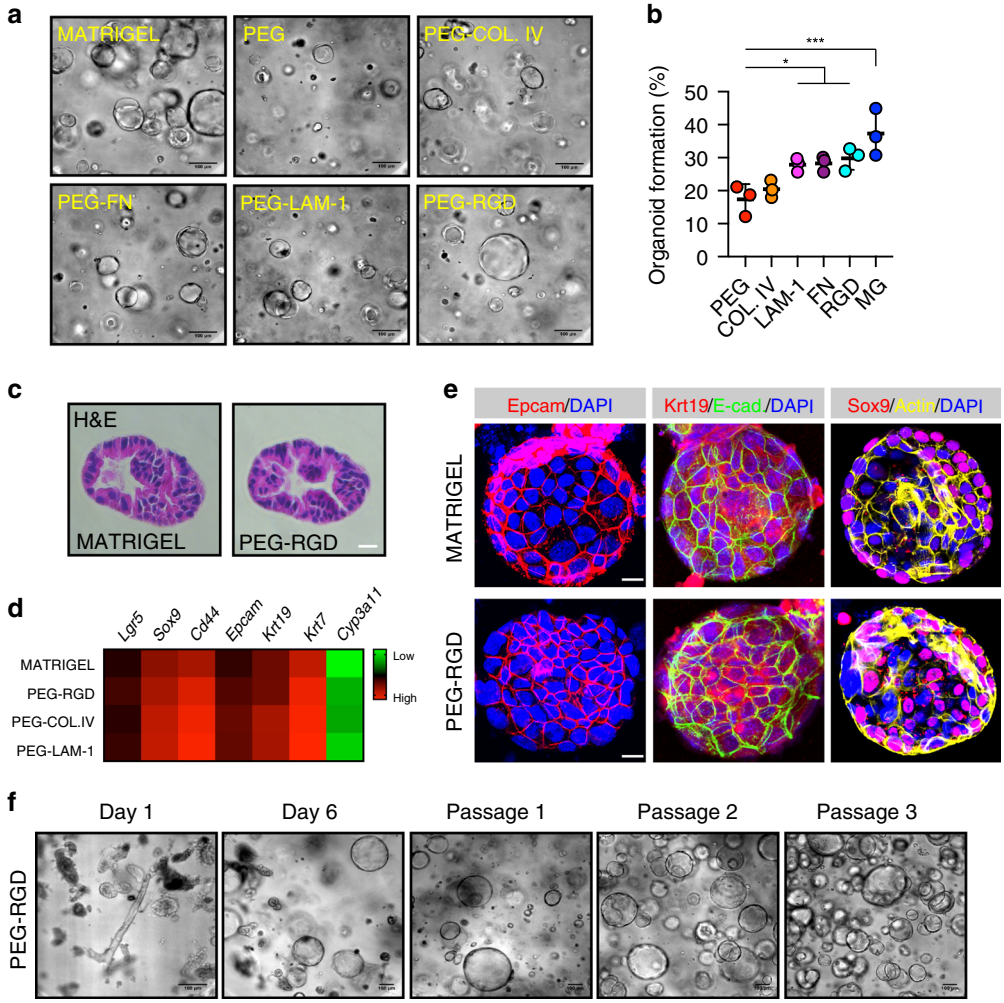

Fig. 1 Liver organoid growth in Matrigel and PEG supplemented with ECM components. a Mouse liver progenitor cells 3 days after embedding in: Matrigel (MG), plain PEG (PEG) and PEG functionalized with the indicated ECM components: COL.IV (collagen IV), FN (fibronectin), LAM-1 (laminin-1) and RGD-representing peptide (RGD). **b** Quantification of organoid formation efficiency relative to panel **a**. Graphs show individual data points derived from $n = 3$ independent experiments and means ± s.d., one-way Anova. $^{*}P < 0.05$, $^{***}P < 0.001$. $P = 0.0321$; $P = 0.0266$; $P = 0.0119$; $P = 0.0003$. Source data are provided as a Source Data file. **c** Hematoxylin and eosin staining of Matrigel- and PEG-derived organoids. Scale bar 25 µm. **d** Gene expression was analysed by qRT-PCR in liver organoids 6 days after embedding in Matrigel and PEG hydrogels supplemented with different ECM factors. The heatmap represents ΔCt values as described in the method section. **e** Liver organoid immunostaining was performed 6 days after embedding of liver progenitor cells in Matrigel or PEG-RGD. **f** Liver organoids can be cultured in PEG hydrogels by directly embedding mouse biliary duct fragments. Representative pictures are shown. Micrographs (**c**, **e**, **f**) are representative of three independent experiments.

Altogether, these results demonstrate that liver organoids grown in PEG-RGD hydrogels can be readily differentiated into hepatocyte-like cells that mimic many of the established hepatic functions.

Matrix stiffness controls liver organoid growth in an actomyosin-independent manner. Mechanical signals can play a critical role in controlling stem cell behaviour and tissue homeostasis[22], but also contribute to the manifestation of diseases[23–25]. Despite the recent progress in establishing novel 3D liver model systems[4,7,9], relatively little is known about the role of mechanics in regulating hepatic stem cell biology. This can be attributed to the fact that current culture systems rely on Matrigel, a matrix from tumour-derived origin, which has batch-to-batch stiffness variability and is not conducive to mechanical modification (Supplementary Fig. 3a). To test whether matrix mechanics affect liver organoid growth, we grew organoids in hydrogel of variable stiffness, ranging from values below the normal mouse liver stiffness (0.3 kPa) to those reaching physiological stiffness (1.3 kPa)[16,17]. Organoid formation efficiency and proliferation was profoundly affected by the mechanical properties of the matrix, with values mimicking physiological liver stiffness (between 1.3 and 1.7 kPa) being optimal (Fig. 3a, b and Supplementary Fig. 3b). Differentiation capacity, however, was unaffected by the degree of stiffness as induction of hepatic genes was maintained also when liver organoids were differentiated in soft gels (Supplementary Figs. 2d and 3c). These data demonstrate that optimizing the mechanical properties of the hydrogel represents a critical step in the efficient generation of liver organoids.

Given the pivotal role of the Hippo pathway nuclear effector, Yes associate protein (YAP), in the transduction of microenvironment mechanical cues downstream of integrins[26], we next tested whether YAP activation could potentially explain the observed matrix stiffness dependence. We monitored the expression of canonical YAP target genes and YAP subcellular localization in organoids cultured in soft (0.3 kPa) and physiologically stiff (1.3 kPa) matrices. Interestingly, in stiffer hydrogels, YAP target genes expression and nuclear accumulation were increased

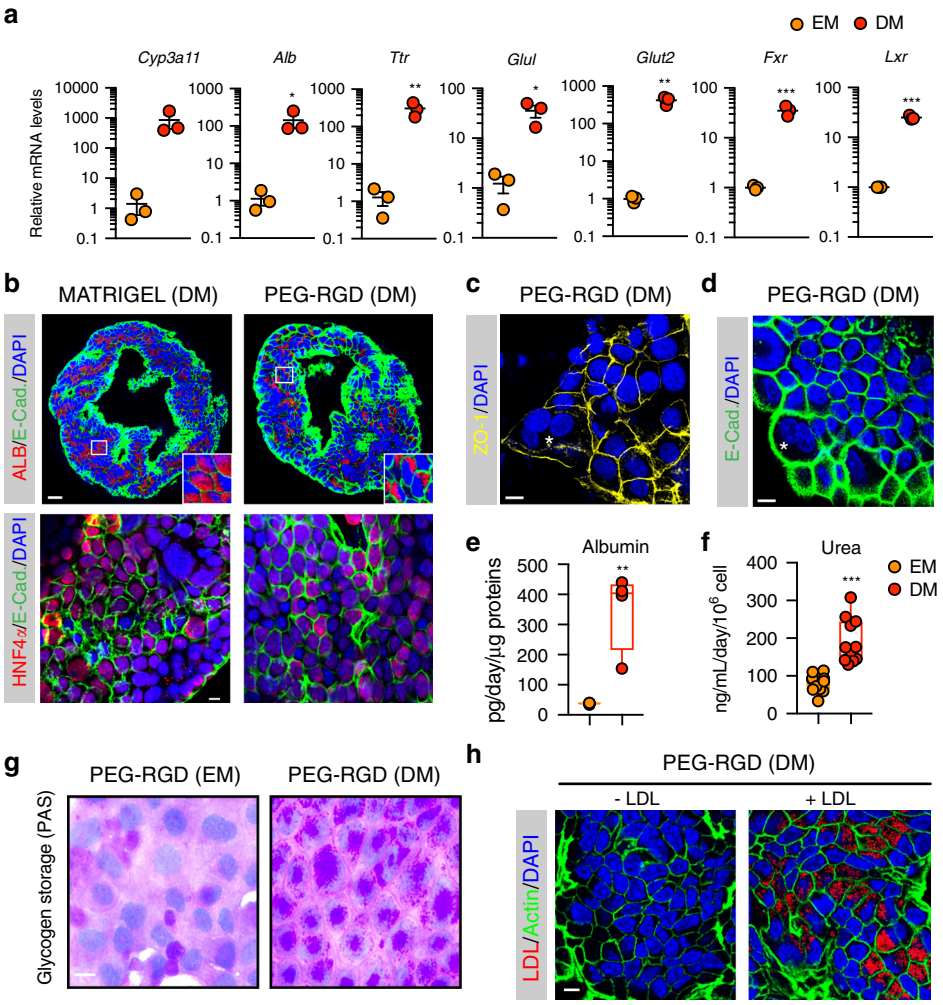

Fig. 2 Differentiation of liver organoids into hepatocyte-like cells in PEG-RGD hydrogels. a Gene expression was analysed by qRT-PCR in liver organoids maintained in expansion medium (EM) or differentiation medium (DM) in PEG-RGD hydrogels. Graphs show individual data points derived from $n = 3$ independent experiments and means ± SEM, unpaired Student's one-tailed *t*-test. $^{*}P < 0.05$, $^{**}P < 0.01$, $^{***}P < 0.001$ ($P = 0.030$; 0.0077; 0.0007; 0.0126; 0.0009; 0.00003). **b** Representative confocal immunofluorescence images of Albumin (ALB), Hnf4a and E-Cadherin (E-CAD.). Scale bars: 25 µm (top), 10 µm (bottom). **c** Representative confocal immunofluorescence images of ZO-1 in liver organoids maintained in differentiation medium (DM) in PEG-RGD hydrogels. The asterisk indicates a binucleated cell. Scale bar 10 µm. **d** Liver organoids maintained in differentiation medium (DM) in PEG-RGD hydrogels. E-cadherin was used to visualize cell borders. The asterisk indicates a binucleated cell. Scale bar 10 µm. **e** Albumin secretion was quantified in the supernatant of organoids embedded in PEG-RGD hydrogels and maintained in EM or DM. Center line, median; box, interquartile range (IQR); whiskers, range (minimum to maximum). Red and orange dots, individual data points derived from $n = 4$, unpaired Student's two-tailed *t*-test. $^{**}P < 0.01$ ($P = 0.0031$). **f** Urea production was quantified in the supernatant of organoids embedded in PEG-RGD hydrogels and maintained in EM or DM. Center line, median; box, interquartile range (IQR); whiskers, range (minimum to maximum). Red and orange dots, individual data points derived from $n = 11$, unpaired Student's two-tailed *t*-test. $^{***}P < 0.001$ ($P < 0.0001$). **g** Glycogen accumulation was assessed by PAS (Periodic-Acid Schiff) staining in liver organoids embedded in PEG-RGD hydrogels and maintained in EM or DM. Scale bar 10 µm. **h** LDL uptake was monitored by Dil-ac-LDL fluorescent substrate in liver organoids maintained in DM in PEG-RGD hydrogels. Scale bar 10 µm. Micrographs (**b**–**d**, **g**, **h**) are representative of three independent experiments. Source data are provided as a Source Data file.

compared to soft matrices (Fig. 3c and Supplementary Fig. 3d). To examine whether an activated integrin/YAP signalling axis is functionally required for organoid derivation in physiologically stiff matrices, we treated organoid cultures with PF-573228 (PF), an inhibitor of the integrin effector focal adhesion kinase (FAK), or with the YAP inhibitor Verteporfin (VP)[27] (Fig. 3d). Both treatments prevented the increase in organoid formation induced in stiffer matrices (Fig. 3e and Supplementary Fig. 3e), indicating that the integrin/YAP module is required in coordinating growth of liver progenitors in response to mechanical stimuli.

We then sought to identify the other components of the FAK-YAP cascade that may play a role in modulating the stiffness response in our system. Since remodelling of the actin cytoskeleton has been identified as a key event upstream of YAP activation[28–30], we assessed its putative involvement in physiological stiffness-induced organoid growth by inhibiting acto-myosin contractility with blebbistatin[31]. Surprisingly, blebbistatin treatment significantly enhanced organoid formation (Fig. 3f) with an efficiency comparable to ROCK inhibitors (Supplementary Fig. 3g), indicating that matrix stiffness promotes organoid growth independently of cytoskeletal dynamics, and that acto-myosin contractility rather interferes with normal liver progenitor expansion. However, tyrosine phosphorylation of YAP by the Src family of kinases (SFK), an alternative route for integrin-dependent and acto-myosin independent YAP activation[32–40], was increased by matrix

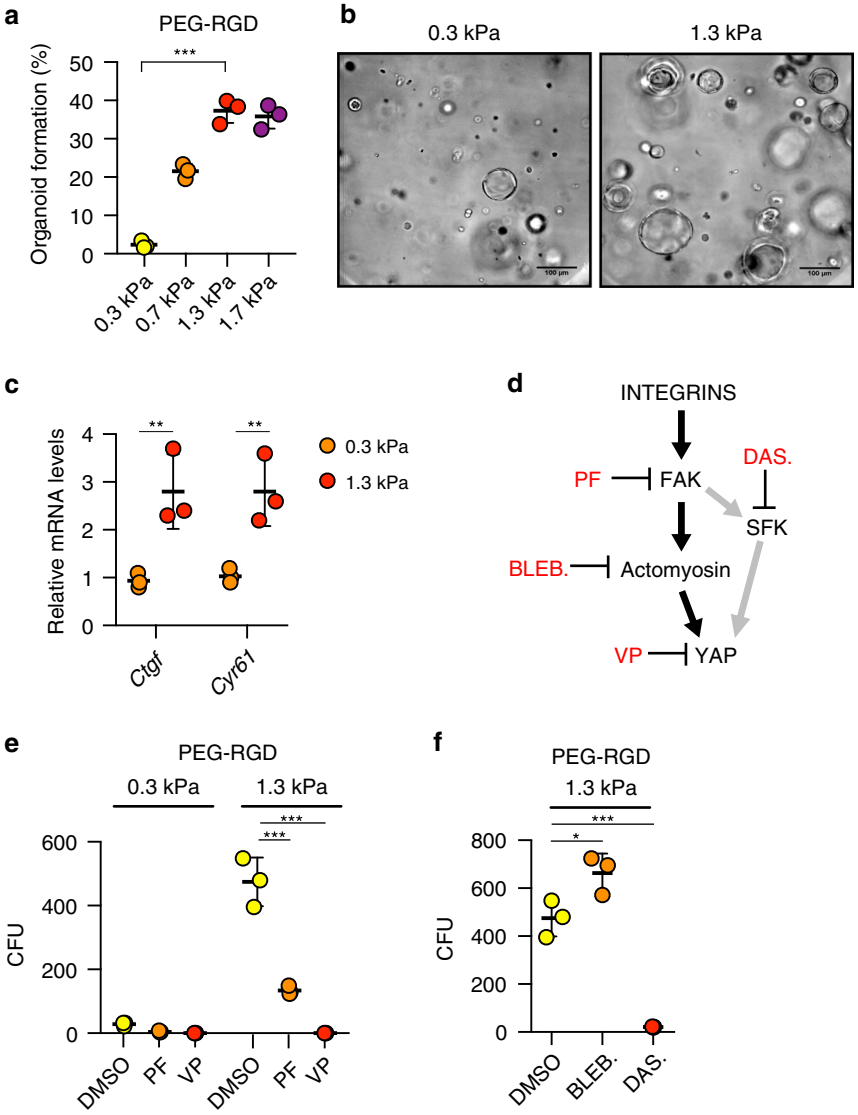

Fig. 3 Effect of matrix stiffness on liver organoid formation. a Effect of matrix stiffness on organoid formation efficiency. Graphs show individual data points derived from $n = 3$ independent experiments and means ± s.d. ($P < 0.0001$). **b** Representative image of organoids 3 days after embedding in PEG-RGD hydrogels of indicated stiffness. **c** Gene expression was analysed by qRT-PCR in liver organoids 6 days after embedding in PEG-RGD hydrogels with indicated stiffness. Graphs show individual data points derived from $n = 3$ independent experiments and means ± s.d. ($P = 0.0088$; 0.0077). **d** Schematic representation of cellular mechano-signalling pathways. Inhibitors of key elements are depicted in red. **e** Effect of indicated inhibitors on organoid formation efficiency in soft (300 Pa) and physiologically stiff (1.3 kPa) PEG-RGD hydrogels. CFU (colony forming unit). Graphs show individual data points derived from $n = 3$ independent experiments and means ± s.d. ($P < 0.0001$). **f** Effect of indicated inhibitors on organoid formation efficiency in physiologically stiff (1.3 kPa) PEG-RGD hydrogels. CFU (colony forming unit). Graphs show individual data points derived from $n = 3$ independent experiments and means ± s.d. ($P = 0.0198$; 0.0003). $^{*}P < 0.05$, $^{**}P < 0.01$, $^{***}P < 0.001$ one-way Anova (**a**, **f**) or two-way Anova (**c**, **e**). Source data are provided as a Source Data file.

stiffness (Supplementary Fig. 3f). Of interest, treatment with Dasatinib[41], a FDA-approved SFK inhibitor, fully abolished YAP phosphorylation and organoid growth in physiologically stiff (1.3 kPa) matrices (Fig. 3f and Supplementary Fig. 3f). These results corroborate the importance of the integrin/SFK/YAP signalling pathway in liver progenitor proliferation in response to differential mechanical inputs.

PEG hydrogels can be tuned to model fibrotic liver mechanics. Liver disease progression is strongly associated with abnormal tissue architecture and mechanotransduction[16,42,43]. Indeed, as a direct effect of aberrant ECM deposition in the fibrotic liver, tissue stiffness increases in time and severely compromises its function[44–46]. In fact, the changes in liver stiffness associated with disease are used for diagnostics based on longitudinal noninvasive monitoring[47]. We reasoned that liver organoids grown in defined hydrogels recapitulating the stiffness of fibrotic liver could serve as physiologically relevant 3D model to investigate how stem cells translate aberrant mechanical inputs into disease-relevant phenotypes. To this aim, we generated fibrosis-mimicking hydrogels with a stiffness of 4 kPa[16,17]. Strikingly, these hydrogels led to a significant impairment of organoid formation (Fig. 4a, b and Supplementary Fig. 3a), demonstrating that an abnormal ECM stiffness is sufficient to decrease the liver progenitor proliferative capacity. In this condition liver organoids showed a reduction in the expression of hepatic progenitor markers (Fig. 4c) and upregulation of genes involved in cellular response to hepatic injury (Fig. 4d and Supplementary Fig. 4a), indicating impaired stemness potential and concomitant induction of a stress

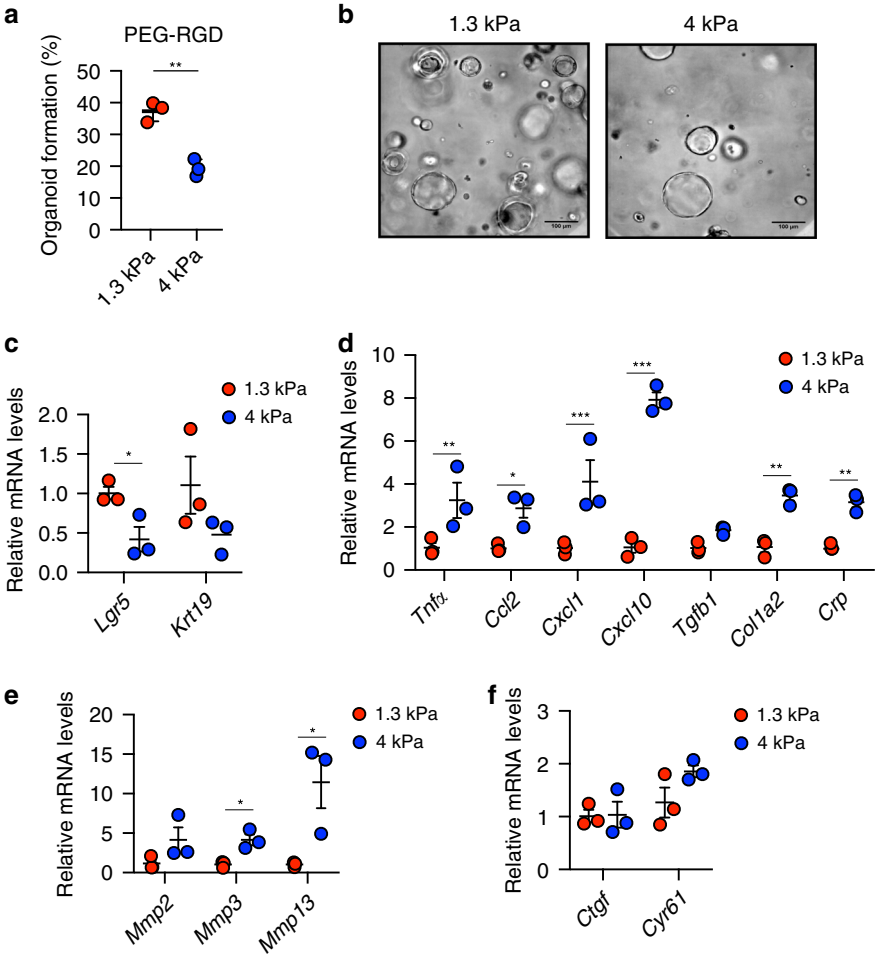

Fig. 4 Hydrogels mimicking the stiffness of native fibrotic liver affect the growth of liver organoids and promote a stress response. a Effect of matrix stiffness on organoid formation efficiency. Graphs show individual data points derived from $n = 3$ independent experiments and means ± SEM, unpaired Student's two-tailed *t*-test ($P = 0.0017$). **b** Representative image of organoids 3 days after embedding in PEG-RGD hydrogels of indicated stiffness. Scale bars: 100 µm. **c**–**f** Gene expression was analysed by qRT-PCR in liver organoids 6 days after embedding in PEG-RGD hydrogels with indicated stiffness. Graphs show individual data points derived from $n = 3$ independent experiments and means ± SEM. c ($P = 0.0218$); **d** ($P = 0.0051$; 0.0223; 0.0001; 0.0001; 0.0021; 0.0056); e (0.0127; 0.033). $^*P < 0.05$, $^{**}P < 0.01$ $^{***}P < 0.001$ unpaired Student's two-tailed *t*-test (**c**, **e**) or two-way Anova (**d**, **f**). Source data are provided as a Source Data file.

response. Finally, fibrosis-mimicking hydrogels led to an increase in the expression of matrix metalloproteases (Fig. 4e), a compensatory phenomenon known to be induced in response to increased ECM stiffness[48–50]. Surprisingly, in these conditions YAP activation was not affected (Fig. 4f), suggesting the existence of other pathways controlling liver progenitor growth in response to increased stiffness. These results suggest that synthetic hydrogels may be a useful tool to assess the contribution of mechanical inputs on liver diseases.

PEG hydrogels allow derivation and culture of human liver organoids. To test the potential clinical relevance of our findings, we assessed whether the PEG-RGD hydrogels, initially designed for expansion and differentiation of mouse liver organoids, were also suitable for culturing human organoids. We first generated Matrigel-derived organoids from human non-tumorigenic liver needle biopsies[5]. Human liver progenitor cells were then embedded in PEG-RGD and cultured in human expansion medium (HEM) (Supplementary Fig. 4b). In these conditions human liver progenitor cells generated organoids that could be expanded over multiple passages (Fig. 5a). Similar to mouse, human organoid generation efficiency in PEG-RGD was comparable to Matrigel (Fig. 5a), and was critically dependent on changes in hydrogel stiffness (Fig. 5b). Moreover, when cultured in HEM, human liver organoids grown in PEG-RGD expressed progenitor cell markers, such as KRT19 (Fig. 5c), but readily differentiated into human hepatocyte-like cells when cultured in human differentiation medium (HDM) (Fig. 5d and Supplementary Fig. 4c).

Finally, in order to generate clinically relevant human liver organoids, we tested the possibility of establishing organoids from human patients without the interference of any animal-derived matrices. To this aim, freshly isolated liver biopsies from six patients were digested and directly embedded in PEG-RGD hydrogels (Fig. 5e). Strikingly, after 8 days of culture, organoid formation was scored from progenitor cells of all patients (Fig. 5f) and could be passaged (Fig. 5g) and differentiated (Supplementary Fig. 4d). Moreover, liver organoids could be frozen-thawed in PEG-RGD hydrogels (Supplementary Fig. 4e).

Altogether, these data provide proof-of-concept that human liver progenitor cells can be derived and maintained in vitro within synthetic matrices.

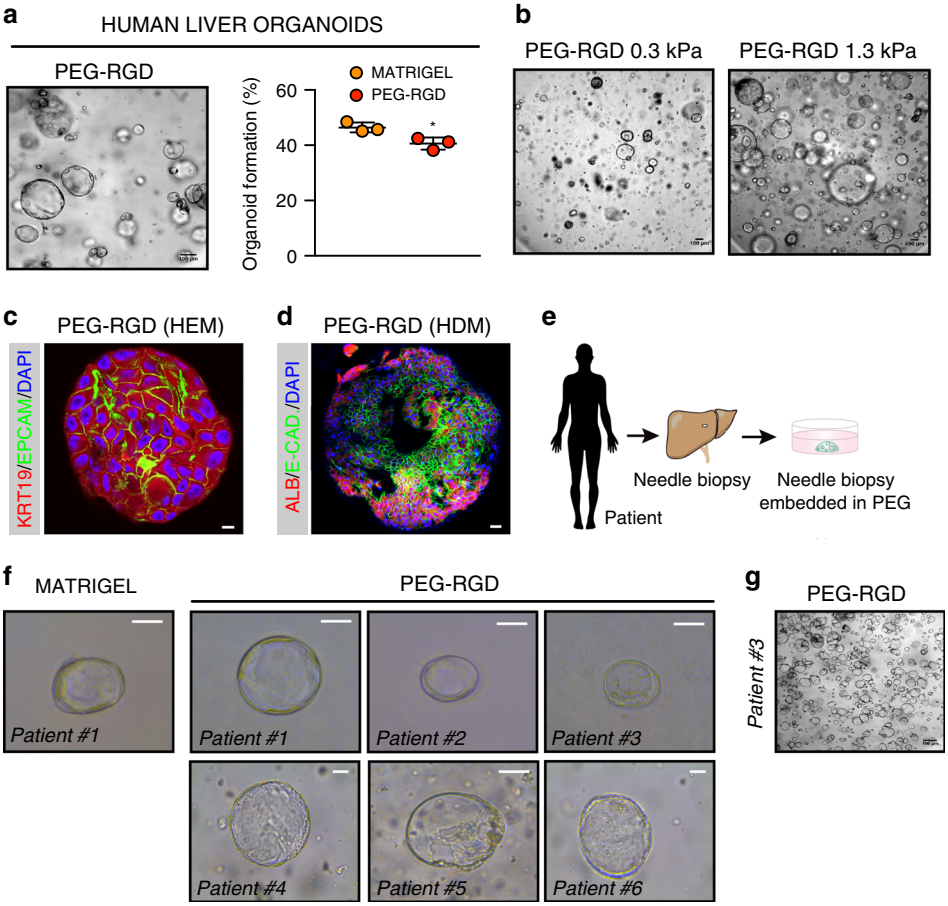

Fig. 5 PEG-RGD hydrogels allow for establishment, expansion and differentiation of patient-derived human liver organoids. a Matrigel-derived human liver progenitor cells were embedded in physiologically stiff PEG-RGD hydrogels and passaged in human expansion medium (HEM) with an efficiency comparable to Matrigel. Representative picture (left) and quantification of organoid formation efficiency (right). Graphs show individual data points derived from $n = 3$ independent experiments and means ± SEM, unpaired Student's two-tailed t-test. $^*P < 0.05$ ($P = 0.0231$). **b** Effect of matrix stiffness on human liver organoid formation. **c** Representative confocal immunofluorescence image of KRT19 and Epcam in liver organoids embedded in physiologically stiff PEG-RGD hydrogels and cultured in HEM. Scale bar 10 µm. **d** Representative confocal immunofluorescence image of Albumin and E-Cadherin in liver organoids cultured in human differentiation medium (HDM), Scale bar 25 µm. **e**, **f** Freshly isolated liver biopsies from six patients were digested and directly embedded in PEG-RGD hydrogels. Scale bar 50 µm. **g** PEG-RGD-derived human liver progenitor cells were embedded in physiologically stiff hydrogels and passaged in human expansion medium (HEM). Scale bar 100 µm. Micrographs (**c**, **d**, **g**) are representative of three independent experiments. Source data are provided as a Source Data file.

Discussion

We report here the establishment of a fully defined 3D culture system for mouse and human hepatic progenitors and organoids. We demonstrated that liver organoids can be expanded and maintained in such minimal environments with an efficiency that is comparable to Matrigel, but without its main disadvantages of structural instability, batch-to-batch variability and clinical incompatibility. By tuning the stiffness of the synthetic networks to match the physiological levels of the liver, we optimized the efficiency of liver organoid derivation, and identified integrin-SFK-YAP as a mechano-sensitive axis that is required for liver organoid growth. Interestingly, in contrast to intestinal organoids[12], we found that liver progenitor cells transduce mechanical signals in an acto-myosin independent manner and instead require activation of the tyrosine kinase Src to support epithelial tissue formation. Moreover, we used PEG hydrogels to accurately model the aberrant mechanical properties of the fibrotic liver, providing evidence that aberrant liver stiffness negatively impacts liver progenitor proliferation. This experimental setup provides a standardized framework to study hepatic progenitor cells in a defined mechanical environment, which may further our understanding of the underappreciated role of mechanical cues in modulating the molecular properties and signatures of this cell population in healthy and fibrotic liver. Finally, our data showing that clinically relevant human stem/progenitor cells can be grown in vitro without any requirement of animal-derived matrices, may open exciting perspectives for the establishment of protocols for liver organoid-based clinical applications.

Methods

Data reporting. The experiments were not randomized and the investigators were not blinded to allocation during experiments and outcome assessment. No statistical methods were used to determine sample size. The experiments were repeated at least three times or with at least three different donors to control biological variations.

Animals and ethical approval. Liver tissues were harvested from 8–12-weeks-old euthanized C57BL/6 J male mice. All the animal experiments were authorized by the Veterinary Office of the Canton of Vaud, Switzerland under the license authorization no. 3263. The mice were housed in groups of five mice per cage with access to food and water. The temperature of the animal facility was set at 22 ± 2 °C, the hygrometry at 40–60% and the light cycle (12:12) from 7:00 to 19:00.

Enzymatically crosslinked hydrogel precursor synthesis. Hydrogel precursors were synthesized as previously reported[51]. Briefly, vinylsulfone functionalized 8-arm PEG (PEG-VS) was purchased from NOF. The transglutaminase (TG) factor XIII (FXIIIa) substrate peptides Ac-FKGG*GPQGIWGQ*-ERCG-NH2 with matrix metalloproteinases (MMPs)-sensitive sequence (in italics), Ac-FKGG-GDQGIAGF-ERCG-NH2, H-NQEQVSPLERCGNH2 and the RGD-presenting adhesion peptide H-NQEQVSPLRGDSPG-NH2, were purchased from GL Biochem. FXIIIa substrate peptides and 8-arm PEG-VS were dissolved in triethanolamine (0.3 M, pH 8.0) and mixed at 1.2 stoichiometric excess (peptide-to-VS group), and allowed to react for 2 h under inert atmosphere. The reaction solution was dialysed (Snake Skin, MWCO 10 K, PIERCE) against ultrapure water for 3 days at 4 °C, after which the products were lyophilized and dissolved in ultrapure water to make 13.33% w/v stock solutions.

Formation and dissociation of PEG hydrogels. PEG precursor solutions were mixed in stoichiometrically balanced ratios to form hydrogel networks of a desired final PEG content. Addition of thrombin-activated FXIIIa (10 U ml−1; Galexis) triggered the hydrogel formation in the presence of Tris-buffered saline (TBS; 50 mM, pH 7.6) and 50 mM CaCl2. The spare reaction volume was used for the incorporation of dissociated liver stem cells, fragments of liver bile ducts, and ECM components: RGD-presenting adhesion peptide, fibronectin (0.5 mg ml−1; R&D systems), laminin-111 (0.2 mg ml−1; Invitrogen), collagen IV (0.2 mg ml−1; BD Bioscience). Gels cast on PDMS-coated 24-well plate were allowed to crosslink by incubation at 37 °C for 10 min. To release the grown colonies for further processing, gels were detached from the bottom of the plates using a tip of a metal spatula and transferred to 15-ml Falcon tube containing 1 ml of Dispase (1 mg/ml, Thermo Fisher Scientific). After 10 minutes enzymatic digestion, the reaction was quenched using 10% FBS containing 1 mM EDTA, washed with cold basal medium and centrifuged for 3 min at 1000 rpm.

Mechanical characterization of PEG hydrogels. Elastic modulus (G') of hydrogels was measured by performing small-strain oscillatory shear measurements on a Bohlin CVO 120 rheometer with plate-plate geometry. Briefly, 1–1.4 mm thick hydrogel discs were prepared and allowed to swell in water for 24 h. The mechanical response of the hydrogels sandwiched between the parallel plates of the rheometer was recorded by performing frequency sweep (0.1–10 Hz) measurements in a constant strain (0.05) mode at 25 °C.

Quantification of liver organoid formation efficiency. Phase contrast z-stacks images were collected through the entire thickness of the PEG gels (every 15 µm) at four different locations within the gels (Nikon Eclipse Ti). The Cell Counter plugin in ImageJ (NIH) was used to quantify the percentage of single cells that formed colonies after 3 days of culture in expansion medium.

Culture of mouse and human liver organoids. Mouse liver organoids were established from biliary duct fragments as previously described with some modifications[4]. Briefly, liver tissues were digested in digestion solution (Collagenase type XI 0.012%, dispase 0.012%, FBS 1% in DMEM medium) for 2 h. When digestion was complete, bile ducts were pelleted by mild centrifugation (200 rpm for 5 min) and washed with PBS. Isolated ducts were then resuspended either in Type I Collagen (8–11 mg/ml prepared following manufacturer's instruction—from Corning), Matrigel (BD Bioscience) or PEG precursor solution and cast in 10 µl droplets in the centre of the wells in a 48-well plate. After the gels were formed, 250 µl of isolation medium was added to each well. Isolation medium was composed of AdDMEM/F-12 (Invitrogen) supplemented with B-27 and N-2 (both GIBCO), 1.25 µM N-acetylcysteine (Sigma–Aldrich), 10 nM gastrin (Sigma–Aldrich) and the following growth factors: 50 ng ml^{-1} EGF (Peprotech), 1 µg ml^{-1} Rspo1 (produced in-house), 100 ng ml^{-1} Fgf10 (Peprotech), 10 mM nicotinamide (Sigma–Aldrich), 50 ng ml^{-1} HGF (Peprotech), Noggin (100 ng ml^{-1} produced in-house), Wnt 3a (1 µg ml^{-1}, Peprotech) and Y-27632 (10 µM, Sigma). After the first 4 days, isolation medium was changed with expansion medium (EM), which consists of isolation medium without Noggin, Wnt and Y-27632. One week after seeding, organoids were removed from the Matrigel or PEG hydrogel, dissociated into single cells using TrypLE express (Gibco), and transferred to fresh Matrigel or PEG hydrogels. Passaging was performed in 1:3 split ratio once per week. Plasmids for Rspo1 and Nog production were a kind gift from Joerg Huelsken. Liver progenitor cells were treated with the following compounds for YAP-inhibition experiments: Verteporfin (10 µM, Sigma), Dasatinib (10 µM, Selleckchem), Blebbistatin (10 µM StemCell Technologies), PF-573228 (10 µM Tocris).

Human liver biopsies and generation of human organoids. Human tissues were obtained from patients undergoing diagnostic liver biopsy at the University Hospital Basel. Written informed consent was obtained from all patients. The study was approved by the ethics committee of the northwestern part of Switzerland (Protocol Number EKNZ 2014-099). Ultrasound (US)-guided needle biopsies were obtained with a coaxial liver biopsy technique as described previously[50]. One biopsy cylinder was fixed in formalin and paraffin-embedded for histopathological diagnosis. Additional cylinders were collected in advanced DMEM/F-12 (GIBCO) for organoid generation. Patient clinical information are shown in Supplementary Table 2. Human liver organoids were generated as previously described with some modifications[5,50]. Briefly, biopsies were placed in advanced DMEM/F-12 (GIBCO) and transported to the laboratory on ice. Liver samples were then digested to small-cell clusters in basal medium containing 2.5 mg/mL collagenase IV (Sigma) and 0.1 mg/mL DNase (Sigma) at 37 °C. Cell clusters were embedded in Matrigel or PEG gels, cast and after the gels were formed, human isolation medium (HIM) was added. HIM is composed of advanced DMEM/F-12 (GIBCO) supplemented with B-27 (GIBCO), N-2 (GIBCO), 10 mM nicotinamide (Sigma), 1.25 mM N-acetyl-L-cysteine (Sigma), 10 nM [Leu15]-gastrin (Sigma), 10 µM forskolin (Tocris), 5 µM A8301 (Tocris), 50 ng/mL EGF (PeproTech), 100 ng/mL FGF10 (PeproTech), 25 ng/ml HGF (PeproTech), 1 µg ml^{-1} Rspo1 (produced in-house), Wnt 3a (1 µg ml^{-1}, Peprotech), Y-27632 (10 µM, Sigma) and Blebbistatin (10 µM StemCell Technologies). After the first 4 days, isolation medium was changed with human expansion medium (HEM), which consists of HIM without Noggin, Wnt and Y-27632.

Mouse hepatocyte differentiation. Single cells were seeded and kept for 6 days in EM. Then the medium was changed to differentiation medium (DM), which no longer contains Rspo1, HGF and nicotinamide and instead contains A8301 (50 nM, Tocris Bioscience) and DAPT (10 nM, Sigma–Aldrich). Cells were maintained in DM for 12 days. During the last 3 days DM was also supplemented with dexamethasone (Sigma, 3 µM). Medium was changed every 2 days.

Human hepatocyte differentiation. Single cells were seeded and kept 6 days in HEM. Then the medium was changed to differentiation medium (HDM), which no longer contains Rspo1, HGF and nicotinamide and instead contains A8301 (50 nM, Tocris Bioscience) and DAPT (10 nM, Sigma–Aldrich), BMP7 (25 ng/ml Peprotech) and human Fgf19 (100 ng/ml, R&D). Cells were maintained in DM for 10 days. During the last 3 days DM was also supplemented with dexamethasone (3 µM). Medium was changed every 2 days.

Immunohistochemical analysis of human organoids. Human organoids were fixed in 10% neutral buffered formalin, washed with PBS, dehydrated, and embedded in paraffin. Five-micrometre thick sections were made from paraffin-embedded samples and sections were stained with H&E and PAS.

Immunofluorescence analysis. Liver organoids were extracted from Matrigel (with Cell Recovery Solution, Corning) or PEG gels (with 1 mg ml− 1 Dispase (Gibco) for 10 min at 37 °C) and fixed with 4% paraformaldehyde (PFA) in PBS (20 min, room temperature). Organoids in suspension were centrifuged (1000 r.p.m., 5 min) to remove the PFA, washed with ultrapure water and pelleted. The organoids were then spread on glass slides and allowed to attach by drying. Attached organoids were rehydrated with PBS and permeabilized with 0.2% Triton X-100 in PBS (1 h, room temperature) and blocked (1% BSA in PBS) for 1 h. Samples were then incubated overnight with phalloidin-Alexa 488 (Invitrogen) and primary antibodies against Epcam (1:50, eBioscience, G8.8), Krt19 (1:100, Abcam, ab15463), E-cadherin (1:100, Cell Signaling, 24E10), Sox9 (1:50, Millipore, AB5535), Albumin (1:50, R&D systems, MAB1455), Hnf4α (1:50, Santa Cruz, C19), ZO-1 (1:50, Invitrogen, 61-7300); YAP (1:50, Cell Signaling, 4912 S). Samples were washed with PBS and incubated for 3 h with secondary antibodies Alexa 488 donkey-α-rabbit, Alexa 568 donkey-α-mouse, Alexa 647 donkey-α-goat (1:1000 in blocking solution; Invitrogen). Following extensive washing, stained organoids were imaged by confocal (Zeiss LSM 710) mode. Dapi was used to stain nuclei.

Western blotting. Samples were lysed in lysis buffer (50 mM Tris (pH 7.4), 150 mM KCl, 1 mM EDTA, 1% NP-40, 5 mM NAM, 1 mM sodium butyrate, protease and phosphatase inhibitors). Proteins were separated by SDS–PAGE and transferred onto nitrocellulose or polyvinylidene difluoride membranes. Blocking (30 min) and antibody incubations (overnight) were performed in 5% BSA in TBST. YAP1 (Santa Cruz sc101199, 1:1000), phospho-YAP1^{Y357} (Abcam ab62751, 1:1000), ACTIN (Santa Cruz sc47778, 1:1000), CXCL10 (RD system AF-466-NA, 1:1000), CCL2 (Novus Biologicals NBP2-22115, 1:1000), COL1A2 (Santa Cruz, 1:1000).

Quantitative real-time qRT-PCR for mRNA quantification. Liver organoids were extracted from Matrigel or PEG gels as previously described[12]. RNA was extracted from organoids using the RNAqueous total RNA isolation kit (Thermo Fisher) following manufacturer's instructions. RNA was transcribed to complementary DNA using QuantiTect Reverse Transcription Kit (Qiagen) following manufacturer's instructions. Expression of selected genes was analysed using the LightCycler 480 System (Roche) and SYBR Green chemistry. Quantitative reverse transcription polymerase chain reaction (PCR) results were presented relative to the mean of *Gapdh* (ΔΔCt method). Expression values shown as heatmap are reported as delta cycle threshold (ΔCt) values normalized using *Gapdh* (ΔCt values were calculated as ΔCt = Ct[target gene] − Ct[*Gapdh*] and represented by scale colour of ΔCt values [Green-low expression; Red-high expression])[51]. Primers for qRT-PCR are listed in Supplementary Table 1.

Proliferation assay. Cell proliferation was assessed by EdU assay (Click-iT EdU Alexa Fluor 647) following manufacturer's instructions. Liver organoids were incubated with EdU for 2 h.

For quantification of EdU+ cells, one section per organoid showing the largest dimension of the organoid was analyzed (15 organoid per condition) and from each section EdU+ cells were manually counted and expressed as percentage of cells calculated from nuclear labeling with DAPI.

Functional analysis. LDL uptake was detected with DiI-Ac-LDL (Biomedical Technologies). Mouse albumin secretion was detected with ELISA kit (Abcam, ab108792). Urea secretion was assessed with QuantiChrom™ Urea Assay Kit (BioAssay Systems). All experiments were performed according to the manufacturers' instructions.

Statistical analysis and sample information. Statistically significant differences between the means of two groups were assessed as specified in the legends. All statistical analyses were performed in the GraphPad Prism 7.0 software. A *P*-value <0.05 was considered statistically significant.

Reporting summary. Further information on research design is available in the Nature Research Reporting Summary linked to this article.

Data availability

All summary or representative data generated and supporting the findings of this study are available within the paper. The data underlying Figs. 1b, d, 2a, e, f, 3a, c, e, f, 4a, c–f, 5a and Supplementary Figs. 1b, 2a–c, 3a–c, g, 4c and uncropped blots are provided as a Source Data file. Source data are provided with this manuscript.

Received: 2 September 2019; Accepted: 11 June 2020;
Published online: 10 July 2020

References

1. Michalopoulos, G. K. Liver regeneration. *J. Cell. Physiol.* **213**, 286–300 (2007).
2. Williams, R., Schalm, S. W. & O'Grady, J. G. Acute liver failure: redefining the syndromes. *Lancet* **342**, 273–275 (1993).
3. Klein, A. S. et al. Organ donation and utilization in the United States, 1999-2008: Special feature. *Am. J. Transplant.* **10**, 973–986 (2010).
4. Huch, M. et al. In vitro expansion of single Lgr5+ liver stem cells induced by Wnt-driven regeneration. *Nature* **494**, 247–250 (2013).
5. Huch, M. et al. Long-term culture of genome-stable bipotent stem cells from adult human liver. *Cell* **160**, 299–312 (2015).
6. Evarts, R. P., Nagy, P., Marsden, E. & Thorgeirsson, S. S. A precursor-product relationship exists between oval cells and hepatocytes in rat liver. *Carcinogenesis* **11**, 1737–1740 (1987).
7. Takebe, T. et al. Generation of a vascularized and functional human liver from an iPSC-derived organ bud transplant. *Nat. Protoc.* **9**, 396–409 (2014).
8. Peng, W. C. et al. Inflammatory cytokine TNFα promotes the long-term expansion of primary hepatocytes in 3D culture. *Cell* **175**, 1607–1619.e15 (2018).
9. Hu, H. et al. Long-term expansion of functional mouse and human hepatocytes as 3D organoids. *Cell* **175**, 1591–1606.e19 (2018).
10. Schneeberger, K. et al. Converging biofabrication and organoid technologies: the next frontier in hepatic and intestinal tissue engineering? *Biofabrication* **9**, 013001 (2017).
11. Broguiere, N. et al. Growth of epithelial organoids in a defined hydrogel. *Adv. Mater.* **30**, 1801621 (2018).
12. Gjorevski, N. et al. Designer matrices for intestinal stem cell and organoid culture. *Nature* **539**, 560–564 (2016).
13. Cruz-Acuña, R. et al. Synthetic hydrogels for human intestinal organoid generation and colonic wound repair. *Nat. Cell Biol.* **19**, 1326–1335 (2017).
14. Saheli, M. et al. Three-dimensional liver-derived extracellular matrix hydrogel promotes liver organoids function. *J. Cell. Biochem.* **119**, 4320–4333 (2018).
15. Ehrbar, M. et al. Biomolecular hydrogels formed and degraded via site-specific enzymatic reactions. *Biomacromolecules* **8**, 3000–3007 (2007).
16. Yin, M. et al. Quantitative assessment of hepatic fibrosis in an animal model with magnetic resonance elastography. *Magn. Reson. Med.* **58**, 346–353 (2007).
17. Kumar, P. et al. Periostin promotes liver fibrogenesis by activating lysyl oxidase in hepatic stellate cells. *J. Biol. Chem.* **293**, 12781–12792 (2018).
18. Arriazu, E. et al. Extracellular matrix and liver disease. *Antioxid. Redox Signal* **21**, 1078–1097 (2014).
19. Ishikawa, T. et al. Hepatocyte growth factor/c-met signaling is required for stem-cell-mediated liver regeneration in mice. *Hepatology* **55**, 1215–1226 (2012).
20. Wang, B., Zhao, L., Fish, M., Logan, C. Y. & Nusse, R. Self-renewing diploid Axin2 + cells fuel homeostatic renewal of the liver. *Nature* **524**, 180–185 (2015).
21. Berg, T. et al. Fibroblast growth factor 10 is critical for liver growth during embryogenesis and controls hepatoblast survival via β-catenin activation. *Hepatology* **46**, 1187–1197 (2007).
22. Ingber, D. E. Mechanobiology and diseases of mechanotransduction. *Ann. Med.* **35**, 564–577 (2003).
23. Humphrey, J. D., Dufresne, E. R. & Schwartz, M. A. Mechanotransduction and extracellular matrix homeostasis. *Nat. Rev. Mol. Cell Biol.* **15**, 802–812 (2014).
24. Duscher, D. et al. Mechanotransduction and fibrosis. *J. Biomech.* **47**, 1997–2005 (2014).
25. Halder, G., Dupont, S. & Piccolo, S. Transduction of mechanical and cytoskeletal cues by YAP and TAZ. *Nat. Rev. Mol. Cell Biol.* **13**, 591–600 (2012).
26. Liu-chittenden, Y. et al. Genetic and pharmacological disruption of the TEAD—YAP complex suppresses the oncogenic activity of YAP. *Genes Dev.* **26**, 1300–1305 (2012).
27. Dupont, S. et al. Role of YAP/TAZ in mechanotransduction. *Nature* **474**, 179–183 (2011).
28. Sorrentino, G. et al. Metabolic control of YAP and TAZ by the mevalonate pathway. *Nat. Cell Biol.* **16**, 357–366 (2014).
29. Sorrentino, G. et al. Glucocorticoid receptor signalling activates YAP in breast cancer. *Nat. Commun.* **8**, 14073 (2017).
30. Kovács, M., Tóth, J., Hetényi, C., Málnási-Csizmadia, A. & Seller, J. R. Mechanism of blebbistatin inhibition of myosin II. *J. Biol. Chem.* **279**, 35557–35563 (2004).
31. Taniguchi, K. et al. A gp130-Src-YAP module links inflammation to epithelial regeneration. *Nature* **519**, 5–62 (2015).
32. Calvo, F. et al. Mechanotransduction and YAP-dependent matrix remodelling is required for the generation and maintenance of cancer-associated fibroblasts. *Nat. Cell Biol.* **15**, 637–646 (2013).
33. Kim, N.-G. & Gumbiner, B. M. Adhesion to fibronectin regulates Hippo signaling via the FAK-Src-PI3K pathway. *J. Cell Biol.* **210**, 503–515 (2015).
34. Li, P. et al. E-catenin inhibits a Src–YAP1 oncogenic module that couples tyrosine kinases and the effector of hippo signaling pathway. *Genes Dev.* **30**, 798–811 (2016).
35. Lamar, J. M. et al. The Hippo pathway target, YAP, promotes metastasis through its TEAD-interaction domain. *Proc. Natl Acad. Sci. USA* **109**, 14732–14733 (2012).
36. Abu-Absi, S. F., Hu, W.-S. & Hansen, L. K. Dexamethasone effects on rat hepatocyte spheroid formation and function. *Tissue Eng.* **11**, 415–426 (2005).
37. Smoot, R. L. et al. Platelet-derived growth factor regulates YAP transcriptional activity via Src family kinase dependent tyrosine phosphorylation. *J. Cell. Biochem.* **119**, 824–836 (2018).
38. Sugihara, T. et al. YAP tyrosine phosphorylation and nuclear localization in cholangiocarcinoma cells is regulated by LCK and independent of LATS activity. *Mol. Cancer Res.* **16**, 1556–1567 (2018).
39. Tamm, C., Bower, N. & Anneren, C. Regulation of mouse embryonic stem cell self-renewal by a Yes-YAP-TEAD2 signaling pathway downstream of LIF. *J. Cell Sci.* **124**, 1136–1144 (2011).
40. Araujo, J. & Logothetis, C. Dasatinib: a potent SRC inhibitor in clinical development for the treatment of solid tumors. *Cancer Treat. Rev.* **36**, 492–500 (2010).
41. Tschumperlin, D. J., Ligresti, G., Hilscher, M. B. & Shah, V. H. Mechanosensing and fibrosis. *J. Clin. Invest.* **128**, 74–88 (2018).
42. Mueller, S. & Sandrin, L. Liver stiffness: a novel parameter for the diagnosis of liver disease. *Hepat. Med.* **2**, 49–67 (2010).
43. Herrera, J., Henke, C. A. & Bitterman, P. B. Extracellular matrix as a driver of progressive fibrosis. *J. Clin. Invest.* **128**, 45–53 (2018).
44. Liu, F. et al. Mechanosignaling through YAP and TAZ drives fibroblast activation and fibrosis. *Am. J. Physiol. Lung Cell. Mol. Physiol.* **308**, L344–L357 (2015).
45. Liu, L. et al. Mechanotransduction-modulated fibrotic microniches reveal the contribution of angiogenesis in liver fibrosis. *Nat. Mater.* **16**, 1252–1261 (2017).
46. Degos, F. et al. Diagnostic accuracy of FibroScan and comparison to liver fibrosis biomarkers in chronic viral hepatitis: A multicenter prospective study (the FIBROSTIC study). *J. Hepatol.* **53**, 1013–1021 (2010).
47. Haage, A. & Schneider, I. C. Cellular contractility and extracellular matrix stiffness regulate matrix metalloproteinase activity in pancreatic cancer cells. *FASEB J.* **28**, 3589–3599 (2014).
48. Xie, J. et al. Substrate stiffness-regulated matrix metalloproteinase output in myocardial cells and cardiac fibroblasts: Implications for myocardial fibrosis. *Acta Biomater.* **10**, 2463–2472 (2014).

49. Peeters, S. A. et al. Circulating matrix metalloproteinases are associated with arterial stiffness in patients with type 1 diabetes: Pooled analysis of three cohort studies. *Cardiovasc. Diabetol.* **16**, 139 (2017).
50. Nuciforo, S. et al. Organoid models of human liver cancers derived from tumor needle biopsies. *Cell Rep.* **24**, 1363–1376 (2018).
51. Sebastiani, G. et al. Regulatory T-cells from pancreatic lymphnodes of patients with type-1 diabetes express increased levels of microRNA MIR-125a-5p that limits CCR2 expression. *Sci. Rep.* **7**, 6897 (2017).

Acknowledgements

We thank Andréane Fouassier, Sabrina Bichet, Thibaud Clerc, Laure Vogeleisen-Delpech, Fabiana Fraga, the Phenotyping Unit (UDP) and the Histology core facility (HCF) of EPFL for technical assistance. The work of K.S. was funded by the Swiss National Science Foundation (SNSF 31003A_166695), Sinergia CRSII3_160798/1, the Kristian Gerhard Jebsen Foundation, and the Ecole Polytechnique Fédérale de Lausanne (EPFL). The work of M.P.L. in the area of organoid biology and technology was supported by the Swiss National Science Foundation (grant #310030_179447), the European Union's Horizon 2020 research and innovation programme (INTENS 668294), the Personalized Health and Related Technologies Initiative from the ETH Board, the Vienna Science and Technology Fund and École Polytechnique Fédérale de Lausanne (EPFL). G.S. was funded by a postdoctoral FEBS long-term fellowship.

Author contributions

G.S., S.R., M.L. and K.S. conceived the project and wrote the manuscript. G.S., S.R. and E.Y. planned and performed experiments and analysed data. S.N. and M.H. provided human biopsy samples and critically revised the manuscript.

Competing interests

Ecole Polytechnique Fédérale de Lausanne has filed patent applications pertaining to synthetic gels for epithelial stem cell and organoid cultures (with M.P.L.), as well as liver disease modelling (with K.S., M.P.L., G.S., E.Y. and S.R.). The remaining authors declare no competing interests.

Additional information

Supplementary information is available for this paper at https://doi.org/10.1038/s41467-020-17161-0.

Correspondence and requests for materials should be addressed to M.P.L. or K.S.

Peer review information *Nature Communications* thanks Yunfang Wang and the other anonymous reviewer(s) for their contribution to the peer review of this work. Peer reviewer reports are available.

Reprints and permission information is available at http://www.nature.com/reprints

Publisher's note Springer Nature remains neutral with regard to jurisdictional claims in published maps and institutional affiliations.

eLife

Reviewed Preprint

This Reviewed Preprint was published after peer review and assessment by eLife.

Reviewed Preprint posted
20 October 2022

Posted to bioRxiv
28 July 2022

Sent for peer review
26 July 2022

Stem Cells and Regenerative Medicine

Hepatic lipid overload potentiates biliary epithelial cell activation via E2Fs

Ece Yildiz [1], Gaby El Alam [2 7], Alessia Perino [1 7], Antoine Jalil [1], Pierre-Damien Denechaud [3 4], Katharina Huber [3], Lluis Fajas [3 5], Johan Auwerx [2], Giovanni Sorrentino [1 6] and Kristina Schoonjans [1 * 8]

[1] Laboratory of Metabolic Signaling, Institute of Bioengineering, Ecole Polytechnique Fédérale de Lausanne, Lausanne, Switzerland • [2] Laboratory of Integrative Systems Physiology, Institute of Bioengineering, Ecole Polytechnique Fédérale de Lausanne, Lausanne, Switzerland • [3] Center for Integrative Genomics, Université de Lausanne, Lausanne, Switzerland • [4] Institute of Metabolic and Cardiovascular Diseases (I2MC), UMR1297, INSERM, University of Toulouse, Toulouse, France • [5] INSERM, Occitanie, Montpellier, France • [6] Department of Life Sciences, University of Trieste, Trieste, Italy

* *Correspondence:* *kristina.schoonjans@epfl.ch*

Abstract

During severe or chronic hepatic injury, biliary epithelial cells (BECs), also known as cholangiocytes, undergo rapid reprogramming and proliferation, a process known as ductular reaction (DR), and allow liver regeneration by differentiating into both functional cholangiocytes and hepatocytes. While DR is a hallmark of chronic liver diseases, including advanced stages of non-alcoholic fatty liver disease (NAFLD), the early events underlying BEC activation are largely unknown. Here, we demonstrate that BECs readily accumulate lipids upon fatty acid (FA) treatment in BEC-derived organoids, and during high-fat diet feeding in mice. Lipid overload induces a metabolic rewiring to support the conversion of adult cholangiocytes into active BECs. Mechanistically, we found that lipid overload unleashes the activation of the E2F transcription factors in BECs, which drives cell cycle progression while promoting glycolytic metabolism. These findings demonstrate that fat overload is sufficient to initiate a DR, without epithelial damage, and provide new insights into the mechanistic basis of BEC activation, revealing unexpected connections between lipid metabolism, stemness, and regeneration.

eLife assessment

This **important** study reports that a high-fat diet induces biliary epithelial cell proliferation and suggests this may account for the so-called ductular reaction in advanced fatty liver disease. Convincing data support the finding that the transcription factor E2F1 is required for biliary epithelial cell proliferation in mice fed with a high-fat diet, and organoid models indicate that lipid abundance promotes glycolysis in an E2F-dependent manner. These findings are potentially of broad interest to the field of liver biology and disease.

Introduction

Under physiological conditions, the hepatic epithelium, composed of hepatocytes and BECs (or cholangiocytes), is non-proliferative. Yet upon injury, these two cell types are capable of rapidly changing their phenotype from quiescent to proliferative, contributing to the prompt restoration of damaged tissue (Gadd et al., 2020; Michalopoulos, 2014; Miyajima et al., 2014; Yanger and Stanger, 2011). However, in chronic liver injury, characterized by impaired hepatocyte replication, BECs weigh-in and serve as the cell source for regenerative cellular expansion through the DR process (Choi et al., 2014; Deng et al., 2018; Español–Suñer et al., 2012; Huch et al., 2013; Lu et al., 2015; Raven et al., 2017; Rodrigo-Torres et al., 2014; Russell et al., 2019).

The molecular basis by which BECs expand during the DR has been extensively studied in chemical models of biliary damage and portal fibrosis using the chemical 3,5-diethoxycarbonyl-1,4-dihydrocollidine (DDC). Several signaling pathways involving YAP (Meyer et al., 2020; Pepe-Mooney et al., 2019; Planas-Paz et al., 2019), mTORC1 (Planas-Paz et al., 2019), TET1-mediated hydroxymethylation (Aloia et al., 2019) and NCAM1 (Tsuchiya et al., 2014) have been reported to drive this process. Importantly, DR has also been observed in late-stage NAFLD patients with fibrosis and portal inflammation (Gadd et al., 2014; Sato et al., 2018; Sorrentino et al., 2005). NAFLD, one of the most common chronic diseases, initiates with increased lipid accumulation, a stage called steatosis (Paschos and Paletas, 2009). This pathology progresses into inflammation and fibrosis that can cause cirrhosis and hepatocellular carcinoma, which are the most frequent liver transplantation indications (Byrne and Targher, 2015). YAP has been found to be activated in BECs in fibrotic livers but not in steatosis (Machado et al., 2015), suggesting that YAP activation is necessary to support DR in the late fibrotic NAFLD stages, and thus, leaving the early molecular mechanisms of BEC activation unexplored.

BEC-derived organoids (BEC-organoids) can be established from intrahepatic bile duct progenitors and exhibit a DR-like signature, representing a promising *in vitro* approach to study regenerative mechanisms and therapies (Huch et al., 2015; 2013; Li et al., 2017; Okabe et al., 2009; Shin et al., 2011; Sorrentino et al., 2020). These self-renewing bi-potent organoids are capable of expressing stem cell/progenitor markers and of differentiating into functional cholangiocyte- and hepatocyte-like lineages, which can engraft and repair bile ducts (Hallett et al., 2022; Sampaziotis et al., 2021) and improve liver function when transplanted into a mouse with liver disease (Huch et al., 2015; 2013; Li et al., 2017).

Here, we used BEC-organoids and BECs isolated from chow diet (CD)- or high-fat diet (HFD)-fed mice and reported that they are affected by acute and chronic lipid overload, one of the initial steps of NAFLD. Lipid accumulation turns BECs from quiescent to proliferative cells and promotes their expansion through the E2F transcription factors and the concomitant

induction of glycolysis. These observations hence attribute a pivotal role to E2Fs, regulators of cell cycle and metabolism, in inducing BEC activation before the late fibrotic stage of NAFLD.

Results

BECs and BEC-organoids efficiently accumulate lipids in vivo and in vitro

To gain insight into how chronic lipid exposure, an inducer of liver steatosis, affects biliary progenitor function *in vitro*, we incubated single BECs with a fatty acid mixture (FA mix) of oleic acid (OA) and palmitic acid (PA) – the two most abundant FAs found in livers of NAFLD patients (Araya et al., 2004), for 7 days and allowed BEC-organoid formation (Figure 1A). Surprisingly, we observed that BEC-organoids efficiently accumulated lipid droplets in a dose-dependent manner (Figure 1B) and this process did not affect organoid viability (Figures 1C-D). To investigate how cells adapt their metabolism to lipid overload, we monitored the expression of several genes involved in lipid metabolism, including *Scd1* (*de novo* lipogenesis) (Figure 1E), *Hmgcs2* (ketogenesis), *Pdk4* (inhibition of pyruvate oxidation), and *Aldh1a1* (prevention against lipid peroxidation products) (Figure 1F) and found it to be affected by FA addition. These results suggest that BEC-organoids actively reprogram their metabolism to cope with aberrant lipid overload.

To determine whether the observed phenotype was preserved in fully formed organoids, we treated already established BEC-organoids with the FA mix for 4 days (Figure 1 - figure supplement 1A). In line with our previous observations, BODIPY staining (Figure 1 - figure supplement 1B), and triglyceride (TG) quantification (Figure 1 - figure supplement 1C) showed a pronounced increase in lipid accumulation after 4 days, without affecting cell viability (Figure 1 - figure supplement 1D).

To assess whether chronic lipid exposure affects BECs *in vivo*, we fed C57BL/6JRj mice for 15 weeks with CD or HFD (Figure 1G) and analyzed their bile ducts. As expected, HFD-fed mice gained weight and developed liver steatosis (Figure 1 - figure supplement 1E), but no apparent fibrosis (data not shown). Of note, HFD-feeding led to an accumulation of lipid droplets in the periportal zone (Figure 1 - figure supplement 1F) and within bile ducts, as reflected by colocalization of BODIPY with PANCK, a BEC marker (Figure 1H), without inducing epithelial damage (Figure 1 - figure supplements 1G-H). Together, these *in vitro* and *in vivo* results demonstrate that BECs accumulate lipids upon chronic FA exposure, raising the question of the functional consequences of this previously unrecognized event on BEC behavior.

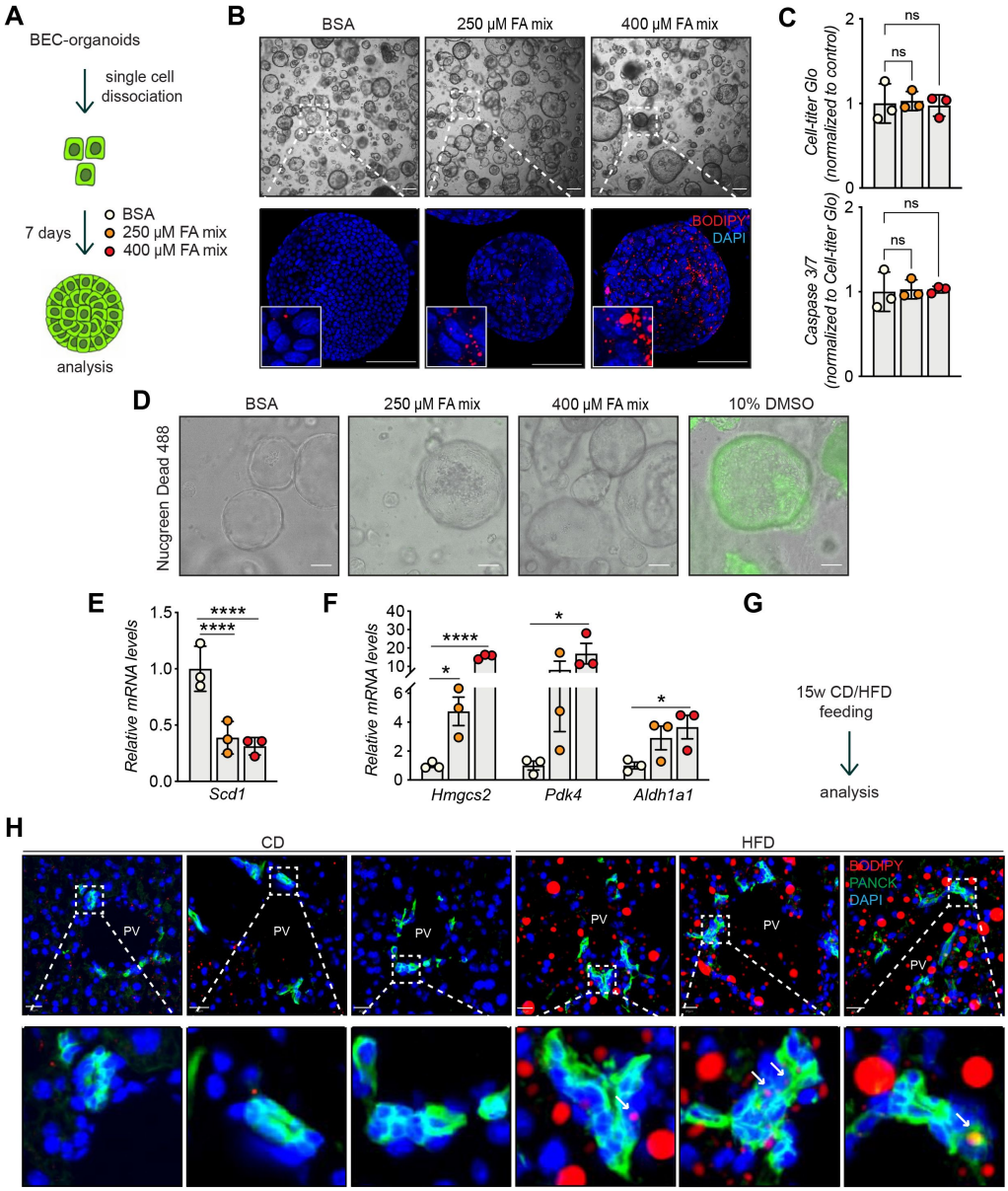

Figure 1.

BECs accumulate lipids.

(A) Schematic depicting fatty acid (FA) treatment of BEC-organoids *in vitro*. **(B)** Representative brightfield and immunofluorescence (IF) images of lipids (BODIPY) in control (BSA) and FA-treated organoids. Close-up IF images were digitally zoomed in four times. n=3. **(C)** Cell-titer Glo and Caspase 3/7 activity measurement for viability and apoptosis detection relative to panel A. n=3. **(D)** Representative Nucgreen Dead 488 staining as composite images from brightfield and fluorescent microscopy. n=3. **(E-F)** Quantification of *Scd1* (**E**) and *Hmgcs2*, *Pdk4,* and *Aldh1a1* (**F**) mRNA in control (BSA) and FA-treated organoids. n=3. **(G)** Schematic depicting CD and HFD feeding *in vivo*. **(H)** Representative images for co-staining of BODIPY and PANCK, relative to panel G. Close-up IF images were digitally zoomed in four times. n=5.

Data are shown as mean ± SD. Absence of stars or ns, not significant ($p > 0.05$); *$p < 0.05$; ****$p < 0.0001$; one-way ANOVA with Dunnett's test (C), and Fisher's LSD test (E, F) was used. PV, portal vein. Arrowheads mark bile ducts. Scale bars, 200 µm (B-brightfield), 100 µm (B-IF, D) and 20 µm (H-I).

The following figure supplements are available for figure 1:

Figure supplement 1. Further characterization of lipid accumulation in BECs.

HFD feeding promotes BEC activation and increases organoid formation capacity

To characterize *in vivo* the impact of chronic lipid overload on BECs at the molecular level, we isolated BECs from livers of CD/HFD-fed mice using EPCAM, a pan-BEC marker (Aloia et al., 2019; Pepe-Mooney et al., 2019; Planas-Paz et al., 2019), by fluorescence-activated cell sorting (FACS) (Figure 2A and Figure 2 - supplement 1A). Performing bulk RNA sequencing (RNA-seq) on $EPCAM^+$ BECs revealed a diet-dependent clustering in Principal Component Analysis (Figure 2 – supplement 1B), indicating that HFD feeding induces considerable transcriptional changes in BECs *in vivo*. Differential expression analysis further revealed a total of 495 significantly changed genes, 121 upregulated and 374 downregulated (Figure 2 - supplement 1C and Appendix 1 - Table 1). At the same time, HFD promoted the upregulation of *Ncam1* (Figure 2 - supplement 1D), a well-established mediator of BEC activation.

To further explore transcriptional changes, we performed gene set enrichment analysis (GSEA) on Gene Ontology (GO) terms (Figure 2B) and KEGG (Figure 2 - supplement 1E) pathways and identified cell proliferation, the most prevalent feature of BEC activation (Sato et al., 2018), as the major upregulated process in these cells upon HFD feeding. Expansion of the reactive BECs requires detachment from their niche and invasion of the parenchyma toward the damaged hepatic area. This process is made possible by reorganizing the extracellular matrix (ECM) and reducing focal adhesion, effectively downregulated in $EPCAM^+$ BECs upon HFD (Figure 2B and Figure 2 - supplement 1E).

To validate the RNAseq data, we monitored the activation of BECs *in vivo* by measuring the number of proliferating BECs in the portal region of the livers of mice fed either CD or HFD (Figures 2C-D). Of note, we found that HFD feeding was sufficient to induce a marked increase in the number of active BECs (i.e., $Ki67^+/OPN^+$ cells- Figure 2D). Similar results were observed in an independent cohort of mice challenged with HFD and injected with EdU to track proliferating cells (Figures 2E-F), confirming that chronic lipid exposure stimulates the appearance of reactive BECs within the bile ducts.

The efficiency of BECs to generate organoids *in vitro* has been shown to mirror their regenerative capacity (Aloia et al., 2019). To functionally assess the impact of lipid overload on this process, we measured the organoid forming capacity of isolated BECs, as a read-out of their regenerative functions. To this aim, we quantified the organoid formation efficiency of BECs isolated from CD- and HFD-fed mouse livers (Figure 2G). Strikingly, we observed that HFD-derived BECs were significantly more efficient in generating organoids than their CD counterparts (Figure 2H). Altogether, these results demonstrate that HFD feeding is sufficient to induce, *in vivo*, the exit of BECs from a quiescent state and the acquisition of both proliferative and pro-regenerative features.

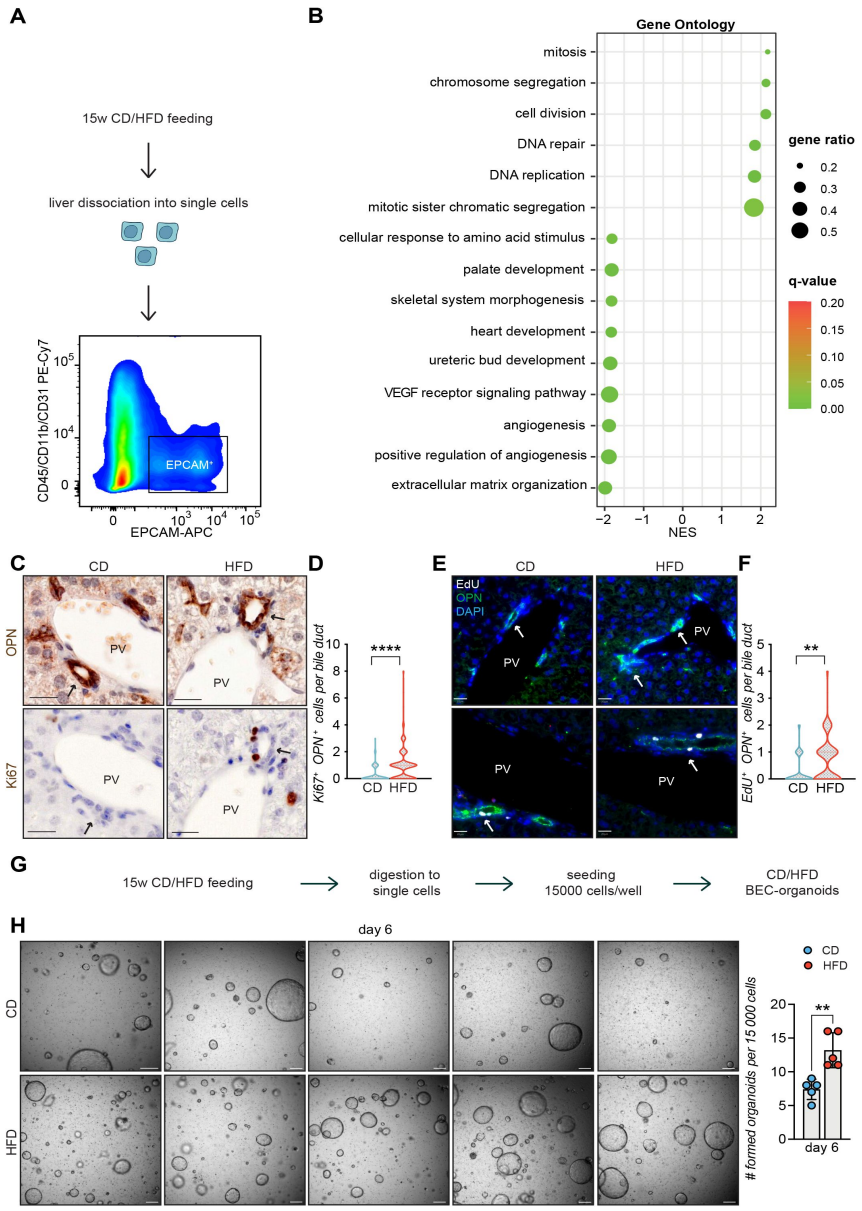

Figure 2.

HFD feeding induces EPCAM$^+$ BEC proliferation.

(A) Scheme depicting the isolation of EPCAM$^+$ BECs from CD- and HFD-fed mice by FACS. **(B)** Gene set enrichment analysis (GSEA) of Gene Ontology (GO) terms. Top 15 upregulated biological processes (BP), ordered by normalized enrichment score (NES). q-value: false discovery rate adjusted p-values. NES: normalized enrichment score. **(C-F)** Representative co-staining images **(C, E)** and quantification **(D, F)** of BECs stained for OPN and Ki67 **(C-D)**, and OPN and EdU **(E-F)** in livers of CD/HFD-fed mice. n=10 for Ki67 and n=5 for EdU. **(G)** Schematic depicting BEC-organoid formation *in vitro* from CD/HFD-fed mouse livers. **(H)** Images of organoid colonies formed 6 days after seeding, and quantification of organoids per well. n=5.

Violin graphs depict the distribution of data points i.e the width of the shaded area represents the proportion of data located there. Other data are shown as mean ± SD. **p < 0.01; ****p < 0.0001; unpaired, two-tailed Student's t-test was used. PV, portal vein. Arrowheads mark bile ducts. Scale bars, 20 µm (C, E), 200 µm (H).

The following figure supplements are available for figure 2:

Figure supplement 1. RNA-seq analysis of EPCAM$^+$ BECs upon HFD.

HFD feeding initiates BEC activation via E2Fs

To understand whether the mechanisms underlying BEC activation upon HFD *in vivo* involve canonical processes found in chronically damaged livers, we compared the transcriptional profile of BECs upon HFD with those of DDC-activated BECs ((Pepe-Mooney et al., 2019); GSE125688). We identified the most pronounced changes shared between HFD and DDC samples by overlapping separate over-representation enrichment analyses (Appendix 1 - Table 2). Cell division, mitosis, and chromosome segregation were the shared enriched pathways for upregulated genes in HFD and DDC samples (Figure 3A), while ECM organization was the shared enriched pathway for the downregulated genes in HFD and DDC conditions (Figure 3 - supplement 1A). We concluded that the mechanisms of BEC activation induced by lipid overload overlap with those induced by biliary epithelial damage.

Of note, a more detailed analysis of DDC- and HFD-derived BECs, revealed the concomitant enrichment of 4 overlapping transcription factor (TF) gene sets, E2F1-4 (Figure 3B) and their target genes (Figure 3 - supplement 1B), which have not been linked to DR previously. Moreover, we identified an enrichment of E2Fs (Figure 3C and Appendix 1 - Table 2) and cell division pathway (Figure 3 - supplement 1C) as the most upregulated genes in proliferating BEC-organoids, further corroborating the role of E2Fs in these two *in vitro* ((Aloia et al., 2019); GSE123133) and *in vivo* ((Pepe-Mooney et al., 2019); GSE125688) DR models.

E2Fs are a large family of TFs with complex functions in cell cycle progression, DNA replication, repair, and G2/M checkpoints (Dimova and Dyson, 2005; Dyson, 1998; 2016; Ren et al., 2002). Therefore, we hypothesized that activation of E2Fs might represent a key event in the process of BEC activation, which is necessary for exiting the quiescent state and driving DR initiation. To test this hypothesis, we focused on E2F1, as it was the most enriched TF in our analysis, and assessed its role in BECs by feeding $E2f1^{+/+}$ and $E2f1^{-/-}$ mice with HFD (Figure 3D). Remarkably, $E2f1^{-/-}$ mice were refractory to BEC activation induced by lipid overload upon HFD, as opposed to $E2f1^{+/+}$ mice (Figures 3E-F). These results *in vivo* demonstrate a previously unrecognized role of E2F1 in controlling BEC activation during HFD-induced hepatic steatosis.

E2F promotes BEC expansion by upregulating glycolysis

The exit of terminally-differentiated cells from their quiescent state requires both energy and building block availability to support cell proliferation. Proliferative cells, therefore, reprogram their glucose metabolism to meet their increased need for biomass and energy (Vander Heiden et al., 2009). Supporting this notion, our interrogation of *in vitro* BEC-organoid formation dataset ((Aloia et al., 2019); GSE123133) revealed the enrichment of purine and pyrimidine metabolism, as well as pentose-phosphate pathway, which are tightly connected to glycolysis (Figure 4 - supplement 1A). In line with these findings, a substrate oxidation test in BEC-organoids revealed a preference for glucose, as reflected by the decrease in maximal respiration, when UK5099, a mitochondrial pyruvate carrier inhibitor, was used (Figures 4A-B), while no changes were observed with inhibitors of glutamine (BPTES) and FA (Etomoxir) metabolism (Figure 4 - supplement 1B and 1C).

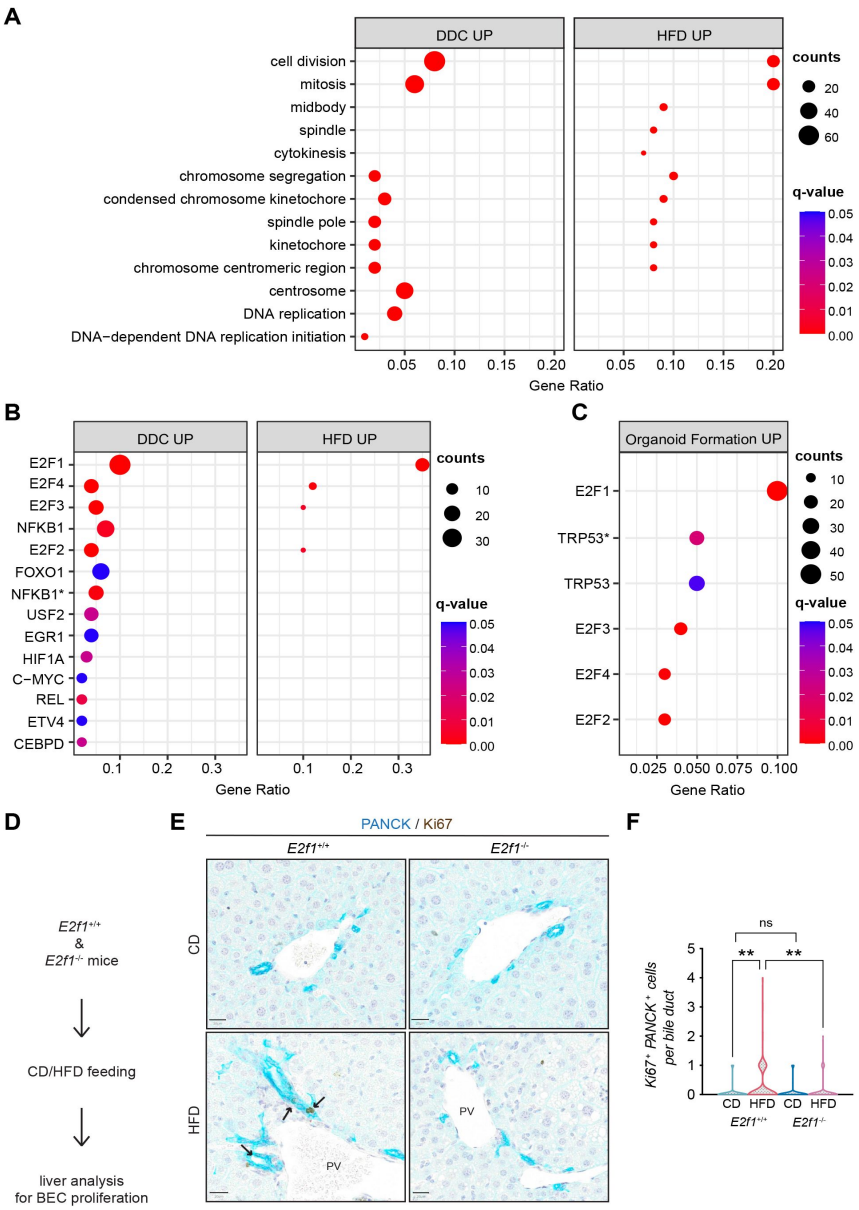

Figure 3.

E2Fs are enriched in DDC and HFD datasets and mediate DR initiation *in vivo*.

(A) Over-representation analysis results. Top 13 enriched biological processes (BP) upon HFD (own data) and DDC (GSE125688) treatment. q-value: false discovery rate adjusted p-values, counts: number of found genes within a given gene set. **(B-C)** Enriched transcription factors (TFs) of upregulated genes identified by over-representation analysis in HFD (own data) and DDC (GSE125688) treatment **(B)**, and during the process of organoid formation from single BECs (Organoids vs T0) (GSE123133) **(C)**. Asterisk (*) marks TFs of the "TF_ZHAO" gene set. **(D)** Schematic depicting *in vivo* E2F1 analysis. **(E-F)** Representative images of PANCK/Ki67 co-staining in livers of *E2f1*$^{+/+}$ and *E2f1*$^{-/-}$ mice fed with CD or HFD **(E)** and quantification of proliferative BECs in the indicated mice **(F)**. For CD, n=5 for *E2f1*$^{+/+}$ and *E2f1*$^{-/-}$. For HFD, n=7 for *E2f1*$^{+/+}$, and n=8 for *E2f1*$^{-/-}$.

Violin graphs depict the distribution of data points i.e the width of the shaded area represents the proportion of data located there. ns, not significant; **p < 0.01; two-way ANOVA with Tukey's test was used. PV, portal vein. Arrowheads mark bile ducts. Scale bars, 20 µm (E).

The following figure supplements are available for figure 3:

Figure supplement 1. Extended analysis of BECs upon HFD, DDC, and during BEC-organoid formation.

To investigate the metabolic changes in BEC-organoids upon HFD, we treated CD/HFD BEC-organoids with FA mix to mimic steatotic conditions *in vitro* (Figure 4C). We hypothesized that the presence of glucose and FA in culture media would reveal a metabolic shift of BEC-organoids. Consistent with our hypothesis, HFD-FA BEC-organoids demonstrated increased compensatory glycolytic rates (Figures 4D-E and Figure 4 - supplement 1D). Of note, there was a reduction in oxidative phosphorylation in HFD-FA BEC-organoids, as evidenced by the decrease in maximal respiration (Figure 4 - supplement 1E-G), which might reflect their preference for glycolytic pathway to generate biomass.

Besides their prominent role in cell cycle progression, E2Fs coordinate several aspects of cellular metabolism (Denechaud et al., 2017; Nicolay and Dyson, 2013), and promote glycolysis in different contexts (Blanchet et al., 2011; Denechaud et al., 2015; Huber et al., 2021). These findings prompted us to postulate that E2F might control glycolysis and thus the glucose preference observed in BEC-organoids. To investigate this hypothesis, we treated BEC-organoids with an E2F inhibitor, HLM006474 (Figure 4F). As expected, HLM006474 treatment reduced the transcriptional levels of several genes involved in cell cycle progression and glycolytic metabolism (Figure 4G), and decreased the glycolytic flux, as evidenced by the blunted proton efflux rate (PER) (Figures 4H-I). Moreover, E2F inhibition was able to reverse the metabolic phenotype only in HFD-FA BEC-organoids (Figures 4J-K).

In conclusion, these results demonstrate that HFD-induced E2F activation controls the conversion of BECs from quiescent to active progenitors by promoting the expression of cell cycle genes while simultaneously driving a shift towards glycolysis.

Discussion

Through DR activation, BECs represent an essential reservoir of progenitors that are crucial for coordinating hepatic epithelial regeneration in the context of chronic liver diseases (Choi et al., 2014; Deng et al., 2018; Español–Suñer et al., 2012; Huch et al., 2013; Lu et al., 2015; Raven et al., 2017; Rodrigo-Torres et al., 2014; Russell et al., 2019). BEC functions are tightly controlled by YAP metabolic pathways (Meyer et al., 2020; Pepe-Mooney et al., 2019; Planas-Paz et al., 2019) and recent studies from different tissues have provided evidence that specific metabolic states play instructive roles in controlling cell fate and tissue regeneration (Beyaz et al., 2016; Capolupo et al., 2022; Miao et al., 2020; Zhang et al., 2016). Aberrant lipid accumulation is a hallmark of early NAFLD, and imbalances in lipid metabolism are known to affect hepatocyte homeostasis, including induction of lipo-toxicity and cell death (X. (Wang et al., 2016); (Sano et al., 2021); (De Gottardi et al., 2007); (Wobser et al., 2009); (Ipsen et al., 2018)). However, the role of lipid dysregulation in BECs and whether it has an impact on the initiation of DR remains unexplored in the setting of NAFLD.

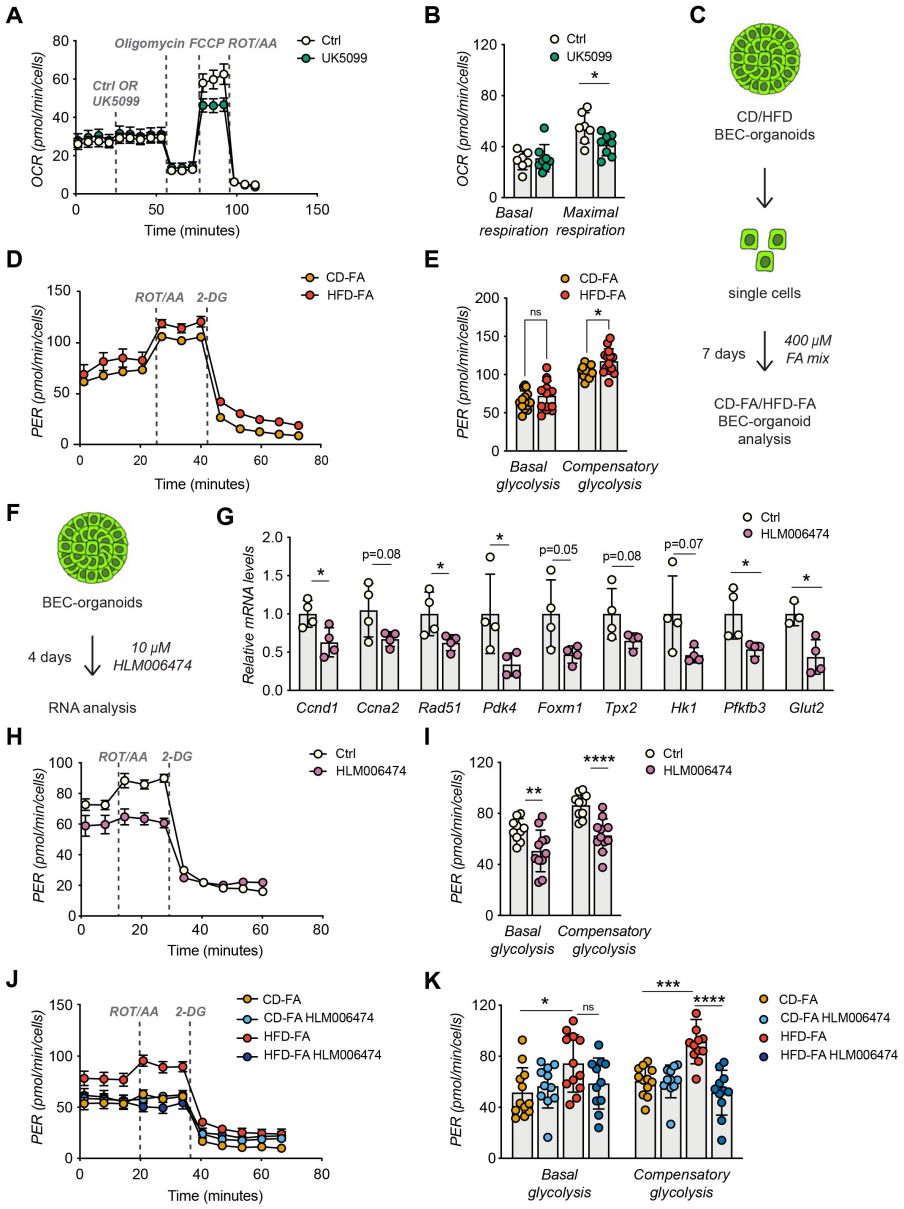

Figure 4.

E2Fs promote glycolysis in BEC-organoids.

(A-B) Seahorse Substrate Oxidation Assay using UK5099, a mitochondrial pyruvate carrier inhibitor **(A)**, and assessment of the glucose dependency **(B)** in CD-derived BEC organoids. n=7 for control (Ctrl), n=8 for UK5099. **(C)** Scheme depicting the treatment of CD/HFD-derived BEC-organoids with FA mix. **(D-E)** Proton efflux rate (PER) **(D)**, and basal and compensatory glycolysis **(E)** measured using Seahorse XF Glycolytic Rate Assay. Relative to panel C. n=13. **(F)** Scheme depicting the treatment of CD-derived BEC-organoids with E2F inhibitor, HLM006474. **(G)** RT-qPCR of selected cell cycle and glycolytic genes, relative to panel H. n=4. (**H-I)** PER during the Seahorse XF Glycolytic Rate Assay **(H)**, and basal and compensatory glycolysis **(I)**, relative to panel F. n=10 for control (Ctrl), n=11 for HLM006474.

(**J-K)** PER during the Seahorse XF Glycolytic Rate Assay **(J)**, and basal and compensatory glycolysis **(K)**, relative to panel C and treatment with HLM006474. n=12 for control (Ctrl), n=11 for HLM006474.

Data are shown as mean ± SD (SEM for A, D, H, J). Absence of stars or ns, not significant ($p > 0.05$); *$p < 0.05$; **$p < 0.01$; ***$p < 0.001$; ****$p < 0.0001$; unpaired, two-tailed Student's t-test (G), two-way ANOVA with Sidak's test (B, E, I, K) were used.

The following figure supplements are available for figure 4:

Figure supplement 1. E2F activation correlates with increased glycolysis.

Here, using HFD-induced mouse models, we studied BEC metabolism in steatosis, the first stage of NAFLD, and demonstrated lipid accumulation in BECs during chronic HFD *in vivo* and their resistance to lipid-induced toxicity. By using BEC-organoids, we observed that FAs directly target BECs, without any involvement of hepatocytes and that BECs functionally respond to lipid overload. Importantly, BEC-organoids derived from CD- and HFD-fed mouse livers were shown to shift their cellular metabolism toward more glycolysis in the presence of lipids. Furthermore, we found that the HFD-induced metabolic shift was sufficient to reprogram BEC identity *in vivo*, allowing their exit from a quiescent state and the simultaneous acquisition of progenitor functions, such as proliferation and organoid-initiating capacity, two hallmarks of DR. These results highlight the metabolic plasticity of BECs and shed light on an unpredicted mechanism of BEC activation in HFD-induced hepatic steatosis. Importantly, we observed that lipid overload is sufficient to induce BEC activation in steatotic livers and that this process precedes parenchymal damage, thus resolving a long-lasting debate on the chronology of DR initiation in chronic liver diseases. While the functional contribution of lipid-activated BECs in liver regeneration during the late stages of NAFLD will require further studies, our data clearly point out the role of BECs as sensors, and possibly effectors, of early liver diseases such as steatosis.

To fully understand the underlying basis of the observed phenotype, we characterized the transcriptome of primary BECs derived from steatotic livers of HFD-fed mice and demonstrated that long-term feeding of a lipid-enriched diet strongly promotes BEC proliferation, suggesting a strong link between metabolic adaptation and progenitor function. By combining our transcriptomic analysis with data mining of publicly available DR datasets (Aloia et al., 2019; Pepe-Mooney et al., 2019), we identified the E2F transcription factors as master regulators of DR in the context of NAFLD. Moreover, the expression of *Pdk4*, an E2F1 target (Hsieh et al., 2008; Wang et al., 2016), was upregulated in FA-treated BEC-organoids and upon HFD. PDK4 limits the utilization of pyruvate for oxidative metabolism while enhancing glycolysis, which reinforces our data demonstrating that E2Fs rewire BEC metabolism toward glycolysis to fuel progenitor proliferation. These observations feature E2Fs as the molecular rheostat integrating the metabolic cell state with the cell cycle machinery to coordinate BEC activation. However, how E2Fs are regulated upon HFD and whether they are interconnected with the already known YAP, mTORC1, and TET1 pathways remain unknown and will require further investigations.

While our data are derived from obese mice, a recent report showed increased numbers of cholangiocytes in steatotic human livers (Hallett et al., 2022) and E2F1 has been found to be upregulated in the livers of obese patients (Denechaud et al., 2015). Moreover, human subjects with elevated visceral fat demonstrated increased glucose metabolism (Broadfield et al., 2021). These observations, while correlative, set the ground for future research in understanding the role and the therapeutic potential of lipid metabolism and E2Fs in controlling BEC activation, thus initiating DR in humans.

Materials and Methods

Mouse studies and ethical approval

All the animal experiments were authorized by the Veterinary Office of the Canton of Vaud, Switzerland under license authorization VD3721 and VD2627.b. C57BL/6JRj mice were obtained from Janvier Labs and *E2f1*$^{+/+}$ and *E2f1*$^{-/-}$ (B6;129S4-E2f1tm1 Meg/J) mice were purchased from The Jackson Laboratory. 8-week-old C57BL/6JRj male mice were fed with Chow Diet (CD - SAFE Diets, SAFE 150) or High Fat Diet (HFD - Research Diets Inc, D12492i) for 15 weeks. 7-week-old *E2f1*$^{+/+}$ and *E2f1*$^{-/-}$ male mice were fed with Chow Diet (CD – Kliba

Nafag 3336) or High Fat Diet (HFD - Envigo, TD93075) for 29 weeks. The well-being of the animals was monitored daily, and body weight was monitored once per week until the end of the experiment. All mice had unrestricted access to water and food and liver tissues were harvested at the end of the experiment.

Data reporting

Mice were randomized into different groups according to their genotype. A previous HFD experiment was used to calculate the sample size for C57BL/6JRj mouse experiments. Mice showing any sign of severity, predefined by the Veterinary Office of the Canton of Vaud, Switzerland were sacrificed and excluded from the data analyses. *In vitro* experiments were repeated with at least 3 biological replicates (BEC-organoids from different mice) or were repeated at least twice by pooling 4 mice per condition (for Seahorse analysis).

Proliferation Assay

Cell proliferation was assessed by EdU assay (Click-iT EdU Alexa Fluor 647, ThermoFisher, C10340) following the manufacturer's instructions. For *in vivo* studies, EdU was resuspended in phosphate-buffered saline (PBS- ThermoFisher, 10010002) and 200 µL of the solution was injected intraperitoneally (50 µg per g of mouse weight) 16 hours before the sacrifice.

EPCAM$^+$ BEC isolation and FACS analysis

23-week-old CD/HFD-fed C57BL/6JRj male mice were used for this experiment and sacrificed in the fed state. To isolate the BECs, mouse livers were harvested and digested enzymatically as previously reported (Broutier et al., 2016). Briefly, livers were minced and incubated in a digestion solution (1% fetal bovine serum (FBS) (Merck/Sigma, F7524) in DMEM/Glutamax (ThermoFisher, 31966-021) supplemented with HEPES (ThermoFisher, 15630-056) and Penicillin/Streptomycin (ThermoFisher, 15140-122) containing 0.0125% (mg/ml) collagenase (Merck/Sigma, C9407), 0.0125% (mg/ml) dispase II (ThermoFisher, 17105-041) and 0.1 mg/ml of DNAase (Merck/Sigma, DN25). This incubation lasted 2-3h on a shaker at 37°C at 150 rpm. Livers were then dissociated into single cells with TrypLE (GIBCO, 12605028) and washed with washing buffer (1% FBS (Merck/Sigma, F7524) in Advanced DMEM/F-12 (GIBCO, 12634010) supplemented with Glutamax (ThermoFisher, 35050061), HEPES (ThermoFisher, 15630-056) and Penicillin/Streptomycin (ThermoFisher, 15140-122)). Single cells were filtered with a 40 µm cell strainer (Falcon, 352340) and incubated with fluorophore-conjugated antibodies CD45–PE/Cy7 (BD Biosciences, 552848), CD11b– PE/Cy7 (BD Biosciences, 552850), CD31–PE/Cy7 (Abcam, ab46733) and EPCAM–APC (eBioscience, 17-5791-82) for 30 min on ice. BECs were sorted using FACSAria Fusion (BD Biosciences) as previously described (Aloia et al., 2019). Briefly, individual cells were sequentially gated based on cell size (forward scatter (FSC) versus side scatter (SSC)) and singlets. BECs were then selected based on EPCAM positivity after excluding leukocytes (CD45$^+$), myeloid cells (CD11b$^+$), and endothelial cells (CD31$^+$), yielding a population of single CD45$^-$/CD11b$^-$/ CD31$^-$/EPCAM$^+$ cells. All flow cytometry data were analyzed with FlowJo v10.8 software (BD Life Sciences).

RNA preparation from EPCAM$^+$ BECs and bulk RNA-seq data analysis

RNA was isolated from sorted BECs using the RNeasy micro kit (QIAGEN, 74104) and the amount and quality of RNA were measured with the Agilent Tapestation 4200 (Agilent Technologies, 5067-1511). As a result, RNA-seq of 5 CD and 7 HFD samples was performed by BGI with the BGISEQ-500 platform. FastQC was used to verify the quality of the reads

RNA was isolated from sorted BECs using the RNeasy micro kit (QIAGEN, 74104) and the amount and quality of RNA were measured with the Agilent Tapestation 4200 (Agilent Technologies, 5067-1511). As a result, RNA-seq of 5 CD and 7 HFD samples was performed by BGI with the BGISEQ-500 platform. FastQC was used to verify the quality of the reads (Andrews, 2010). No low-quality reads were present, and no trimming was needed. Alignment was performed against the mouse genome (GRCm38) following the STAR (version 2.6.0a) manual guidelines (Dobin et al., 2013). The obtained STAR gene counts for each alignment were analyzed for differentially expressed genes using the R package DESeq2 (version 1.34.0) (Love et al., 2014). A threshold of 1 log2 fold change and adjusted p-value smaller than 0.05 were considered when identifying the differentially expressed genes. A principal component analysis (PCA) (Lê et al., 2008) was used to explore the variability between the different samples.

Gene set enrichment analysis (GSEA)

We used the clusterProfiler R package (Yu et al., 2012) to conduct GSEA analysis on various gene sets. Gene sets were retrieved from http://ge-lab.org/gskb/ for *M.musculus*. We ordered the differentially expressed gene list by log2 (Fold-changes) for the analysis with default parameters.

Over-representation enrichment analysis

All significantly changing genes (adjusted p-value < 0.05 and an absolute fold change > 1) were split into 2 groups based on the direction of the fold change (genes significantly up- & down-regulated). An over-representation analysis using the clusterProfiler R package was performed on each of the two groups to identify biologically overrepresented terms.

Figure generation with R

The R packages ggplot2 (Wickham, 2016) retrieved from https://ggplot2.tidyverse.org and ggpubr were used to generate figures.

Culture of mouse liver BEC-organoids from biliary duct fragments and single cells

BEC-organoids were established from bile ducts of C57BL/6JRj male mice as previously described (Broutier et al., 2016; Sorrentino et al., 2020). Thus, the liver was digested as detailed above ($EPCAM^+$ BEC isolation) and bile ducts were isolated, they were pelleted by centrifugation at 200 rpm for 5 min at 4°C and washed with PBS twice. Isolated ducts were resuspended in Matrigel (Corning, 356231) and cast in 10 µl droplets in 48-well plates. When gels were formed, 250 µl of isolation medium (IM-Advanced DMEM/F-12-Gibco,12634010) supplemented with Glutamax (ThermoFisher, 35050061), HEPES (ThermoFisher, 15630-056), and Penicillin/Streptomycin (ThermoFisher, 15140-122), 1X B27 (Gibco, 17504044), 1mM *N*-acetylcysteine (Sigma-Aldrich, A9165), 10 nM gastrin (Sigma-Aldrich, G9145), 50 ng/ml EGF (Peprotech, AF-100-15), 1 µg/ml Rspo1 (produced in-house), 100 ng/ml FGF10 (Peprotech, 100-26), 10 mM nicotinamide (Sigma-Aldrich, N0636), 50 ng/ml HGF (Peprotech, 100-39), Noggin (100 ng/ml produced in-house), 1µg/ml Wnt3a (Peprotech, 315-20) and 10 µM Y-27632 (Sigma, Y0503) was added to each well. Plasmids for Rspo1 and Noggin production were a kind gift from Joerg Huelsken. After the first 4 days, IM was replaced with the expansion medium (EM), which was the IM without Noggin, Wnt3a, and Y-27632. For passaging, organoids were removed from Matrigel a maximum of one week after seeding and dissociated into single

cells using TrypLE Express (Gibco, 12604013). Single cells were then transferred to fresh Matrigel. Passaging was performed in a 1:3 split ratio.

For the FA-treatment of BEC-organoids, palmitic acid (Sigma, P0500) and oleic acid (Sigma, O1008) were dissolved in 100% ethanol into 500 and 800 µM stock solutions respectively, and kept at −20 °C. For each experiment, palmitic acid and oleic acid were conjugated to 1% fatty acid free bovine serum albumin (BSA) (Sigma, A7030), in EM through 1:2000 dilution each (Malhi et al., 2006). The concentration of vehicle, ethanol, was 0.1% ethanol in final incubations and 1% fatty acid free BSA in EM was used as the control for FA treatment.

Liver immunohistochemistry (IHC) and immunofluorescence (IF)

For liver paraffin histology, livers were washed in PBS (Gibco, 10010023), diced with a razor blade, and fixed overnight in 10% formalin (ThermoFisher, 9990244) while shaking at 4°C. The next day fixed livers were washed twice with PBS, dehydrated in ascending ethanol steps, followed by xylene, and embedded in paraffin blocks. 4 µm thick sections were cut from paraffin blocks, dewaxed, rehydrated, and quenched with 3% H_2O_2 for 10 minutes to block the endogenous peroxidase activity (for IHC). Antigen retrieval was performed by incubating the sections in 10 mM citrate buffer (pH 6.0) for 20 min at 95 °C. After the sections cooled to room temperature, they were washed and blocked with blocking buffer (1% BSA (Sigma, A7906) and 0.5% Triton X-100 (Sigma, X100) in PBS), for 1 h at room temperature. The primary antibodies anti-Ki67 (ThermoFisher, MA5-14520), anti-PANCK (Novusbio, NBP600-579), anti-OPN (R&D Systems, AF808), anti-Cleaved caspase-3 (Cell Signaling, 9661) were diluted in a 1:100 dilution of the blocking buffer and incubated overnight at 4 °C. For IHC, ImmpRESS HRP conjugated secondary (VectorLabs MP-74-01-15 and MP-74-02) were incubated for 30 min and detection was performed by using a 3.3'-diaminobenzidine (DAB) reaction. Sections were counterstained with Harris and mounted. For IF, sections were washed and incubated for 1 h with Alexa Fluor conjugated secondary antibodies (1:1000 in blocking solution; Invitrogen). Following extensive washing, sections were counterstained with DAPI (ThermoFisher, 62248), and mounted in ProLong Gold Antifade Mountant (Thermo Fischer, P36930).

For IF of liver cryosections, the livers were frozen in O.C.T. compound (VWR chemicals) on dry ice-filled with isopentane. 10 µm liver sections were cut from O.C.T embedded samples, hydrated, and washed twice in PBS. The sections were blocked in blocking buffer for 1h at room temperature and incubated with BODIPY 558/568 (Invitrogen, D38D35) for 20 minutes. After fixation with 4% paraformaldehyde (PFA) solution (Sigma, 1004960700) for 15 minutes, sections were washed with PBS. Then, sections were permeabilized using 5% BSA in TBS-T and stained with primary antibody anti-PANCK diluted in blocking buffer for 16 h at 4 °C. The next day, the sections were washed three times with PBS and the appropriate Alexa Fluor secondary antibodies were diluted in blocking buffer (1:1000) and incubated with the sections for 1 h at room temperature. The sections were washed in PBS and incubated with DAPI diluted 1:1000 in PBS for 1 h at room temperature. Finally, the sections were mounted in ProLong Gold Antifade Mountant.

Stained sections were imaged by a virtual slide microscope (VS120, Olympus) and analysis was performed using QuPath software (Bankhead et al., 2017).

BEC-organoid whole-mount immunofluorescence

BEC-organoids were incubated with BODIPY 558/568 for 20min, and then washed with PBS and extracted from Matrigel using Cell Recovery Solution (Corning, 354253). After fixing

with 4% PFA in PBS (30 min, on ice), they were pelleted by gravity to remove the PFA and were washed with PBS and ultra-pure water. BEC-organoids were then spread on glass slides and allowed to attach by drying. The attached BEC-organoids were rehydrated with PBS and permeabilized with 0.5% Triton X-100 in PBS (1 h, room temperature) and blocked for 1 h in blocking buffer. After washing with PBS, samples were incubated for 1 h at room temperature with Alexa Fluor Phalloidin 488 (Invitrogen, A12379). Following extensive washing, samples were counterstained with DAPI and were imaged by a confocal microscope (LSM 710, Zeiss). Signal intensity was adjusted on each channel using Fiji software (Schindelin et al., 2012).

Quantitative real-time qPCR for mRNA quantification

BEC-organoids were extracted from Matrigel using Cell Recovery Solution (Corning, 354253). RNA was extracted from organoid pellets using the RNAqueous total RNA isolation kit (Invitrogen, AM1931) and the RNeasy Micro Kit (Qiagen, 74004) following the manufacturer's instructions. RNA was transcribed to complementary DNA using QuantiTect Reverse Transcription Kit (Qiagen, 205314) following the manufacturer's instructions. PCR reactions were run on the LightCycler 480 System (Roche) using SYBR Green (Roche, 4887352001) chemistry. Real-time quantitative polymerase chain reaction (RT-qPCR) results were presented relative to the mean of *36b4* (comparative ΔCt method). Primers for RT-qPCR are listed in Appendix 1 - Table 3.

E2F inhibition

For the E2F inhibition experiment, single BECs were grown for 7 days and allowed to form organoids. For the Seahorse experiment, BEC-organoids were treated with E2F inhibitor, HLM006474 (10 µM, Merck, 324461), overnight before the metabolic assay. For RT-qPCR analysis, BEC-organoids were treated with HLM006474 chronically for 4 days.

Bioenergetics with Seahorse extracellular flux analyzer

The oxygen consumption rate (OCR), extracellular acidification rate (ECAR), and proton-efflux rate (PER) of the BEC-organoids were analyzed by an XFe96 extracellular flux analyzer (Agilent) following the manufacturer's instructions according to assay type.

For Mito Stress Test on CD/HFD-derived BEC-organoids, the organoids were grown with FA mix for 7 days. On day 7, 10 µM HLM006474 or DMSO as vehicle were added overnight. The next morning, BEC-organoids were dissociated, and 20000 cells were seeded with Seahorse Assay Medium in XFe96 Cell Culture Microplates (Agilent, 101085-004), which were previously coated with 10% Matrigel in Advanced DMEM/F-12. Seahorse Assay Medium was unbuffered, serum-free pH 7.4 DMEM supplemented with 10 mM glucose (Agilent, 103577-100), 10 mM pyruvate (Gibco, 11360070), and 2 mM glutamine (Agilent, 103579-100), and 10 µM HLM006474 or DMSO (vehicle) were added when indicated. After 2 h incubation for cell attachment, plates were transferred to a non-CO^2 incubator at 37 °C for 45 minutes. Mitochondrial OCR was measured in a time course before and after the injection of 1.5 µM Oligomycin (Millipore, 495455), 2.5 µM FCCP (Sigma, C2920), and 1 µM Rotenone (Sigma, R8875)/Antimycin A (Sigma, A8674).

For Glycolytic Rate Assay, CD BEC-organoids were grown without FA mix and CD/HFD-derived BEC-organoids were grown with FA mix for 7 days. The Seahorse assay preparations including the E2F inhibitor were the same as mentioned above. GlycoPER was measured in a time course before and after the injection of 1 µM Rotenone/Antimycin A, and 500 µM 2-DG (Sigma, D8375).

For Substrate Oxidation Assay, CD BEC-organoids were grown without FA mix for 7 days. On day 8, they were dissociated and prepared for Seahorse assay, without E2F inhibitor. Mitochondrial OCR was measured in a time course before and after the injection of Oligomycin (1.5 μM), FCCP (2.5 μM), and Rotenone/Antimycin A (1 μM) with or without UK5099 (Sigma, PZ0160), Etomoxir (E1905) and BPTES (SML0601), inhibitors of glucose oxidation, fatty acid oxidation and glutamine oxidation, respectively, in separate experiments.

All Seahorse experiments were normalized by cell number through injection of 10 μM of Hoechst (ThermoFisher,62249) in the last Seahorse injection. Hoechst signal (361/486 nm) was quantified by SpectraMax iD3 microplate reader (Molecular Devices).

BEC-organoid growth assay

BEC-organoid formation efficiency was quantified by counting the total number of cystic/single layer (lumen-containing) CD/HFD-derived BEC-organoids 6 days after seeding and normalizing it to the total number of cells seeded initially (15000 cells). Organoids were imaged by DM IL LED inverted microscope (Leica), selected as regions of interest (ROI) using widefield 4x magnification, and counted manually.

BEC-organoid functional analysis

Grown BEC-organoids were treated with the FA-mix for 4 days and triglyceride levels were measured with a Triglyceride kit (Abcam, ab65336) following the manufacturer's instructions. Cell-titer Glo (Promega, G7570) was used to investigate cell viability. For functional assays involving single BECs, grown organoids were dissociated into single cells. 10000 BECs were seeded, and organoid formation was allowed for 7 days. Cell viability, apoptosis, and cell death were investigated using Cell-titer Glo, Caspase 3/7 activity (Promega, G8091), and Nucgreen Dead 488 staining (Invitrogen, R37109), respectively, according to the protocol of manufacturers. For cell death staining, organoids were imaged using ECLIPSE Ts2 inverted microscope (Nikon).

Quantification and statistical analysis

Data were presented as mean ± standard deviation (mean ± SD.) unless it is stated otherwise in the figure legend. *n* refers to biological replicates and is represented by the number of dots in the plot or stated in the figure legends. For the Seahorse experiments, *n* refers to technical replicates pooled from 4 biological replicates and is represented by the number of dots in the plot or stated in the figure legends. The statistical analysis of the data from bench experiments was performed using Prism (Prism 9, GraphPad). The differences with $p<0.05$ were considered statistically significant. No samples (except outliers) or animals were excluded from the analysis. Data are expected to have a normal distribution.

For two groups comparison, data significance was analyzed using a two-tailed, unpaired Student's t-test. In case of comparisons between more than two groups, one- or two-way ANOVA was used. Dunnet's, Tukey's, or Sidak's tests were used to correct for multiple comparisons. Statistical details of each experiment can be found in the respective figure legends.

Data availability

Computational analysis was performed using established packages mentioned in previous sections, and no new code was generated. Two publicly available RNA-Seq datasets of mouse BECs with accession numbers GSE123133 (Aloia et al., 2019) and GSE125688 (Pepe-Mooney et al., 2019) were downloaded from the GEO and used for GSEA and over-representation enrichment analysis as mentioned previously.

References

Aloia L., McKie M.A., Vernaz G., Cordero-Espinoza L., Aleksieva N., van den Ameele J., Antonica F., Font-Cunill B., Raven A., Aiese Cigliano R., Belenguer G., Mort R.L., Brand A.H., Zernicka-Goetz M., Forbes S.J., Miska E.A., Huch M. , 2019 **Epigenetic remodelling licences adult cholangiocytes for organoid formation and liver regeneration** *Nature Cell Biology* **21:**1321–1333

Andrews S. , 2010 **Andrews, S., 2010. FastQC: a quality control tool for high throughput sequence data.**

Araya J., Rodrigo R., Videla L.A., Thielemann L., Orellana M., Pettinelli P., Poniachik J , 2004 **Increase in long-chain polyunsaturated fatty acid n–6/n–3 ratio in relation to hepatic steatosis in patients with non-alcoholic fatty liver disease** *Clinical Science* **106:**635–643

Bankhead P., Loughrey M.B., Fernández J.A., Dombrowski Y., McArt D.G., Dunne P.D., McQuaid S., Gray R.T., Murray L.J., Coleman H.G., James J.A., Salto-Tellez M., Hamilton P.W , 2017 **QuPath: Open source software for digital pathology image analysis** *Sci Rep* **7:**16878

Beyaz S., Mana M.D., Roper J., Kedrin D., Saadatpour A., Hong S.-J., Bauer-Rowe K.E., Xifaras M.E., Akkad A., Arias E., Pinello L., Katz Y., Shinagare S., Abu-Remaileh M., Mihaylova M.M., Lamming D.W., Dogum R., Guo G., Bell G.W., Selig M., Nielsen G.P., Gupta N., Ferrone C.R., Deshpande V., Yuan G.-C., Orkin S.H., Sabatini D.M., Yilmaz Ö.H , 2016 **High-fat diet enhances stemness and tumorigenicity of intestinal progenitors** *Nature* **531:**53–58

Blanchet E., Annicotte J.-S., Lagarrigue S., Aguilar V., Clapé C., Chavey C., Fritz V., Casas F., Apparailly F., Auwerx J., Fajas L , 2011 **E2F transcription factor-1 regulates oxidative metabolism** *Nat Cell Biol* **13:**1146–1152

Broadfield L.A., Duarte J.A.G., Schmieder R., Broekaert D., Veys K., Planque M., Vriens K., Karasawa Y., Napolitano F., Fujita S., Fujii M., Eto M., Holvoet B., Vangoitsenhoven R., Fernandez-Garcia J., Van Elsen J., Dehairs J., Zeng J., Dooley J., Rubio R.A., van Pelt J., Grünewald T.G.P., Liston A., Mathieu C., Deroose C.M., Swinnen J.V., Lambrechts D., di Bernardo D., Kuroda S., De Bock K., Fendt S.-M. , 2021 **Fat Induces Glucose Metabolism in Nontransformed Liver Cells and Promotes Liver Tumorigenesis** *Cancer Res* **81:**1988–2001

Broutier L., Andersson-Rolf A., Hindley C.J., Boj S.F., Clevers H., Koo B.-K., Huch M , 2016 **Culture and establishment of self-renewing human and mouse adult liver and pancreas 3D organoids and their genetic manipulation** *Nature Protocols* **11:**1724–1743

Byrne C.D., Targher G. , 2015 **NAFLD: A multisystem disease** *Journal of Hepatology* **62:**

Capolupo L., Khven I., Lederer A.R., Mazzeo L., Glousker G., Ho S., Russo F., Montoya J.P., Bhandari D.R., Bowman A.P., Ellis S.R., Guiet R., Burri O., Detzner J., Muthing J., Homicsko K., Kuonen F., Gilliet M., Spengler B., Heeren R.M.A., Dotto G.P., La Manno G., D'Angelo G , 2022 **Sphingolipids control dermal fibroblast heterogeneity** *Science* **376:**

Choi T., Ninov N., Stainier D.Y.R., Shin D , 2014 **Extensive Conversion of Hepatic Biliary Epithelial Cells to Hepatocytes After Near Total Loss of Hepatocytes in Zebrafish** *Gastroenterology* **146:**776–788

De Gottardi A., Vinciguerra M., Sgroi A., Moukil M., Ravier-Dall'Antonia F., Pazienza V., Pugnale P., Foti M., Hadengue A. , 2007 **Microarray analyses and molecular profiling of steatosis induction in immortalized human hepatocytes** *Lab Invest* **87:**792–806

Denechaud P.-D., Fajas L., Giralt A , 2017 **E2F1, a Novel Regulator of Metabolism** *Front. Endocrinol* **8:**311

Denechaud P.-D., Lopez-Mejia I.C., Giralt A., Lai Q., Blanchet E., Delacuisine B., Nicolay B.N., Dyson N.J., Bonner C., Pattou F., Annicotte J.-S., Fajas L , 2015 **E2F1 mediates sustained lipogenesis and contributes to hepatic steatosis** *Journal of Clinical Investigation* **126:**137–150

Deng X., Zhang X., Li W., Feng R.-X., Li L., Yi G.-R., Zhang X.-N., Yin C., Yu H.-Y., Zhang J.-P., Lu B., Hui L., Xie W.-F , 2018 **Chronic Liver Injury Induces Conversion of Biliary Epithelial Cells into Hepatocytes** *Cell Stem Cell* **23:**114–122

Dimova D.K., Dyson N.J , 2005 **The E2F transcriptional network: old acquaintances with new faces** *Oncogene* **24:**2810–2826

Dobin A., Davis C.A., Schlesinger F., Drenkow J., Zaleski C., Jha S., Batut P., Chaisson M., Gingeras T.R. , 2013 **STAR: ultrafast universal RNA-seq aligner** *Bioinformatics* **29:**15–21

Dyson N , 1998 **The regulation of E2F by pRB-family proteins** *Genes Dev* **12:**2245–2262

Dyson N.J , 2016 **RB1 : a prototype tumor suppressor and an enigma** *Genes Dev* **30:**1492–1502

Español–Suñer R., Carpentier R., Van Hul N., Legry V., Achouri Y., Cordi S., Jacquemin P., Lemaigre F., Leclercq I.A. , 2012 **Liver Progenitor Cells Yield Functional Hepatocytes in Response to Chronic Liver Injury in Mice** *Gastroenterology* **143:**1564–1575

Gadd V.L., Aleksieva N., Forbes S.J , 2020 **Epithelial Plasticity during Liver Injury and Regeneration** *Cell Stem Cell* **27:**557–573

Gadd V.L., Skoien R., Powell E.E., Fagan K.J., Winterford C., Horsfall L., Irvine K., Clouston A.D , 2014 **The portal inflammatory infiltrate and ductular reaction in human nonalcoholic fatty liver disease** *Hepatology* **59:**1393–1405

Hallett J.M., Ferreira-Gonzalez S., Man T.Y., Kilpatrick A.M., Esser H., Thirlwell K., Macmillan M.T., Rodrigo-Torres D., Dwyer B.J., Gadd V.L., Ashmore-Harris C., Lu W.-Y., Thomson J.P., Jansen M.A., O'Duibhir E., Starkey Lewis P.J., Campana L., Aird R.E., Bate T.S.R., Fraser A.R., Campbell J.D.M., Oniscu G.C., Hay D.C., Callanan A., Forbes S.J , 2022 **Human biliary epithelial cells from discarded donor livers rescue bile duct structure and function in a mouse model of biliary disease** *Cell Stem Cell* **29:**355–371

Hsieh M.C.F., Das D., Sambandam N., Zhang M.Q., Nahlé Z. , 2008 **Regulation of the PDK4 Isozyme by the Rb-E2F1 Complex** *Journal of Biological Chemistry* **283:**27410–27417

Huber K., Mestres-Arenas A., Fajas L., Leal-Esteban L.C. , 2021 **The multifaceted role of cell cycle regulators in the coordination of growth and metabolism** *FEBS J* **288:**3813–3833

Huch M., Dorrell C., Boj S.F., van Es J.H., Li V.S.W., van de Wetering M., Sato T., Hamer K., Sasaki N., Finegold M.J., Haft A., Vries R.G., Grompe M., Clevers H. , 2013 **In vitro expansion of single Lgr5+ liver stem cells induced by Wnt-driven regeneration** *Nature* **494:**247–250

Huch M., Gehart H., van Boxtel R., Hamer K., Blokzijl F., Verstegen M.M.A., Ellis E., van Wenum M., Fuchs S.A., de Ligt J., van de Wetering M., Sasaki N., Boers S.J., Kemperman H., de Jonge J., Ijzermans J.N.M., Nieuwenhuis E.E.S., Hoekstra R., Strom S., Vries R.R.G., van der Laan L.J.W., Cuppen E., Clevers H. , 2015 **Long-Term Culture of Genome-Stable Bipotent Stem Cells from Adult Human Liver** *Cell* **160:**299–312

Ipsen D.H., Lykkesfeldt J., Tveden-Nyborg P , 2018 **Molecular mechanisms of hepatic lipid accumulation in non-alcoholic fatty liver disease** *Cell. Mol. Life Sci* **75:**3313–3327

Lê S., Josse J., Husson F , 2008 **FactoMineR : An R Package for Multivariate Analysis** *J. Stat. Soft* **25:**

Li B., Dorrell C., Canaday P.S., Pelz C., Haft A., Finegold M., Grompe M. , 2017 **Adult Mouse Liver Contains Two Distinct Populations of Cholangiocytes** *Stem Cell Reports* **9:**478–489

Love M.I., Huber W., Anders S , 2014 **Moderated estimation of fold change and dispersion for RNA-seq data with DESeq2** *Genome Biol* **15:**550

Lu W.-Y., Bird T.G., Boulter L., Tsuchiya A., Cole A.M., Hay T., Guest R.V., Wojtacha D., Man T.Y., Mackinnon A., Ridgway R.A., Kendall T., Williams M.J., Jamieson T., Raven A., Hay D.C., Iredale J.P., Clarke A.R., Sansom O.J., Forbes S.J. , 2015 **Hepatic progenitor cells of biliary origin with liver repopulation capacity** *Nat Cell Biol* **17:**971–983

Machado M.V., Michelotti G.A., Pereira T.A., Xie G., Premont R., Cortez-Pinto H., Diehl A.M , 2015 **Accumulation of duct cells with activated YAP parallels fibrosis progression in non-alcoholic fatty liver disease** *Journal of Hepatology* **63:**962–970

Meyer K., Morales-Navarrete H., Seifert S., Wilsch-Braeuninger M., Dahmen U., Tanaka E.M., Brusch L., Kalaidzidis Y., Zerial M. , 2020 **Bile canaliculi remodeling activates YAP via the actin cytoskeleton during liver regeneration** *Mol Syst Biol* **16:**

Miao Z.-F., Adkins-Threats M., Burclaff J.R., Osaki L.H., Sun J.-X., Kefalov Y., He Z., Wang Z.-N., Mills J.C , 2020 **A Metformin-Responsive Metabolic Pathway Controls Distinct Steps in Gastric Progenitor Fate Decisions and Maturation** *Cell Stem Cell* **26:**910–925

Michalopoulos G.K , 2014 **The Liver Is a Peculiar Organ When It Comes to Stem Cells** *The American Journal of Pathology* **184:**1263–1267

Miyajima A., Tanaka M., Itoh T , 2014 **Stem/Progenitor Cells in Liver Development, Homeostasis, Regeneration, and Reprogramming** *Cell Stem Cell* **14:**561–574

Nicolay B.N., Dyson N.J , 2013 **The multiple connections between pRB and cell metabolism** *Current Opinion in Cell Biology* **25:**735–740

Okabe M., Tsukahara Y., Tanaka M., Suzuki K., Saito S., Kamiya Y., Tsujimura T., Nakamura K., Miyajima A , 2009 **Potential hepatic stem cells reside in EpCAM+ cells of normal and injured mouse liver** *Development* **136:**1951–1960

Paschos P., Paletas K , 2009 **Non alcoholic fatty liver disease and metabolic syndrome** *Hippokratia* **13:**9–19

Pepe-Mooney B.J., Dill M.T., Alemany A., Ordovas-Montanes J., Matsushita Y., Rao A., Sen A., Miyazaki M., Anakk S., Dawson P.A., Ono N., Shalek A.K., van Oudenaarden A., Camargo F.D. , 2019 **Single-Cell Analysis of the Liver Epithelium Reveals Dynamic Heterogeneity and an Essential Role for YAP in Homeostasis and Regeneration** *Cell Stem Cell* **25:**23–38

Planas-Paz L., Sun T., Pikiolek M., Cochran N.R., Bergling S., Orsini V., Yang Z., Sigoillot F., Jetzer J., Syed M., Neri M., Schuierer S., Morelli L., Hoppe P.S., Schwarzer W., Cobos C.M., Alford J.L., Zhang L., Cuttat R., Waldt A., Carballido-Perrig N., Nigsch F., Kinzel B., Nicholson T.B., Yang Y., Mao X., Terracciano L.M., Russ C., Reece-Hoyes J.S., Gubser Keller C., Sailer A.W., Bouwmeester T., Greenbaum L.E., Lugus J.J., Cong F., McAllister G., Hoffman G.R., Roma G., Tchorz J.S , 2019 **YAP, but Not RSPO-LGR4/5, Signaling in Biliary Epithelial Cells Promotes a Ductular Reaction in Response to Liver Injury** *Cell Stem Cell* **25:**39–53

Raven A., Lu W.-Y., Man T.Y., Ferreira-Gonzalez S., O'Duibhir E., Dwyer B.J., Thomson J.P., Meehan R.R., Bogorad R., Koteliansky V., Kotelevtsev Y., Ffrench-Constant C., Boulter L., Forbes S.J , 2017 **Cholangiocytes act as facultative liver stem cells during impaired hepatocyte regeneration** *Nature* **547:**350–354

Ren B., Cam H., Takahashi Y., Volkert T., Terragni J., Young R.A., Dynlacht B.D , 2002 **E2F integrates cell cycle progression with DNA repair, replication, and G 2 /M checkpoints** *Genes Dev* **16:**245–256

Rodrigo-Torres D., Affò S., Coll M., Morales-Ibanez O., Millán C., Blaya D., Alvarez-Guaita A., Rentero C., Lozano J.J., Maestro M.A., Solar M., Arroyo V., Caballería J., van Grunsven L.A., Enrich C., Ginès P., Bataller R., Sancho-Bru P. , 2014 **The biliary epithelium gives rise to liver progenitor cells: RODRIGO-TORRES ET AL** *Hepatology* **60:**1367–1377

Russell J.O., Lu W., Okabe H., Abrams M., Oertel M., Poddar M., Singh S., Forbes S.J., Monga S.P , 2019 **Hepatocyte-Specific β-Catenin Deletion During Severe Liver Injury Provokes Cholangiocytes to Differentiate Into Hepatocytes** *Hepatology* **69:**742–759

Sampaziotis F., Muraro D., Tysoe O.C., Sawiak S., Beach T.E., Godfrey E.M., Upponi S.S., Brevini T., Wesley B.T., Garcia-Bernardo J., Mahbubani K., Canu G., Gieseck R., Berntsen N.L., Mulcahy V.L., Crick K., Fear C., Robinson S., Swift L., Gambardella L., Bargehr J., Ortmann D., Brown S.E., Osnato A., Murphy M.P., Corbett G, Gelson W.T.H., Mells G.F., Humphreys P., Davies S.E., Amin I., Gibbs P., Sinha S., Teichmann S.A., Butler A.J., See T.C., Melum E., Watson C.J.E., Saeb-Parsy K., Vallier L. , 2021 **Cholangiocyte organoids can repair bile ducts after transplantation in the human liver** *Science* **371:**839–846

Sano A., Kakazu E., Hamada S., Inoue J., Ninomiya M., Iwata T., Tsuruoka M., Sato K., Masamune A , 2021 **Steatotic Hepatocytes Release Mature VLDL Through Methionine and Tyrosine Metabolism in a Keap1-Nrf2–Dependent Manner** *Hepatology* **74:**1271–1286

Sato K., Marzioni M., Meng F., Francis H., Glaser S., Alpini G , 2018 **Ductular reaction in liver diseases: pathological mechanisms and translational significances** *Hepatology*

Schindelin J., Arganda-Carreras I., Frise E., Kaynig V., Longair M., Pietzsch T., Preibisch S., Rueden C., Saalfeld S., Schmid B., Tinevez J.-Y., White D.J., Hartenstein V., Eliceiri K., Tomancak P., Cardona A , 2012 **Nat Methods** 676–682

Shin S., Walton G., Aoki R., Brondell K., Schug J., Fox A., Smirnova O., Dorrell C., Erker L., Chu A.S., Wells R.G., Grompe M., Greenbaum L.E., Kaestner K.H , 2011 **Foxl1-Cre-marked adult hepatic progenitors have clonogenic and bilineage differentiation potential** *Genes & development* **25:**1185–92

Sorrentino G., Rezakhani S., Yildiz E., Nuciforo S., Heim M.H., Lutolf M.P., Schoonjans K , 2020 **Mechano-modulatory synthetic niches for liver organoid derivation** *Nature Communications* **11:**1–10

Sorrentino P., Tarantino G., Perrella A., Micheli P., Perrella O., Conca P , 2005 **A Clinical–Morphological Study on Cholestatic Presentation of Nonalcoholic Fatty Liver Disease** *Dig Dis Sci* **50:**1130–1135

Tsuchiya A., Lu W.-Y., Weinhold B., Boulter L., Stutchfield B.M., Williams M.J., Guest R.V., Minnis-Lyons S.E., MacKinnon A.C., Schwarzer D., Ichida T., Nomoto M., Aoyagi Y., Gerardy-Schahn R., Forbes S.J , 2014 **Polysialic acid/neural cell adhesion molecule modulates the formation of ductular reactions in liver injury: HEPATOLOGY, Vol. XX, No. X, 2014 TSUCHIYA ET AL** *Hepatology* **60:**1727–1740

Vander Heiden M.G., Cantley L.C., Thompson C.B. , 2009 **Understanding the Warburg Effect: The Metabolic Requirements of Cell Proliferation** *Science* **324:**1029–1033

Wang L.-Y., Hung C.-L., Chen Y.-R., Yang J.C., Wang J., Campbell M., Izumiya Y., Chen H.-W., Wang W.-C., Ann D.K., Kung H.-J. , 2016 **KDM4A Coactivates E2F1 to Regulate the PDK-Dependent Metabolic Switch between Mitochondrial Oxidation and Glycolysis** *Cell Reports* **16:**3016–3027

Wang X., Zheng Z., Caviglia J.M., Corey K.E., Herfel T.M., Cai B., Masia R., Chung R.T., Lefkowitch J.H., Schwabe R.F., Tabas I. , 2016 **Hepatocyte TAZ/WWTR1 Promotes Inflammation and Fibrosis in Nonalcoholic Steatohepatitis** *Cell Metabolism* **24:**848–862

Wickham H , 2016 **ggplot2: Elegant Graphics for Data Analysis, 2nd ed. 2016. ed, Use R! Springer International Publishing**

Wobser H., Dorn C., Weiss T.S., Amann T., Bollheimer C., Büttner R., Schölmerich J., Hellerbrand C , 2009 **Lipid accumulation in hepatocytes induces fibrogenic activation of hepatic stellate cells** *Cell Res* **19:**996–1005

Yanger K., Stanger B.Z , 2011 **Facultative stem cells in liver and pancreas: Fact and fancy** *Dev. Dyn* **240:**521–529

Yu G., Wang L.-G., Han Y., He Q.-Y. , 2012 **clusterProfiler: an R Package for Comparing Biological Themes Among Gene Clusters** *OMICS: A Journal of Integrative Biology* **16:**284–287

Zhang H., Ryu D., Wu Y., Gariani K., Wang X., Luan P., D'Amico D., Ropelle E.R., Lutolf M.P., Aebersold R., Schoonjans K., Menzies K.J., Auwerx J. , 2016 **NAD + repletion improves mitochondrial and stem cell function and enhances life span in mice** *Science* **352:**1436–1443

Author information

Ece Yildiz
Laboratory of Metabolic Signaling, Institute of Bioengineering, Switzerland

Gaby El Alam
Laboratory of Integrative Systems Physiology, Institute of Bioengineering, Switzerland

Alessia Perino
Laboratory of Metabolic Signaling, Institute of Bioengineering, Switzerland

Antoine Jalil
Laboratory of Metabolic Signaling, Institute of Bioengineering, Switzerland

Pierre-Damien Denechaud
Center for Integrative Genomics, Université de Lausanne, Switzerland, Institute of Metabolic and Cardiovascular Diseases (I2MC), UMR1297, INSERM, University of Toulouse, France

Katharina Huber
Center for Integrative Genomics, Université de Lausanne, Switzerland

Lluis Fajas
Center for Integrative Genomics, Université de Lausanne, Switzerland, INSERM, Occitanie, France

Johan Auwerx
Laboratory of Integrative Systems Physiology, Institute of Bioengineering, Switzerland

Giovanni Sorrentino
Laboratory of Metabolic Signaling, Institute of Bioengineering, Switzerland, Department of Life Sciences, University of Trieste, Italy

Kristina Schoonjans
Laboratory of Metabolic Signaling, Institute of Bioengineering, Switzerland

Peer review

Editors

Reviewing Editor

Peter Tontonoz

University of California, Los Angeles, United States

Senior Editor

Carlos Isales

Medical College of Georgia at Augusta University, United States

Reviewer #1 (Public Review):

This manuscript explores how biliary epithelial cells respond to excess dietary lipids, an important area of research given the increasing prevalence of NAFLD. The authors utilize in vivo models complemented with cultured organoid systems. Interesting, E2F transcription factors appear important for BEC glycolytic activation and proliferation.

Much of the work utilizes the BEC-organoid model, which is complicated by the fact that liver cell organoid models often fail to maintain exclusive cell identity in culture. The method used by the authors (Broutier et al., 2016) can lead to organoids with a mixture of ductal and hepatocyte markers. It would be helpful for the authors to further demonstrate the cholangiocyte identity of the organoid cells.

The authors suggest that BECs form lipid droplets in vivo by detecting BODIPY immunofluorescence of liver cryosections. While confocal microscopy would ensure that the BODIPY fluorescence signal is within the same plane as the cell of interest, the authors use a virtual slide microscope that cannot exclude fluorescence from a different focal plane. The conclusion that BECs accumulate lipids does not seem to be fully supported by this analysis.

Several mouse experiments rely heavily on rare BEC proliferation events with the median proliferation event per bile duct being 0-1 cell. While the proliferative effect appears consistent across experiments, a more quantitative approach, such as performing Epcam+ BEC FACS and flow cytometry-based cell cycle analyses, would be helpful.

Finally, it is not yet clear how relevant the findings in this study are to ductular reaction, which is a non-specific histopathologic indicator of liver injury in the context of severe liver disease. In NAFLD, the ductular reaction is uncommon in benign steatosis, and if seen at all, occurs in the setting of substantial liver inflammation and fibrosis (Gadd et al., Hepatology 2014). The authors use a dietary model containing 60 kcal% fat, which causes adipose lipid accumulation as well as subsequent liver lipid accumulation. This diet does not cause overt inflammation or fibrosis that would represent experimental NASH, which typically requires the addition of cholesterol in dietary lipid NASH models (Farrell et al., Hepatology, 2019). While the E2F-driven proliferation may be important for physiologic bile duct function in the setting of obesity, the claim that E2Fs mediate DR initiation would require an additional pathophysiologic model or human data to demonstrate relevance. The authors could clarify this point in their discussion.

Reviewer #2 (Public Review):

The manuscript by Yildiz et al investigates the early response of BECs to high fatty acid treatment. To achieve this, they employ organoids derived from primary isolated BECs and treat them with a FA mix followed by viability studies and analysis of selected lipid metabolism genes, which are upregulated indicating an adjustment to lipid overload. Both organoids with lipid overload and BECs in mice exposed to a HFD show increased BEC proliferation, indicating BEC activation as seen in DR. Applying bulk RNA-sequencing analysis to sorted BECs from HFD mice identified four E2F transcription factors and target genes as upregulated. Functional analysis of knock-out mice showed a clear requirement for E2F1 in mediating HFD induced BEC proliferation. Given the known function of E2Fs the authors performed cell respiration and transcriptome analysis of organoids challenged with FA treatment and found a shift of BECs towards a glycolytic metabolism.

The study is overall well-constructed, including appropriate analysis. Likewise, the manuscript is written clearly and supported by high-quality figures. My major point is the lack of classification of the progression of DR, since the authors investigate the early stages of DR associated with lipid overload reminiscent of stages preceding late NAFLD fibrosis. How are early stages distinguished from later stages in this study? Molecularly and/or morphologically? While the presented data are very suggestive, a more substantial description would support the findings and resulting claims.